March 10, 1961

To the Graduate Council:

I am submitting herewith a dissertation written by Robert I. Gray entitled "The Dynamics of a Packed Gas Absorber by Frequency Response Analysis." I recommend that it be accepted in partial fulfillment of the requirements for the degree of Doctor of Philosophy, with a major in Chemical Engineering.

John W. Prados
Major Professor

We have read this dissertation and recommend its acceptance:

Edgar D. Eads

W. D. Johnson

M. Jury

J. D. Tillman

E. E. Stansbury

D. C. Boyce

M. Peebles

Accepted for the Council:

W. E. Spivey
Acting Dean of the Graduate School

THE DYNAMICS OF A PACKED GAS ABSORBER BY FREQUENCY RESPONSE ANALYSIS

A Dissertation

Presented to

The Graduate Council of

The University of Tennessee

In Partial Fulfillment

of the Requirements for the Degree

Doctor of Philosophy

---

by

Robert I. Gray

March 1961

337

ACKNOWLEDGEMENT

The author wishes to acknowledge and to express his gratitude to his major professor, Dr. John W. Prados, for the initial suggestion which led to the selection of this research problem and for his continued interest, suggestions, and constructive criticism.

The members of the faculty of the Department of Chemical and Metallurgical Engineering have individually contributed helpful suggestions on numerous aspects of the work. The author is particularly grateful to the late Dr. R. M. Boarts for his encouragement and financial assistance in the form of positions as a graduate assistant and later as an instructor in the Department of Chemical Engineering.

This research has been financially supported by a National Science Foundation grant. The author wishes to express his sincere appreciation to the Fellowship Committees of the Foundation and the University of Tennessee for this Fellowship.

Mr. E. H. Honeycutt, Supervisor of Laboratories, and his staff have been of great assistance in the construction of the experimental equipment of this work. The author is particularly grateful to H. B. Thompson for his numerous suggestions concerning the design of this equipment and for his unique craftsmanship in the construction of the individual

479920

components.

Mrs. Dorothy Norton, who has skillfully typed and has suggested format improvements of this thesis, is gratefully acknowledged.

The author finds that the terms acknowledgement, gratitude, or appreciation are inadequate in describing his feelings for his wife's contributions to this work. Thank you, Elise.

SUMMARY

The unsteady state behavior of physical gas absorption in a packed bed was studied by comparing the results of experimental frequency response tests of such a system with theoretical frequency responses determined for several postulated flow models.

Rapidly expanding automatic process control technology has resulted in a great increase in the number of experimental and theoretical studies of process dynamics in the last five years. Countercurrent, diffusional operations in distributed systems, however, have received little attention. Therefore, this study was undertaken to provide a more thorough understanding of the dynamic behavior of such an interphase mass transfer process and to investigate the effects of the system's physico-chemical and operational variables on this behavior.

The absorption column consisted of a 6-inch ID, Pyrex pipe packed to a depth of 5.12 ft with 5/8-inch ceramic Raschig rings. The gas phase was a mixture of carbon dioxide and air, while the solvent was water. Both phases were handled in open systems.

The frequency response tests were conducted by introducing a gas mixture with a sinusoidally varying carbon dioxide concentration to the inlet of the column and measur-

ing the resulting steady state concentration wave at the column outlet. The concentration sinusoid was generated by mixing with a constant flow air stream the carbon dioxide flow from a sinusoidally varying linear valve specifically designed for the application. The sinusoid generator was capable of frequencies of 0.1 to 15 cycles/min.

The gas phase steady state concentration sinusoids at the inlet and outlet of the column were measured continuously with specially designed, high speed thermal conductivity cells and were recorded with a single channel oscillograph. The dynamic response of the column was tested for liquid phase flow rates of 222, 55, and 0 lb moles/hr-ft^2 at each of three gas phase flow rates (nominally 1, 10, and 20 lb moles/hr-ft^2, corresponding to Reynolds numbers of 30, 300, and 600, respectively). The responses of the packing section alone were determined from the total column responses by deducting the effects of the column inlet and outlet sections which were evaluated from frequency response tests of a mock-up of these sections.

The experimental frequency response results obtained for a spectrum of concentration sinusoid frequencies at each set of column operating conditions were expressed graphically in Bode plots (phase shift and logarithm of the amplitude ratio versus logarithm of the sinusoid frequency).

Theoretical frequency responses for the packing section

were calculated for three flow models: a "slug flow" model which presumed no radial velocity gradients, a "mixing cell," and an "axial diffusion" model which attempted quantitative descriptions of the packing section mixing or dispersion phenomena.

The experimental results showed that the greatest portion of the column response was associated with the inlet and outlet sections for all the gas flows tested.

Comparison of the theoretical and experimental packing section frequency responses indicated that, while the "slug flow" model most closely described the absorption dynamics, no model was completely satisfactory in this respect. The deviations of the experimental responses from those of the "slug flow" model were attributed to mixing of the gas phase in the packing section. The presence of these dispersion effects was clearly demonstrated in the nonabsorption (dry packing) tests. While neither the "mixing cell" nor the "axial diffusion" models adequately described the observed responses, it was established that the relative degree of mixing was considerably larger than had been previously reported for gas flow in packed beds.

The applicability of a flow model could not be established from comparison of experimental and theoretical phase shifts as all models resulted in similar data which were, generally, in good agreement with the observed values.

The effect of column operating conditions on the degree of mixing was masked by an apparent complex interaction of these variables and by the lack of a satisfactory single mixing parameter.

TABLE OF CONTENTS

CHAPTER		PAGE
I.	INTRODUCTION	1
	Historical Background	1
	Objectives	5
	Frequency Response Analysis	7
	Gas Analysis	9
	Absorption System	10
	Theoretical Models	11
II.	MATHEMATICAL DEVELOPMENT OF THE THEORETICAL FREQUENCY RESPONSE EQUATIONS	14
	Slug Flow Models	14
	Two Phase Countercurrent Flow with Absorption	14
	Single Phase Flow without Absorption	27
	Cell Mixing Models	29
	Two Phase Countercurrent Flow with Absorption	29
	Single Phase Flow without Absorption	39
	Axial Diffusion Model	41
	Two Phase Countercurrent Flow with Absorption	41
	Single Phase Flow without Absorption	45
III.	EXPERIMENTAL EQUIPMENT	49
	The Column	49
	Gas Phase Flow System	49
	Liquid Phase Flow System	56

CHAPTER PAGE

Thermal Conductivity Cells and Detection Equipment 59
Gas Sampling and Cell Thermostatting Equipment . 63
Column Inlet and Outlet Sections Mock-up 68
IV. EXPERIMENTAL PROCEDURE 71
Column Packing 71
Calibrations 72
Bridge Operation 78
Column Frequency Response Tests 82
Mock-up System Frequency Response Tests 87
V. RESULTS AND DISCUSSION 89
Experimental Data Analysis 89
Total System and Mock-up System Responses . . . 99
Experimental and Theoretical Packing Section Responses 110
Nominal Gas Flow of 1 lb mole/hr-ft^2 123
Nominal Gas Flow of 10 lb mole/hr-ft^2 127
Nominal Gas Flow of 20 lb mole/hr-ft^2 130
Discussion 132
Axial Mixing 133
Effects of System Parameter on Theoretical Frequency Responses 137
Experimental Difficulties at Low Gas Flows . . 138

CHAPTER PAGE

VI. CONCLUSIONS AND RECOMMENDATIONS 141

Conclusions 141

Recommendations for Future Work 143

Recommendations for Equipment Modifications . . 145

BIBLIOGRAPHY 147

APPENDICES 158

A.. Use of Boundary Conditions in the Development of the Theoretical Response Equations 159

B. Determination of the Amplitude Ratio and Phase Shift from the Theoretical Transfer Functions . 165

Slug Flow Model 165

Mixing Cell Model 169

Axial Diffusion Model 176

C. Concentration Sinusoid Generator 179

Historical Background 179

Linear Valve Development 181

Theoretical Frequency Response Analysis 184

Discussion 194

D. Thermal Conductivity Cell Development 196

Historical Background 196

Thermal Conductivity Cell Design 201

Wheatstone Bridge Theory and Development 205

Cell Tests and Calibrations 213

Discussion 237

APPENDICES PAGE

E. Calibration Data 239

F. Experimental Frequency Response Data 249

G. Amplitude Ratio and Phase Shift Sample Calculations 263

Experimental Responses 263

Theoretical Responses 265

Slug Flow Models 273

Cell Mixing Models 277

Axial Diffusion Model 282

H. Notation 284

VITA 289

LIST OF TABLES

TABLE		PAGE
I.	Summary of Experimental Operating Conditions . .	98
II.	Matched Bridge Relative Characteristics	211
III.	Experimental Data - Run 1	250
IV.	" " - Run 3	251
V.	" " - Run 2	252
VI.	" " - Run 10	253
VII.	" " - Run 11	254
VIII.	" " - Run 4	255
IX.	" " - Run 9	256
X.	" " - Run 8	257
XI.	" " - Run 12	258
XII.	" " - Run 5	259
XIII.	" " - Run 7	260
XIV.	" " - Run 6	261
XV.	" " - Run 13	262

LIST OF FIGURES

FIGURE		PAGE
1.	Packing Increment	15
2.	Mixing Cell Increment	29
3.	Absorption Column and Associated Equipment	50
4.	Schematic Diagram of Column Flow Systems	52
5.	Linear Valve and Drive Arrangement	54
6.	Liquid Distributor Layout	58
7.	Schematic Diagram of Thermal Conductivity Cell Bridge Circuit	61
8.	Capillary Flowmeter	64
9.	Schematic Diagram of Thermal Conductivity Cell Flow Systems	66
10.	Column Inlet and Outlet Section Mock-up	69
11.	Soap Film Flowmeter Equipment	75
12.	Oscillograph Concentration Traces	90
13.	Experimental System Block Diagram	91
14.	Column Inlet and Outlet Mock-up Block Diagram . .	93
15.	Total Amplitude Ratio vs. Frequency, G = 1 $\frac{\text{lb mole}}{\text{hr-ft}^2}$	100
16.	" " " " " G =10 "	102
17.	" " " " " G =20 "	103
18.	Total Phase Shift vs. Frequency, G = 1 $\frac{\text{lb mole}}{\text{hr-ft}^2}$.	104
19.	" " " " " G =10 " .	105
20.	" " " " " G =20 " .	106

FIGURE PAGE

21. Total Amplitude Ratio Reproducibility 111

22. Total Phase Shift Reproducibility 112

23. Packing Section Amplitude Ratio, G = 1 $\frac{\text{lb mole}}{\text{hr-ft}^2}$ . . 114

24. Packing Section Phase Shift--Absorption,
G = 1 $\frac{\text{lb mole}}{\text{hr-ft}^2}$ 115

25. Packing Section Phase Shift--No Absorption,
G = 1 $\frac{\text{lb mole}}{\text{hr-ft}^2}$ 116

26. Packing Section Amplitude Ratio, G = 10 $\frac{\text{lb mole}}{\text{hr-ft}^2}$. 117

27. Packing Section Phase Shift--Absorption,
G = 10 $\frac{\text{lb mole}}{\text{hr-ft}^2}$ 118

28. Packing Section Phase Shift--No Absorption,
G = 10 $\frac{\text{lb mole}}{\text{hr-ft}^2}$ 119

29. Packing Section Amplitude Ratio, G = 20 $\frac{\text{lb mole}}{\text{hr-ft}^2}$. 120

30. Packing Section Phase Shift--Absorption,
G = 20 $\frac{\text{lb mole}}{\text{hr-ft}^2}$ 121

31. Packing Section Phase Shift--No Absorption,
G = 20 $\frac{\text{lb mole}}{\text{hr-ft}^2}$ 122

C-1. Valve Linearity Test Setup 180

C-2. Linear Valve 182

C-3. Linear Valve Position Characteristic 185

C-4. Analog Computer Solution of Sinusoid Generator
Behavior 191

C-5. Analog Simulation of Pressure Regulator Supply . . 194

C-6. Sinusoid Generator Dynamic Response 195

FIGURE PAGE

D-1. Thermistor Resistance Temperature Characteristic . 200
D-2. Thermal Conductivity Cell 202
D-3. Thermistor Mounting Arrangement 204
D-4. Wheatstone Bridge 206
D-5. Schematic Diagram of Calibration Gas Mixer 215
D-6. Thermal Conductivity Cell Test and Calibration Equipment 220
D-7. Bridge Signal vs. Thermistor Current 222
D-8. Bridge Signal vs. Cell Flow Rate 224
D-9. Null Point and Sensitivity Temperature Effects . . 228
D-10. Transient Test Equipment Modification 233
D-11. Thermal Conductivity Cell Calibration Data 236

E-1. Air Orifice Meter Calibration Data 240
E-2. Air Rotameter Calibration Data 241
E-3. Water Rotameter Calibration Data 242
E-4. Capillary Flowmeter Calibration Data for Air . . . 243
E-5. Mixer Capillary Flowmeter Calibration Data for Carbon Dioxide and Air 244
E-6. Mixer Rotameter Calibration, G-9143 245
E-7. Mixer Rotameter Calibration, G-9144 246
E-8. Inlet and Outlet Thermal Conductivity Cell Calibration Data 247
E-9. Sinusoid Generator Frequency Calibration Data . . 248

FIGURE PAGE

G-1. Packing Liquid Phase Holdup 267

G-2. Loading and Flooding Limiting Conditions 269

G-3. Liquid Film Mass Transfer Coefficients 271

G-4. Equilibrium Data Temperature Dependence 272

CHAPTER I

INTRODUCTION

The advanced design procedures currently used in the chemical process industry have resulted in the establishment of large integrated systems of process and operational equipment. The successful design and operation of such installations have required the chemical engineer to become familiar with the concepts and theories of automatic process control. As a result of this increased interest and knowledge, extremely rapid progress in the field of process dynamics has been made in the last five years. A large portion of this activity has been concerned with the application of servomechanism theory to the analysis of closed or feed-back loops and networks, particularly with regard to the stability of such systems (44). These loop and network studies require as primary information the dynamic or unsteady-state behavior of each unit operation or process which is integral to the system. It is the dynamic behavior of these individual components or "open loops" that will be considered here.

I. HISTORICAL BACKGROUND

Since 1954 an increasingly large number of experimental,

theoretical, and analog studies of individual operational equipment have been published in the literature. Some of the best of these are worth mentioning as examples of the type of work now being carried out.

In the field of heat transfer several analytical and experimental studies of concentric tube heat exchangers have been presented (73, 23). The dynamics of shell and tube heat exchangers were studied by Lees (63) and Aikman (2), while Reilly (85) and Dusinberre (39) gave transient analyses for a packed bed and cross-flow heat exchanger, respectively. The subject of rapid thermal transients in nuclear reactors has also been adequately covered (84).

Numerous studies have been made on pressure and fluid flow transients, particularly for pulsed incompressible flow and for wave propagation in gaseous systems. In this area the works of Alves (4) and Rohmann (86) are of interest. An extensive number of experimental and analytical investigations have been carried out on the dispersion or mixing of a single phase flow in packed beds (28, 33, 7, 59, 67, 40, 20, 108, 16).

Bilous and Amundson (11, 12) and Aris and Amundson (6) have published extensive theoretical calculations on chemical reactor stability and control. The equations for transients of second-order chemical reactions in continuous stirred-tank

reactors have been developed by Acton and Lapidus (1).

A comprehensive series of papers on the mathematics of adsorption in fixed beds has been presented by Amundson and co-workers (62). Other analytical adsorption studies by this group include work on agitated and moving beds (41, 53). Deisler and Wilhelm (33) carried out an interesting frequency response experiment on a fixed bed of adsorbent.

In the field of interphase mass transfer, a large number of papers have been presented on the unsteady-state behavior of plate distillation columns. Wilkinson (122), Jackson (49), and Rosenbrock (89) have studied the analytical and experimental transients of such columns. The control of a continuous plate distillation column has been investigated in two papers by Williams and Rose (87, 123). Several interesting studies of transients in batchwise fractional extraction have also been reported (78, 93).

In addition to the above references, two other sources of process dynamic studies can be recommended to the interested reader. The first is the proceedings of a conference on the subject held at Cambridge, England, in 1956 (81), and gives many comprehensive reports on experimental dynamics of operating plant instruments and equipment. The second is a text, Process Dynamics by D. P. Campbell (18), which attempts to apply the theories of servomechanisms to a number of chemical engineering processes with particular

emphasis on closed loop behavior.

Noticeably absent from the literature are significant studies of the unsteady-state behavior of countercurrent diffusional operations in "distributed parameter" systems, i.e., those systems which are properly described by partial differential equations as opposed to ordinary differential equations. Examples of such diffusional operations are: gas absorption and distillation in packed columns, and liquid-liquid extraction in spray or packed columns. While general solutions of the time dependent equations for a simplified system of this type are available (52, 66), to this author's knowledge, only one experimental study has been presented. McMillan (68) has published some rather limited frequency response measurements on an industrial, packed, HCl absorber, but has included no theoretical considerations.

In contrast, there has been a considerable amount of work on distributed parameter systems in general. The previously mentioned heat exchanger studies (73, 23, 2), the theoretical heat exchanger transfer functions of Takahashi (109), Amundson and co-workers' mathematical studies of adsorption (62, 41, 53), and the previously mentioned investigations of single phase mixing in packed beds are but a few examples that could be mentioned. Of these, though, only two have dealt with gas system dynamics (33, 67), and only one--the work of Lapidus (61)--has considered the transient

behavior of two phases in contact.

II. OBJECTIVES

It was felt, therefore, that a theoretical and experimental investigation of a two phase, countercurrent diffusion operation in a packed bed could provide valuable information to the field of process dynamics. Specifically, it was decided to investigate the dynamic behavior of a packed gas absorber of sufficient size to simulate industrial equipment and still meet the practical limitations of a controlled laboratory experiment.

In general terms, the dynamic behavior of the gas absorption process was studied by constructing a suitable absorption column and subjecting it to a known disturbance, thus forcing it to operate in a time dependent manner. The response of the column to the disturbance was measured in terms of the time variation of a phase concentration. Tests of this type were carried out for a number of column operating conditions in an effort to determine the qualitative and, if possible, quantitative effects of the operating conditions on the column's dynamic response.

In addition to these experimental tests, the column theoretical response was determined by writing the general time dependent equations for a particular mass transfer and flow model, and solving these equations for a phase concen-

tration-time behavior when initially disturbed in the same manner as was the experimental column. Theoretical responses for several models were obtained, using the same column operating conditions as in the experimental tests.

Conclusions concerning the nature of gas absorption dynamics, concerning the applicability of the several models and the assumptions upon which they were based, and concerning the effects of the column operating conditions were obtained by direct comparison of the theoretical and experimental column responses.

Three basic types of initial disturbances have been used to study the experimental dynamics of process equipment. In the "step function" method the initial disturbance is an instantaneous change in the measured variable (temperature, composition, etc.) of an incoming stream from one constant value to another (28, 16). A somewhat similar disturbance is the "pulse function" where the inlet stream measured variable instantaneously increases to a very high (or low) value and then returns to its original state (28, 20). This is the experimental equivalent of the Dirac delta function.

Both these types of disturbances have two disadvantages. The first is associated with the difficulty of obtaining a sharp and uniform step or pulse under experimental conditions. An additional problem is encountered in attempting to obtain a complete solution of the time dependent

equations with these disturbances for anything other than the most simple system.

III. FREQUENCY RESPONSE ANALYSIS

The third type of disturbance consists of a sinusoidal variation of the inlet stream measured variable. This initial sinusoidal disturbance causes the measured variables of outlet streams--after the transient has passed--to vary in a steady oscillatory fashion. If the system behaves linearly the output stream variable will also vary sinusoidally with the same frequency as the input disturbance but with a different amplitude and phase relation. The dynamic characteristics of the system are measured in terms of the ratio of a steady-state output wave amplitude to the disturbing input wave amplitude--the so-called "amplitude ratio"--and the "phase shift" or displacement between the two waves.

This technique for determining the dynamic response of an experimental system is called "frequency response analysis." It has two advantages over the methods mentioned previously: 1) a uniform sinusoidal variation of the measured variable is considerably easier to generate experimentally than the sharp concentration changes of the "step" and "pulse" methods, and, 2) since it is the steady state values of the amplitude ratio and phase shift that are desired, there is no necessity for the accurate determination of the

initial time condition. In addition the method permits the determination of the theoretical amplitude ratios and phase shifts, for a linear system, without a complete solution of the general boundary value problem. For these reasons frequency response analysis was selected for the experimental and analytical studies of this investigation.

Although frequency response techniques have been used for many years to analyze the behavior of electrical loops and networks, it was not until 1950 when Rutherford (90) suggested its application to process control problems that it found use in the process industry. Since that time a great variety of frequency response experiments have been carried out. To cite a few examples, the method has been applied to stirred tank reactors (43), heat exchangers (23, 2, 73), a spray drier (2), turbulent flow systems (56, 116), bubble-cap plates (45), packed beds (40, 33, 59), and even to rotameters (47).

The first significant theoretical frequency response study of chemical processing equipment was presented by Rosen and Winsche (88) in which a number of fixed-bed adsorption mechanisms were investigated. Several other interesting theoretical studies have since been carried out: the complex flow models of Turner (115), the characteristics of air-operated controllers by Ackman and Rutherford (3), and Bilous' (13) study of continuous-flow chemical reactor control are

examples. Also worth mentioning are the theoretical methods used to calculate frequency responses from the transient response to a step function disturbance and vice versa (92, 64).

IV. GAS ANALYSIS

A major deterent to experimental studies of the dynamics of mass transport phenomena has been the general lack of a satisfactory method to continuously measure rapidly changing liquid or gas phase compositions. In previous liquid phase analyses electrical conductivity (59, 16) and continuous colorimetric photometry (40, 20, 108) have been employed with some success. The problem of continuous high speed analysis of a gas phase is more difficult and, correspondingly, there has been less work done with such systems. Mass spectroscopy has been used by Lapidus (61), while Deisler et al. (34) have developed an α-ionization method explicitly for the frequency response analysis of a gas system (33, 67). Keyes (56) attempted to apply thermal conductivity analysis to his frequency response studies.

The particular two phase countercurrent flow conditions of this investigation made it difficult to analyze the liquid phase without significant time lags. This was caused by the uncertain flow conditions that might exist in any electrical conductivity or photometric cells. In addition,

the gas-solvent systems considered for this work did not have satisfactory specific conductance sensitivity.

A survey of available gas analyzers (105, 24, 74) indicated that continuous-mass spectroscopy and non-dispersed infra-red spectrophotometry might meet the speed-of-response requirement of this experiment; but, unfortunately, the cost of these instruments was prohibitive. The α-ionization method of Deisler et al. (34) was not applicable to the wet gas mixtures which would be encountered in the column.

Thus, with little choice in the matter, thermal conductivity analysis was selected for use in these frequency response studies. Although the method, as used commercially (105, 24), is very slow and although its previous use in frequency response analysis created significant experimental difficulties (56), it was believed that considerable improvement could be made in the design and application of the equipment. The special, high speed device developed for this investigation is described in detail in Appendix D.

V. ABSORPTION SYSTEM

The selection of the solute-carrier-solvent system to be used in the absorption experiments of this work was influenced by a number of considerations. The size of the proposed column (see Chapter III) encouraged the use of a common, inexpensive carrier gas and solvent. Thus, logically, air

and water were chosen for these functions. Although considerations such as availability, cost, ease of handling, etc., were pertinent to the selection of the solute gas, the most influential consideration was that of detectability by thermal conductivity methods. Ammonia, for example, was not acceptable because the thermal conductivity of ammonia-air mixtures is not sensitive to the changes in ammonia concentration (65). As a compromise, carbon dioxide was selected for use as the solute gas in this investigation. In addition to possessing very satisfactory thermal conductivity properties, the CO_2-air mixture has a linear equilibrium relationship with water and many mass transfer data were available for the system. A disadvantage of carbon dioxide was its relative insolubility, necessitating large L/G ratios in order to obtain significant absorption rates.

VI. THEORETICAL MODELS

The mathematical models used in this work to calculate the theoretical responses (amplitude ratios and phase shifts) of the absorption process were based on application of several simplifying assumptions used in steady-state absorption theory. The distinction between these models concerns the means by which the axial dispersion or mixing of mass in the column packing can be analytically described. Specifically, it is assumed, in the first model, that the liquid and gas

molar flow rates are constant with radial position or that these flows experience no radial velocity variation--the so-called "slug" or "piston flow" assumption. Actually, though, the "slug flow" assumption is known to be incorrect (17, 96) and the combined action of the radial velocity gradients and the turbulence from wakes around the packing pieces causes mixing or dispersion of mass in the column. The second and third theoretical models are attempts to develop hypothetical conditions which will adequately describe this dispersion phenomenon.

Although these various models are distinctly different in form, they have a number of common concepts. Since it is generally agreed that the resistance to absorption of carbon dioxide by water is predominantly in the liquid phase (99, 102), the "overall" driving force concept was used for the mass transfer rate equation in all the models. In addition, this mass transfer rate equation is written in the classic form:

$$N = k_L(x^*-x)$$

since, as pointed out by Danckwerts (29), all three of the currently postulated physical absorption mechanisms (the "film," "penetration," and "surface renewal" theories) accept this form and differ only in the physical significance attributed to the coefficient, k_L.

The assumptions that the liquid and gas molar flow rates are constant with axial position in the column--the so-called "dilute solution" assumption--and that the solvent-solute equilibrium data obey Henry's law--the so-called "linear equilibrium line" assumption--are used in all the mathematical models of this work.

The additional details of these models and their mathematical development are presented in Chapter II.

In the remaining body of this presentation the experimental equipment and procedure will be described, followed by a discussion of the experimental and theoretical results and the conclusions which they suggest.

CHAPTER II

MATHEMATICAL DEVELOPMENT OF THE THEORETICAL FREQUENCY RESPONSE EQUATIONS

The theoretical response developments presented in this chapter are divided into separate analyses according to the type of flow model assumed. The three models considered in this work are: (1) "slug flow" model, (2) "mixing cell" model, and (3) "axial diffusion" model. In general the "slug flow" model assumes no axial mixing or dispersion by presuming that all axial velocities are independent of radial position. The "mixing cell" and "axial diffusion" models, on the other hand, attempt to account for the axial mixing phenomenon by assuming the system acts as a series of non-interacting perfect mixers and that axial mixing is described by a Fickian diffusion term, respectively.

Two types of processes are considered for each flow model: (1) two phase countercurrent flow with absorption, and (2) single phase flow without absorption.

I. SLUG FLOW MODELS

Two Phase Countercurrent Flow with Absorption

Consider the countercurrent motion of a gas and a liquid phase over some continuous vertical contacting medium.

Figure 1, below, shows the general arrangement of the system and introduces the nomenclature.

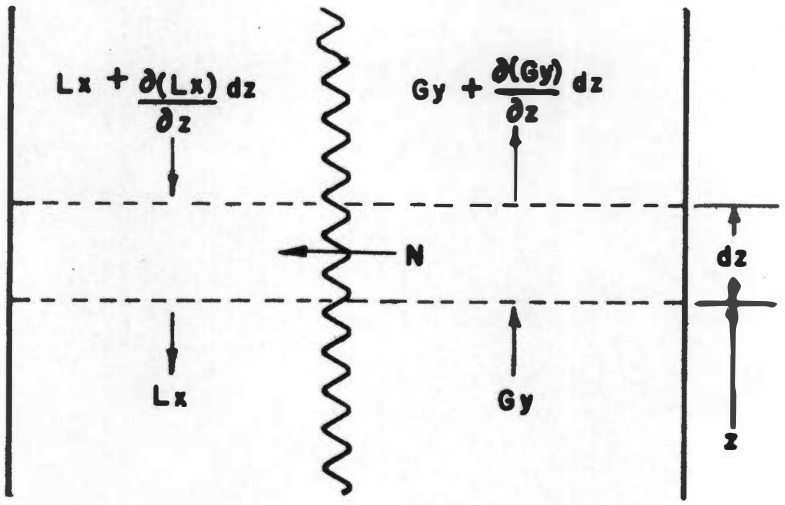


Figure 1. Packing Increment

where

L = molar mass velocity of liquid phase, lb mole/hr-ft^2

G = " " " " gas " "

x = mole fraction solute in liquid phase

y = " " " " gas "

N = mass transfer rate, lb moles/hr-ft^2 transfer area

z = length dimension, ft

Conservation of the solute component in the liquid phase for the incremental section dz gives the following:

input - output = accumulation

or

$$(Lx + \frac{\partial(Lx)}{\partial z}\, dz) + Na\, dz - Lx = \frac{\partial(h_L\, x\, dz)}{\partial t}$$

and assuming L is constant in z and h_L constant in time,

$$L \frac{\partial x}{\partial z} + Na = h_L \frac{\partial x}{\partial t} \qquad (1)$$

where

h_L = total liquid holdup, $\frac{\text{lb moles}}{\text{ft}^3}$

a = mass transfer area, $\frac{\text{ft}^2}{\text{ft}^3 \text{ packing}}$

Similarly, conservation of the solute component in the gas phase for the increment dz, assuming that the gas molar velocity is constant throughout the column and that the holdup is constant in time, gives

$$G \frac{\partial Y}{\partial z} + Na = - h_G \frac{\partial Y}{\partial t} \qquad (2)$$

This analysis will be restricted to systems where physical absorption is controlled by the liquid side resistance or, as discussed in the introduction, where the rate equation can be written

$$Na = k_L\, a\, (x^* - x) \qquad (3)$$

where

k_L = mass transfer coefficient, $\frac{\text{lb moles}}{\text{hr-ft}^2\text{-mole fraction}}$

x^* = that liquid phase solute composition which would be in equilibrium with the gas phase composition, y

It will be presumed that the gas-liquid interface is at equilibrium at all times and that this equilibrium can be described quantitatively by the Henry's Law expression,

$$y = mx^* \tag{4}$$

where m is a constant.

Substitution of Equations 3 and 4 into Equations 1 and 2 yields the following:

$$L \frac{\partial x}{\partial z} + k_L a (y/m-x) = h_L \frac{\partial x}{\partial t} \tag{5}$$

$$G \frac{\partial Y}{\partial z} + k_L a (y/m-x) = h_G \frac{\partial Y}{\partial t} \tag{6}$$

Consider the absorber in steady state operation at t=0 and then consider the variation of compositions from this initial condition at any time, t. Thus it shall be understood that the values of the dependent variables of Equations 5 and 6 are deviations from the absorber steady state conditions and are zero at t=0.

With this in mind one can now take the Laplace

transformation of Equations 5 and 6 where the transformation is defined by:

$$\mathcal{L} f(t) = \bar{f}(s) = \int_0^\infty f(t)e^{-st}\, dt \tag{7}$$

Here it is assumed that x and y and their time derivatives are sectionally continuous and of exponential order (22). Thus

$$L \frac{d\bar{x}}{dz} + k_L a (\bar{y}/m - \bar{x}) = h_L s \bar{x} \tag{8}$$

and

$$G \frac{d\bar{y}}{dz} + k_L a (\bar{y}/m - \bar{x}) = h_G s \bar{y} \tag{9}$$

Upon rearranging, these become

$$\frac{d\bar{x}}{dz} - \alpha\bar{x} = -\beta\bar{y} \tag{10}$$

and

$$\frac{d\bar{y}}{dz} + \gamma\bar{y} = \delta\bar{x} \tag{11}$$

where

$$\alpha = \frac{k_L a - h_L s}{L} \qquad \beta = \frac{k_L a}{mL}$$
$$\gamma = \frac{k_L a/m + h_G s}{G} \qquad \delta = \frac{k_L a}{G} \tag{12}$$

Differentiation of Equation 11 with respect to z gives

$$\frac{d^2\bar{y}}{dz^2} + \gamma\frac{d\bar{y}}{dz} = \delta\frac{d\bar{x}}{dz}$$

or

$$\frac{d\bar{x}}{dz} = \frac{1}{\delta}\frac{d^2\bar{y}}{dz^2} + \frac{\gamma}{\delta}\frac{d\bar{y}}{dz} \qquad (13)$$

Substitution of Equations 11 and 13 into Equation 10 yields

$$\frac{1}{\delta}\frac{d^2\bar{y}}{dz^2} + \frac{\gamma}{\delta}\frac{d\bar{y}}{dz} - \frac{\alpha}{\delta}\frac{d\bar{y}}{dz} - \frac{\alpha\gamma}{\delta}\bar{y} = -\beta\bar{y}$$

or

$$\frac{d^2\bar{y}}{dz^2} + (\gamma-\alpha)\frac{d\bar{y}}{dz} + (\beta\delta-\alpha\gamma)\bar{y} = 0 \qquad (14)$$

This ordinary second order differential equation in the transformed gas phase composition, $\bar{y}$, can be solved by standard methods to yield

$$\bar{y} = C_1 e^{p_1 z} + C_2 e^{p_2 z} \qquad (15)$$

where C_1 and C_2 are constants and $p_{1,2}$ are roots of the characteristic equation and are given by

$$p_{1,2} = \frac{(\alpha-\gamma) \pm \sqrt{(\gamma-\alpha)^2 - 4(\beta\delta-\alpha\gamma)}}{2} \qquad (16)$$

The constants C_1 and C_2 of Equation 15 are determined from the boundary conditions, which are:

$$\text{at } z=0 \qquad \bar{y} = \bar{y}_o \tag{17a}$$

and

$$\text{at } z=\infty \qquad \bar{y} = 0 \tag{17b}$$

The subject of boundary condition for this type of flow system has received great attention in the literature (28, 120, 77, 33, 7). Equations 17 were chosen as representing the conditions with the greatest physical significance for this problem.

It is shown in Appendix A that the infinity condition of Equation 17b requires that the constant associated with the positive root of characteristic equation be zero. Thus, from Appendix A, $C_1=0$, since the positive root is

$$p_1 = \frac{(\alpha-\gamma) + \sqrt{(\gamma-\alpha)^2 - 4(\beta\delta-\alpha\gamma)}}{2}$$

With condition 17a requiring that $C_2=\bar{y}_o$, the general solution of Equation 14 becomes

$$\bar{y} = \bar{y}_o \exp\left\{\left[\frac{(\alpha-\gamma) - \sqrt{(\gamma-\alpha)^2 - 4(\beta\delta-\alpha\gamma)}}{2}\right] z\right\} \tag{18}$$

Thus, at the outlet of the contacting medium where $z=Z$, the transformed gas phase composition is

$$\bar{y}_Z = \bar{y}_o \exp\left\{\left[\frac{(\alpha-\gamma) - \sqrt{(\gamma-\alpha)^2 - 4(\beta\delta-\alpha\gamma)}}{2}\right] Z\right\} \tag{19}$$

A term used frequently in automatic control and servomechanism theory is "transfer function."* The transfer function of a system is defined as the ratio of the transformed output signal from the system to the transformed input signal to that system (97). Thus, from Equation 19, the transfer function for the continuous gas absorber under consideration here is

$$\frac{\bar{y}_Z}{\bar{y}_o} = \exp\left\{\left[\frac{(\alpha-\gamma) - \sqrt{(\gamma-\alpha)^2 - 4(\beta\delta-\alpha\gamma)}}{2}\right] Z\right\} \qquad (20)$$

By the substitutions of Appendix A, Equation 20 may be reduced to the following form:

$$\frac{\bar{y}_Z}{\bar{y}_o} = \exp\left\{\left[(d+cs) - \sqrt{(c^2+a)s^2 + (b+2dc)s + d^2}\right]\frac{Z}{2GL}\right\} \qquad (21)$$

where

$$\begin{aligned} a &= 4GL\, h_L\, h_G \\ b &= 4GL\,(h_G + \tfrac{h_L}{m})\, k_L\, a \\ c &= Gh_L - Lh_G \\ d &= (G - \tfrac{L}{m})\, k_L\, a \\ s &= \text{Laplace transform parameter of Equation 7} \end{aligned} \qquad (22)$$

---

*The term "transfer function" has widespread use in this country while abroad it is frequently called the "harmonic response function" or "complex transference."

If, at time zero, the input gas phase composition is forced to vary harmonically in time the output gas phase composition will also, after sufficient time, form a periodic steady state composition wave of the same frequency. For any linear system, such as the one discussed here, it can be shown that the ratio of steady state output wave amplitude to the input wave amplitude--the so-called "amplitude ratio"*-- and the phase shift between the two waves can be determined directly from the transfer function of the system by substitution of $i\omega$, where i is the imaginary unit ($\sqrt{-1}$) and ω is the circular frequency of the input wave, for the Laplace transform parameter, s. The modulus of the complex number resulting from this substitution can be shown to be equal to the amplitude ratio while the argument gives the phase shift (98, 75).

Thus, the theoretical dynamic response of the continuous gas absorption process under consideration can be obtained directly from the transfer function of Equation 21 when the inlet gas phase composition is given by

$$y(0)=A(0) \sin \omega t$$

noting, again, that y represents the deviation from the steady state gas phase compositions. Thus, substituting

---

*Also frequently termed "magnitude ratio," "attenuation," or "gain."

$s=i\omega$ in Equation 21 yields:

$$\left[\frac{\bar{y}_Z}{\bar{y}_o}\right]_{i\omega} = \exp\left\{\frac{Z}{2GL}\left[(d+c\,\omega i) - \sqrt{\left[a^2 - (c^2+a)\omega^2\right] + (b+2dc)\omega i}\right]\right\} \tag{23}$$

The extraction of the modulus and argument of the complex number of Equation 23 is described in detail in Appendix B. There the amplitude ratio and phase shift are found to be, respectively:

$$\frac{A(Z)}{A(0)} = \exp\left\{\frac{Z}{2GL}\left[(G-\frac{L}{m})\,k_L\,a - (\frac{r+n}{2})^{\frac{1}{2}}\right]\right\} \tag{24}$$

$$\phi = \frac{Z}{2GL}\left[(Gh_L - Lh_G)\omega - (\frac{r-n}{2})^{\frac{1}{2}}\right] \tag{25}$$

where

$$n = (G-\frac{L}{m})^2\,(k_L\,a)^2 - (Gh_L+Lh_G)^2\omega^2$$

$$r = \sqrt{\left[(G-\frac{L}{m})^2\,(k_L a)^2 - (Gh_L+Lh_G)^2\omega^2\right]^2 + \left[2k_L a(G+\frac{L}{m})(Gh_L+Lh_G)\omega\right]^2} \tag{26}$$

It is of interest to investigate the behavior of the amplitude ratio and phase shift in the limits of the frequency, ω .

a) Frequency, ω , approaches zero

Equation 26 shows that

$$\lim_{\omega \to 0} n = (G - \frac{L}{m})^2 (k_L a)^2$$

and

$$\lim_{\omega \to 0} r = (G - \frac{L}{m})^2 (k_L a)^2$$

Thus, from

Equation 24, $\lim_{\omega \to 0} (\frac{A(Z)}{A(0)}) = 1.0$

and from (27)

Equation 25, $\lim_{\omega \to 0} \phi = 0$

b) Frequency, ω, approaches ∞

From Equations 26 and 22, or B5 of Appendix B,

$$r+n = \sqrt{\left[d^2-(c^2+a)\omega^2\right]^2 + \left[(b+2dc)\omega\right]^2} + (d^2-(c^2+a)\omega^2)$$

or

$$r+n = \sqrt{(c^2+a)^2\omega^4+\left[(b+2dc)^2-2d^2(c^2+a)\right]\omega^2+d^4} + (d^2-(c^2+a)\omega^2)$$

Multiplying and dividing by ω^2 :

$$r+n = \omega^2\left[\sqrt{(c^2+a^2)^2+\frac{(b+2dc)^2+2d^2(c^2+a)}{\omega^2}+\frac{d^4}{\omega^4}}+\frac{d^2}{\omega^2}-(c^2+a)\right] \quad (28)$$

From the above equation it can be seen that the limit of r+n as $\omega \to \infty$ approaches the indeterminate form $(\infty)(0)$. An

alternate form, subject to the application of L'Hospital Rule, can be obtained by rearrangement. Thus,

$$r+n = \frac{f(\omega)}{g(\omega)}$$

where

$$\lim_{\omega \to 0} f(\omega) = 0$$

and

$$\lim_{\omega \to 0} g(\omega) = 0$$

since

$$f(\omega) = \sqrt{(c^2+a^2)^2 + \frac{(b+2dc)^2+2d^2(c^2+a)}{\omega^2} + \frac{d^4}{\omega^4} + \frac{d^2}{\omega^2}} - (c^2+a) \tag{29}$$

and

$$g(\omega) = \frac{1}{\omega^2}$$

By L'Hospital Rule,

$$\lim_{\omega \to \infty} (r+n) = \lim_{\omega \to \infty} \frac{df/d\omega}{dg/d\omega} \tag{30}$$

From Equation 29:

$$\frac{df/d\omega}{dg/d\omega} = \left[\frac{(b+2dc)^2-2d^2(c^2+a)}{2} + \frac{d^4}{\omega^2}\right]\left[(c^2+a)^2 + \frac{(b+2dc)^2-2d^2(c^2+a)}{\omega^2} + \frac{d^4}{\omega^4}\right]^{-\frac{1}{2}} + d^2$$

Thus, from Equation 30 and the above result,

$$\lim_{\omega \to \infty} (r+n) = \frac{(b+2dc)^2}{2(c^2+a)}$$

and by Equation 22,

$$\lim \left(\frac{r+n}{2}\right)^{\frac{1}{2}} = \frac{b+2dc}{2\sqrt{(c^2+a)}} = k_L a\left(G+\frac{L}{m}\right) \qquad (31)$$

Therefore, by Equation 24, it is found that the value of the amplitude ratio approaches a finite limit as $\omega \to \infty$. This limit is given by

$$\lim_{\omega \to \infty} \left(\frac{A(Z)}{A(0)}\right) = e^{-\frac{Z\, k_L\, a}{Gm}} \qquad (32)$$

From Equation 28 it can be seen that r-n is unbounded for increasing ω and therefore, by Equation 25, the phase shift, ϕ, is also unbounded. That is,

$$\lim_{\omega \to \infty} \phi = \infty \qquad (33)$$

Since, as has been pointed out in the above discussion, the amplitude ratio approaches, asymptotically, finite limits as ω approaches both zero and infinity the plot of amplitude ratio versus frequency, ω , must have an inflection point. From the trigonometric forms of Equation A7 in Appendix A, it can be shown that the frequency at which this inflection occurs is given by

$$\omega_i = \frac{d}{\sqrt{c^2+a}} = \frac{(k_L a)(G-\frac{L}{m})}{(Gh_L + Lh_G)} \tag{34}$$

For computational purposes it is convenient to know the amplitude ratio and phase shift at the inflection frequency, ω_i. Substitution of Equation 34 into Equations 24 and 25 and subsequent reduction gives, respectively:

$$\left[\frac{A(Z)}{A(0)}\right]_i = \exp\left\{\frac{Z(k_L a)}{2GL}\left[(G-\frac{L}{m}) - (G^2 - \frac{L^2}{m^2})^{\frac{1}{2}}\right]\right\} \tag{35}$$

and

$$\phi_i = \frac{Z(k_L a)}{2GL}\left[\left(\frac{Gh_L - Lh_G}{Gh_L + Lh_G}\right)(G-\frac{L}{m}) - (G^2 - \frac{L^2}{m^2})^{\frac{1}{2}}\right] \tag{36}$$

Single Phase Flow without Absorption

The development of the response equations for single phase flow without absorption is similar to that of the two phase absorption system. If the single flow involved is considered to be the gas phase and if no mass transfer occurs, Equation 2 reduces to:

$$G\frac{\partial Y}{\partial z} = -h_G\frac{\partial Y}{\partial t} \tag{37}$$

Proceeding again with the understanding that the dependent variable, y, is only the deviation from the steady state gas stream concentration and has value zero at time t=0,

the Laplace transform of Equation 37 yields:

$$G\frac{d\bar{y}}{dz} + h_G s\bar{y} = 0$$

the solution of this first order differential equation is:

$$\bar{y} = C_1 e^{-\frac{h_G s}{G} z} \tag{38}$$

With the boundary condition $\bar{y}=\bar{y}_o$ at $z=0$, $C_1=\bar{y}_o$, and

$$\bar{y} = \bar{y}_o e^{-\frac{h_G s}{G} z} \tag{39}$$

Thus, by the definition given in the previous section, the transfer function for this system becomes:

$$\frac{\bar{y}_Z}{\bar{y}_o} = e^{-\frac{h_G s}{G} Z} \tag{40}$$

Again, substituting $s=i\omega$ yields a complex number of the form

$$\left[\frac{\bar{y}_Z}{\bar{y}_o}\right]_{i\omega} = e^{-\frac{h_G Z}{G} \omega i} \tag{41}$$

From the discussion of Appendix B, the phase shift and amplitude ratio for this system can be obtained from Equation 41 by direct comparison with Equation B4. Thus, the amplitude

ratio is identically unity for all frequency, ω, and the phase shift is given by:

$$\phi = - \frac{h_G Z}{G} \omega \qquad (42)$$

In the limits as frequency, ω, approaches zero and infinity the phase shift approaches these limits also.

II. CELL MIXING MODELS

Two Phase Countercurrent Flow with Absorption

In this model the dynamics of the interphase mass transfer and mixing process are described by the behavior of a series of non-interacting* mixing cells, a typical example of which is shown below:

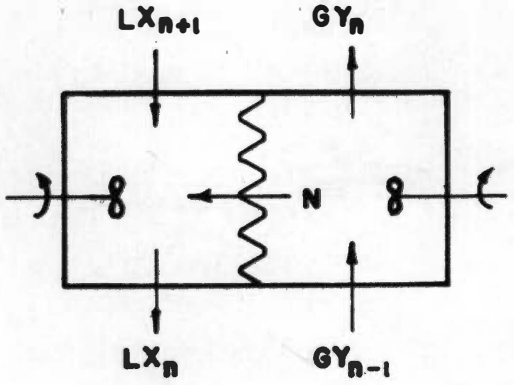


Figure 2. Mixing Cell Increment

*By non-interacting is meant that no dynamic element of one mixing cell is also an element of any other mixing cell.

This absorption mixing-cell concept is an extension of a similar model for axial mixing of a single phase nonabsorbing system first suggested by Kramers and Alberda (59). The gas and liquid components of each mixing cell are assumed independently well mixed at all times--that is, the gas and liquid compositions of the nth cell, y_n and x_n respectively, are constant throughout the cell and equal to the composition of the fluid streams leaving the cell. From these conditions the following analysis is developed, the nomenclature of which, except as noted, is identical to that used in Section I of this chapter.

The conservation of the liquid phase component yields the equation,

$$x_{n+1}L - x_nL + NaH = Hh_L \frac{dx_n}{dt} \tag{43}$$

A similar equation for the gas phase gives,

$$y_{n-1}G - y_nG - NaH = Hh_G \frac{dy_n}{dt} \tag{44}$$

where

H = packing height equivalent to a mixing cell

$H = \frac{Z}{N}$ when N = number of mixing cells in packing
Z = packing height

These equations assume; (1) that concentrations are dilute enough that mass transfer occurring in the cell does not

significantly alter the molar flows of the phases in and out of the cell, (2) that the packing height equivalent to a mixing cell is the same for both phases, and (3) that the liquid and gas holdups are independent of time.

As in the previous section, the mass transfer rate equation will be written for a physical absorption process where the liquid film controls and a linear equilibrium relationship exists. Thus, by Equations 3 and 4,

$$Na = k_L a(y_n/m - x_n) \tag{45}$$

Substitution of Equation 45 into 43 and 44 with rearrangement gives,

$$x_{n+1} - (1+\frac{Hk_La}{L})x_n + \frac{Hk_La}{Lm} y_n = \tau_L \frac{dx_n}{dt} \tag{46a}$$

and

$$y_{n-1} - (1+\frac{Hk_La}{Gm})y_n + \frac{Hk_La}{G} x_n = \tau_G \frac{dy_n}{dt} \tag{46b}$$

where

$$\tau_L = \frac{Hh_L}{L} \quad \text{liquid cell transit time} \tag{47a}$$

$$\tau_G = \frac{Hh_G}{G} \quad \text{gas cell transit time} \tag{47b}$$

These equations are now subjected to Laplace transformation,

where, as in the previous section, the dependent variables are understood to be deviations from the steady state solution and have zero value at time equal zero. Thus Equations 46a and 46b become,

$$\bar{x}_{n+1} - (1+\frac{Hk_La}{L})\bar{x}_n + \frac{Hk_La}{Lm}\bar{y}_n = \tau_L s\bar{x}_n$$

$$\bar{y}_{n-1} - (1+\frac{Hk_La}{Gm})\bar{y}_n + \frac{Hk_La}{G}\bar{x}_n = \tau_G s\bar{y}_n$$

These can be rearranged to the form:

$$\bar{x}_{n+1} - T_L\,\bar{x}_n + f\,\bar{y}_n = 0 \qquad (48)$$

and

$$\bar{y}_{n-1} - T_G\,\bar{y}_n + g\,\bar{x}_n = 0 \qquad (49)$$

where

$$T_L = \tau_L s + \frac{Hk_La}{L} + 1 \qquad (50a)$$

$$T_G = \tau_G s + \frac{Hk_La}{Gm} + 1 \qquad (50b)$$

$$f = Hk_La/Lm \qquad (51a)$$

$$g = Hk_La/G \qquad (51b)$$

Equations 48 and 49 are a set of simultaneous linear difference equations which are solved as follows:

The variable $\bar{x}_n$ is eliminated from 48 and 49, resulting in:

$$(T_G T_L - fg)\bar{y}_n = T_L\,\bar{y}_{n-1} + g\,\bar{x}_{n+1} \qquad (52)$$

Since Equations 48 and 49 are derived for the arbitrary nth mixing cell and are thus valid for other cells, Equation 49 can be written for the (n+1) mixing cell as:

$$\bar{y}_n - T_G\,\bar{y}_{n+1} + g\,\bar{x}_{n+1} = 0 \qquad (53)$$

The variable $\bar{x}_{n+1}$ can now be eliminated from Equations 52 and 53. Thus,

$$T_G\,\bar{y}_{n+1} - (T_L T_G - fg + 1)\bar{y}_n + T_L\,\bar{y}_{n-1} = 0$$

or

$$T_G\,\bar{y}_{n+2} - (T_L T_G - fg + 1)\bar{y}_{n+1} + T_L\,\bar{y}_n = 0 \qquad (54)$$

The above second order linear difference equation in the transformed gas phase composition, $\bar{y}_n$, can be solved by assuming a solution of the form,

$$\bar{y}_n = C\,A^n \qquad (55)$$

where C and A are constants. Substituting Equation 55 into 54 gives

$$T_G\,A^2 - (T_L T_G - fg + 1)A + T_L = 0$$

The solution of this quadratic equation in A is:

$$A_{1,2} = \frac{(T_L T_G - fg + 1) \pm \sqrt{(T_L T_G - fg + 1)^2 - 4\, T_L T_G}}{2\, T_G} \qquad (56)$$

and the general solution of Equation 54 becomes,

$$\bar{y}_n = C_1 A_1^{\,n} + C_2 A_2^{\,n} \qquad (57)$$

where C_1 and C_2 are arbitrary constants to be evaluated from the boundary conditions of the system and A_1 and A_2 are given by Equation 56.

The boundary conditions for this system are as follows: The gas phase composition of the flow to the first mixing cell is y_o. Thus,

$$y_n = y_o \quad \text{at} \quad n=o \qquad (58)$$

Also, the liquid phase composition of the flow to the last, or Nth, mixing cell is constant in time. Therefore, since the variable x_n in the above development represents the deviation of the liquid phase composition from the steady state, this requires that

$$x_{N+1} = 0 \quad \text{at} \quad n=N \qquad (59)$$

Boundary condition 58 substituted in Equation 57 gives

$$\bar{y}_o = C_1 + C_2 \qquad (60)$$

or

$$C_1 = \bar{y}_o - C_2$$

and by 57

$$\bar{y}_n = \bar{y}_o A_1^n + C_2(A_2^n - A_1^n) \tag{61}$$

If the transformed gas phase composition, $\bar{y}_n$, as given by Equation 61, is substituted in its appropriate form for both $\bar{y}_n$ and $\bar{y}_{n-1}$ in Equation 52, an expression is established which can be solved directly for C_2. This gives

$$C_2 = \frac{\left[T_L A_1^{n-1} - (T_L T_G - fg) A_1^n\right] \bar{y}_o + g\,\bar{x}_{n+1}}{(T_L T_G - fg)(A_2^n - A_1^n) - T_L(A_2^{n-1} - A_1^{n-1})} \tag{62}$$

Substitution of this value of the constant, C_2, back into Equation 61--with substantial algebraic reduction--yields:

$$\bar{y}_n = \frac{T_L(A_2 - A_1)(A_1 A_2)^{n-1}\,\bar{y}_o}{(T_L T_G - fg)(A_2^n - A_1^n) - T_L(A_2^{n-1} - A_1^{n-1})} + \frac{g(A_2^n - A_1^n)\,\bar{x}_{n+1}}{(T_L T_G - fg)(A_2^n - A_1^n) - T_L(A_2^{n-1} - A_1^{n-1})} \tag{63}$$

This equation represents the final solution of the set of simultaneous difference equations, 48 and 49. It expresses the transformed gas phase composition, $\bar{y}_n$, of the gas

stream leaving the nth mixing cell in terms of the liquid phase composition, $\bar{x}_{n+1}$, entering the nth cell and the gas phase composition, $\bar{y}_o$, of the gas stream entering the first mixing cell. Writing this equation for the last mixing cell, N, yields

$$\bar{y}_N = \frac{T_L(A_2-A_1)(A_1A_2)^{N-1}\bar{y}_o}{(T_LT_G-fg)(A_2^N-A_1^N)-T_L(A_2^{N-1}-A_1^{N-1})} + \frac{g(A_2^N-A_1^N)\,\bar{x}_{N+1}}{(T_LT_G-fg)(A_2^N-A_1^N)-T_L(A_2^{N-1}-A_1^{N-1})} \tag{64}$$

Since boundary condition 59 states that

$$x_{N+1} = 0$$

then

$$\bar{x}_{N+1} = 0$$

and Equation 64 becomes

$$\frac{\bar{y}_N}{\bar{y}_o} = \frac{T_L(A_2-A_1)(A_1A_2)^{N-1}}{(T_LT_G-fg)(A_2^N-A_1^N)-T_LT_G(A_2^{N-1}-A_1^{N-1})} \tag{65}$$

where $A_{1,2}$ is given by Equation 56.

This relation is the gas phase transfer function for a series of N mixing cells. As discussed in the previous section,

the frequency response, i.e., amplitude ratio and phase shift, of any linear system can be obtained from the complex number which results by substitution of $i\omega$ for the Laplace transform parameter, s, in the transfer function. By Equation 56,

$$A_1 A_2 = \frac{T_L}{T_G}$$

and

$$A_2 - A_1 = \frac{\sqrt{(T_L T_G - fg + 1)^2 - 4T_G T_L}}{T_G}$$

Substitution of these values into Equation 65 and subsequent rearrangement gives the following form:

$$\frac{\overline{y}_n}{\overline{y}_o} = \frac{T_L{}^N \sqrt{(T_L T_G - fg + 1)^2 - 4T_G T_L}}{(T_L T_G - fg)(D_2{}^N - D_1{}^N) - T_L T_G (D_2{}^{N-1} - D_1{}^{N-1})} \tag{66}$$

where

$$D_1 = \frac{(T_G T_L - fg + 1) - \sqrt{(T_G T_L - fg + 1)^2 - 4T_G T_L}}{2}$$

$$D_2 = \frac{(T_G T_L - fg + 1) + \sqrt{(T_G T_L - fg + 1)^2 - 4T_G T_L}}{2} \tag{67}$$

The establishment of the complex number resulting from the substitution of $s=i\omega$ in Equation 50 and then in Equation 66, and the extraction of the amplitude ratio and phase shift from this complex number is a rather involved calculation. A detailed outline of the procedure is presented in Appendix B. For brevity's sake it will simply be said here that the amplitude ratio and phase shift are given by:

$$\frac{A(Z)}{A(0)} = \frac{r_L^N \, r_T}{r_{LG} \, r_N} \tag{B30}$$

and

$$\phi = N\theta_L + \theta_T - \theta_{LG} - \theta_N \tag{B31}$$

where the significance of the variables r and θ are stated in Appendix B.

It can be shown that the amplitude ratio, $\frac{A(Z)}{A(0)}$, approaches zero and phase shift approaches infinity as the frequency, ω, approaches infinity while the phase shift approaches zero and amplitude ratio approaches the steady state value,

$$\lim_{\omega \to 0} \frac{A(Z)}{A(0)} = \frac{\left[\frac{Hk_L a}{L}+1\right]^N \left[\frac{Hk_L a}{L} - \frac{Hk_L a}{Gm}\right]}{\left[\frac{Hk_L a}{L}+1\right]^{N+1} - \left[\frac{Hk_L a}{Gm}+1\right]^{N+1} - \left[\frac{Hk_L a}{L}+1\right]^{N} + \left[\frac{Hk_L a}{Gm}+1\right]^{N}} \tag{68}$$

as the frequency approaches zero.

Single Phase Flow without Absorption

The response equations for this case can be derived from the initial forms of the previous case. Here, since N=0, Equation 44 becomes

$$y_{n-1} - y_n = \tau_G \frac{dy_n}{dt} \tag{69}$$

With the variable y, as before, representing only deviations from the steady state and equal to zero at time zero, the Laplace transformation of Equation 69 gives,

$$\bar{y}_{n-1} - \bar{y}_n = \tau_G \, s \, \bar{y}_n$$

or

$$(\tau_G s+1)\, \bar{y}_{n+1} - \bar{y}_n = 0 \tag{70}$$

Assume the solution of this simple difference equation has the form $\bar{y}_n = CA^n$, where, as before, C and A are constants. Substitution of this solution in Equation 70 leads to

$$A = \frac{1}{\tau_G s+1}$$

Thus

$$\bar{y}_n = C\left(\frac{1}{\tau_G s+1}\right)^n \tag{71}$$

It is clear, from boundary condition 58, that for n=0

$$\bar{y}_n = \bar{y}_o$$

Thus, from Equation 71,

$$C = y_o$$

and

$$\bar{y}_n = \bar{y}_o \left(\frac{1}{\tau_G s+1}\right)^n$$

Therefore, the transfer function for a series of N mixing cells is simply,

$$\frac{\bar{y}_N}{\bar{y}_o} = \left(\frac{1}{\tau_G s+1}\right)^N \qquad (72)$$

Substitution of $i\omega$ for the transform parameter, s, gives

$$\left[\frac{\bar{y}_N}{\bar{y}_o}\right]_{i\omega} = \left(\frac{1}{\tau_G \omega i+1}\right)^N$$

Since $\tau_G \omega i+1 = r_G e^{\theta_G i}$ (73)

where

$$r_G = \sqrt{\tau_G^2 \omega^2+1} = \sqrt{\left(\frac{Hh_G \omega}{G}\right)^2+1}$$

$$\theta = \tan^{-1} \tau_G \omega = \tan^{-1}\left(\frac{Hh_G}{G}\right) \qquad (74)$$

then

$$\left[\frac{\bar{y}_N}{\bar{y}_o}\right]_{i\omega} = r_G^{-N} e^{-N\theta_G i}$$

It is clear, from the above equations, that the amplitude ratio and phase shift are given by

$$\frac{A(Z)}{A(0)} = r_G^{-N} = \left[\left(\frac{Hh_G\omega}{G}\right)^2 + 1\right]^{-\frac{N}{2}} \tag{75}$$

and

$$\phi = -N\,\theta_G = -N \tan^{-1}\left(\frac{Hh_G\omega}{G}\right) \tag{76}$$

where, as before,

$$H = \frac{Z}{N}$$

It is obvious from Equations 75 and 76 that the amplitude ratio vanishes and the negative phase shift increases without limit as the frequency, ω, approaches infinity while the amplitude ratio approaches unity and the phase shift approaches zero in the limit as ω approaches zero.

III. AXIAL DIFFUSION MODEL

Two Phase Countercurrent Flow with Absorption

This model attempts to describe the axial mixing or

dispersion phenomenon through the use of a Fickian diffusion component in the axial direction. Apparently first suggested by Wicke (121) and more recently revived by Lapidus and Amundson (62) the model has been the subject of a number of experimental studies in recent years. The use of the concept in the case of two phase countercurrent flow with absorption is as follows: Referring to Figure 1, the liquid phase solute imput flux at $z+dz$ is,

$$Lx + \frac{\partial(Lx)}{\partial z}dz - E_L \frac{\partial}{\partial z}\left(h_L x + \frac{\partial(h_L x)}{\partial z}\,dz\right)$$

The solute mass transfer to the element dz is $Nadz$ while the liquid phase solute output flux at z can be expressed as,

$$Lx - E_L \frac{\partial(h_L x)}{\partial z}\,dz$$

Conservation of the liquid phase solute in the packing element dz gives,

$$Lx + \frac{\partial(Lx)}{\partial z}dz - E_L \frac{\partial}{\partial z}\left(h_L x + \frac{\partial(h_L x)}{\partial z}dz\right) + Nadz - \left(Lx - E_L \frac{\partial(h_L x)}{\partial z}\right) = \frac{\partial(h_L\, x\, dz)}{\partial t}$$

or if, as in the previous cases, it is assumed that the molar liquid phase flow, L, is constant in z and that the liquid phase holdup, h_L, is constant in time, t, and z,

$$\frac{L}{\partial z}\frac{\partial x}{} - h_L E_L \frac{\partial^2 x}{\partial z^2} + Na = h_L \frac{\partial x}{\partial t} \qquad (77)$$

The coefficient, E_L, associated with the axial diffusion term of the above equation, has been variously termed: the axial eddy diffusivity, the effective axial diffusivity, the longitudinal diffusivity, the diffusion coefficient, the axial eddy diffusion coefficient, and the dispersion coefficient. This author prefers the name axial eddy diffusivity because it indicates that the term acts quantitatively as a Fickian diffusion component in a specified direction and, at the same time, acts not as a pure molecular diffusion effect.

A similar conservation of the gas phase solute in the increment dz, with the above assumptions, gives the equation:

$$-G\frac{\partial Y}{\partial z} + h_G E_G \frac{\partial^2 Y}{\partial z^2} - Na = h_G \frac{\partial Y}{\partial t} \qquad (78)$$

Here, the axial eddy diffusivity, E_G, refers to the gas phase.

The mass transfer rate equation is, from Equations 3 and 4:

$$Na = k_L a(y/m - x) \qquad (79)$$

Substitution of Equation 79 in Equations 78 and 77 followed

by Laplace transformation, where the dependent variables have the same significance as those of the slug flow model, gives:

$$L\frac{d\bar{x}}{dz} - h_L E_L \frac{d^2\bar{x}}{dz^2} + k_L a(\bar{y}/m - \bar{x}) = h_L s\bar{x}$$

and

$$-G\frac{d\bar{y}}{dz} + h_G E_G \frac{d^2\bar{y}}{dz^2} - k_L a(\bar{y}/m - \bar{x}) = h_G s\bar{y}$$

or, on rearrangement

$$h_L E_L \frac{d^2\bar{x}}{dz^2} - L\frac{d\bar{x}}{dz} - (k_L a + h_L s)\bar{x} = -\frac{k_L a}{m}\bar{y} \qquad (80)$$

and

$$h_G E_G \frac{d^2\bar{y}}{dz^2} - G\frac{d\bar{y}}{dz} - \left(\frac{k_L a}{m} + h_G s\right)\bar{y} = -k_L a\,\bar{x} \qquad (81)$$

When Equation 81 is expressed explicitly in $\bar{x}$, it can be differentiated twice with respect to z to obtain $\frac{d\bar{x}}{dz}$ and $\frac{d^2x}{dz^2}$ as functions of $\bar{y}$. These values, with Equation 81 expressed explicitly in $\bar{x}$, can then be substituted into Equation 80 to obtain a differential equation in $\bar{y}$ only. This, upon rearrangement, becomes:

$$\kappa\frac{d^4\bar{y}}{dz^4} + \zeta\frac{d^3\bar{y}}{dz^3} + \eta\frac{d^2\bar{y}}{dz^2} + \lambda\frac{d\bar{y}}{dz} + \mu\bar{y} = 0 \qquad (82)$$

where

$$\kappa = -\frac{h_G E_G}{k_L a} \tag{83a}$$

$$\delta = \frac{G}{k_L a} + \frac{L E_G h_G}{k_L a E_L h_L} \tag{83b}$$

$$\eta = \left(\frac{1}{m} - \frac{LG}{h_L E_L k_L a} - \frac{h_G E_G}{h_L E_L}\right) + \left(\frac{h_G}{k_L a} - \frac{h_G E_G}{k_L a E_L}\right)s \tag{83c}$$

$$\lambda = \left(\frac{G}{h_L E_L} - \frac{L}{h_L E_L m}\right) + \left(\frac{G}{k_L a E_L} - \frac{h_G L}{h_L k_L a E_L}\right)s \tag{83d}$$

$$\mu = \left(\frac{k_L a + h_L s}{h_L E_L}\right)\left(\frac{k_L a/m + h_G s}{k_L a}\right) - \frac{k_L a}{h_L E_L m} \tag{83e}$$

Since this differential equation in the transformed gas phase composition, $\bar{y}$, is of fourth order no general analytical solution can be obtained and, hence, no general transfer function can be derived for this system. Considering the complexity of the above coefficients, any attempts to determine the frequency response of the system by numerical methods would require use of digital computation techniques (69)(106).

Single Phase Flow without Absorption

Again, when no absoprtion takes place, N=0, and the previously developed equations are considerably reduced. Thus Equation 78 becomes:

$$h_G E_G \frac{\partial^2 Y}{\partial z^2} - G\frac{\partial Y}{\partial z} = h_G \frac{\partial Y}{\partial t} \tag{84}$$

The Laplace transform of this equation gives

$$h_G E_G \frac{d^2\bar{y}}{dz^2} - G \frac{d\bar{y}}{dz} - h_G s \bar{y} = 0 \qquad (85)$$

The general solution of this second order differential equation in $\bar{y}$ is,

$$\bar{y} = C_1 e^{K_1 z} + C_2 e^{K_2 z} \qquad (86)$$

where C_1 and C_2 are arbitrary constants and

$$K_{1,2} = \frac{G \pm \sqrt{G^2 + 4h_G{}^2 s E_G}}{2 h_G E_G} \qquad (87)$$

or

$$K_{1,2} = \left[1 \pm \sqrt{1 + \frac{4 h_G{}^2 E_G s}{G^2}}\right] \frac{G}{2h_G E_G}$$

The form of the solution 86 depends, of course, upon the nature of the system boundary conditions. As discussed in Section I, a number of different approaches have been used for this flow system. This author believes that the following are the most direct and reasonable of the boundary conditions that have been suggested (33, 40, 67).

$$\bar{y} = \bar{y}_o \quad \text{at} \quad z=0 \qquad (88a)$$

$$\bar{y} = 0 \quad \text{at} \quad z= \infty \qquad (88b)$$

Since E_G, h_G, G, and s are positive, the radical of Equation 87 is greater than one and

$$K_1 = \left[1 + \sqrt{1 + \frac{4\, h_G^2\, E_G\, s}{G^2}}\right] \frac{G}{2h_G E_G} > 0$$

while

$$K_2 = \left[1 - \sqrt{1 + \frac{4\, h_G^2\, E_G\, s}{G^2}}\right] \frac{G}{2h_G E_G} < 0$$

Thus, from 88b, $C_1=0$ and Equation 86 becomes

$$\bar{y} = C_2\, e^{K_2 z}$$

With boundary condition 88a, $C_2=\bar{y}_o$ and the above equation can be written

$$\bar{y} = \bar{y}_o\, e^{K_2 z} \tag{89}$$

The transfer function of the system, therefore, becomes,

$$\frac{\bar{y}_Z}{\bar{y}_o} = \exp\left\{\left[1 - \sqrt{1 + \frac{4\, h_G^2\, E_G\, s}{G^2}}\right] \frac{GZ}{2h_G E_G}\right\} \tag{90}$$

As has been discussed in the previous sections, the substitution of $s=i\omega$ in the transfer function of a linear system yields a complex number from which the frequency response (amplitude ratio and phase shift) can be obtained. In addition, the transfer function of this particular system lends

itself to a major simplification which significantly alters the form of Equation 90. The details of this approximation and the subsequent determination of the amplitude ratio and phase shift are given in Appendix B. The results are:

$$\frac{A(Z)}{A(0)} \cong \exp\left(\frac{-ZE_G h_G^3 \omega^2}{G^3}\right) \qquad \text{(B39)}$$

$$\phi \cong \frac{-h_G Z \omega}{G} \qquad \text{(B40)}$$

subject to the restriction that

$$\frac{5\omega^2 E_G^2}{U^4} \ll 1$$

Under the above approximation, it is apparent that amplitude ratio (Equation B39) approaches unity and the phase shift (Equation B40) approaches zero as the frequency, ω, tends to zero, while the amplitude ratio approaches zero and the phase shift approaches infinity as the frequency becomes large.

CHAPTER III

EXPERIMENTAL EQUIPMENT

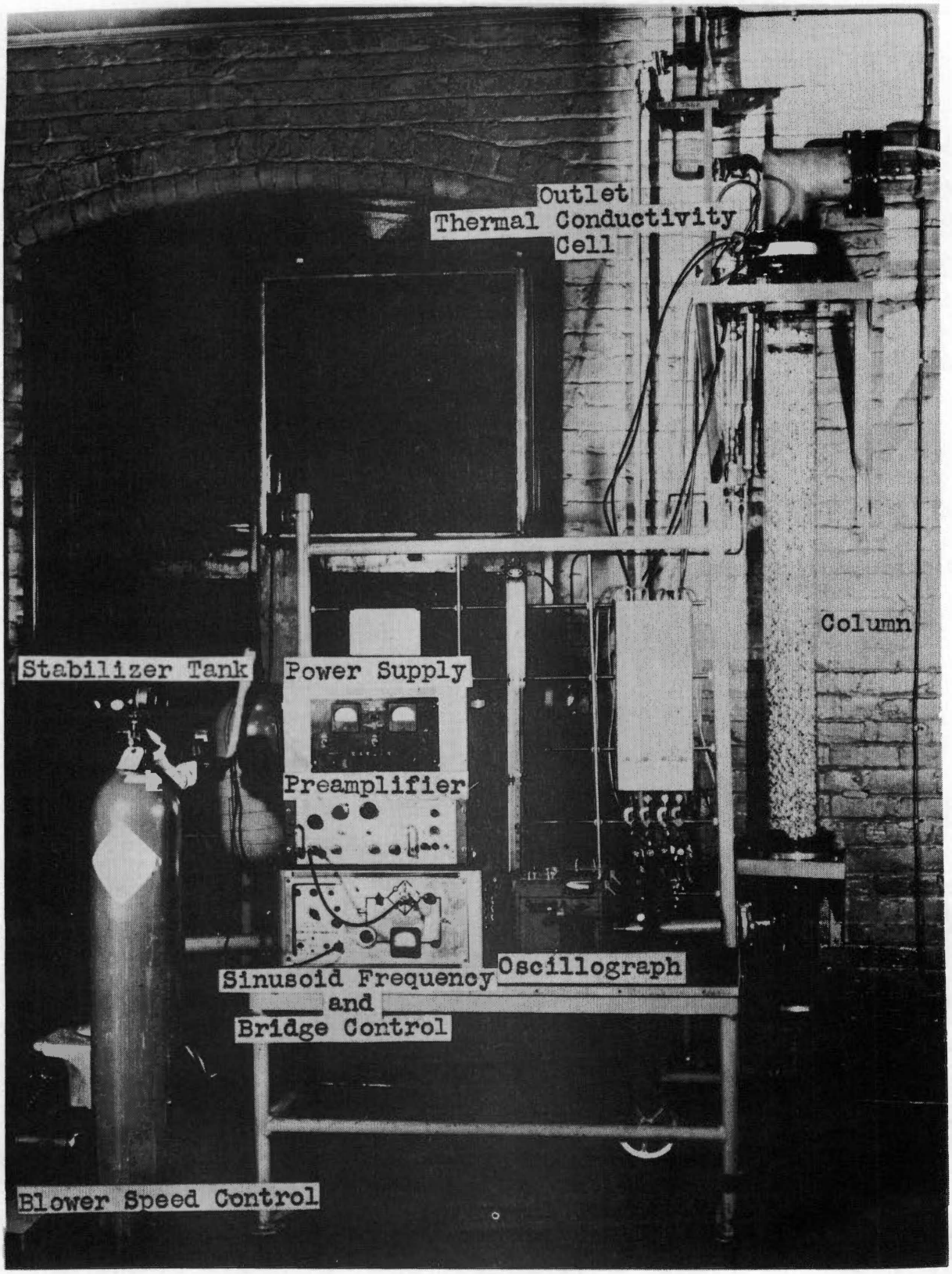
I. THE COLUMN

The dynamic gas absorption process studied in this work was carried out in a 6-inch ID, Pyrex glass pipe 6 feet long, packed with 5/8-inch Raschig rings to a depth of 5.12 feet (61.5 inches). This column and its location with respect to the rest of the experimental equipment is shown in Figure 3. The column was supported on a 3/4-inch thick aluminum plate which, in turn, was bolted to an angle-iron wall frame. The Raschig ring packing was supported by a 1/4-inch stainless steel screen (free area = 87 per cent) which was attached to the aluminum plate by a special ring which allowed removal of the packing without entirely disassembling the column.

The carrier and solute gas mixture passed upward through the packing, countercurrent to water flowing by gravity from the top of the packing. The equipment associated with the flow and measurement of the gas and liquid phases is described in detail in the following sections.

II. GAS PHASE FLOW SYSTEM

Atmospheric air was brought to the system from a point


Outlet
Thermal Conductivity
Cell
Column
Stabilizer Tank
Power Supply
Preamplifier
Sinusoid Frequency
and
Bridge Control
Oscillograph
Blower Speed Control

outside the building through a standard 2-inch wrought iron pipe. Figure 4 is a schematic diagram of the column gas and liquid flow systems. The air passed through a filter before passing to the blower. This filter consisted of a canister packed with a 6-inch by 6-inch roll of fine stainless steel Demister packing and acted as a trap for any solids suspended in the incoming air.

The blower was a Suitorbuilt, Roots type driven through a variable concentric, pulley speed control device by a Delta, 1/2-hp, 110-volt, 60-cycle repulsion-induction motor. The variable speed control adjusted the blower speed from 290 to 1400 rpm which resulted in a flow rate variation of 0.7 to 35 cu ft/min at atmospheric discharge. To obtain flows of less than 0.7 cu ft/min the main 2-inch discharge line valve was closed and air flow by-passed to a vent by throttling through an exit valve. A portion of this by-pass flow was returned to the gas flow system through a Tri-flat Predictability rotameter (G9148 - glass float) which measured its flow rate. For the high flows, where the control was by blower speed adjustment, the flow rates were measured by the pressure drop resulting from flow through a 3/4-inch square-edged orifice plate equipped with radius taps. The orifice pressure drop was measured with a 30-inch water manometer.

The solute carbon dioxide used in the absorption studies was obtained from cylinders of medical grade (U.S.P.)

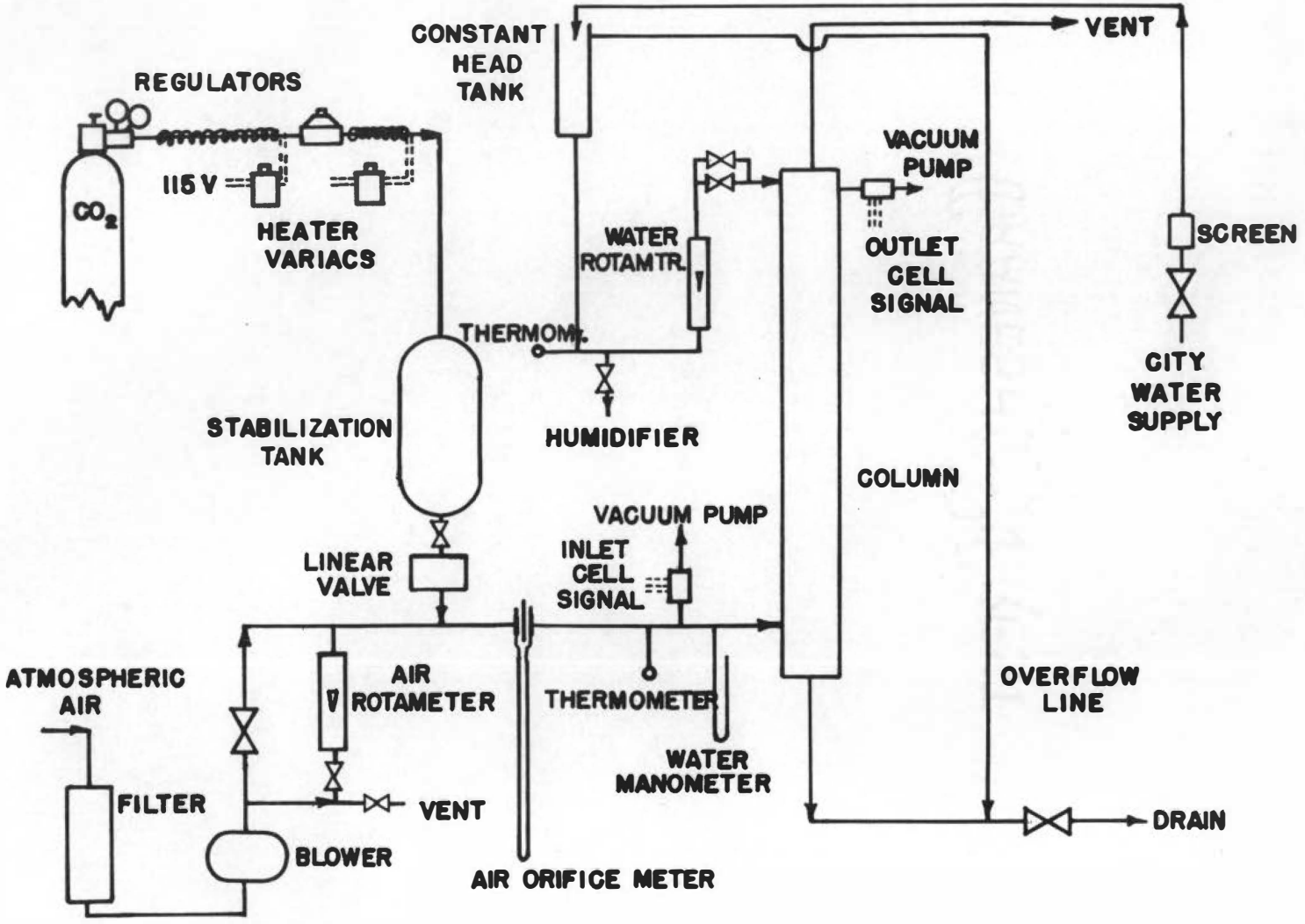


Figure 4. Schematic diagram of column flow systems.

gas. The cylinder pressure (~950 psig) was reduced to 50 psig.by a Matheson "two-stage" pressure regulator placed directly at the main cylinder valve. The line running to a second pressure regulator was heated by a 300-watt, 110-volt Calrod heater and properly insulated with asbestos tape. The second pressure regulator (Matheson low pressure "pancake") was used to obtain a less rapid pressure drop in the flowing CO_2 and also to provide a more accurate and sensitive regulation of the stabilizer tank pressure. The line between the second regulator and stabilizer tank was also heated electrically (one 300-watt Calrod) and insulated.

This two stage pressure reduction with intermediate heating was found necessary to avoid the large Joule-Thompson cooling which accompanied the continuous expansion of carbon dioxide. Before the heaters and second pressure regulator were added to the system, the cooling at the high CO_2 flow rates was great enough that solid CO_2 was formed which then passed through the stabilization tank and caused momentary flow stoppages at the linear valve.

The 2100 cu in. stainless steel stabilization tank between the second pressure regulator and the linear valve of the sinusoid generator was introduced to act as a pressure capacitance element for the CO_2 flow system. A full description of the action of this tank is given in Appendix C.

Figure 5 is a photograph of the sinusoid generator

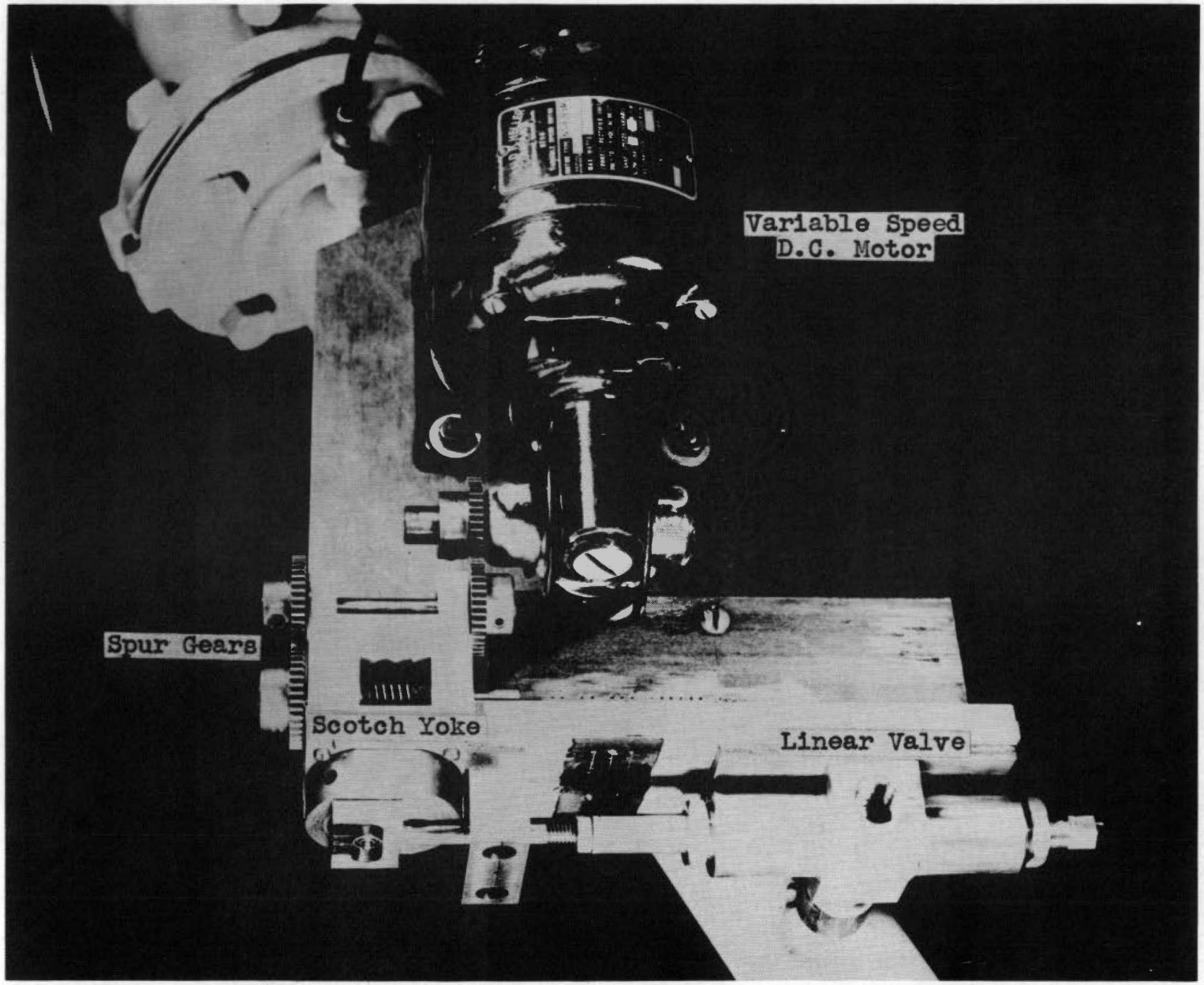


Figure 5. Linear valve and drive arrangement.

with the stabilizer tank removed. In general terms, this device consisted of a specially designed linear valve driven in a sinusoidal manner by a scotch yoke and variable-speed Gerald K. Heller DC motor. The motor speed controls (Gerald K. Heller Company, Model C-25) were placed in the cabinet with the thermal conductivity bridge controls (see Figure 3). The design and construction details of the concentration sinusoid generator are given in Appendix C.

The sinusoidal flow of carbon dioxide from the linear valve of the sinusoid generator mixed with the incoming air stream at a point approximately 12 inches upstream of the orifice plate. About 4-1/2 feet of 2-inch pipe separated the sinusoid generator and the inlet thermal conductivity cell. This length of pipe, which included the orifice plate, acted as a mixing section and served the duel function of creating a uniform gas mixture and filtering some of the distorting higher harmonics from the original concentration sinusoid.

The temperature of the inlet gas mixture was measured with a thermometer inserted in the 2-inch pipe leading to the column at a point just downstream of the inlet thermal conductivity cell sampling probe. The column inlet pressure (essentially the column pressure drop) was also measured at this point with a 12-inch water manometer which was open to the atmosphere.

The carbon dioxide-air mixture entered the column

through the 3-inch side of a 6-inch by 6-inch by 3-inch Pyrex reducer tee and made a 90-degree turn to enter the packing section. At the top of the column the gas phase passed through a 6-inch Pyrex elbow followed by 6-inch by 2-inch Pyrex reducer. A 2-inch galvanized tube was flanged to the glass reducer to take the depleted gas mixture to a vent point outside the building. The air intake and gas mixture exit were approximately 13 feet apart and were positioned so that the prevailing winds prevented recirculation of the carbon dioxide.

III. LIQUID PHASE FLOW SYSTEM

The solvent used in these absorption experiments was tap water taken directly from the building supply. Figure 4 shows the flow diagram for this system. The water entered through a 1/2-inch globe valve. A 3/8-inch copper tube carried the water from the inlet valve to the constant head tank. A strainer was placed in this line to keep solids from entering the system.

The fixed liquid level in the constant head tank was maintained by forcing a continual runoff through a 3/4-inch overflow line located at the top of the tank. The overflow line was connected to the drain. From the bottom of the constant head tank the water flowed by gravity to the column through a 1/2-inch brass pipe. A rotameter was placed in

this line to measure the water flow rate which was controlled by a valve and by-pass arrangement. A 3/4-inch globe valve made the coarse flow adjustment and a 1/8-inch globe valve in the by-pass was used for fine adjustments. The inlet water temperature was measured with a thermometer mounted in the brass pipe just ahead of the rotameter.

The water entered the column directly through a 1-1/2-inch thick aluminum flange plate located between the column Pyrex pipe and the upper, 6-inch Pyrex elbow. From the flange plate the water flowed through a 1/2-inch pipe to 3/8-inch tube, stainless steel elbow and a 3/8-inch inconel tube to the liquid distributor at the top of the packing. To avoid the formation of dissimilar metal corrosion cells, the brass pipe and stainless steel fitting were joined to the aluminum flange plate with 1/2-inch plastic close nipples.

The liquid distributor was in the form of a ring of 3/8-inch inconel tubing which supplied water to nine 1/8-inch inconel distribution tubes mounted 1/2 inch apart in a parallel array across the ring. Figure 6 shows this arrangement and the location of the 39 liquid distribution points. A cut-off wheel was used to cut the holes in the 1/8-inch tubes. The holes located in the center of the ring were made somewhat larger to compensate for the loss in pressure in that region. Before installation in the column the effectiveness of the distributor was checked visually by noting the height

to which the water from the individual holes would rise when the distributor was inverted. Adjustment of the size of individual holes was then made until a satisfactory distribution was obtained.

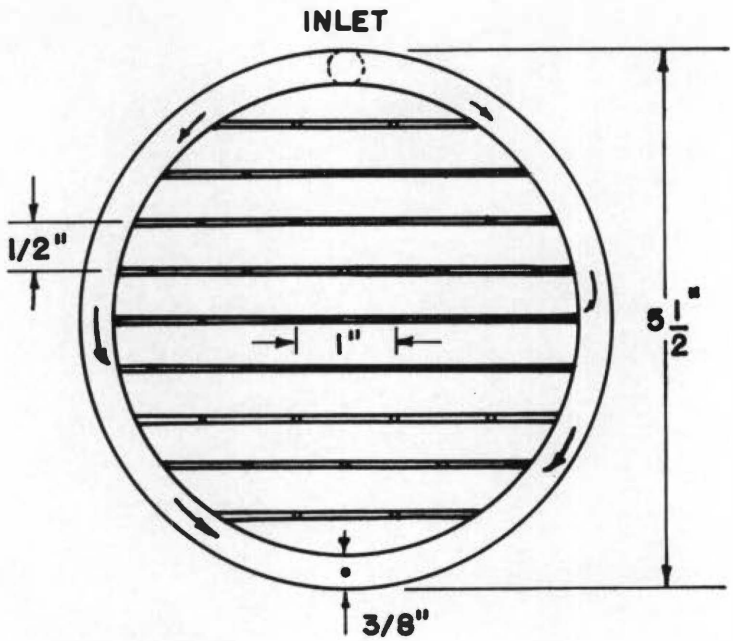


Figure 6. Liquid Distributor Layout

The water drained by gravity over the packing and dropped through the glass tee located at the bottom of the tower. From here the liquid flowed through a 12-inch high water leg which acted as a seal to the incoming gas stream.

The exit liquid from the column was dumped to the sewer through a 1-1/2-inch pipe.

IV. THERMAL CONDUCTIVITY CELLS AND DETECTION EQUIPMENT

The sinusoidal concentration variations of the gas phase were measured by thermal conductivity analysis. Because commercial thermal conductivity analyzers did not have suitable speeds of response, a special high speed cell utilizing thermistors was designed for these experiments. A complete description of the design and calibration of these thermal conductivity cells is given in Appendix D.

The location of the thermal conductivity cells with respect to the column is shown in Figure 3. The inlet cell was mounted on the 2-inch gas-phase inlet pipe immediately before the Pyrex tee at the bottom of the column. The outlet cell was supported by the 3/16-inch sample tube which passed through the aluminum flange plate placed on top of the column. These positions were chosen as close as possible to the inlet and outlet of the packing section in an effort to minimize the sampling time lags. The sampling tubes were positioned so as to place the sampling points at the center of the gas inlet pipe and the column.

The direct current Wheatstone bridge used in conjunction with the thermal conductivity cells for the continuous

gas analysis is shown in Figure 7. The design considerations used to select the thermistors and fixed resistors of this bridge are discussed in Appendix D. Only the thermistor elements (R_s and R_r), which are shown as dashed lines in Figure 7, were actually placed in the cells. The rest of the bridge components were mounted on a control panel and placed in the cabinet seen in Figure 3. A three-pole, three-way, rotary switch simultaneously made or broke the connections at points 1, 2, and 3. The middle position was used as open circuit. This allowed the inlet cell thermistors (R_{si} and R_{ri}) to be switched out of the bridge circuit and the outlet cell thermistor (R_{so} and R_{ro}) to be connected in their place.

The source of DC potential for the bridge was an Oregon Electronic Manufacturing Company, Variable Voltage, Regulated Power Supply (Model A3A) which could supply 200 ma at 0 to 300 volts. The total bridge current, I_t, was adjusted with two potentiometers: a 5000-ohm Ohmite potentiometer for coarse adjustment and a 1000-ohm Micropot for fine control. The total bridge current was calculated from the measured potential drop across the $1\Omega \pm 1$ per cent precision wire wound (P.W.W.) resistor, R_M. The same detecting equipment used to measure the unbalanced bridge signal also measured the potential drop across the current-measuring resistor, R_M. A double pole-double throw toggle switch was used to remove the preamplifier and oscillograph from across

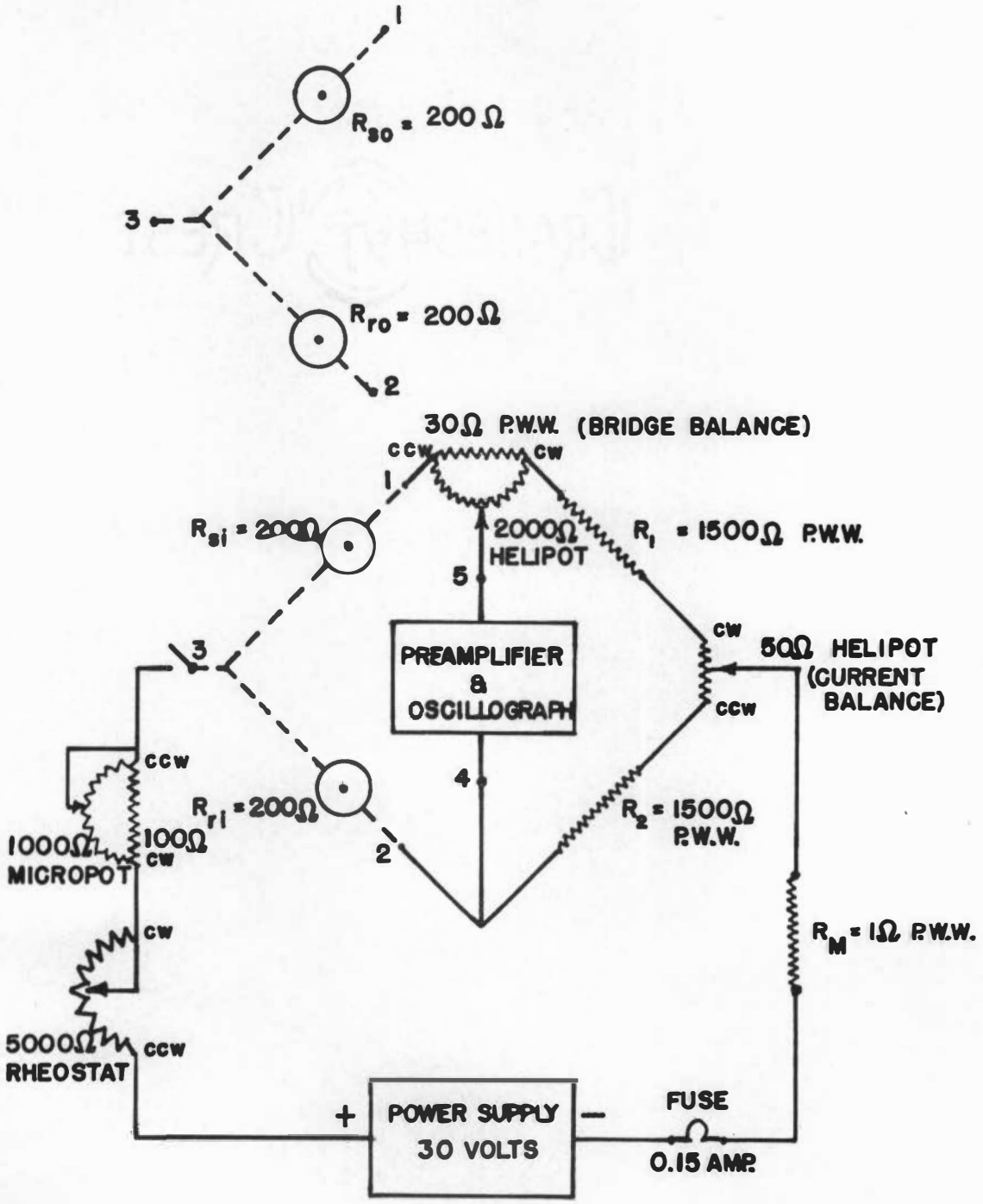


Figure 7. Schematic diagram of thermal conductivity cell bridge circuit.

the bridge at points 4 and 5 and to place it across the current measuring resistor, R_M, at these same points. A 0.15 amp fuse was placed in the circuit to protect the thermistors against burnout by direct shorts.

The 50 Ω Helipot placed at the bridge supply point allowed the individual bridge arm currents to be adjusted. The 2000 Ω Helipot included within the sample thermistor bridge arm was used to obtain a bridge null or balance point under various conditions and, as is explained in Chapter IV, to provide a means for measuring the individual bridge arm currents.

The unbalanced bridge signals were detected and recorded by the combination of a Sanborn low level preamplifier (Model 150-1500), driver amplifier and power supply (Model 150-200A-400) and single channel oscillograph (Model 151-100A). This equipment offered several desirable features the most attractive of which was its speed-of-response. The combined frequency response (amplitude ratio) of the preamplifier, driver amplifier, and galvanometer is completely flat to one cycle per second and down only 20 per cent at 10 cps. The preamplifier also provided a wide range of sensitivities (0.1 to 100 mv/cm in ten steps) and zero suppression (up to ±100 mv). With its high input impedance (5300 ohms) the instrument closely approached the desirable absolute potentiometric detector (27). In addition the oscillo-

graph was equipped with a manually and remotely activated marking pen. This pen was used for phasing the inlet and outlet concentration sinusoids by activating the pen on every cycle through a microswitch mounted on the rotary element of the sinusoid generator's scotch yoke. The relative size and location of this detection and recording equipment can be seen in Figure 3.

Initial tests of the thermal conductivity cells, bridge and detecting equipment indicated the necessity for proper grounding and shielding. The arrangement which proved most satisfactory was to ground all instrument chassis together (power supply, preamplifier, and bridge control cabinets) at the power supply positive potential and to shield all leads between the different components. In addition, the leads from the thermal conductivity cells were carefully twisted and shielded to avoid stray magnetic and capacitive coupling. The bridge end of the shielding for these leads was grounded at the power supply positive potential while the cell end was left floating (insulated from the cell). A natural ground was found unnecessary.

V. GAS SAMPLING AND CELL THERMOSTATTING EQUIPMENT

The requirement for continuous gas analysis in these frequency response experiments necessitated a continuous

sampling procedure. In addition, a quantitative measure of the sampling flow rates was required to assure similarity of calibrating and operating conditions. Thus, a simple capillary flowmeter was designed for this purpose. Figure 8 shows a cross section of this flowmeter and indicates its construction details. The body of the meter was brass while the capillary section was made of a 1-1/4-inch long piece of thermometer tubing with the ends cut square. A seal between the capillary and the brass body was made with low melting vacuum wax which was melted after the capillary was inserted in the body.

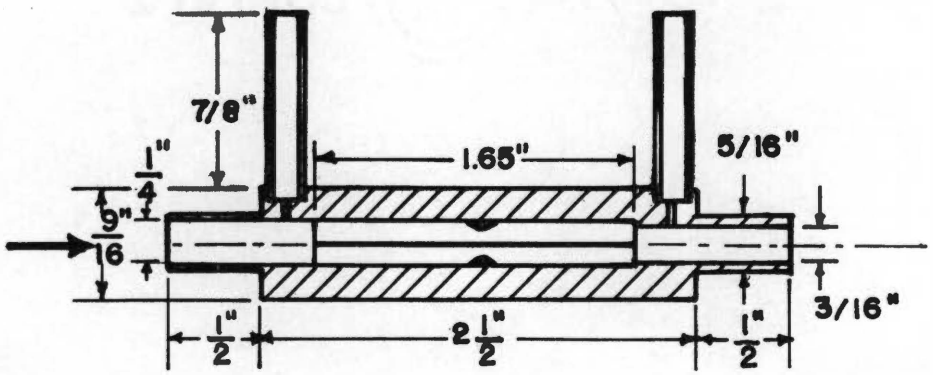


Figure 8. Capillary Flowmeter

Four such flowmeters were constructed: one each for the sample gas and reference gas of both thermal conductivity cells. The capillary section for each meter was cut from the same thermometer and, as closely as possible, to the same

length.

The flow rates through the meters were measured in terms of the pressure drops across the capillaries which were indicated by a rack of 48-cm water manometers (see Figure 3). The capillary flowmeters were all carefully calibrated by a method described in Chapter IV.

Since the column was to operate at, or slightly above, atmospheric pressure some method to continuously withdraw samples had to be provided. A vacuum pump was used for this purpose and Figure 9 shows its position in the sample and reference gas flow system. The sample streams for the inlet and outlet cells were withdrawn from the column through 3/16-inch inconel tubes and directly entered the thermal conductivity cells. From the cells, the sample flows passed through 1/4-inch polyethylene tubing to the capillary flowmeter and then to a vacuum manifold. The sample gas flow rates were controlled by small needle valves placed between the flowmeters and the vacuum manifold. The manifold was maintained at approximately 10 cm of mercury vacuum by a Duo-Seal vacuum pump which ran continuously. Gas flow from the manifold was throttled through a small tubing valve which acted as a critical orifice and thereby eliminated the effects of the downstream pressure pulsations caused by the rotary action of the vacuum pump.

The reference gas flows for the inlet cell and for the

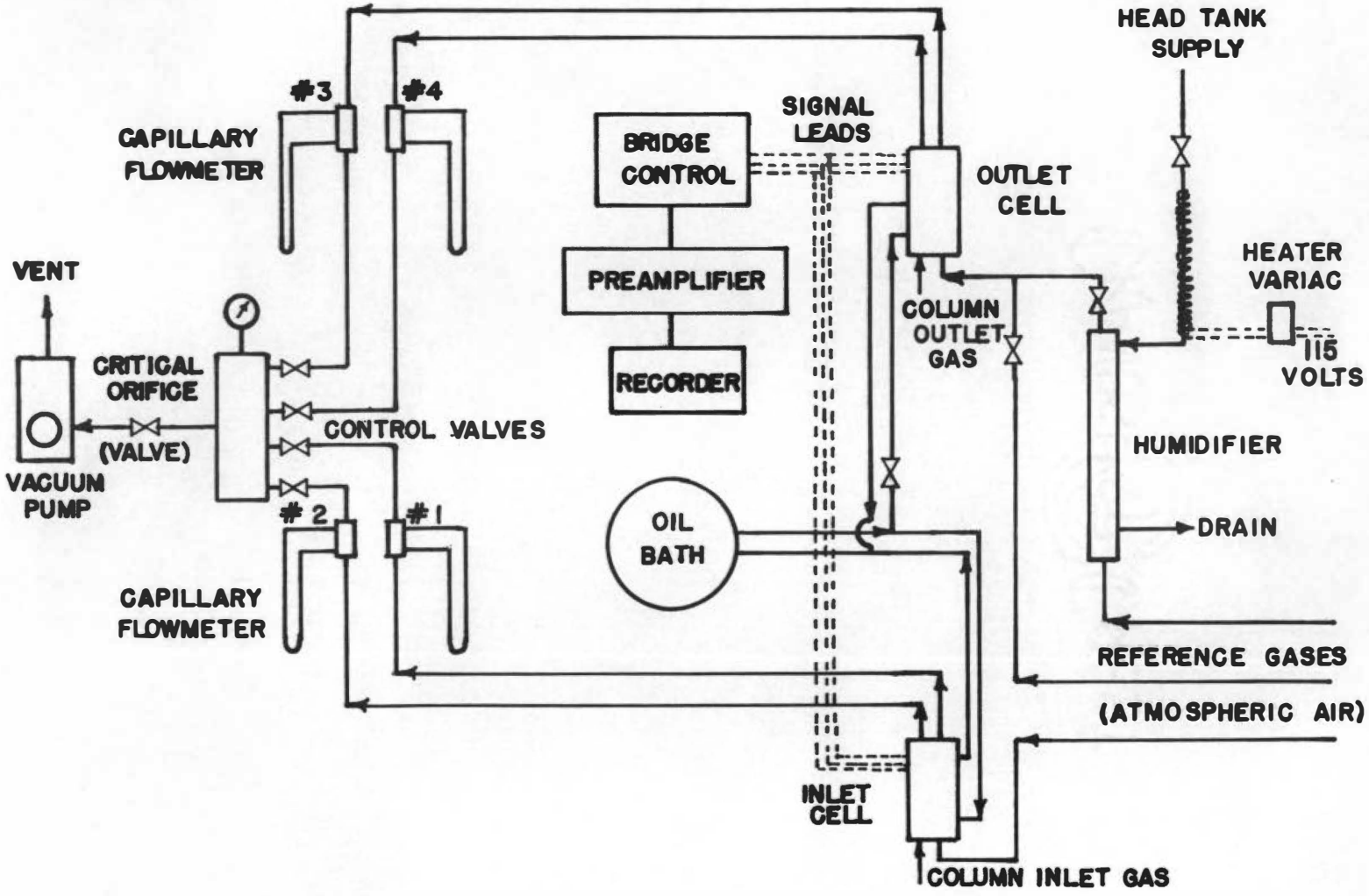


Figure 9. Schematic diagram of thermal conductivity cell flow systems.

outlet cell, in the nonabsorption runs, were atmospheric air taken from the same point outside the building as the blower inlet air. These streams passed to and from the thermal conductivity cells through 1/4-inch polyethylene tubes. Their flow rates were controlled and measured with capillary flowmeters in exactly the same manner as were the sample gas flows.

In the case of the absorption runs the reference gas flow, for the outlet thermal conductivity cell only, was passed through a small humidification column before it entered the cell (see Figure 9). This humidification column consisted of a 1-inch ID by 20 inch long Pyrex glass tube packed with 3/16-inch ceramic rings. Water from the constant head tank was introduced to the top of this column, passed downward over the packing, and ran to the drain through a suitable gas seal water leg. The reference gas was humidified by passing it up the column, countercurrent to the dispersed water stream. A small variable control, electric heater was wrapped around the water inlet tube so that the absolute humidity of the column outlet air stream could be controlled. The purpose of this humidifier was to supply a reference gas to the thermal conductivity cell with the same absolute humidity as the sample gas taken from the top of the column. In this way the bridge signal from the outlet cell would reflect only the carbon dioxide concentration of the

column outlet gas stream. A discussion of these humidity effects is presented in greater detail in Appendix D.

The inlet and outlet thermal conductivity cell temperatures were controlled by the continuous circulation of a constant temperature oil through built-in chambers in the cell bodies (see Appendix D). The constant temperature oil was supplied by a "Precision Constant Temperature Circulating System" (Model K-12), made by Precision Scientific Company. This system was capable of flow rates of 2 gallons per minute at a 6-foot head. A Roto-stat thermostat (Model S209), could control the bath temperature to $\pm$ 0.02°C over a range of -10° to 110°C. The circulation system for the cells is shown in Figure 9. A parallel flow arrangement was used in which the bath outlet stream was split into two separate flows--one for each thermal conductivity cell. The return streams from the cells were then joined to form a single bath inlet stream. Uninsulated 1/2-inch tygon tubing was used for the oil lines between the circulation bath and the cells. An adjustable pinch clamp restricted the inlet line of the inlet cell so as to obtain an even distribution of oil to each cell.

VI. COLUMN INLET AND OUTLET SECTIONS MOCK-UP

A replica of the column inlet and outlet sections was constructed to test separately the dynamic response of these sections. Figure 10 shows the construction of this mock-up.

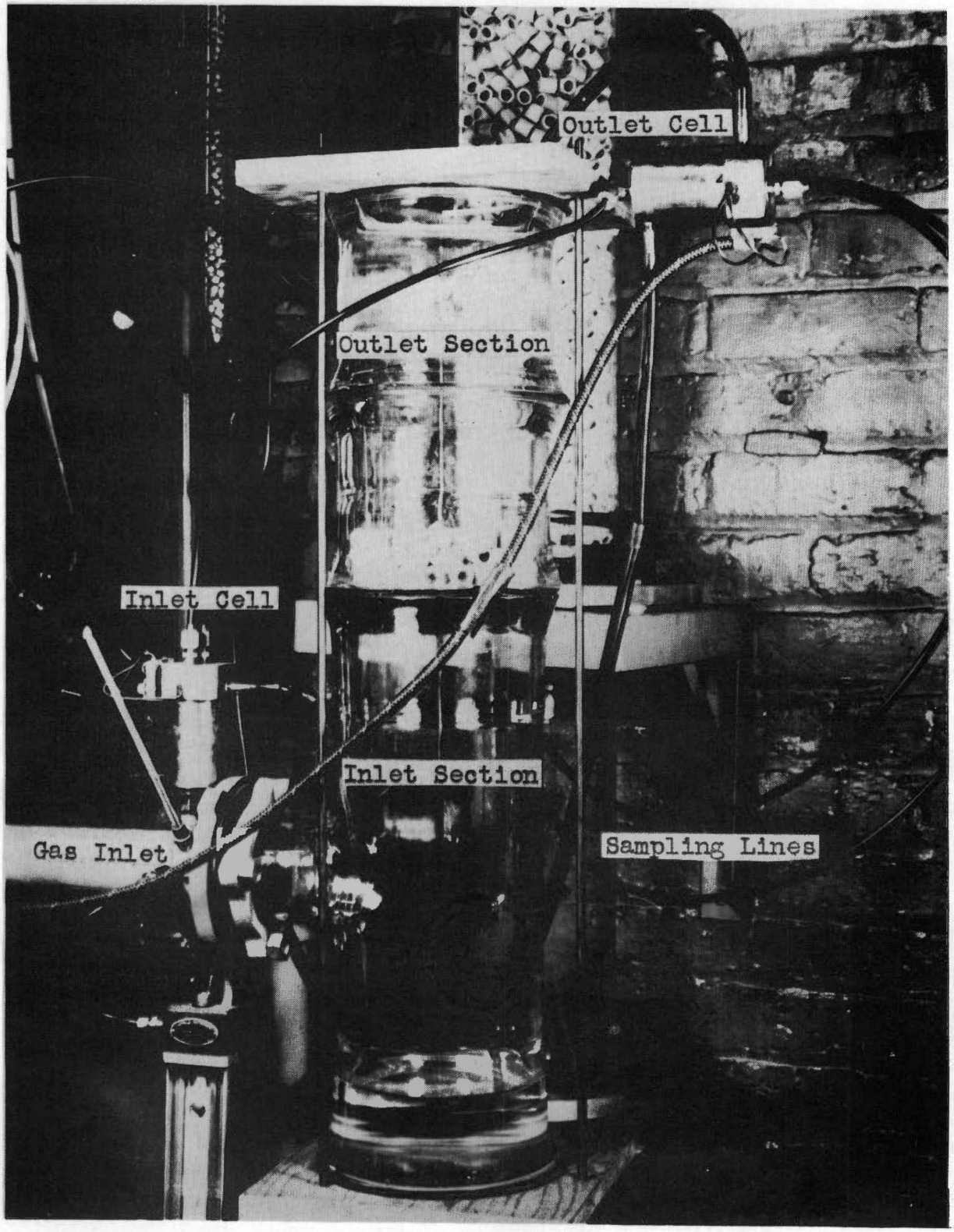


Figure 10. Column inlet and outlet section mock-up.

The lower section consisted of a 6-inch by 6-inch by 3-inch Pyrex glass tee identical to the inlet section of the column. Two 6-inch long sections of 6-inch ID glass pipe were placed on top of the tee to simulate the foot-long section of empty column between the top of the packing and the outlet cell sampling probe. These sections were held together by two 3/4-inch plywood support pieces connected by three 1/4-inch rods which were threaded on their ends. The bottom support piece was solid, while the top piece had a 6-inch hole to allow the gas to pass through. The gas was vented to a point outside the building through a 6-inch by 1-1/2-inch reducer and a length of 2-inch rubber hose (not shown in Figure 10). A piece of 1/4-inch stainless steel screen was placed between the tee and the first 6-inch pipe section to support a 2-inch layer of 5/8-inch Raschig rings. This layer of rings was similar to a layer placed above the liquid distributor in the experimental column to eliminate entrainment. The inlet thermal conductivity cell held the same position that it had in the full column tests while the outlet cell, along with its sampling probe, was removed from the top of the column and inserted in the mock-up through a 3/16-inch hole drilled in the side of the top support piece. The sampling points for both cells were the same as those in the full column experiments.

CHAPTER IV

EXPERIMENTAL PROCEDURE

I. COLUMN PACKING

A number of tests and calibrations of portions of the experimental equipment were necessary before any frequency response data could be taken. Among these, the column packing porosity measurements merit first consideration.

The column packing porosity or void fraction was required for the determination of gas phase holdup in the packing. Although porosity values for 5/8-inch Raschig rings were available in the literature, it was believed that a more accurate value--one peculiar to the packing methods used here--could be obtained from a relatively simple test.

The column packing was installed after the column was erected and the water flow system was completed but before the gas inlet and outlet lines were attached. A gasketted, 4-inch flange plate was placed over the air inlet side of the reducer tee to make a water tight seal. Thus, when the drain valve was closed, the column could be completely filled with water supplied by the constant head tank. The Raschig rings were then dumped into the water and allowed to fill the Pyrex pipe to a depth of 62 inches. This packing method resulted in a lower porosity than alternate methods (113) and, in

addition, avoided breakage of the ceramic packing rings.

After the packing was installed, the column was filled with water and drained several times to settle the packing into a fixed position. The average porosity of this final arrangement was calculated from the ratio of the volume of water necessary to fill the complete packing section to the volume of the empty packing section. The volume of water necessary to fill the packing section was determined from the time necessary to fill the section at a known and constant water flow rate. The water flow was maintained constant with the constant head tank (with no overflow) and was measured with the previously calibrated inlet water rotameter. The filling times were measured with a stopwatch. Because of the location of the drain valve the filling volume had to be decreased by the amount of water which filled the overflow line. Four runs were made with excellent reproducibility and resulted in a porosity value of 0.604.

II. CALIBRATIONS

A large number of flowmeter and analyzer calibrations were carried out at the start of this experimental study. The purpose of this section is to describe, in some detail, the procedures and techniques used to obtain these calibrations. The calibration data resulting from these tests are presented in the form of graphs in Appendix E.

The gas system orifice meter used to measure large air flow rates was calibrated by three methods. Initially, data were taken over the full range of the blower speed control with a large (10 liters per revolution) wet-test meter. Unforunately, this meter was unable to measure flows over 10 ft^3/min and the data at flows above this value had to be obtained by other means. A vane anemometer was used for this purpose. This device was calibrated from the wet-test meter data at the low flow rates and the proportionality between measured and actual flow rates was assumed to be constant throughout the entire flow range. In addition, the largest flow rates were checked from the manufacturer's blower characteristic (volume flow rate versus blower speed) and hand tachometer measurements of blower speed. The results of these tests are shown in Figure E-1. Also shown is the theoretical calibration curve calculated from the standard orifice equation with a coefficient of 0.61.

The gas system rotameter, which was used to measure air flow for the low flow rate runs, was calibrated with a smaller (0.1 ft^3/revolution) wet-test meter. Since the capacity of this meter was approximately 0.4 ft^3/min the upper end of the rotameter scale had to be calibrated from the Triflat Predictability Rotameter curves given by the manufacturer. The calibration curve for this rotameter is shown in Figure E-2.

The calibration of the water flow rotameter was accomplished most conveniently after it was installed on the column. In this way the constant head tank could be used to maintain constant flow rates through the meter. A 1-inch diameter tygon tube connected to the water passage at the inside of the aluminum flange plate allowed the water to be diverted from the top of the column to a weigh bucket. With this arrangement, 25-pound samples were collected in the weigh bucket for a number of rotameter settings. The filling time for each run was measured with a stopwatch. The rotameter calibration data are shown in Figure E-3.

The thermal conductivity cells' sample stream flowmeters were calibrated with a modified "soap-film flowmeter." The sample stream flowmeters were the special capillary tube orifices described in Chapter III. A soap-film flowmeter is a simple device in which gas flow rates are measured by timing the volume displaced by a moving soap film (51, 55). The experimental equipment used in these calibrations is shown schematically in Figure 11.

Compressed air from the building supply was used as the calibration gas for these meters. The air pressure in the system was maintained at 1/2-psig by a Matheson low pressure "pancake" regulator. The flow rate was controlled with a small needle valve placed at the exit of the pressure regulator. Air flow passed from the regulator into a 100-ml gas

burette through 1/4-inch tygon tubing and a glass tee located at the inlet of the burette. The gas flowed from the outlet of the burette through the capillary flowmeter and was vented to the atmosphere. The calibration procedure was to estab-

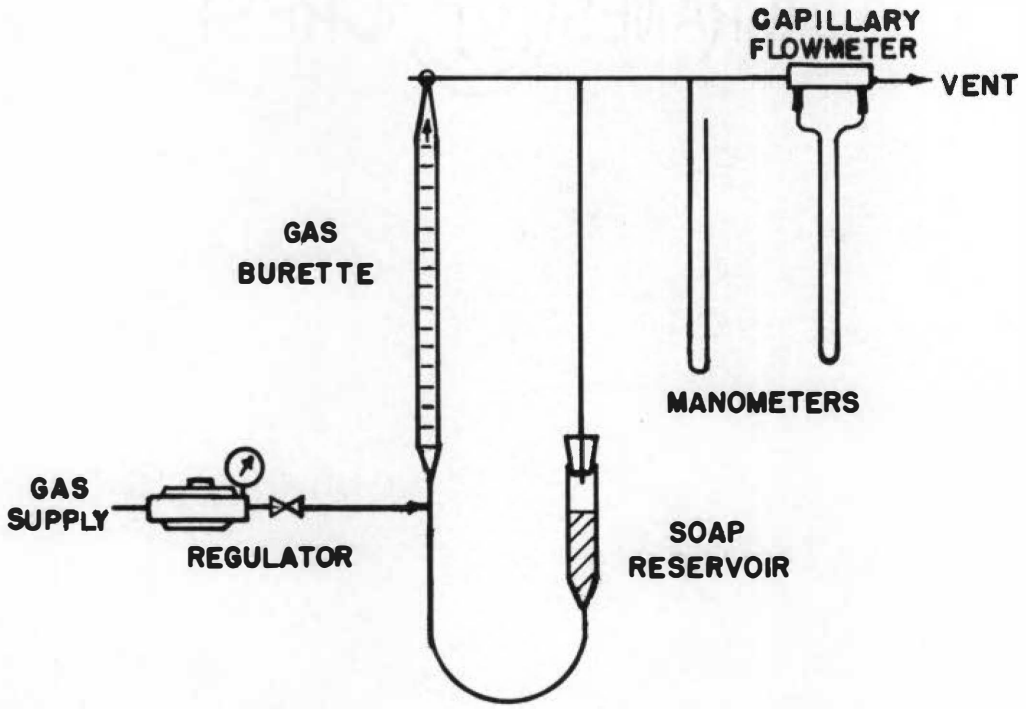


Figure 11. Soap Film Flowmeter Equipment

lish a fixed flow rate through the burette and the capillary flowmeter and to record the reading of the 48-cm water manometer used to measure the pressure drop across the meter. A soap reservoir containing household liquid detergent was then raised so as to form a soap bubble across the tee located at the inlet of the burette. The gas flow rate was

determined from the time necessary for the soap film to sweep the 100-ml volume of the gas burette. The sweep times were measured with a stopwatch to the nearest 0.1 second.

This soap-film flowmeter, which was capable of measurements to better than 1 per cent for a wide range of flow rates, was used to calibrate all four sampling stream capillary flowmeters. The results of these tests are shown in Figure E-4. In addition, the device was used to calibrate the flowmeters used in the standard gas mixer discussed in Appendix D. These data are shown in Figures E-5 through E-7.

The calibration equipment and procedure for the thermal conductivity cells used for continuous column gas phase analysis are presented in Appendix D. Briefly, the cells are calibrated by measuring the unbalanced bridge signal for various air-carbon dioxide mixtures of known composition. The cells were calibrated in the special equipment stand shown in Figure D-6 and then transferred to the absorption column.

Shortly after the thermal conductivity cells were installed on the column and some preliminary response data had been obtained, an outlet cell thermistor lead failed and could not be repaired. Since the manufacturer could not supply a replacement matched pair of thermistors for a number of months, an available but unmatched pair was installed in the cell. The use of this unmatched pair of thermistors resulted

in an unbalanced bridge signal which was beyond the balancing and zero suppression capacity of the bridge and preamplifier, respectively. In an effort to rematch the thermistor side of the bridge a 20-ohm precision wire-wound resistor was added to the low resistance arm (reference thermistor). In addition to bringing the bridge into balance, this added resistance decreased the bridge sensitivity, as would be predicted by Equation D13, and required that the cell be recalibrated.

The outlet cell recalibration was carried out with the cell in place on the column by recording the bridge signals for various steady gas phase compositions. The gas concentration for each calibration point was measured with the previously calibrated inlet thermal conductivity cell. The results of the outlet cell recalibration, along with the original inlet cell calibration, are shown in Figure E-8 of Appendix E.

The linear valve of the sinusoid generator was driven by a direct current motor which was controlled by a variable rheostat. It was found convenient to have a calibration of the rheostat settings versus the sinusoid generator frequencies. This was accomplished by measuring with a stopwatch the period of valve oscillation for various rheostat settings. The remotely activated flasher on the Sanborn recorder described in Chapter III was used to indicate the periods. These frequency calibration data are presented in

Figure E-9 for a one-to-one spur gear combination.

III. BRIDGE OPERATION

The first step to proper operation of the Wheatsone bridge was to calibrate and standardize the Sanborn Low Level Preamplifier. This calibration and standardization used instrument internal references and was carried out according to the manufacturer's recommended procedure. Calibration established an accurate chart scale reading for the various instrument sensitivities while standardization fixed the no-load scale reading and calibrated the zero suppression potentiometer.

The variable voltage supply was set at 30.0 volts for all tests, calibrations, and operations of the Wheatsone bridge and thermal conductivity cells. This value was chosen arbitrarily as a bridge voltage which could provide a satisfactory range of bridge currents for the particular current control rheostats used in the bridge (see Figure 7).

The total bridge current was determined from the potential drop across the measuring resistor, R_M. The detecting equipment was transferred to the measuring resistor with a toggle switch mounted on the bridge control panel. The potential drop across the resistor was measured by returning the galvanometer stylus to its no-load position (chart center position) with the precision 10-turn zero

suppression potentiometer at the maximum sensitivity level of 0.1 mv/cm. Since the measuring resistor had a resistance of 1 ohm±1 per cent, the total bridge current in milliamperes was read from the zero suppression potentiometer scale directly in millivolts.

The thermal conductivity cell tests discussed in Appendix D have shown that the maximum cell sensitivity occurred at a thermistor current of approximately 8.0 ma. Thus a total bridge current of 16.0 ma was used for all the experimental analyses of this work. This total bridge current was established by setting the zero suppression potentiometer at 16.0 mv and adjusting the 5000-ohm rheostat of Figure 7 to bring the galvanometer reading on scale. The fine current adjust Micropot was then used to establish a no-load reading (chart center line) at the maximum sensitivity scale (0.1 mv/cm).

The current flow in the individual bridge arms was determined as follows: The bridge balancing Helipot shown in Figure 7 was adjusted fully to the thermistor side of the bridge (counterclockwise, or ccw) and the bridge signal recorded. The Helipot was turned completely to the fixed resistor side of the bridge (clockwise, or cw) and the bridge signal again recorded. The difference between these two signals, assuming that the Sanborn equipment acted as a potentiometric detector, was the potential drop across the bridge

balancing resistors. Since the measured resistance of the wire-wound resistor was 30.70 ohms, the equivalent resistance of the balancing resistors was 30.22 ohms. Thus, the sample stream thermistor current in milliamperes was the above potential drop in millivolts divided by 30.22. The reference stream thermistor current was obtained by subtracting the sample stream thermistor current from the total bridge current.

The 50-ohm current balance Helipot was used to equalize the bridge arm currents. This was accomplished by the trial and error process of adjusting the Helipot and, at a total bridge current of 16.0 ma, measuring the resulting sample stream thermistor current until a value of 8.0 ma was obtained.

After the bridge currents had been established, the cell was prepared to make continuous gas analyses. The sample and reference gas stream flow rates were individually adjusted to 60 ml/min. Figure D-8 shows that the thermal conductivity cells, with the thermistors in the retracted position, exhibited no flow sensitivity and, there, the sampling gas stream flow rates were selected for convenience of operation. Figure E-4 of Appendix E shows that all the capillary flowmeter calibration curves pass the flow rate 60 ml/min at the same manometer reading (9.0 cm of water). Thus, this flow rate was used because it permitted equal

manometer settings for similar sample flow rates.

Once the sample and reference gas flow rates were established (both 100 per cent air) the bridge could be "nulled" or "balanced." In balancing the bridge, the galvanometer stylus is adjusted to the chart centerline position with the bridge balancing 2000-ohm Helipot. The maximum possible preamplifier sensitivity level is used for this process.

The unbalanced bridge signal resulting from the introduction of an air-carbon dioxide mixture to the sample side of the thermal conductivity cell was measured in two ways. The signal (millivolts) could be read directly from the galvanometer deflection as indicated by the recorded chart trace and the known sensitivity level; or the zero suppression potentiometer could be used to return the stylus to the chart center line at maximum sensitivity and the signal read directly from the potentiometer dial. It was found that the former method was suited for only small signals while the latter technique would yield accurate measurements for a full range of signals and, therefore, was used for most of the cell tests and calibrations.

A rotary switch mounted on the control panel was used to connect either the inlet or outlet thermal conductivity cell thermistors into the bridge circuit. The above description of bridge operation applies to either cell. It was

found, however, that the thermistors of the inlet and outlet cells were closely enough matched (even with the fixed 20-ohm resistor added to the outlet cell reference arm) to obviate the need for readjustment of the total and individual bridge currents when one cell's thermistors were replaced by the other cell's thermistors.

IV. COLUMN FREQUENCY RESPONSE TESTS

In general terms, the frequency response analysis of the gas absorption process was carried out by introducing a carbon dioxide-air mixture with a sinusoidally varying CO_2 concentration to the inlet of the packed gas absorber and measuring the column outlet CO_2 concentration wave. The outlet wave amplitude and phase were then compared to those of the inlet wave. The procedure for these experiments is explained in detail below.

The gas absorption tests were initiated by thoroughly wetting the column packing. Since Schulman (104) has found that a considerable length of time is necessary to establish a constant liquid holdup condition, the column was operated at the maximum water flow rate for several hours before any absorption runs were made. After this packing saturation period, the proper water flow rate was adjusted using the control valves and rotameter shown in Figure 4. The air flow rate necessary to obtain a particular total flow rate of the

air-carbon dioxide mixture, was calculated from an estimated value of the mean carbon dioxide concentration. The resulting air flow rate was then established with the control valves and rotameter or orifice-meter (depending on the magnitude of the gas phase flow rate) of the gas phase flow system.

A mean carbon dioxide concentration of the same value as used in the air flow calculation was obtained through proper adjustment of the linear valve of the concentration sinusoid generator. With the scotch yoke set at its mean, or center line position, the valve mean position was adjusted to a value estimated to give the desired carbon dioxide concentration. The blower was then started and sample and 100-per cent air reference streams were drawn through the inlet thermal conductivity cell with the vacuum pump. The bridge was balanced and the stabilization tank was filled with CO_2 to the appropriate pressure (approximately 1/2 psig for the low gas flow rates and 5 psig for the large flows). The carbon dioxide was introduced to the system by opening the valve between the stabilization tank and the linear valve (see Figure 4) and the concentration of the resulting gas mixture was determined from the signal indicated by the inlet thermal conductivity cell. If the proper concentration was not obtained, the valve mean position was readjusted and the new concentration measured. This process was repeated until

the desired mean carbon dioxide concentration was obtained. Although the mean composition of the gas mixture could be altered by changing the stabilizer tank pressure, this was found to be considerably less sensitive than variation of mean position of the linear valve.

Once the gas mixture mean concentration had been established the amplitude of the concentration sinusoid was adjusted by lengthening or decreasing the stroke of the scotch yoke as required.

At the start of a frequency response measurement the carbon dioxide flow through the linear valve was cut off and the inlet thermal conductivity cell was switched to the bridge which was then balanced with the column and reference sampling flow rates controlled at 60 ml/min. The sinusoid generator frequency was adjusted to the proper value with the DC motor speed control device and the frequency marking pen was activated through a toggle switch on the bridge control panel.

An oscillograph chart speed was chosen such that one complete concentration cycle was recorded on at least 2 inches of chart paper. This was required for the accurate determination of phase shifts.

The carbon dioxide flow to the linear valve was then started and the steady-state inlet gas phase concentration sinusoid was recorded. The concentration variation was

recorded so that the mean carbon dioxide concentration was depressed with the zero suppression potentiometer, and the preamplifier sensitivity was selected so that the concentration sinusoid was plotted over a large portion of the chart paper width. In this manner the concentration sinusoid amplitude could be measured with greater accuracy. Four to six complete steady-state concentration cycles were recorded at each frequency.

The column outlet gas phase concentration sinusoid was obtained at every frequency by introducing the outlet cell thermistors to the bridge by use of the rotary switch mounted on the bridge control panel. Immediately after recording the inlet cell response, the outlet cell signal was recorded without any readjustment of the bridge controls (balance, current, etc.). Again, the outlet gas phase mean concentration signal was eliminated by use of the zero suppression potentiometer and only the sinusoidal concentration variation was recorded.

After the inlet and outlet gas phase concentration sinusoids had been recorded for one sinusoid generator frequency, the DC motor speed control was adjusted to give a higher (or lower) sinusoid frequency and traces of the inlet and outlet gas phase concentration were again recorded. This process was repeated until a full spectrum of frequency responses were obtained for a particular set of column operating

conditions. Inlet and outlet concentration traces were made for 6 to 12 values of the sinusoid frequency for each set of column conditions.

The column operating conditions were taken by recording the initial gas system rotameter (or orifice meter) reading, the inlet gas mixture temperature and pressure, the water rotameter reading, and the inlet water temperature. Since the dial settings on the DC motor speed control were very coarse, the actual sinusoid generator frequency was measured by timing the period between flashes of the oscillograph remote marker indicator light with a stopwatch. The measured period was recorded to the nearest 0.1 second on the oscillograph chart for each sinusoid frequency. The preamplifier sensitivity level and zero suppression for each concentration trace were also recorded on this chart.

The column frequency response data for the nonabsorption runs (no liquid flow) were obtained in exactly the same manner as were the absorption column responses described above. However, in these tests no water flow was used and the packing was thoroughly dried before any response data were taken. The packing was dried by passing air through the column at the maximum blower speed for several hours. Because of the difficulty in drying the packing, all of the nonabsorption tests, after the first, were made in sequence.

V. MOCK-UP SYSTEM FREQUENCY RESPONSE TESTS

In order to carry out frequency response tests of the column inlet and outlet sections mock-up, the 2-inch gas phase inlet pipe was disconnected from the column and rotated about 10 degrees so that it could be reconnected to the mock-up section as shown in Figure 10. This arrangement allowed the sinusoid generator, orifice meter, and inlet thermal conductivity cell to be rapidly and simultaneously transferred to the mock-up system. The outlet thermal conductivity cell, however, had to be removed from the column and positioned in the mock-up section upper support piece. This could be carried out without disconnecting the thermistor leads although the polyethylene sampling tubes had to be removed for the transfer.

The Pyrex tee of the mock-up system was filled with water to a depth of 6 inches to simulate a condition which existed in the full column due to the height of the water leg gas seal. Because of the major equipment modifications required, the mock-up system did not include facilities to simulate the liquid which fell through the column tee from the bottom of the packing during the absorption tests.

The frequency response data for the mock-up system were obtained by the same procedures used in the full column absorption and nonabsorption runs. A complete frequency

spectrum was obtained at gas phase flow rates which were as similar as possible to the gas flows of the full column tests.

CHAPTER V

RESULTS AND DISCUSSION

I. EXPERIMENTAL DATA ANALYSIS

The dynamic response of the gas absorption system considered in this work was expressed in terms of the ratio of the gas phase inlet concentration sinusoid amplitude to the gas phase steady-state outlet concentration sinusoid amplitude and the phase shift between these two waves. The amplitude ratio and phase shift data were obtained, as described in Appendix G, from the oscillograph concentration traces similar to those of Figure 12. Because of the placement of the thermal conductivity cells, these experimental response data included not only the behavior of the packed section of the column but also the dynamic response of the column inlet and outlet sections. It was possible to reduce the original data so as to eliminate the effects of the inlet and outlet sections by application of the following theory:

The dynamic elements of the experimental system can be schematically represented by a block diagram (19) shown in Figure 13. In this diagram, G_i and G_o represent the transfer functions of the column inlet and outlet sections, respectively, while G_p is the packing transfer function and G_{ic} and G_{oc} the transfer functions of the respective inlet

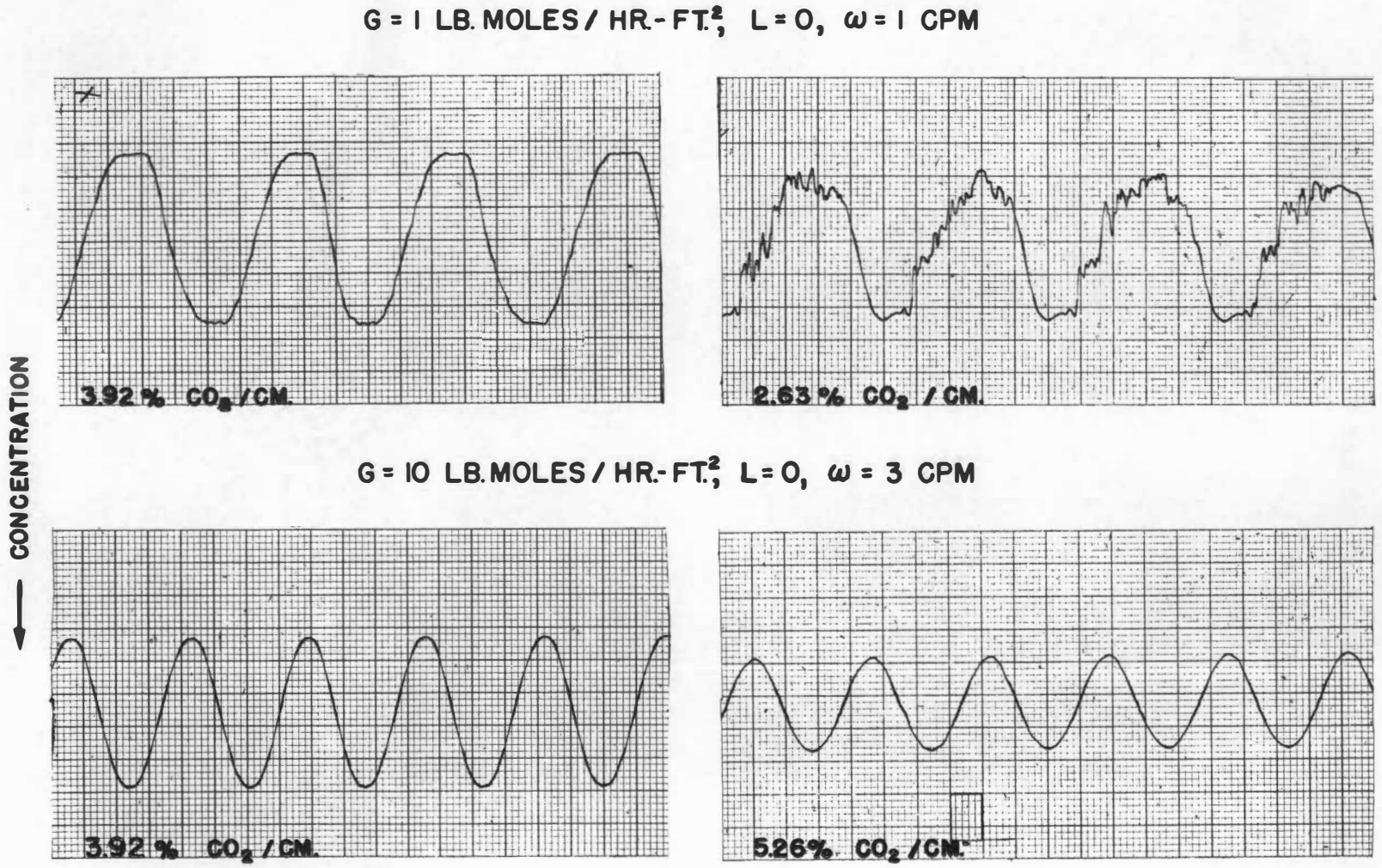


Figure 12. Oscillograph concentration traces

and outlet thermal conductivity cells. S represents the transformed dependent variable which, in the present case, is the gas phase composition. The concentration variations

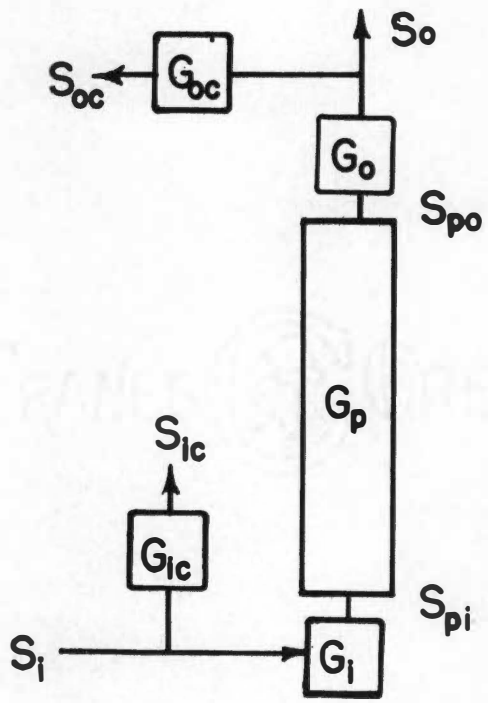


Figure 13. Total System Block Diagram

which the thermal conductivity cells attempt to measure are, therefore, S_i and S_o while those actually recorded by the oscillograph are S_{ic} and S_{oc}. The problem is to determine the experimental packing section transfer function, G_p, from the measured signals, S_{ic} and S_{oc}.

By the definition of a transfer function given in Chapter II, G_p becomes:

$$G_p = \frac{S_{po}}{S_{pi}} \tag{91}$$

Also,

$$G_i = \frac{S_{pi}}{S_i} \qquad \text{and} \qquad G_o = \frac{S_o}{S_{po}}$$

but

$$S_i = \frac{S_{ic}}{G_{ic}} \qquad \text{and} \qquad S_o = \frac{S_{oc}}{G_{oc}}$$

Therefore,

$$G_i = \frac{S_{pi}}{S_{ic}} G_{ic} \qquad \text{and} \qquad G_o = \frac{1}{G_{oc}} \frac{S_{oc}}{S_{po}}$$

or

$$S_{pi} = S_{ic} \frac{G_i}{G_{ic}} \qquad \text{and} \qquad S_{po} = \frac{S_{oc}}{G_o G_{oc}}$$

Substitution of these equations into the above expression for the packing section transfer function gives:

$$G_p = \left(\frac{G_{ic}}{G_o G_{oc} G_i}\right) \frac{S_{oc}}{S_{ic}} \tag{92}$$

Now define the ratio S_{oc}/S_{ic} as the total system transfer system, G_s or

$$G_s \equiv \frac{S_{oc}}{S_{ic}} \tag{93}$$

Thus

$$G_p = \left(\frac{G_{ic}}{G_o G_{oc} G_i}\right) G_s \qquad (94)$$

The transfer function representing the bracketted term of the above equation can be determined from the dynamic response of a mock-up of only the column inlet and outlet sections. The block diagram for such a system is shown in Figure 14.

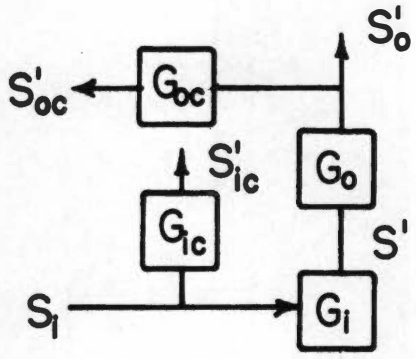


Figure 14. Column Inlet-Outlet Mock-up Block Diagram

Again, by the definition of a transfer function, for this system,

$$G_i = \frac{S'}{S_i} \qquad \text{and} \qquad G_o = \frac{S_o'}{S'}$$

Also

$$G_{ic} = \frac{S_{ic}'}{S_i} \qquad \text{and} \qquad G_{oc} = \frac{S_{oc}'}{S_o'}$$

or

$$S_i = \frac{S_{ic}'}{G_{ic}} \qquad \text{and} \qquad S_o' = \frac{S_{oc}'}{G_{oc}}$$

Elimination of S' from the first pair of equations gives

$$G_o G_i = \frac{S_o'}{S_i}$$

Direct substitution of the last pair of equations into the above relation results in the expression

$$\frac{G_o G_{oc} G_i}{G_i} = \frac{S_{oc}'}{S_{ic}} \equiv G_s' \tag{95}$$

where the ratio $\frac{S_{oc}'}{S_{ic}}$ is defined as the mock-up system transfer function, G_s'.

With the above definition the packing section transfer function of Equation 94 becomes

$$G_p = \frac{G_s}{G_s'} \tag{96}$$

As discussed in Chapter II, substitution of $i\omega$ for the Laplace transformation parameter, s, in a system transfer function will result in a complex number whose modulus is the amplitude ratio and whose argument equals the phase shift between the steady-state input and output sinusoidal signals. Thus, presuming the substitution, $s=i\omega$, to be made and the resulting complex number to be written in polar

form, the above expression for the packing section transfer function becomes:

$$r_p\, e^{\theta_p i} = \frac{r_s\, e^{\theta_s i}}{r_s'\, e^{\theta_s' i}} = \frac{r_s}{r_s'}\, e^{(\theta_s - \theta_s')i} \qquad (97)$$

where

r = appropriate modulus (amplitude ratio)

θ = appropriate argument (phase shift)

From this expression it is seen that the packing section amplitude ratio, given by r_p, is simply the measured total system amplitude ratio, r_s, divided by the measured mock-up system amplitude ratio, r_s'. Similarly, the packing section phase shift, θ_p, is the difference between the measured total system phase shift, θ_s, and the mock-up phase shift, θ_s'.

The mechanics of determining the packing section amplitude ratio and phase shift can be simplified by taking the logarithm of each side of Equation 97, resulting in a more direct form. Thus,

$$\log r_p + \theta_p i = \log r_s - \log r_s' + (\theta_s - \theta_s')i \qquad (98)$$

Now the logarithm of packing section amplitude ratio is equal to the differences in the logarithms of the measured amplitude ratios. Equation 98 suggests that the experimental

amplitude ratios and phase shifts are most conveniently expressed as a function of the sinusoidal frequency, ω, by plotting the logarithm of the amplitude ratio as the ordinate versus the logarithm of the frequency, ω, as the abscissa and, separately, the phase shift versus the logarithm of the frequency. Such graphs are called "Bode Plots" (14), and are extensively used to present the results of theoretical and experimental frequency response studies. These log amplitude-phase plots have the advantage that the products or quotients of several transfer functions at any frequency, ω, may be obtained by direct addition or subtraction of the linear vertical coordinates at that frequency. The addition and subtraction operations may be carried out graphically by the use of dividers. Thus, by Equation 98, the logarithms of the packing section amplitude ratio and the packing section phase shift are simply the vertical coordinate differences between the Bode plots of the total system and mock-up system responses.

This method of separating some part of an overall transfer function has been used, with modification, by McHenry and Wilhelm (67) and Turner (116). Implicit in its use is the requirement that the transfer function, G_1, be the same for both the total system and mock-up system measurements. This was not quite the case for the absorption runs where the gas inlet section had the packing exit liquid

dropping through it. Since, in an effort to avoid extensive column modifications, the mock-up system tests did not include this falling liquid, some difference between the absorption inlet section and the mock-up inlet section transfer functions existed. No difference existed, of course, for the total system dry packing runs, (L=0).

Although the magnitude of the difference between the two transfer functions could not be quantitatively evaluated, the similarity in shape of the packing section responses for the absorption and non-absorption runs suggests that the error introduced by the dissimilarity was not serious.

Because of the ease by which the packing section frequency response may be determined from the experimental amplitude ratio and phase shift measurements, and because of the convenience in comparing the experimental and theoretical responses, Bode plots were used to present all the results of this work.

The experimental data consisted of amplitude ratio and phase shift measurements for a number of gas phase concentration sinusoid frequencies, ω, with the absorption column operating at fixed flow conditions. This frequency response spectrum was obtained for three column gas phase flow rates at each of two liquid phase flow rates and at zero liquid flow over dry packing. The column experimental operating conditions are summarized in Table I, in which the runs

TABLE I

SUMMARY OF EXPERIMENTAL OPERATING CONDITIONS

Nominal Gas Flow lb-moles /hr-ft^2	Run	Actual Gas Flow lb-moles /hr-ft^2	Liquid Flow lb-moles /hr-ft^2	Temperature Gas °F	Temperature Water °F	Column Pressure Drop-in. of H_2O	Column Exit Pressure psia	Mean Inlet Gas Composition mole %
1	1	0.87	0	82	-	0	14.36	9.1
	3	0.87	55	80	74	11	14.35	10.0
	2	0.87	222	78	74	11	14.35	9.5
	10	0.93	222	72	71	11	14.42	14.9
	11*	0.93	0	75	-	11	14.40	14.5
10	4	7.7	0	83	-	0.3	14.43	13.7
	9	6.8	55	82	72	0.4	14.40	13.7
	8	7.4	222	82	72	0.7	14.40	14.1
	12*	7.7	0	76	-	0.1	14.34	12.8
20	5	17.2	0	88	-	1.55	14.42	5.61
	7	16.9	55	88	74	2.6	14.42	7.52
	6	17.5	222	88	73	4.6	14.42	6.74
	13*	16.8	0	77	-	0.4	14.34	4.65

*Column inlet-outlet mock-up runs.

are numbered chronologically. The order of the runs was influenced by the desire to run the dry packing tests in sequence--the packing being difficult to dry--and by the major equipment modifications that were necessary to obtain the frequency response of the mock-up system.

Although it was intended that the gas phase flow rate be constant for a series of runs, it was found difficult to re-establish a fixed gas flow with the run-to-run variations in the gas phase temperature, pressure, and mean solute composition. In addition, the blower variable speed control used to regulate gas flow in the high flow rate runs was found difficult to adjust for small changes in flow rate. For these reasons some variation in the gas phase flow rates was observed, as can be seen from Table I. For convenience of identification, though, both Table I and all the Bode plots were labeled by the nominal flow rates of 1, 10, or 20 lb-moles/hr-ft^2.

II. TOTAL SYSTEM AND MOCK-UP SYSTEM RESPONSES

The experimentally measured amplitude ratios and phase shifts for the various operating conditions of Table I are tabulated in Appendix F. These data were expressed graphically by Bode plots in which the series of runs associated with each of the three nominal gas flow rates were plotted on a single graph. Thus, Figure 15 gives the amplitude ratio

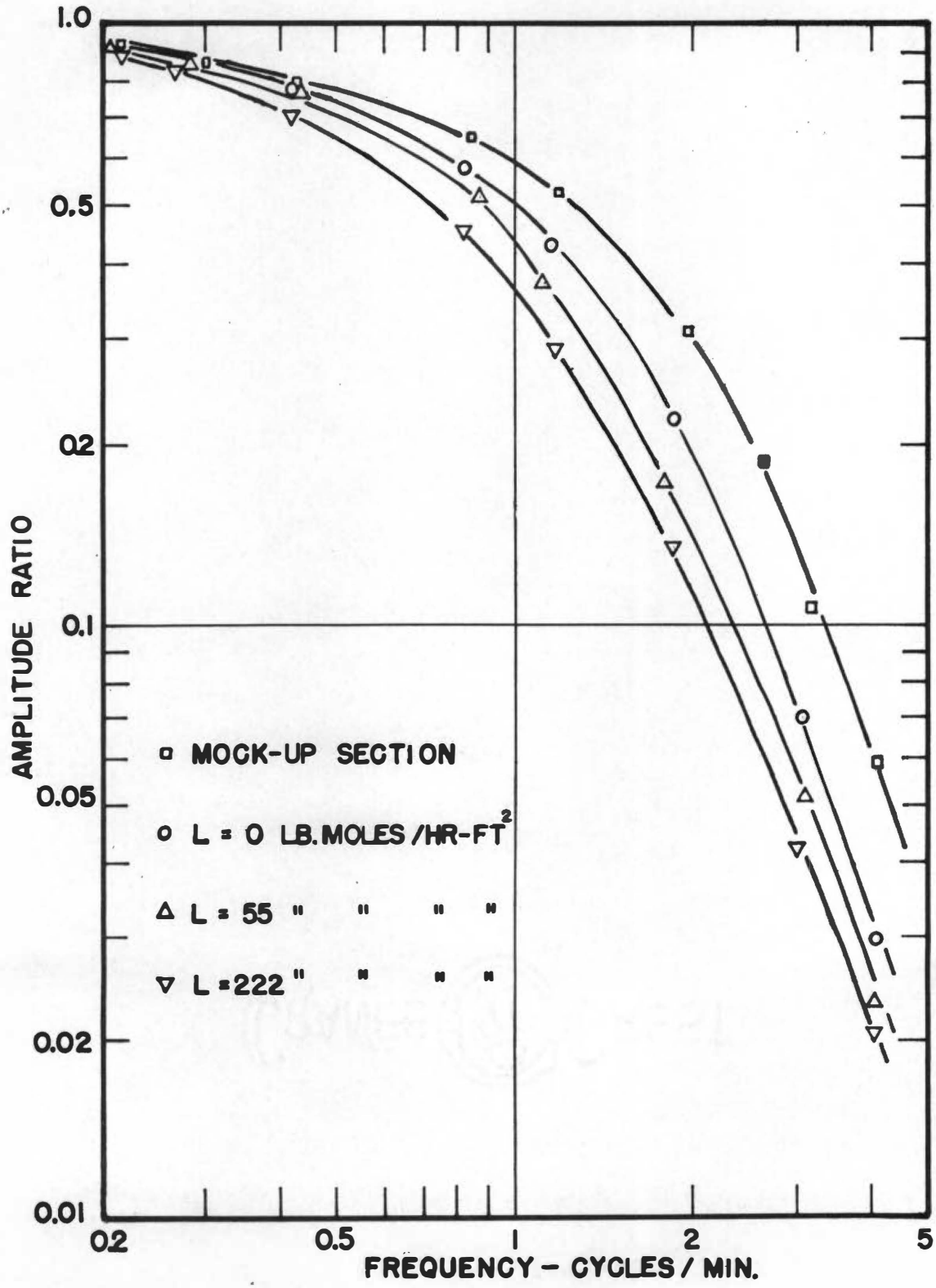


Figure 15. Total amplitude ratio vs. frequency, G=1 lb-mole/hr-ft^2.

and Figure 18 the phase shift versus various values of the concentration sinusoid frequency, ω, for the nominal gas phase flow rate of 1 lb-moles/hr-ft^2. The separate responses of the total system for each of the three liquid phase flow conditions (0, 55, and 222 lb-moles/hr-ft^2), as well as the mock-up system response are shown in these figures. Similarly, the responses of runs at the nominal gas flow of 10 lb-moles/hr-ft^2 are given in Figures 16 and 19 while the amplitude ratio and phase shift data for the runs at a gas flow of 20 lb-moles/hr-ft^2 are shown in Figures 17 and 20.

The qualitative behavior the log amplitude ratio-log frequency plots (Figures 15, 16, and 17) is reasonable in all respects. It was to be expected that the amplitude ratio would decrease with increasing frequency in all cases; and, at fixed liquid phase flow and frequency, that the amplitude ratio would decrease with decreasing gas phase flow rate. This latter effect can be deduced from the inverse proportionality of residence time for the column gas phase to gas phase flow rate; or, in a general sense, the column time constant increases with decreased gas phase flow rate. Also, the observed decrease in amplitude ratio with increasing liquid phase flow rate, at fixed gas phase flow and frequency, can be reasoned from steady-state absorption theory which shows that the column gas phase outlet composition decreases as the

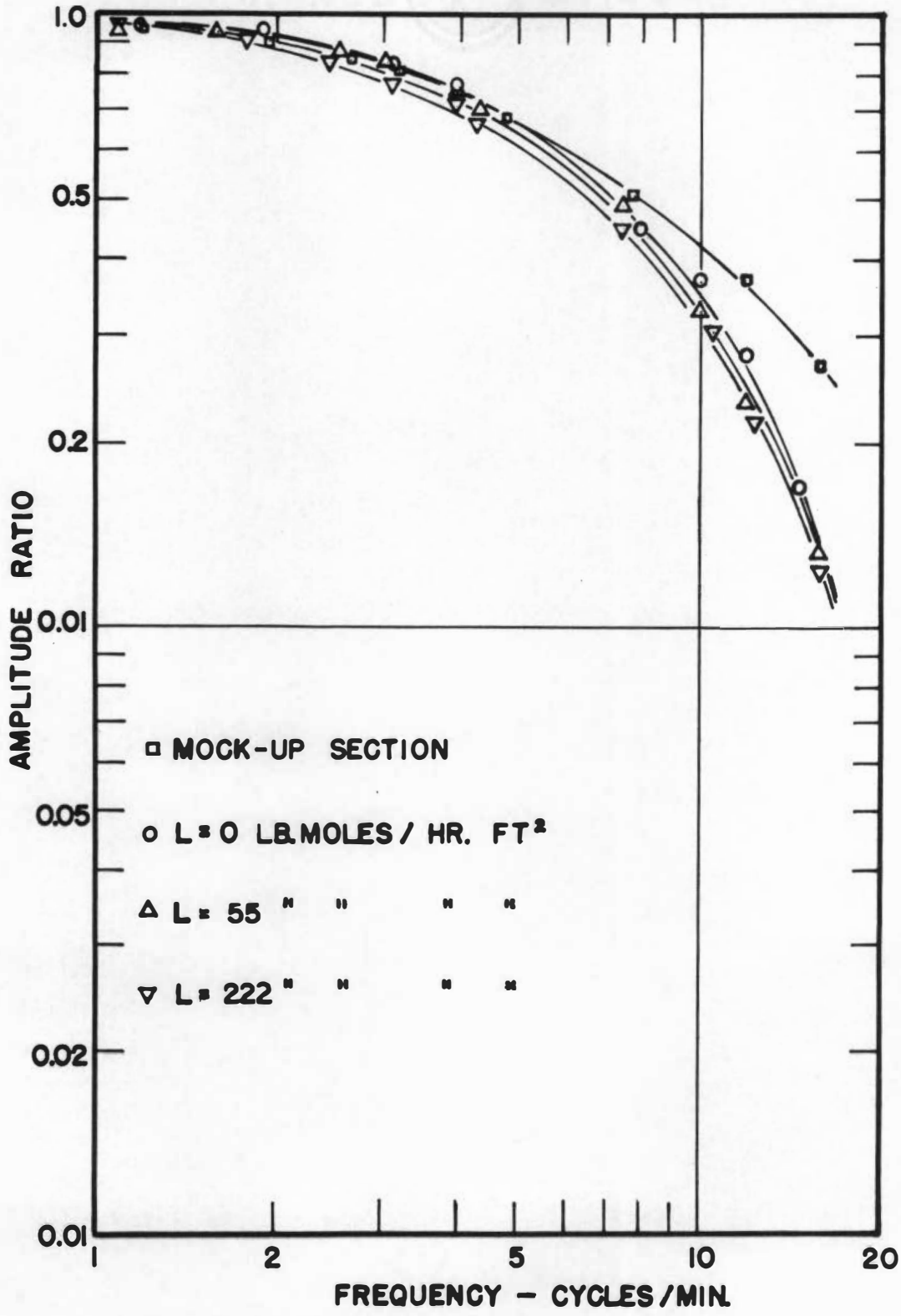


Figure 16. Total amplitude ratio vs. frequency, G=10 lb-mole/hr-ft^2.

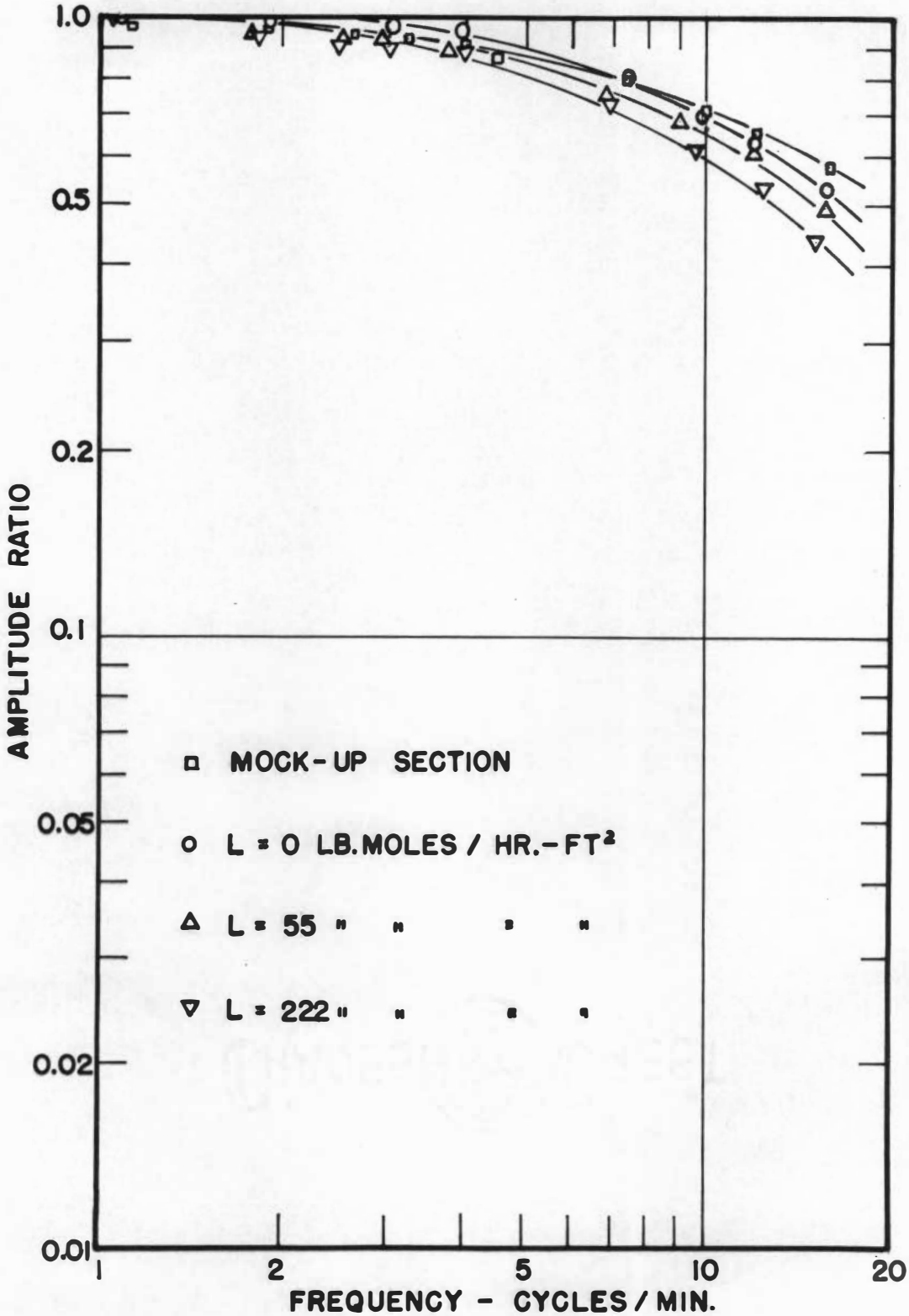


Figure 17. Total amplitude ratio vs. frequency, G=20 lb-mole/hr-ft^2.

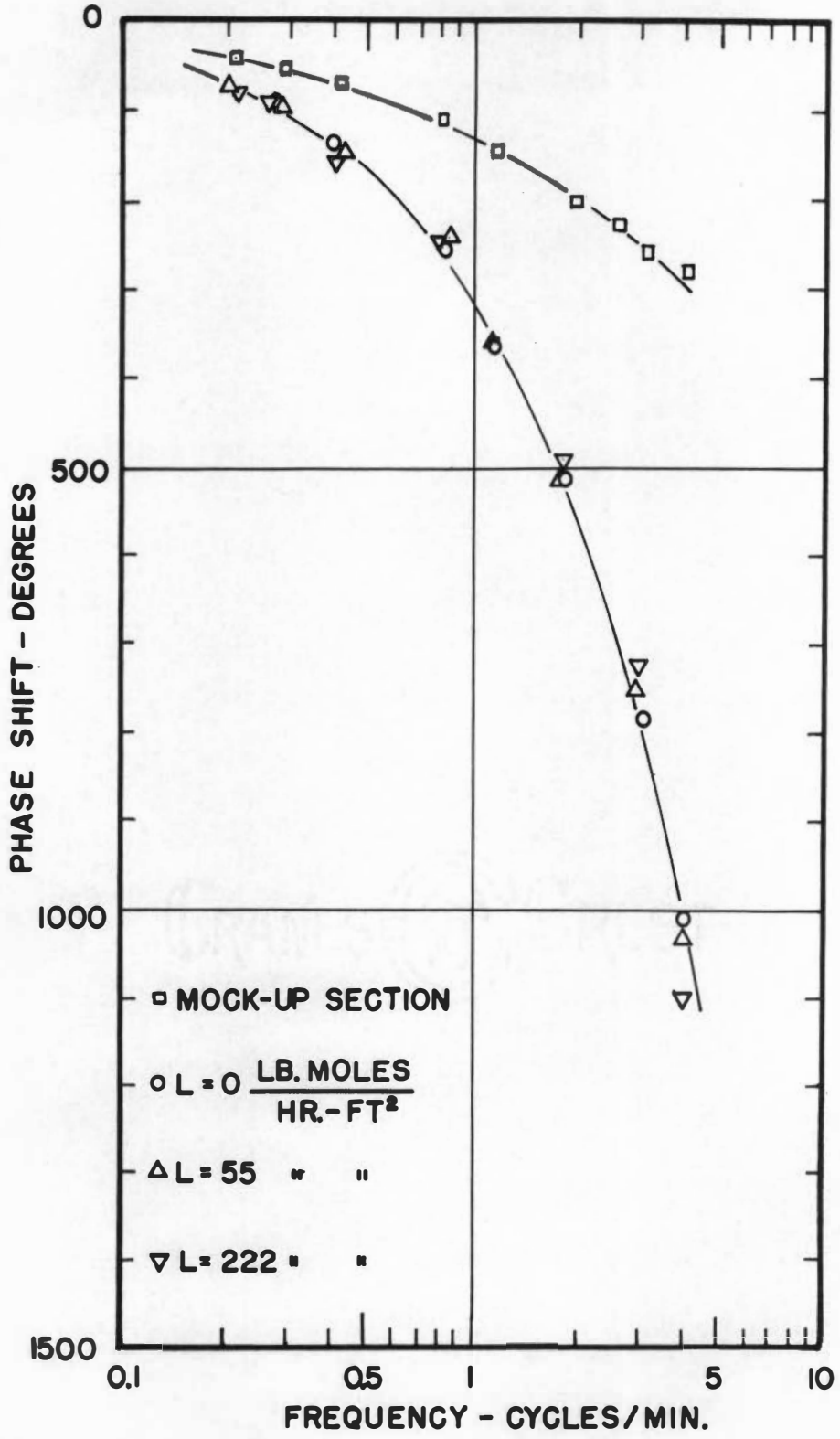


Figure 18. Total phase shift vs. frequency, G=1 lb-mole/hr-ft^2.

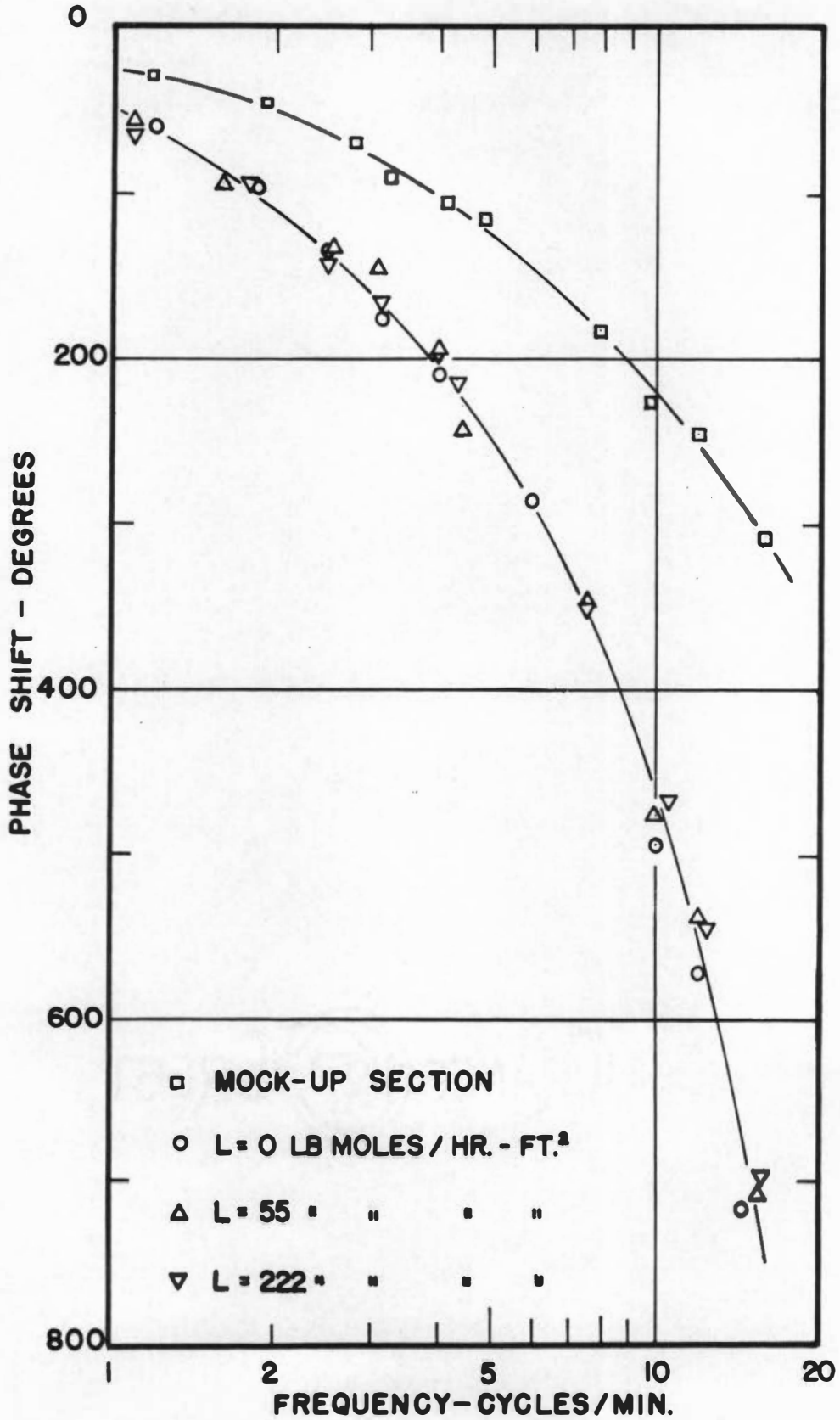


Figure 19. Total phase shift vs. frequency, G=10 lb-mole/hr-ft^2.

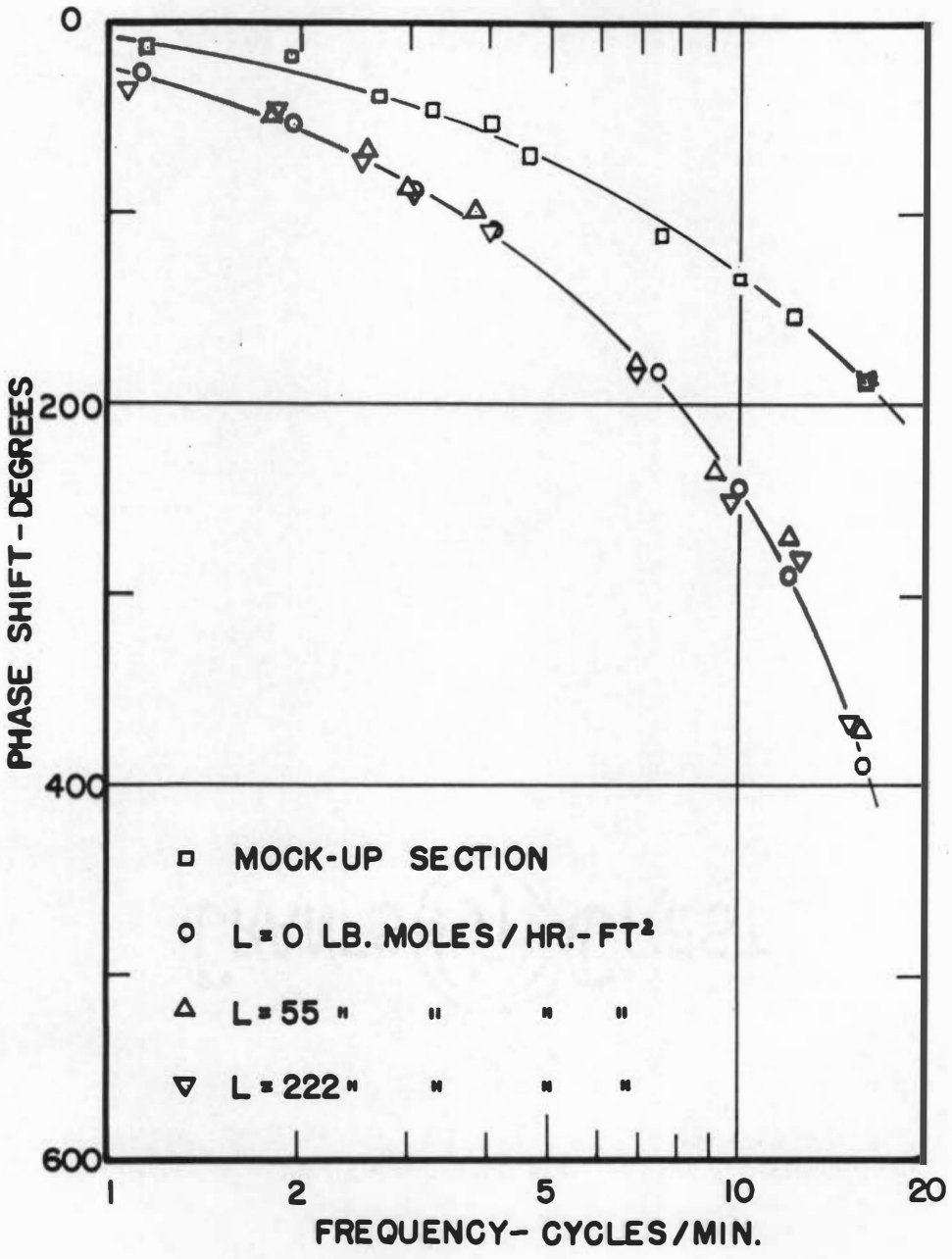


Figure 20. Total phase shift vs. frequency, G=20 lb-mole/hr-ft^2.

L/G ratio increases.

Since the mock-up system does not include the packing section (see Figure 10), it was significantly smaller than the total column and the amplitude ratio for any frequency should be greater than that for the total system operating at the same gas phase flow rate. This is seen from Figures 15, 16, and 17, for all runs made at gas flows of 1 and 10 lb-moles/hr-ft^2 and for the absorption runs at G=20 lb-moles/hr-ft^2. Figure 17, however, shows that the dry packing amplitude ratio for G-20 lb-moles/hr-ft^2 was greater than the mock-up amplitude ratio. A careful check of the original data verified this situation and also indicated that the discrepancy could not be wholly attributed to experimental error. Since the data for the dry packing column were disproportionately higher than those of the absorption system, there was reason to suspect that amplitude ratios for the dry packing were in error, particularly at the lower frequencies. A possible explanation for this anomaly is that the gas phase flow rate gradually increased throughout the duration of the dry packing run--the run was started at the high frequency end of the spectrum. An increase of approximately 15 per cent could account for the observed discrepancy at the lower frequencies. This increase is within the range of flow rate changes which were occasionally observed and corrected during operation.

The experimentally measured phase shifts for the three gas phase flows considered in this work are shown in Figures 18, 19, and 20. These data are also reasonable in that, in all cases, the phase shift increases with increased sinusoid frequency, ω. In the case of the phase shifts, the effects of liquid phase flow rate changes were considerably less noticeable. This was reasonable since, at a constant gas phase flow rate, the average gas phase residence time would be approximately constant. It would vary only as the changing liquid phase flow affected the bed void volume through changes in liquid hold-up. Thus, increasing the liquid phase flow rate resulted in small increases in liquid hold-up (see Figure G-1, Appendix G), which caused the void volume and, correspondingly, the average residence time and phase shift to decrease. Although some scatter in the phase shift data was observed, particularly for the gas phase flow rate of 1 lb-mole/hr-ft^2 where the phase shifts were quite large, the general effect of decreased phase shift with increasing liquid phase flow rate can be noted.

The phase shift data for the mock-up system shown in Figures 18, 19, and 20 indicate considerably smaller values than those of the total column at the same frequency. This was to be expected since the average residence time of the mock-up system was obviously much smaller than the average residence time in the full column system.

It can be noted, from the amplitude ratio and phase shift data of the inlet-outlet mock-up, that a significant amount of the total system response was associated with the column inlet and outlet section, the thermal conductivity cells, and the sampling lines. Since the thermal conductivity cells were geometrically identical and had the same measured time constants (see Appendix D), it was reasonable to assume that they possessed similar transfer functions. Thus, by Equation 95, since $G_{oc} \cong G_{ic}$, the data of the mock-up tests represented the combined responses of only the column inlet and outlet section. Since the amplitude ratios of the mock-up data represent a much greater proportion of the total system amplitude ratios than do the mock-up phase shifts of the total system phase shift data, it can be concluded that the inlet and outlet sections caused the gas phase to be rather well mixed but without significant time delay. Most of this effect probably occurred at the inlet section where the gas phase made a 90 degree change in direction which suggests that a relocation of the inlet cell sampling line closer to the inlet of the packing section might eliminate a great deal of the inlet effects.

In an effort to check the reproducibility of the experimental data, Run 2 (G=1 lb-mole/hr-ft^2, L=222 lb-mole/hr-ft^2) was repeated under conditions as similar as were possible to obtain except for the inlet gas phase mean concen-

tration, which was intentionally increased from 9 to 15 mole per cent. From the theoretical considerations of Chapter II, such a change in the mean concentration of the gas phase should not have altered the frequency response of the system if all the other variables remain constant. The amplitude ratio and phase shift data for this second test are shown in Figures 21 and 22, respectively. As can be seen, the agreement between the two runs was in general very good, with some slight scatter occurring at the highest frequencies.

III. EXPERIMENTAL AND THEORETICAL PACKING SECTION RESPONSES

The frequency response of the packing section alone was determined from the Bode plots of the total system and inlet-outlet mock-up responses by the method discussed earlier in this chapter. The linear vertical distances between the total system curves at any frequency were obtained graphically with dividers and transferred to a separate Bode plot of similar scale. This process, which is described in more detail in Appendix G, was carried out for all the runs. The experimental results are shown as a series of points, the locus of which represents the response of the packing section alone. These points do not necessarily occur at the same frequencies as the original data since they are obtained from the response curves drawn through the original experi-

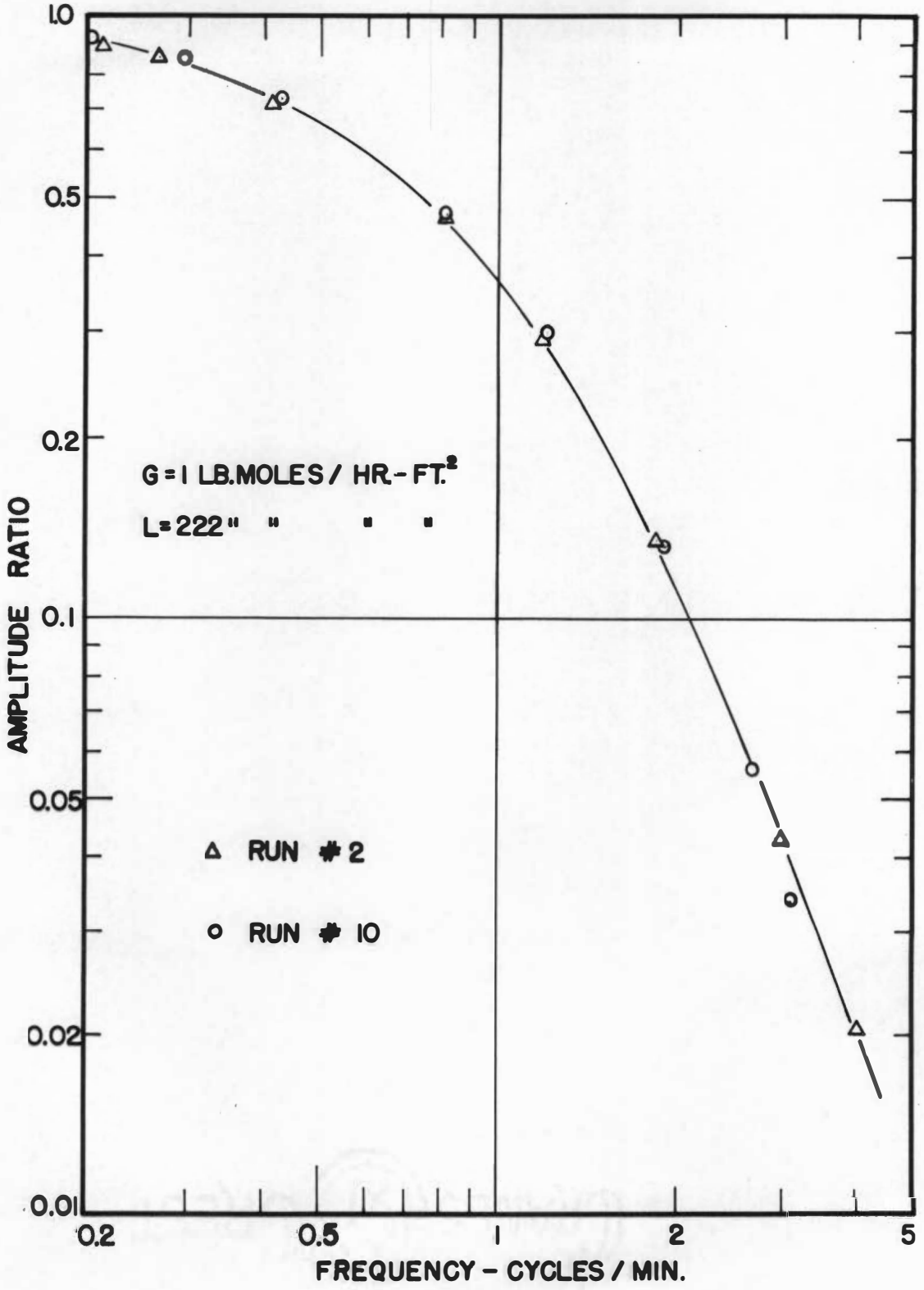


Figure 21. Total amplitude ratio reproducibility.

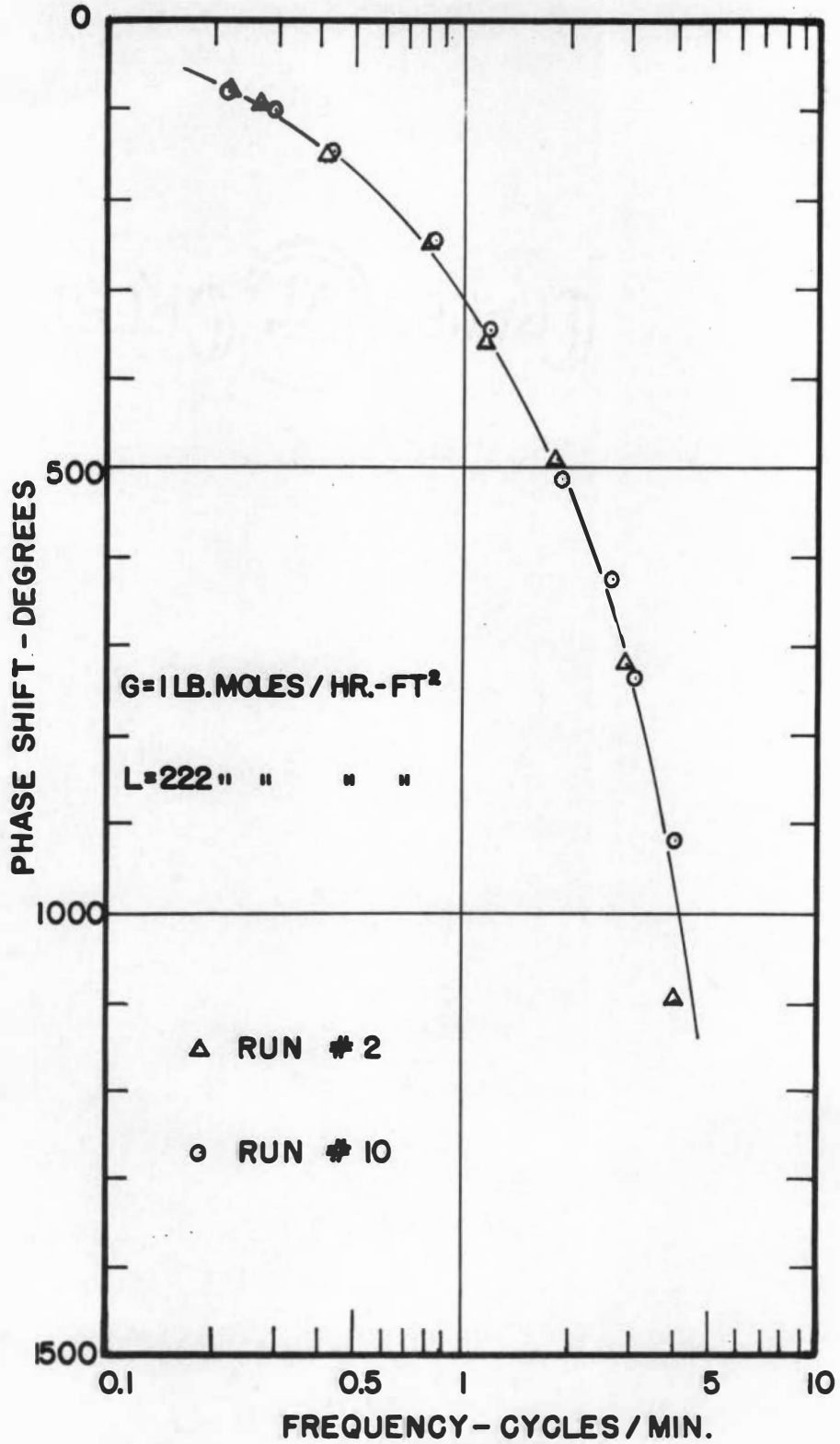


Figure 22. Total phase shift reproducibility.

mentally measured responses. This method of representing the experimental data was used to provide a clear distinction between it and the theoretical curves.

The packing section amplitude ratio spectrum for the absorption runs at G=1 lb-mole/hr-ft^2 is given in Figure 23, and the dry packing amplitude ratio (no absorption or L=0), is also shown in Figure 23. The phase shift data for these respective conditions are given in Figures 24 and 25. The packing section amplitude ratios and phase shifts for the nominal gas phase flow of 10 lb-moles/hr-ft^2 are presented in Figure 26 and Figures 27 and 28, respectively. Figure 29 shows the absorption and dry packing amplitude ratio data for the flow G=20 lb-moles/hr-ft^2 while the phase shift data, for this gas phase flow, are given in Figures 30 and 31.

The amplitude ratio data for dry packing at G=20 lb-moles/hr-ft^2, as shown in Figure 30, were obtained by arbitrarily lowering the total system data for the run to an estimated reasonable value based on the total system absorption amplitude ratios. Thus, the curve of Figure 30 is completely artificial although it represents, in all probability, a good approximation to the actual packing section amplitude response at the indicated gas flow.

The development of the theoretical frequency response equations for the three flow models considered in this work is given in Chapter II and Appendices A and B. Illustrated

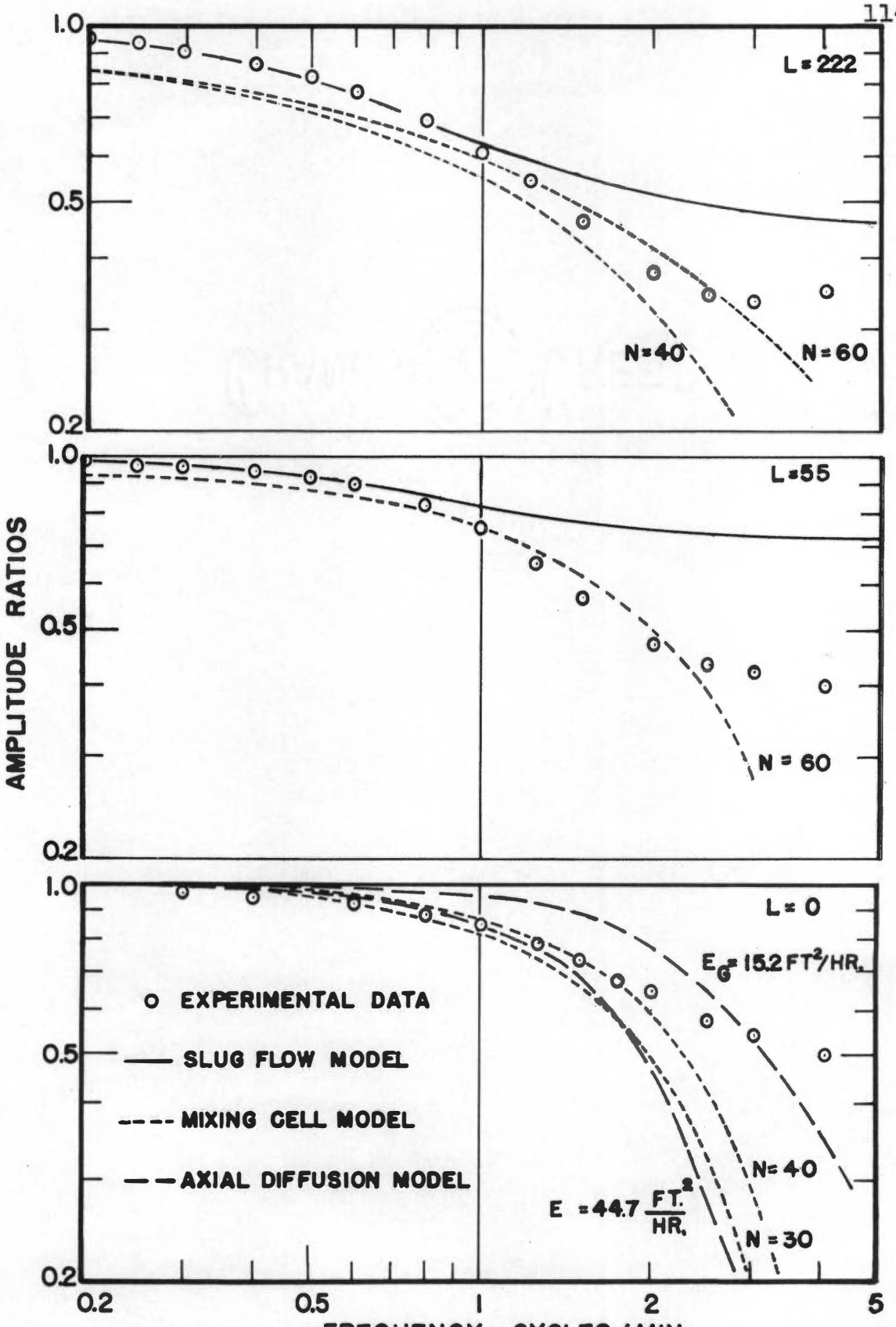


Figure 23. Packing section amplitude ratio, $\dot{G}$=1 lb-mole/hr-ft^2.

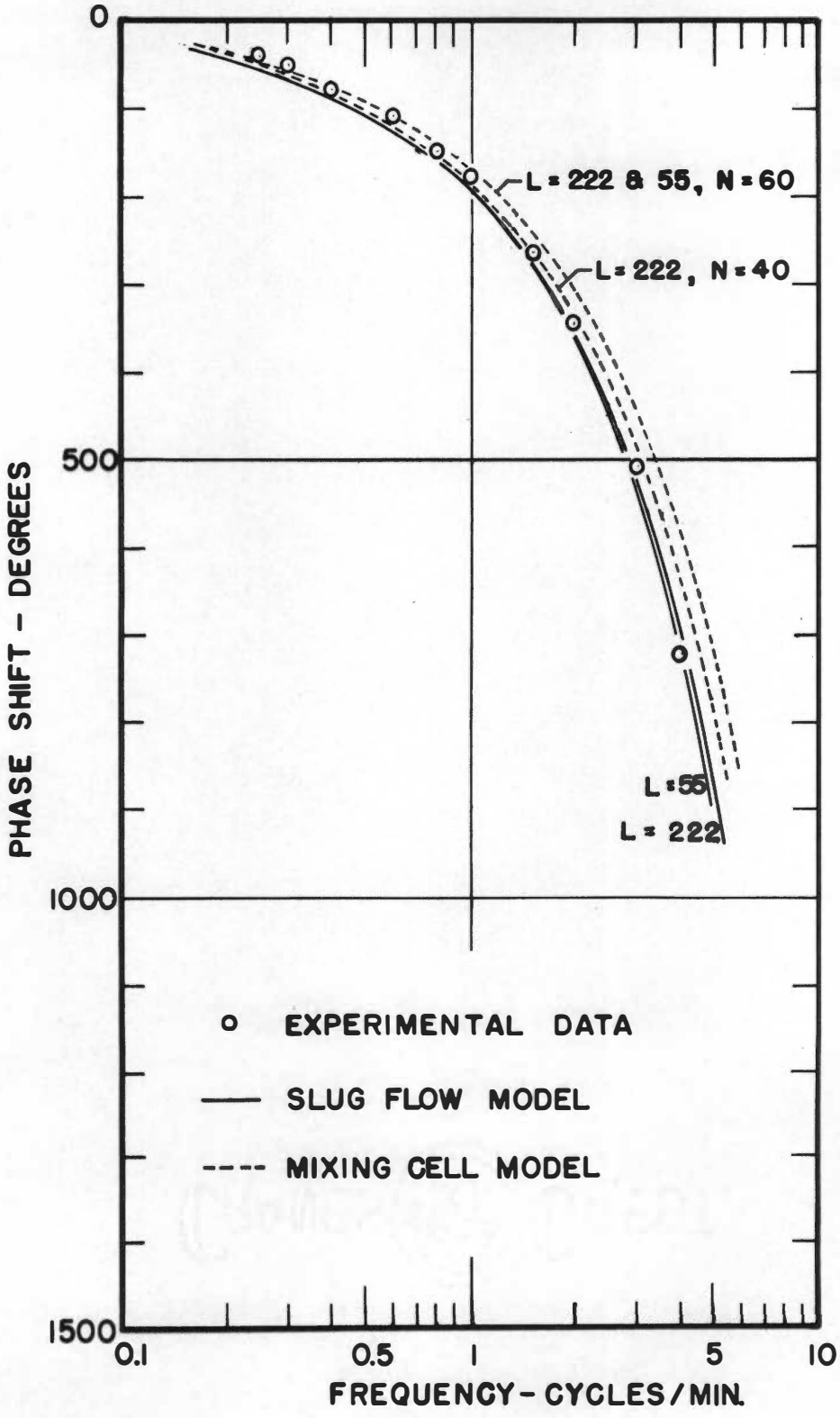


Figure 24. Packing section phase shift - absorption, G=1 lb-mole/hr-ft^2.

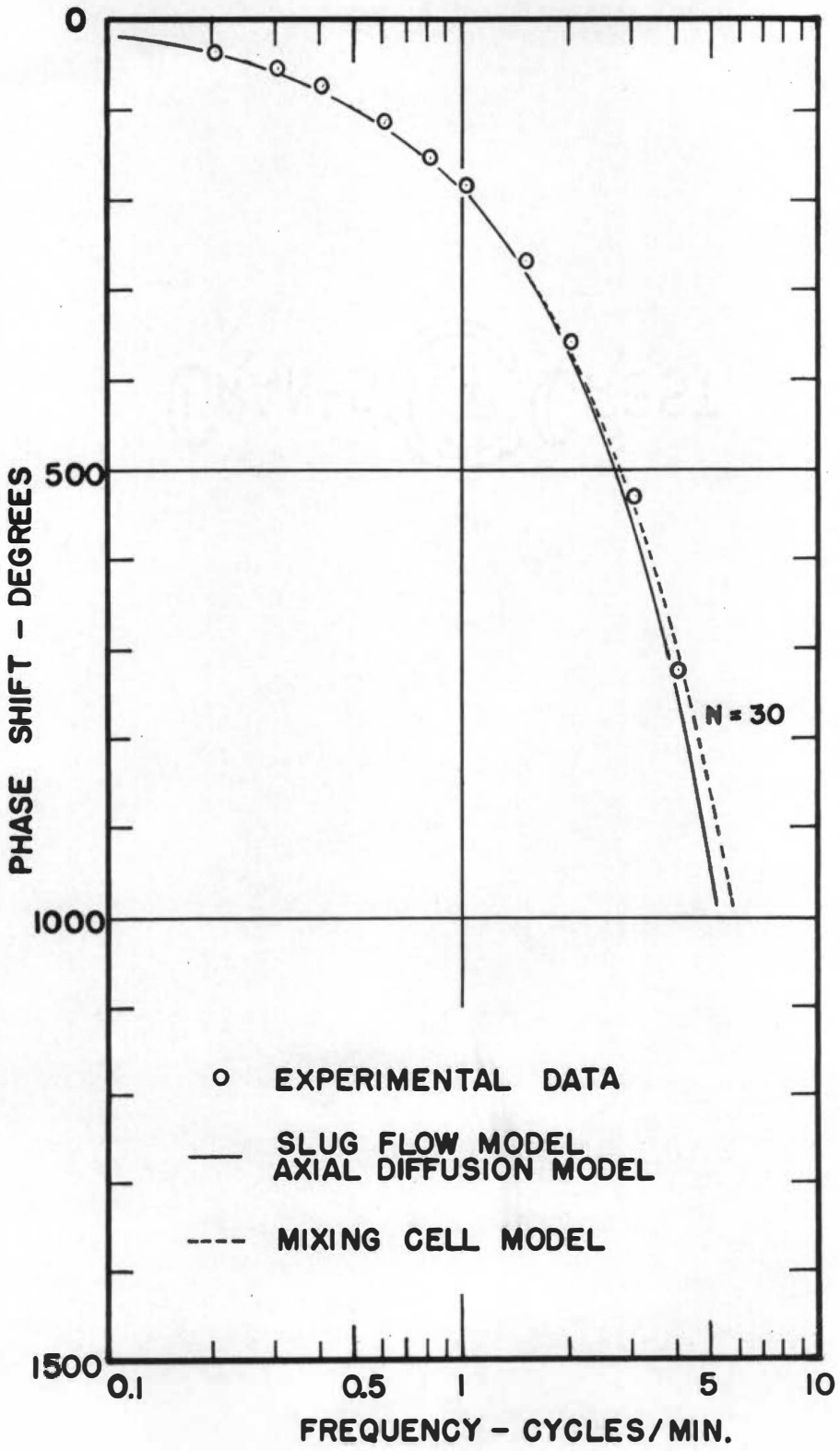


Figure 25. Packing section phase shift - no absorption, G=1 lb-mole/hr-ft^2.

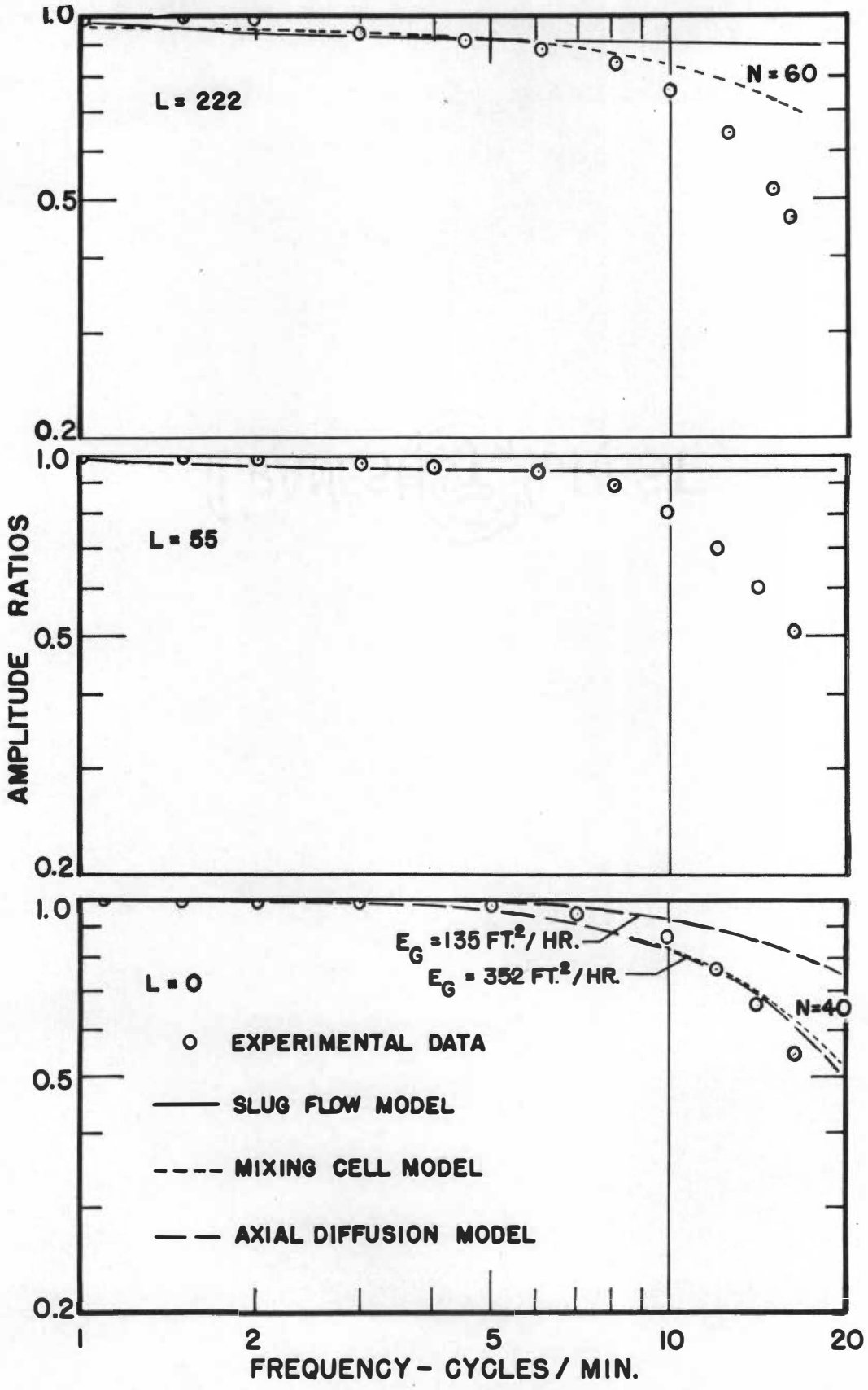


Figure 26. Packing section amplitude ratio, G=10 lb-mole/hr-ft^2.

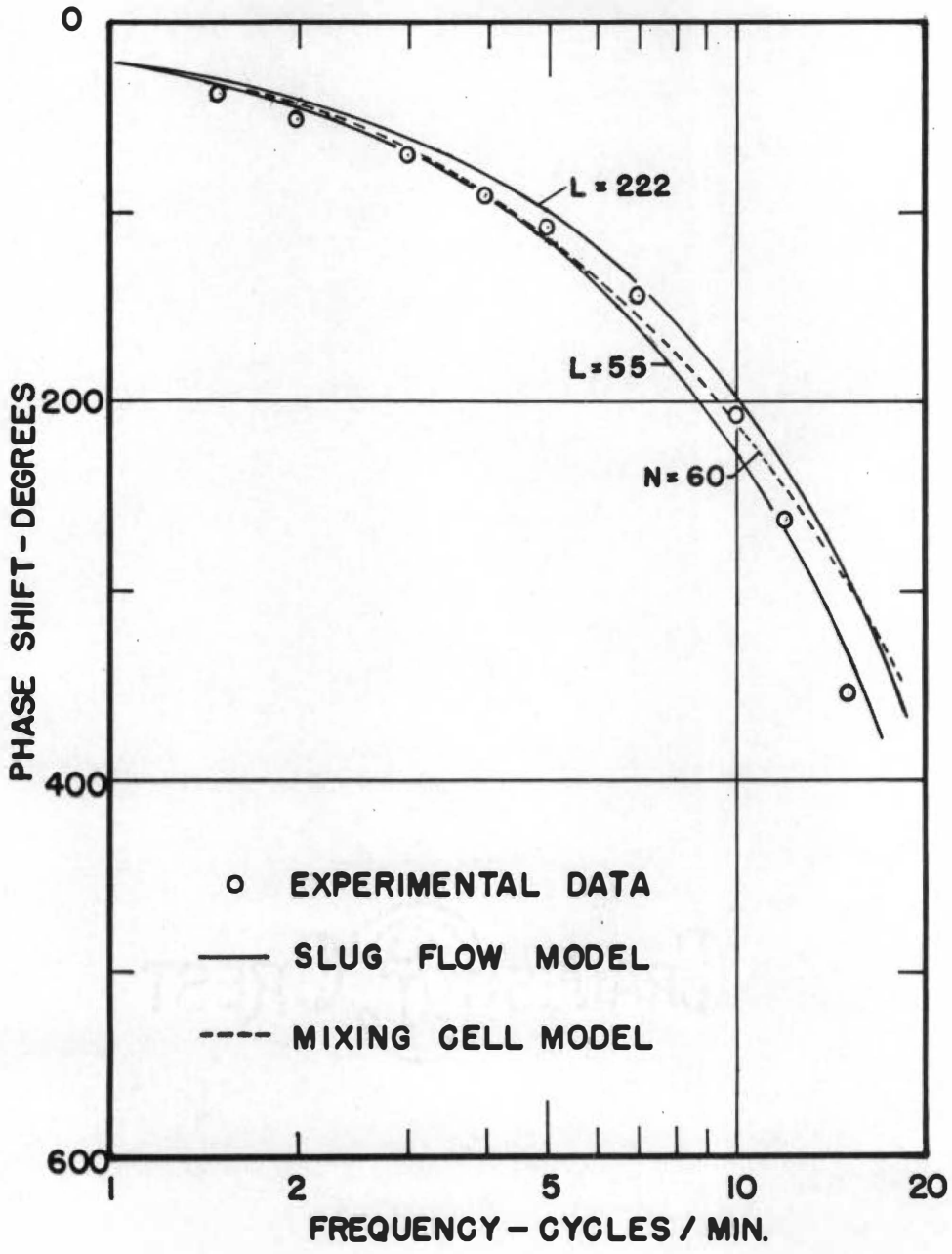


Figure 27. Packing section phase shift - absorption, G=10 lb-mole/hr-ft^2.

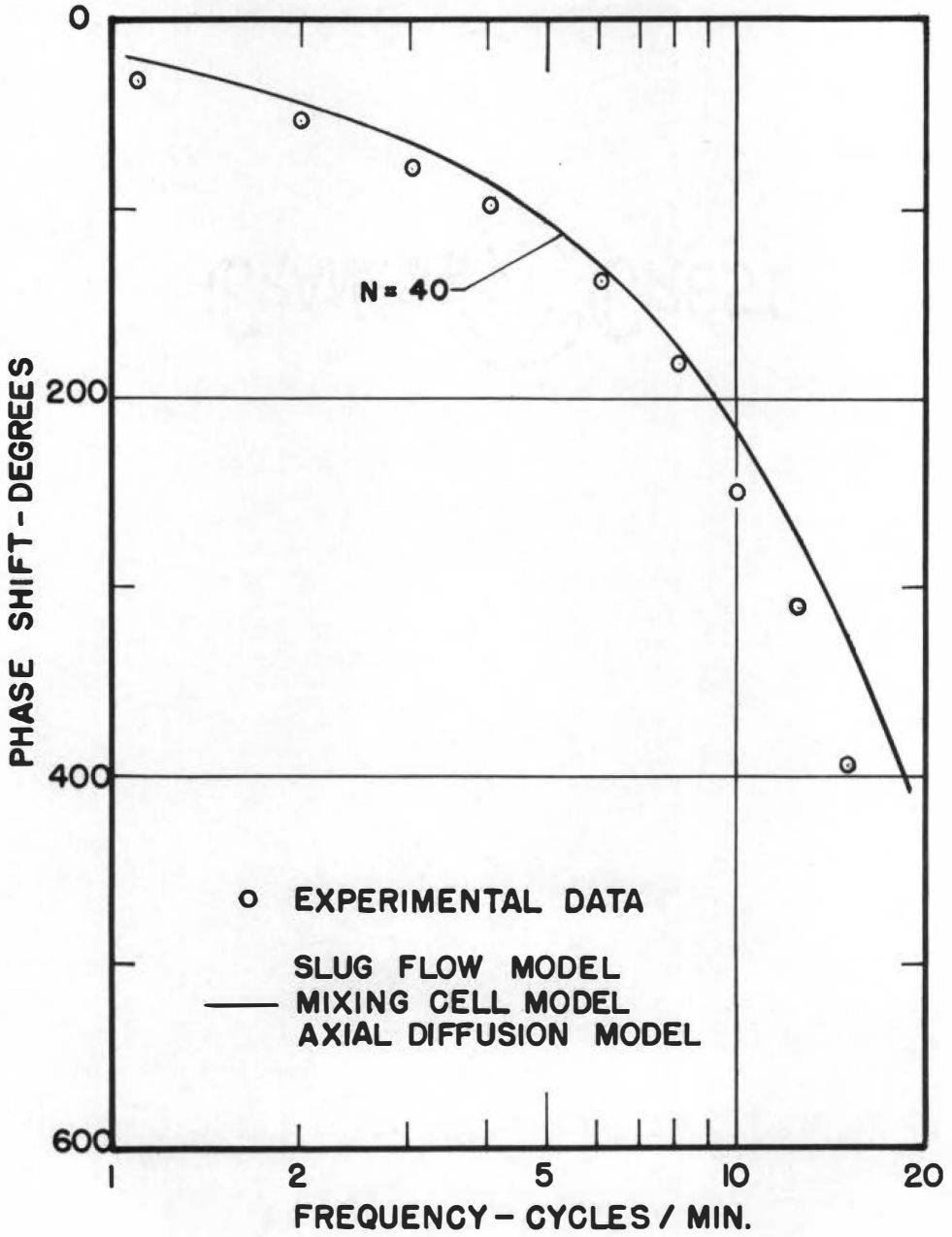


Figure 28. Packing section phase shift - no absorption, G=10 lb-mole/hr-ft^2.

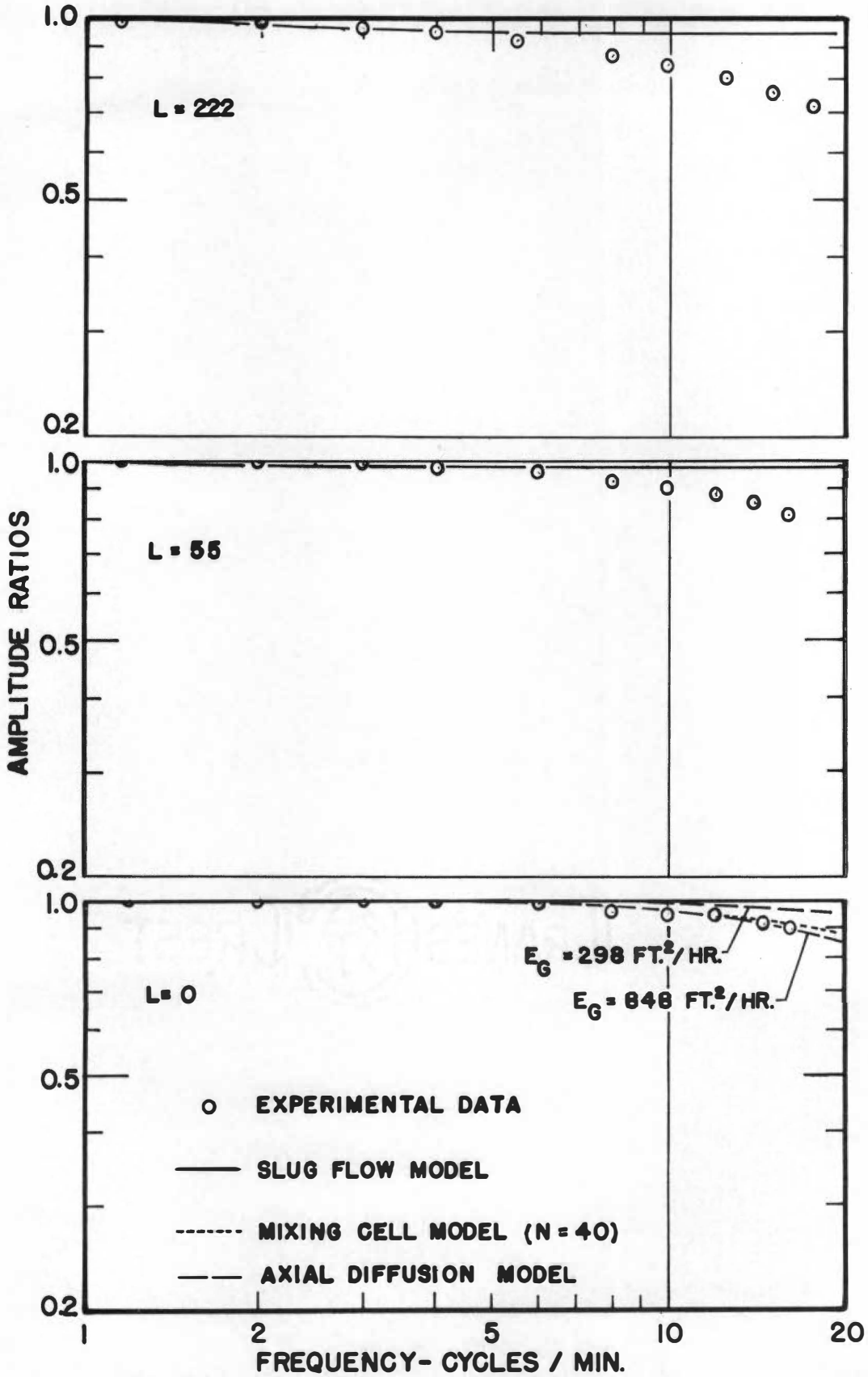


Figure 29. Packing section amplitude ratio, G=20 lb-mole/hr-ft^2.

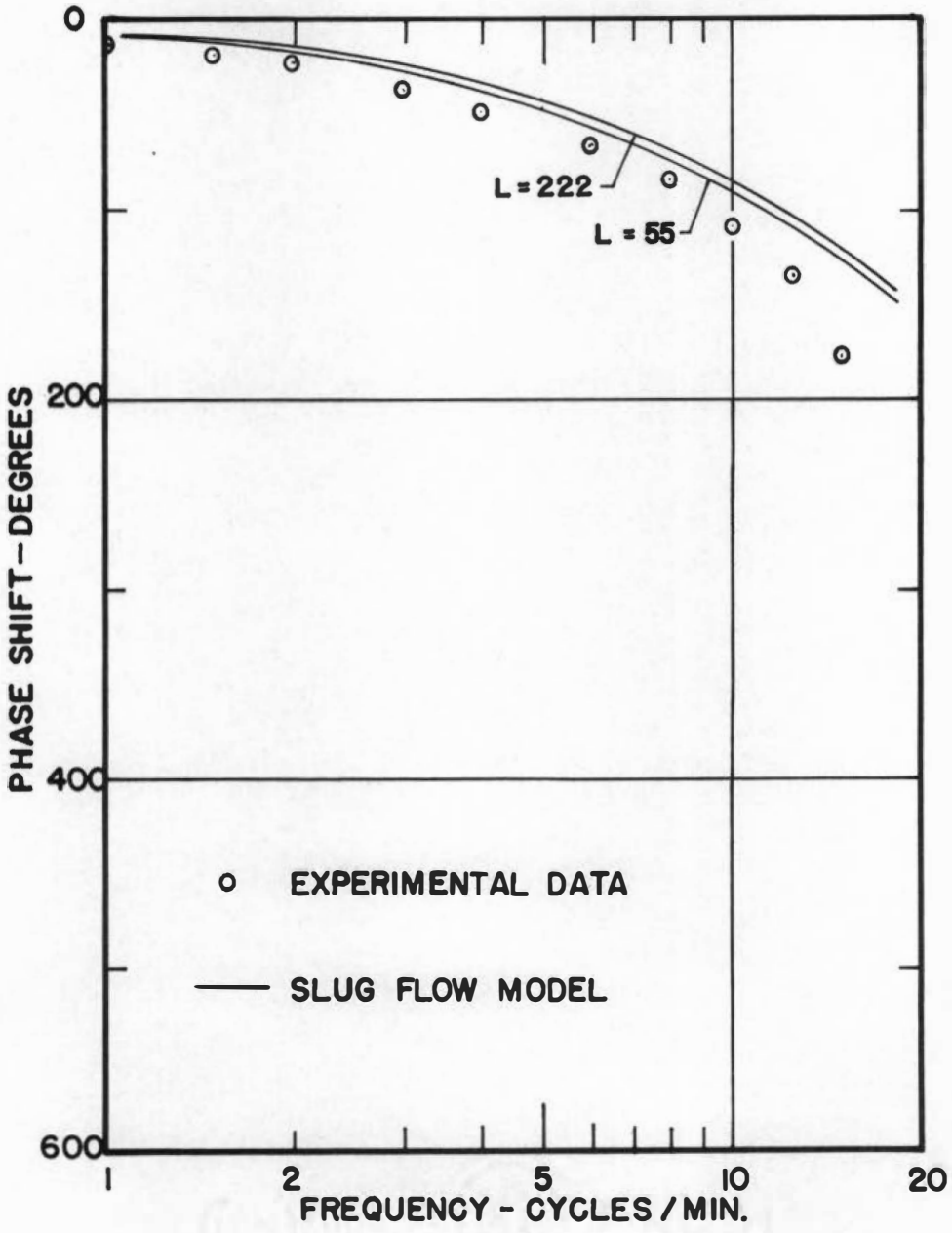


Figure 30. Packing section phase shift - absorption, G=20 lb-mole/hr-ft^2.

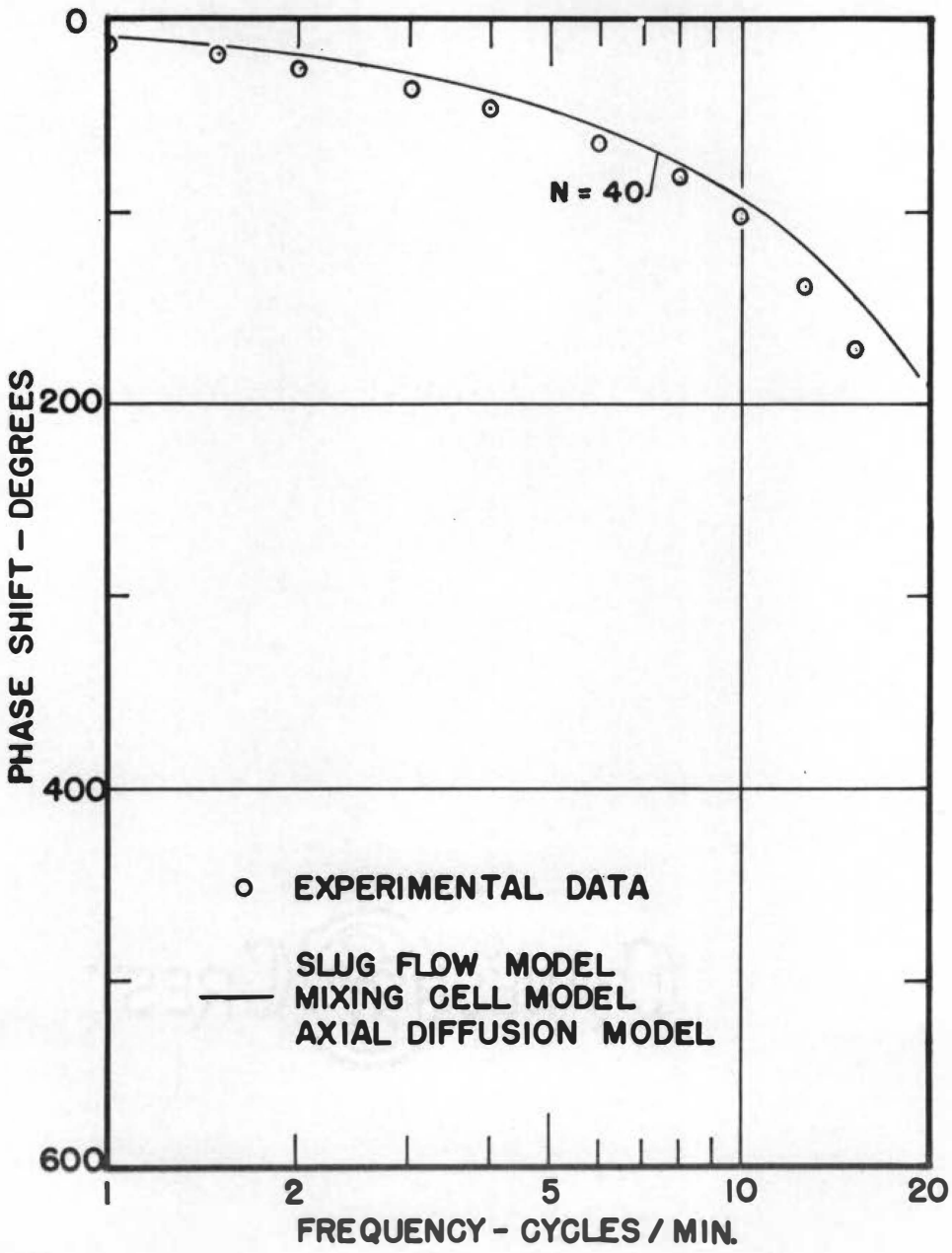


Figure 31. Packing section phase shift - no absorption, G=20 lb-mole/hr-ft^2.

examples of the amplitude ratio and phase angle calculations are presented in Appendix G. From these calculations and the developments of Chapter II, it can be seen that any response calculation requires knowledge not only of the gas and liquid phase flow rates but also of the gas and liquid phase holdups, the mass transfer coefficients, $k_L a$, and the slope of the equilibrium line, m. The values of these properties used in the theoretical amplitude ratio and phase shift calculations were taken from the most reliable data available in the literature and from porosity measurements made on the packing section of the experimental column. A detailed discussion of the data obtained for the theoretical calculations and of their sources is given in Appendix G.

The results of the calculation of the theoretical amplitude ratios and phase shifts, for the three general models discussed in Chapter II, are shown in the same figures used to demonstrate the experimentally measured frequency responses (Figures 23 through 31). These calculated values will be discussed in order of increasing nominal gas flow rate.

Nominal Gas Flow Equal 1 lb-mole/hr-ft^2

Two phase countercurrent flow with absorption. Figure 23 shows the theoretical amplitude ratio for the slug flow and the mixing-cell models in the case of absorption with

G=1 lb-mole/hr-ft^2. As can be seen, the slug flow amplitude ratios approach the constant values given by Equation 32 as the frequency becomes large. This limiting of the theoretical amplitude ratio has also been demonstrated by Cohen and Johnson (23) in their studies of the dynamics of double-pipe heat exchangers. Apparently, this type of response is a characteristic of distributed systems under slug-flow conditions where the inlet and outlet signals of the system transfer function represent conditions of the same phase or flow stream.

In this work the theoretical values of the asymptotes are 0.435 and 0.714 for the liquid phase flows of 222 and 55 lb-moles/hr-ft^2, respectively. The change of the limiting amplitude ratio with changing liquid phase flow is due to the variation of the mass transfer coefficient, $k_L a$, with changing liquid flow (see Figure G-3, Appendix G).

While the theoretical amplitude ratio, for the slug-flow model, agrees well with the experimentally measured amplitude ratios at frequencies below 1 cycle per minute, the experimental values fall considerably below the theoretical curve at higher frequencies. Still there appears to be a definite flattening of the experimental curves for both liquid flows at frequencies above 2 cycles per minute.

The theoretical amplitude ratio curves for the mixing-cell model are also shown in Figure 23. The response of a

40 cell and a 60 cell cascade are given for the liquid flow of 222 lb-moles/hr-ft^2 and of a 60 cell cascade with a liquid flow of 55 lb-moles/hr-ft^2. As can be seen, the agreement between the experimental and theoretical amplitude ratios for this model was poor for both values of the number of mixing cells per cascade, N. It is interesting to note the relative position of the theoretical curve for N=60 in the case of L=55 lb-moles/hr-ft^2 as compared to that at the flow of L=222 lb-moles/hr-ft^2. While the theoretical curves do not agree well with the experimental data, their positions with respect to the experimental amplitude ratios in each case were approximately the same.

The theoretical phase shifts are shown in Figure 24 for both flow-models and all liquid phase flow and cascade conditions. The experimental data are plotted as a single curve since, as can be seen in Figure 16, separation according to liquid phase flow would be difficult and unnecessary. Both models give relatively similar phase shift responses which agree approximately with the observed data. This is reasonable when it is remembered that the analyses of Chapter II force each model to have approximately similar mean residence times, i.e., that of the packing section under the existing operating conditions. It can be noted that the slug-flow model agrees with the observed phase shift slightly better at the higher frequencies while the mixing-cell model

(N=40), better describes the experimental data at the lower frequencies ($\omega < 1$ cpm). This is counter to the tendency observed for the amplitude ratios.

The theoretical responses for the axial diffusion model are not given since, as discussed in Chapter II, an analytical solution for the absorption system was not possible.

Single phase flow without absorption. Figure 23 shows the theoretical amplitude ratios for the dry packing response (no absorption or L=0), at G=1 lb-mole/hr-ft^2 for the slug flow, mixing-cell, and axial diffusion models. Mixing-cell model curves are given for two values of the number of cells per cascade or column (N=30 and N=40). The axial diffusion curves are shown for two values of the axial eddy diffusivity, i.e., E_G=15.2 ft^2/hr (Peclet number $\frac{D_p U}{E_G}$ = 2.0) and E_G=44.7 ft^2/hr (Peclet number = 0.68). The agreement between the theoretical and the experimental amplitude ratios at the high frequencies is poor for all models.

The value of E_G=15.2 ft^2/hr was calculated from the data of McHenry and Wilhelm (67) for an experimental Reynolds number of 32. These authors tested the validity of the axial diffusion model for a 2-inch column of randomly packed 1/8-inch spheres over a Reynolds number range of 10 to 400. As can be seen, the theoretical amplitude ratio spectrum for this value of the axial dispersion coefficient was

in strong disagreement with the experimental data.

It is of interest to note the similarity of the theoretical amplitude ratio responses for the axial diffusion and the mixing cell models. Thus, the curve for the axial diffusion model for E_G=44.7 ft^2/hr, in Figure 23, lies very close to that for the mixing cell model with N=30. This similarity of the two models for long beds has been demonstrated from theoretical considerations by Kramers and Alberda (59) and by Aris and Amundson (7).

The theoretical phase angle results for this system are shown in Figure 25. By comparing Equations 42 and B40 it can be seen that the phase angle approximation for the axial diffusion model is identical to the exact relationship for the slug-flow model. Thus, a single curve in Figure 25 represented both these models. The mixing-cell model phase shift was also similar, due to, as in the absorption system, the similarity of the packing section mean residence time. The agreement between the theoretical and experimental phase shift for the gas phase flow of 1 lb-mole/hr-ft^2 was excellent.

Nominal Gas Flow Equal 10 lb-moles/hr-ft^2

Two phase countercurrent flow with absorption. The theoretical amplitude ratios for the slug-flow and mixing-cell models at a gas phase flow of 10 lb-moles/hr-ft^2 are

shown in Figure 26. The high frequency asymptotes of the slug-flow model for this gas flow are 0.904 and 0.956 for the liquid flows of 222 and 55 lb-moles/hr-ft^2, respectively. These high values and the flat response curves result from the substantial reduction of the exponent of e in Equation 32.

The response for the mixing-cell model was calculated for only the higher liquid flow rate since little additional information could be gained from the results of the extremely tedious calculation necessary to obtain a second curve. As in the case of the previous flow rate, the agreement between experimental and theoretical amplitude ratios is poor for both the mixing-cell model and the slug-flow model. In addition, the experimental amplitude ratio data deviate considerably more strongly from the theoretical calculations than did the similar data for the gas phase flow of 1 lb-mole/hr-ft^2.

The theoretical phase shift calculations for the slug-flow model at both liquid flow rates and for the mixing-cell model at L=222 lb-moles/hr-ft^2 are shown in Figure 27. The significant difference between the two curves of the slug-flow model, not observed in previous calculations, results more from the larger gas phase flow rate (7.4 vs. 6.8 lb-moles/hr-ft^2) used in the calculation of the higher liquid flow curve than from the variation of column hold-up with

liquid flow rate. These curves demonstrate the sensitivity of theoretical phase shift calculations to small changes in gas phase flow rate and point out the necessity for accurate and reproducible gas flow rate control. Unlike the low gas flow case, the mixing-cell model gave approximately the same phase shifts as the slug-flow model. The experimental data are again expressed as a single curve since Figure 19 does not clearly indicate separate responses.

Single phase flow without absorption. The theoretical amplitude ratios of the three flow models for the dry packing or non-absorption system are shown in Figure 26. Two values of the axial eddy-diffusivity were used to obtain these curves-- E_G=135 ft^2/hr (Peclet number = $\frac{D_p U}{E_G}$ = 2) and E_G=352 ft^2/hr (Peclet number = 0.77). The former value was obtained from the data of McHenry and Wilhelm (67) for the experimental Reynolds number of 280 while the latter was arbitrarily chosen in an attempt to fit the experimental amplitude ratio spectrum. Coincidentally, the theoretical amplitude ratio for the mixing-cell model (N=40) was almost identical to that of the axial diffusion model (E_G=352 ft^2/hr), for the frequency range of the experimental data.

The agreement between theory and experiment was, in general, poor particularly for the amplitude ratios calculated with the data of McHenry and Wilhelm. As in the low gas flow case (G=1 lb-mole/hr-ft^2), the experimental data

fall considerably below the E_G=135 ft^2/hr curve, thus indicating a higher degree of mixing than was observed by these authors.

The theoretical phase shift calculations for the three flow models at the flow G=10 lb-moles/hr-ft^2 were given by a single curve, as can be seen in Figure 28. The axial diffusion and slug-flow models agreed because of the similarity of Equations 42 and B40. The mixing-cell model was also similar because, by Equations 75 and 76, the responses of this model approach those of the slug-flow model as the number of mixing cells per cascade or column becomes large.

Although the agreement between the theoretical and experimental phase shifts appears to be less satisfactory than in previous cases, a comparison of this figure with Figure 25 will show that this effect is due to a doubling of the ordinate scale and that the absolute deviation between theory and experiment is approximately the same in each case.

Nominal Gas Flow Equal 20 lb-moles/hr-ft^2

Two phase countercurrent flow with absorption. The theoretical amplitude ratios for the slug-flow model with absorption at G=20 lb-moles/hr-ft^2 are compared with the experimental values observed at similar operating conditions in Figure 29. The theoretical curves are extremely flat with asymptotes of 0.959 and 0.983 for the liquid flows of

222 and 55 lb-moles/hr-ft^2, respectively. The theoretical mixing-cell amplitude ratios were not calculated for this gas phase flow rate since the experimental data were too limited to warrant the extensive calculations which would have been required. The small variation of the amplitude ratios measured at this gas flow resulted from approach to the maximum frequency of the sinusoid generator (16 cpm).

Again, at the higher frequencies, the experimental amplitude ratios fell considerably below the theoretical curves for the slug-flow model.

Figure 30 shows the theoretical phase shift calculations for the slug-flow model at G=20 lb-moles/hr-ft^2. A single curve is presented to represent the experimental data for the same reasons as in the previous flow rates. Although the absolute deviations are not large, the experimental data fall consistently lower than the theoretical curve due, in all probability, to a small error in gas phase flow rate measurement.

Single phase flow without absorption. The theoretical dry packing amplitude ratios at G=20 lb-moles/hr-ft^2 for the axial diffusion model (E=298 ft^2/hr - Peclet number = 2 and E=848 ft^2/hr - Peclet number = 0.71) and the mixing-cell model (N=40) are given in Figure 29. The axial diffusion response curve for E=848 ft^2/hr (Peclet number = 0.71) resulted from an attempt to fit the data with this model. The curve for

E=298 ft^2/hr (Peclet number = 2) was not calculated from the data of McHenry and Wilhelm as in the previous cases, since these authors did not measure axial eddy diffusivities at Reynolds numbers as high as existed in the column at this gas phase flow rate (Reynolds number = 620). The curve was included only for comparison purposes.

Since the range of the experimental amplitude ratios at this gas flow rate was quite limited, no specific statement of agreement can be made except that the response curve for the greater axial-eddy diffusivity appears to represent the experimental results more closely.

Figure 31 shows the theoretical phase shift calculations for the slug-flow model at G=20 lb-moles/$hr\text{-}ft^2$. As in the absorption runs at this flow rate, the experimental phase shifts fell slightly below the theoretical calculations, again, possibly due to a small error in gas flow rate measurement. An error of approximately 10 per cent on the high side could account for the observed differences.

IV. DISCUSSION

At the conclusion of this presentation of the experimental and theoretical results, several general observations can be made concerning the absorption and non-absorption runs.

Axial Mixing

The experimental amplitude ratio data shown in Figures 23, 26, and 29 clearly indicate that the slug-flow model is not completely satisfactory in describing the dynamics of the absorption process. It is not surprising that the experimental data at the higher frequencies fall below the predicted values, since it is well known that the velocity profiles in packed beds such as used in this work are not flat but tend to peak near the walls of the column where there is some increase in the packing void fraction (17, 96). These non-uniform velocity profiles as well as the wakes and eddies formed by flow around the packing particles should effect some radial and axial mixing of the gas phase which, in turn, can influence the dynamic behavior of the bed (25, 37, 58). Thus it seems likely that the deviation of the experimental responses from the slug-flow theory is a manifestation of a radial and/or axial mixing phenomenon.

The idealistic--perhaps naive--attempt to describe this mixing action quantitatively by the mixing-cell model appears to be unsuccessful as Figures 23 and 26 indicate. The agreement between experiment and theory for this model was worse than that for the slug-flow model. In addition, from the relative position of the N=40 and N=60 curves in Figure 23, it appears that significant improvement of agreement would not result from a different choice of the

parameter, N.

The effects of gas phase mixing were even more apparent in the dry packing or non-absorption runs shown in Figures 23, 26, and 29. Here, the amplitude ratios deviated strongly from the response of the slug-flow model and, again, the attempts to describe the mixing process, i.e., the mixing cell model and the axial diffusion model, were not satisfactory, particularly at the low gas velocities. This poor agreement between experimental and theoretical responses based on the axial diffusion model substantiates similar conclusions by Kramers and Alberda (59) and Carberry and Bretton (20). On the other hand, McHenry and Wilhelm (67) and Eback and White (40) have found that the experimentally determined axial-diffusivity was independent of sinusoid frequency. Strang (108) apparently did not consider the possibility. The inapplicability of the axial diffusion model to single phase flow through packed beds could certainly explain the great variation of eddy diffusivities which have been reported in the literature (16).

It is interesting to note that, while the axial diffusion model did not seem appropriate, the best fit of the theoretical amplitude ratio response curve for this model to the experimental data resulted in values of the axial-eddy diffusivity which were consistently higher than those reported by McHenry and Wilhelm (67). In addition, these diffusivities

resulted in Peclet numbers which were not, in general, independent of Reynolds number as has been the case in previously reported work (67, 40, 108). Also the mixing-cell model, though equally poor in describing the experimental amplitude ratios over the complete frequency range, indicated that the best fit of the experimental data would not result in the same number of mixing-cells for all three gas phase flows. Thus, for the dry packing or non-absorption system, the relative degree of axial mixing seemed to increase somewhat with gas phase flow rate.

A similar effect can be seen in the absorption runs where the mixing-cell model for N=60 had approximately the same relative position with respect to the experimental data for both liquid flows at G=1 lb-mole/hr-ft^2 (see Figure 23), but the amplitude ratio response for G=10 (Figure 26) fell below the theoretical mixing-cell curve for N=60, thus indicating a greater relative degree of mixing for this gas flow rate.

Therefore, it would appear that the axial and/or radial transport of mass in countercurrent two phase flow in a packed bed is affected by some complex interaction of the liquid and gas phases. Jacques and Vermeulen (50) observed such complexities in their study of axial mixing in packed liquid-liquid extraction columns.

A comparison of the experimental amplitude ratio

responses at G=1 lb-moles/hr-ft^2 with the responses at the two higher gas flow rates for both the absorption and non-absorption runs indicate a subtle but consistent difference. While the curves at the low gas flow (Reynolds number $\cong$ 30) have a gradual slope with a distinct leveling tendency, the curves at the high gas flows (Reynolds number $\cong$ 300 and 600) break sharply downward and show no similar leveling. Although this apparent difference might be due to the lack of data at higher sinusoid frequencies for the high gas flow cases, it is possible that the distinction results from the existence of a different gas phase fluid dynamic state for the respective conditions. This explanation is consistent with the observations of Carberry and Bretton (20) who have noted changes in the correlations of both axial eddy diffusivities and friction factors in the Reynolds number range 100-300 and also with the data of Dorweiler and Fahien (37) who, in their studies of radial diffusion in a packed column, observed a strong variation in the radial Peclet number at Reynolds numbers from 10 to 50. Also, Jacques and Vermeulan (50) show a fourfold increase in the axial eddy-diffusivity in the transition region between laminar and turbulent flow of a single liquid phase in a packed bed of 0.65-inch Raschig rings (20 <Reynolds number > 200).

Effects of System Parameter on Theoretical Frequency Responses

Because of the complexity of the theoretical amplitude ratio and phase shift relationships (see Appendix B) it was quite difficult to assess the effects of uncertainties in the system's operational and physico-chemical parameters. The results of the variation of liquid and gas phase flow rates can be ascertained from the several cases which have been given in Figures 23 through 31. It is believed that the experimental errors in flow rate measurement would not effectively alter the theoretical responses shown in these figures. The effects of errors in the literature values of mass transfer coefficients, equilibrium data and liquid phase hold-ups, however, are more difficult to estimate.

The maximum relative experimental errors of the literature data used in the theoretical calculations of this work are estimated to be as follows: mass transfer coefficient, k_La, $\pm$10 per cent; slope of equilibrium line, m, $\pm$2 per cent; liquid phase hold-up, h_L, $\pm$5 per cent. Since the amplitude ratio for the slug-flow model, as the frequency, ω, approaches infinity, is $\exp(-Zk_La/Gm)$ (Equation 32), the error in the linear displacement of the ordinate on a Bode plot of this limiting amplitude ratio is the error in the term Zk_La/Gm. Also the inflection frequency, as can be seen from Equation 34, is directly propor-

tional to $k_L a$. Thus, considering the magnitude of the estimated errors in the mass transfer coefficients, etc., it appears that the relative positions of the amplitude ratio responses for the slug-flow model would not be shifted by more than 12 per cent by these errors.

Because of the complexity of the mixing-cell model theoretical response calculations, no general statements can be made concerning the effect of errors on this model.

Experimental Difficulties at Low Gas Flows

An experimental difficulty was encountered while the column was operated at the low gas phase flow rate (G=1 lb-mole/hr-ft^2) which caused a margin of uncertainty for the amplitude ratios and phase shifts measured at frequencies above 2 cycles per minute. When operating at the low gas phase flow rate approximately two-thirds of the output cell concentration wave behaved in an erratic manner. This phenomenon can be seen in Figure 12. As is shown, the erratic behavior always began as the outlet gas concentration started to decrease and it seemed to terminate as the concentration started to rise. A careful check indicated that this behavior was apparently due to an actual concentration variation and not to stray signal pickup or noise in the bridge or preamplifier circuit. Since, as can also be seen in Figure 12, this anomaly disappeared at the higher gas phase flow rates,

it was thought that erratic mixing in the space above the packing might be the cause. To check this possibility, three concentration traces were made with the sampling point placed at the wall of the column, at a point half way between the column wall and center and at the column center point. The results of these traces showed that the output cell signal was essentially independent of sampling position--the amplitude increased only 6 per cent at the wall for G=1 lb-mole/hr-ft^2 and remained constant (within 1 per cent) for G=10 lb-moles/hr-ft^2--and that the low flow rate trace showed the same erratic behavior at all three positions.

Conceivably, the fluctuations might be associated with slight sample flow eccentricities caused by the small cyclic nature of the column gas phase flow, but this too seems remote since the column upstream pressure, as indicated by a water manometer, did not show the slightest variation at the low gas flow rates.

No adequate explanation was found for this erratic behavior of the outlet cell concentration trace, and the phenomenon occurred in all the runs including the run on the mock-up of the column inlet and outlet sections. Although the accuracy of the data at low frequencies was not significantly affected by this behavior, the erratic portions of the wave became proportionally more dominant at the high frequencies ($\omega > 2$ cpm), thus making it rather difficult to

measure reliably the considerably attenuated output wave amplitudes at these conditions. The combined effects of large attenuations and erratic signals restricted the frequency range which could be investigated at these low gas phase flow rates. It is estimated that these conditions introduced an uncertainty of approximately ±15 per cent in the values of the amplitude ratios of Figure 15 and, correspondingly, of Figure 23 for frequencies above two cycles per minute.

The slight flattening of the inlet gas concentration sinusoid seen in Figure 12 was also a manifestation of the low gas phase flow rate tests. Because, at the low flow rate, the carbon dioxide flow through the linear valve of the sinusoid generator was very small, the total linear displacement of the valve stem was approximately only 1/32 inch. With these small amplitudes the clearances of the scotch yoke parts caused a slight "dead zone" at the end of each valve stroke which resulted in the flattened portions of the concentration waves. At the higher gas flow rates, where the linear displacements or amplitudes of the valve stem were considerably larger, these clearance effects were negligible as can be seen from Figure 12.

CHAPTER VI

CONCLUSIONS AND RECOMMENDATIONS

I. CONCLUSIONS

The major conclusions drawn from the results of the experimental and analytical portions of this work are briefly states as follows:

1. Frequency response analysis offers an accurate and convenient method to measure the dynamic behavior of a packed gas absorption tower. The techniques developed here could be adapted to both larger and smaller installations.
2. The specially designed thermal conductivity cells developed for continuous measurement of the gas phase solute concentration possess both the sensitivity and speed of response necessary for frequency response analysis. The cells are suitable for frequencies considerably in excess of those used in this study (ω_{max}=16 cpm).
3. The dynamic behavior of a packed gas absorber or, for that matter, any piece of operational equipment may be very significantly influenced by the mixing and hold-up characteristics of its inlet and outlet sections. The dynamics of these sections can represent

the most significant portion of the total process response.

4. Conclusions concerning the agreement between theoretical and experimental frequency response measurements should be based on only amplitude ratio data since quite different mathematical models tend to give similar phase shift responses.
5. The slug-flow model does not completely describe the unsteady-state behavior of a countercurrent packed gas absorber. This is presumably the result of significant axial and/or radial mixing of the gas phase in the packing of the column.
6. The quantitative effects of the gas phase mixing phenomenon in the two phase absorption system are not accounted for by the mixing-cell model as developed in this work.
7. Although the qualitative effects of the complex interaction of the gas and liquid flow rates upon the relative degree of gas phase mixing could not be completely ascertained, a somewhat greater relative degree of mixing occurs with increasing gas phase flow rate.
8. The flow of a single gas phase through a dry packed bed is not of the slug or piston type and the axial and/or radial mixing in the packing is significant.

9. Neither the mixing-cell model nor the axial diffusion model adequately describes the dispersion or mixing of a single phase gas flow in the packed bed of this experimental study.
10. Although--for the lack of a justifiable index of mixing--no quantitative measure can be made, the relative degree of mixing in the dry packing or non-absorption system is considerably greater than previously reported data for gas flow in packed beds.

II. RECOMMENDATIONS FOR FUTURE WORK

The above conclusions are by no means absolute and should be verified by future work on this subject. The present investigation has suggested a number of approaches which could yield additional information on the problem of gas absorber dynamics. These are:

1. A careful study should be made of the effect of taking concentration samples from a single point in the column. This study should consider the radial and axial variation of the sample point location and the possibility of moving the sampling points to the inlet and outlet of the packing section, thereby eliminating the significant response of the column inlet and outlet sections.
2. It is suggested that future absorption tests use a

more soluble solute gas such as SO_2. In this manner significant absorption can be obtained without use of the very large L/G ratios which were necessary in this work. Thus, considerably larger gas flow rates can be used and the problems of concentration sinusoid generation and measurement encountered at low gas flow rates can be avoided.

3. The effects and interaction of gas and liquid phase flow rates on the degree of mixing of the gas phase in the packing section can be best studied by using an essentially insoluble solute as the sinusoidally varying component in the gas phase. The Freons are ideal for this application since they are available, insoluble, relatively inexpensive, and ideally suited for thermal conductivity detection.

4. Attempts should be made to obtain a suitable mathematical model for the unsteady-state absorption process. Two approaches might be used. The first would be to complete or modify the models suggested in this work. For example, a numerical solution for the axial diffusion model might be attempted or a solution of the mixing-cell model with a different number of cells for the gas phase than for the liquid phase might be tried. Both these models would require, in all probability, digital computer solution. The

possibility of application of alternate boundary conditions and a full study of their significance also should be considered.

The second and possibly more reasonable approach would be to attempt to develop a model based on random walk theory (50, 80) since the transport and interphase transfer of mass in a packed bed is describable by a statistical model (82).

5. The presence of axial and/or radial mixing in a packed gas absorber could explain the difficulty in obtaining satisfactory correlations for both gas and liquid film mass transfer coefficients. A combination of steady state and frequency response absorption tests with the same mean gas concentration, together with frequency response tests using a non-absorbent solute gas at the same column operating conditions, could yield information on the extent to which these film coefficients are affected by gas phase mixing (76, 117, 69).

III. RECOMMENDATIONS FOR EQUIPMENT MODIFICATIONS

Before any further frequency response studies are made with the equipment constructed for this study, certain modifications are suggested. Thus:

1. The unmatched thermistors of the outlet thermal-

conductivity cell should be replaced with a matched pair and the balancing resistor should be removed from that portion of the bridge circuit.

2. The effectiveness of temperature control of the thermal conductivity cells should be improved either through use of a larger supply bath or by relocation of the present one. This is particularly needed for the outlet cell where better thermostating and a matched pair of thermistors should result in considerably improved null point stability.
3. The frequency range of the concentration sinusoid generator should be extended to at least one cycle per second so that significant responses can be obtained at higher gas phase flow rates.
4. The blower variable speed control should be modified to assure a constant and easily regulated gas flow that can be accurately re-established whenever necessary.

BIBLIOGRAPHY

BIBLIOGRAPHY

1. Acton, F.S. and L. Lapidus, "Design Equations for Continuous Stirred-Tank Reactors," Ind. Eng. Chem., 47, 706 (1955).

2. Aikman, A.R. "Frequency Response Analysis and Controllability of a Chemical Plant," Frequency Response, R. Oldenburger, ed. New York: The Macmillan Company, 1956. P. 141.

3. Aikman, A.R., and C. I. Rutherford. "The Characteristics of Air-operated Controllers," Automatic and Manual Control, A. Tustin, ed. London: Butterworths Scientific Publications, 1952. P. 175.

4. Alves, G.E., "Hydraulic Analyses of Sudden Flow Changes in a Complex Pumping Circuit," A.I.Ch.E.J., 2, 143 (1956).

5. Ambrose, D. and R. R. Collerson, "A Thermal Conductivity Gauge for Use in Gas-Liquid Partition Chromatography," Journ. of Scient. Inst., 32, 323 (1955).

6. Aris, R., and N. R. Amundson, "An Analysis of Chemical Reactor Stability and Control," Chem. Eng. Sci., 7, 121 (1958).

7. _____, _____, _____, "Some Remarks on Longitudinal Mixing or Diffusion in Fixed Beds," A.I.Ch.E.J., 3, 280 (1957).

8. Baron, T., "Generalized Graphical Method for the Design of Fixed Bed Catalytic Reactors," Chem. Eng. Progr., 48, 119 (1952).

9. Beeker, J.A., C. B. Green, and G. L. Pearson, "Properties and Uses of Thermistors--Thermally Sensitive Resistors," Trans.A.I.E.E., 65, 711 (1946).

10. Berg, C., et al., "Instrumentation for Pilot Plants," Ind. Eng. Chem., 45, 1836 (1953).

11. Bilous, O., and N. R. Amundson, "Chemical Reactor Stability and Sensitivity," A.I.Ch.E.J., 1, 513 (1955) and 2, 117, (1956).

12. _____, et al., "Control of Continuous Flow Chemical Reactors," A.I.Ch.E.J., 3, 249 (1957).

13. _____, H.D. Block, and E.L. Piret, "Control of Continuous-flow Chemical Reactors," A.I.Ch.E.J., 3, 248 (1957).

14. Bode, H.D. Network Analysis and Feedback Amplifier Design. New York: Van Nostrand Company, Inc., 1945.

15. Bohemen, J., and J. H. Purnell, "The Behavior of Katharometers for Gas Chromatography in Carrier Gases of Low Thermal Conductivity," Journ. App. Chem., 8, 433 (1958).

16. Cairns, E.J., and J.M. Prausnitz, "Longitudinal Mixing in Packed Beds," Chem. Eng. Sci., 12, 20 (1960).

17. _____ _____, "Velocity Profile in Packed and Fluidized Beds," Ind. Eng. Chem., 51, 1441 (1959).

18. Campbell, D.P. Process Dynamics. New York: John Wiley and Sons, Inc., 1958.

19. _____. Process Dynamics. New York: John Wiley and sons, Inc., 1958. P. 293.

20. Carberry, J.J., and R. H. Bretton, "Axial Dispersion of Mass in Flow Through Fixed Beds," A.I.Ch.E.J., 4, 367 (1958).

21. Cherry, R.H., "Thermal-Conductivity Gas Analysis," Process Instruments and Controls Handbook, D.M. Considine, ed. New York: McGraw-Hill Book Company, Inc., 1957.

22. Churchill, R.V. Operational Mathematics. New York: McGraw-Hill Book Company, Inc. 1958.

23. Cohen, W.C., and E. F. Johnson, "Dynamic Characteristics of Double-Pipe Heat Exchangers," Ind. Eng. Chem., 48, 1031 (1956).

24. Considine, D.M., ed. Process Instruments and Controls Handbook. New York: McGraw-Hill Book Company, Inc., 1957.

25. Converse, A.O., "The Effect of Velocity Profile on Axial Dispersion in Packed Beds," A.I.Ch.E.J., 6, 344 (1960).

26. Cornell, D., W. G. Knapp, and J. R. Fair, "Mass Transfer Efficiency--Packed Columns--Part I," Chem. Eng. Prog., 56, #7, 68 (1960).

27. Cowan, C.B., and P.H. Stirling. "The Selection and Operation of Thermistors for Katharometers," Gas Chromatography, V.J. Coats, et al., eds. New York: Academic Press Inc., 1958. P. 165.

28. Danckwerts, P.V., "Continuous Flow Systems--Distribution of Residence Times," Chem. Eng. Sci., 2, 1 (1953).

29. _____, and A.M. Kennedy, "Kinetics of Liquid-Film Process in Gas Absorption--Part 1: Models of the Absorption Process," Trans. Instn. Chem. Engrs., 32, s49 (1954).

30. Davis, A.D., and G. A. Howard, "Thermistor Detector in Gas Chromatography," J. App. Chem., 8, 183 (1958).

31. Daynes, H.A. Gas Analysis by Measurement of Thermal Conductivity. London: Cambridge University Press, 1933.

32. Deed, D.W., P.W. Schutz, and T.B. Drew, "Comparison of Rectification and Desorption in Packed Columns," Ind. Eng. Chem., 39, 766 (1947).

33. Deisler, P.F., Jr., and R.H. Wilhelm, "Diffusion in Beds of Porous Solids--Measurement by Frequency Response Techniques," Ind. Eng. Chem., 45, 1219 (1953).

34. _____, et al., "Rapid Gas Analysis Using Ionization by α Particles," Anal. Chem., 27, 1366 (1955).

35. Desty, D.H., "Detectors for Gas Chromatography," Nature, 180, 22 (1957).

36. Dinbat, M., P.E. Porter, and F.H. Stross, "Gas Chromatography," Anal. Chem., 28, 290 (1956).

37. Dorweiler, V.P., and R. W. Fahien, "Mass Transfer at Low Flow Rates in a Packed Column," A.I.Ch.E.J., 5, 139 (1959).

38. Drew, C.M. "Detectors," Principles and Practice of Gas Chromatography, R.L. Peesak, ed. New York: John Wiley and Son, Inc., 1959. Pp. 116 and 153.

39. Dusinberre, G.M., "Calculation of Transients in Cross Flow Heat Exchangers," J. Heat Trans., 81, 61 (1959).

40. Ebach, E.A., and R.R. White, "Mixing of Fluids Flowing through Beds of Packed Solids," A.I.Ch.E.J., 4, 161 (1958).

41. Edeskuty, F.J., and N.R. Amundson, "Effect of Intra-particle Diffusion--I Agitated Nonflow Adsorption Systems," Ind. Eng. Chem., 44, 1698 (1952).

42. Eykman, E.G.J., and C.J.D.M. Verhagen. "Response and Phase-Lag of Thermometers," Frequency Response, R. Oldenburger, ed. New York: The MacMillan Company, 1956. P. 158.

43. Fanning, R.J., and C.M. Sliepevich, "The Dynamics of Heat Removal from a Continuous Agitated-Tank Reactor," A.I.Ch.E.J., 5, 240 (1959).

44. Fuchs, A.M. "A Bibliography of the Frequency-Response Method as Applied to Automatic-Feedback-Control Systems," Frequency Response, R. Oldenburger, ed. New York: McMillan Company, 1956. P. 43.

45. Gilbert, T.J., "Liquid Mixing on Bubble-cap-Sieve Plates," Chem. Eng. Sci., 10, 243 (1959).

46. Hainsworth, B.D., and H.M. Paynter, "Dynamic Analysis of Heat Exchanger Control," I.S.A.J., 4, #6, 2 (1957).

47. Harrison, G.S., and W.D. Armstrong, "The Frequency Response of Rotameters," Chem. Eng. Sci., 12, 253 (1960).

48. Harvey, D., and G.O. Morgan. "Factors Affecting Thermal Conductivity Detectors in Vapour Phase Partition Chromatography," Vapour Phase Chromatography, D.H. Desty, ed. London: Butterworths Scientific Publications, 1957. P. 74.

49. Jackson, R.F., and R.L. Pigford, "Rate of Approach to Steady-State by Distillation Column," Ind. Eng. Chem., 48, 1020 (1956).

50. Jacques, G.L., and T. Vermeulen. "Longitudinal Dispersion in Solvent Extraction Columns: Peclet Numbers for Ordered and Random Packing," University of California Radiation Laboratory Report, UCRL 8209, (1957).

51. James, A.T., and A.J.P. Martin, "Gas-Liquid Partition

Chromatography for the Separation and Microestimation of Volatile Fatty Acids from Formic Acid to Dodecamoic Acid," Biochem.J., 50, 679 (1952).

52. Jaswon, M.A., and W. Smith, "Countercurrent Transfer processes in the Non-Steady State," Proc. Roy. Soc., A225, 226 (1954).

53. Kasten, P.R., and N.R. Amundson, "Effect of Intraparticle Diffusion--II Analytical Solution of Single Systems in Moving Beds," Ind. Eng. Chem., 44, 1704 (1952).

54. Keppler, J.G., et al. "Vapour Phase Chromatography at High Temperatures," Vapour Phase Chromatography, D.H. Desty, ed. London: Butterworths Scientific Publications, 1957. P. 222.

55. Keulemans, A.I.M. Gas Chromatography. New York: Reinhold Publishing Corporation, 1957.

56. Keyes, J.J., Jr., "Diffusion Film Characteristics in Turbulent Flow: Dynamic Response Method," A.I.Ch. E.J., 1, 305 (1955).

57. Kirkland, J.J. "An Apparatus for Laboratory Preparative-Scale Vapor Phase Chromatography," Gas Chromatography V.J. Coates, et al., eds. New York: Academic Press Inc., 1958. P. 207.

58. Klinkenberg, A., H.J. Krajenbrink, and H.A. Lauwerier, "Diffusion in a Fluid Moving at Uniform Velocity in a Tube," Ind. Eng. Chem., 45, 1202 (1953).

59. Kramers, H., and G. Alberda, "Frequence-Response Analysis of Continuous-Flow Systems," Chem. Eng. Sci., 2, 173 (1953).

60. Langer, H.S., and C. Zahn. "Bibliography on Gas Chromatography," Gas Chromatography, V.J. Coates, et al., eds. New York: Academic Press Inc., 1958. P. 287.

61. Lapidus, L., "Flow Distribution and Diffusion in Fixed-Bed Two-Phase Reactors," Ind. Eng. Chem., 49, 1000 (1957).

62. _____, and N.R. Amundson, "Mathematics of Adsorption in Beds. VI. The Effect of Longitudinal Diffusion in Ion Exchange and Chromatographic Column," J. Phys. Chem., 56, 984 (1952).

63. Lees, S., and J. O. Hougen, "Pulse Testing a Model Heat Exchanger," Ind. Eng. Chem., 48, 1064 (1956).

64. Leonhard, A. "Determination of Transient Response from Frequency Response," Frequency Response, R. Oldenberger, ed. New York: The Macmillan Company, 1956.

65. Lindsay, A.L., and L.A. Bromley, "Thermal Conductivity of Gas Mixtures," Ind. Eng. Chem., 42, 1508 (1950).

66. Marshall, W.R., Jr., and R.L. Pigford. The Application of Differential Equations to Chemical Engineering Problems. Newark: University of Delaware, 1947. P. 148.

67. McHenry, K.W., Jr., and R.H. Wilhelm, "Axial Mixing of Binary Gas Mixtures Flowing in a Random Bed of Spheres," A.I.Ch.E.J., 3, 83 (1957).

68. McMillan, J., "The Dynamics of Process Plants," Trans. Instn. Chem. Engrs., 33, 169 (1955).

69. McMullen, A.K., T. Miyauchi, and T. Vermeulen. "Longitudinal Dispersion in Solvent Extraction Columns," University of California Radiation Laboratory Report, UCRL 3911 and UCRL 3911 Supplement, 1957.

70. Mellor, N. "Factors Affecting Katharometer Sensitivity and Column Efficiency in Vapour Phase Partition Chromatography," Vapour Phase Chromatography, D.H. Desty, ed. London: Butterworths Scientific Publications, 1957. P. 63.

71. Minter, C.C., and L.M. Burdy, "Thermal Conductivity Bridge for Gas Analysis," Anal. Chem., 23, 143 (1951).

72. Morris, G.A., and J. Jackson. Absorption Towers. London: Butterworths Scientific Publications, 1953. P. 143.

73. Mozley, J.M., "Predicting Dynamics of Concentric Pipe Heat Exchangers," Ind. Eng. Chem., 48, 1035 (1956).

74. Mullen, P.W. Modern Gas Analysis. New York: Interscience Publications Inc., 1955.

75. Oldenbourg, R.C., and H. Sartorius. The Dynamics of Automatic Controls. New York: The American Society of Mechanical Engineers, 1948. P. 22.

76. Otake, T., E. Kunugita, and A. Kauabe, "Mixing Characteristics of Irrigated Packed Beds--Absorption of CO_2 Gas," Kagaku Kogaku, 23, 81 (1959)--(CA. 53, 7680h).

77. Pearson, J.R.A., "A Note on the Danckwerts Boundary Conditions for Continuous Flow Reactors," Chem. Eng. Sci., 10, 281 (1959).

78. Peppard, D.F., and M.A. Peppard, "Batchwise Fractional Extraction--Holdup and Approach to Steady State," Ind. Eng. Chem., 46, 34 (1954).

79. Percival, W.C., "Quantitative Determination of Fluorinated Hydrocarbons by Gas Chromatography," Anal. Chem., 29, 20 (1957).

80. Perry, J.H., ed. Chemical Engineer's Handbook. New York: McGraw-Hill Book Company, Inc., 1950. P. 674.

81. Plant and Process Dynamic Characteristics, The Society of Instrument Technology. London: Butterworths Scientific Publications, 1957.

82. Prausnitz, J.M., and R.H. Wilhelm, "Turbulent Concentration Fluctuations in a Packed Bed," Ind. Eng. Chem., 49, 978 (1957).

83. Pritchard, F.W., "A Modified Thermal Conductivity Analyser for Measuring Methane in Air or Carbon Dioxide," J. Sci. Instr., 29, 116 (1952).

84. Reactor Heat Transfer Conference of 1956. TID-7529.

85. Reilly, P.M., "Unsteady State Heat Transfer in Stationary Packed Beds," A.I.Ch.E.J., 3, 513 (1952).

86. Rohmann, C.P., "On the Dynamics of Pneumatic Transmission Lines," Trans. A.S.M.E., 79, 853 (1957).

87. Rose, A., and T.J. Williams, "Automatic Control in Continuous Distillation," Ind. Eng. Chem., 47, 2284 (1955).

88. Rosen, J.B., and W.E. Winsche, "The Admittance Concept in Kinetics of Chromatography," J. of Chem. Phys., 18, 1587 (1950).

89. Rosenbrock, H.H., "Calculations of the Transient Behavior of Distillation Columns," Brit. Chem. Eng., 3, 364, 432, 491 (1958).

90. Rutherford, C.I., "The Practical Application of Frequency Response Analysis to Automatic Process Control," Instn. of Mech. Eng. (Eng), 162, 334 (1950).

91. Rice, S.A., et al., "Thermal Conductivity Cell for Gas Chromatography," nal. Chem., 29, 1386 (1957).

92. Schechter, R.S., and E.H. Wessler, "Frequency Response from Step Input Response," Ind. Eng. Chem., 51, 945, (1959).

93. Scheibel, E.G., "Batchwise Fractional Extraction Calculation of Deviation from Steady State," Ind. Eng. Chem., 46, 43 (1954).

94. Schmauch, L.J., "Response Time and Flow Sensitivity of Detectors for Gas Chromatography," Anal. Chem., 31, 225 (1959).

95. Schnelle, P.D., "A Precision Gas Mixer for Calibrating Analyzers," I.S.A.J., 4, #4, 5 (1957).

96. Schwartz, C.E., and J.M. Smith, "Flow Distribution in Packed Beds," Ind. Eng. Chem., 45, 1209 (1953).

97. Sevant, C.J., Jr. Basic Feedback Control System Design. New York: McGraw-Hill Book Company, Inc., 1958. P. 16.

98. _____. Basic Feedback Control System Design. New York: McGraw-Hill Book Company, Inc., 1958. P.124.

99. Sherwood, T.K., and F.A.L. Holloway, "Performance of Packed Towers--Experimental Studies of Absorption and Desorption," A.I.Ch.E. Trans., 36, 20 (1940).

100. _____ _____, "Performance of Packed Towers--Liquid Film Data for Several Packings," A.I.Ch.E. Trans., 36, 39 (1940).

101. _____, and R.L. Pigford. Absorption and Extraction. New York: McGraw-Hill Book Company, Inc., 1958. P. 278.

102. _____ __ _____. Absorption and Extraction. New

York: McGraw-Hill Book Company, 1952. P. 287.

103. Shulman, H.L., and J.J. DeGouff, Jr., "Mass Transfer Coefficients on Interfacial Areas for 1-Inch Raschig Rings," Ind. Eng. Chem., 44, 1915 (1952).

104. _____, C.F. Ullrich, and N. Wells, "Performance of Packed Columns--I. Total, Static, and Operating Holdups," A.I.Ch.E.J., 1, 247 (1955).

105. Siggia, S. Continuous Analysis of Chemical Process Systems. New York: John Wiley and Sons, Inc., 1959. P. 245.

106. Sleicher, C.A., Jr., "Axial Mixing and Extraction Efficiency," A.I.Ch.E.J., 5, 145 (1959).

107. St. Clair, D.W., et al. "Sine-Wave Generators," Frequency Response, R. Oldenburger, ed. New York: The Macmillan Company, 1956. P. 70.

108. Strang, D.A., and C.J. Geankoplis, "Longitudinal Diffusivity of Liquids in Packed Bed," Ind. Eng. Chem., 50, 1305 (1958).

109. Takahashi, Y. "Transfer Function Analysis of Heat Exchange Processes," Automatic and Manual Control, A. Tustin, ed. London: Butterworths Scientific Publications, 1952. P. 235.

110. Thermistor Manual, EMC-4. Framingham, Mass.: Fenwal Electronics Inc.

111. Thomas, C.O. "An Investigation of Techniques for the Separation of Hydrogen and Deuterium," Ph.D. Dissertation, Chemistry Department, University of Tennessee (1957), p. 110.

112. Timms, D.G., H.J. Konreth, and R.C. Chirnside, "The Determination of Impurities in Carbon Dioxide by Gas Chromatography with Special Reference to Coolant Gas for Nuclear Reactors," Analyst, 83, 600 (1958).

113. Trebal, R.E. Mass-Transfer Operations. New York: McGraw-Hill Book Company, Inc. 1955. P. 140.

114. Troy, D.J., "Measurement of Atmospheric Pollution by Ultraviolet Photometry," Anal. Chem., 27, 1217 (1955).

115. Turner, G.A., "The Flow Structure in Packed Beds--A Theoretical Investigation Utilizing Frequency Response," Chem. Eng. Sci., 7, 156 (1958).

116. _____, "The Frequency Response of Some Illustrative Models of Porous Media," Chem. Eng. Sci., 10, 14 (1959).

117. van Deemter, J.J., F.J. Zuiderweg, and A. Klinbenberg, "Longitudinal Diffusion and Resistance to Mass Transfer as Causes of Nonideality in Chromatography," Chem. Eng. Sci., 5, 271 (1956).

118. Walker, R.E., and A.A. Westenberg, "Precision Thermal-Conductivity Gas Analyzer Using Thermistors," Rev. Sci. Instr., 28, 789 (1957).

119. Weaver, E.R. "Gas Analysis by Methods Depending on Thermal Conductivity," Physical Methods in Chemical Analysis, W.G. Berl, ed. New York: Academic Press Inc., 1951. Vol. II, 387.

120. Wehner, J.F., and R.H. Wilhelm, "Boundary Conditions of Flow Reactor," Chem. Eng. Sci., 6, 89 (1956).

121. Wicke, E., Kolloid Z., 86, 307 (1939); 93, 129 (1940).

122. Wilkinson, W.L., and W.D. Armstrong, "An Approximate Method of Predicting Composition Response of a Fractionating Column," Chem. Eng. Sci., 7, 1 (1957).

123. Williams, T.J., R.T. Harnett, and A. Rose, "Automatic Control in Continuous Distillation," Ind. Eng. Chem., 48, 1008 (1956).

APPENDICES

APPENDIX A

USE OF BOUNDARY CONDITIONS IN THE DEVELOPMENT OF THE THEORETICAL RESPONSE EQUATIONS

Consider the general root of the characteristic equation of differential Equation 14:

$$p_{1,2} = \frac{(\alpha - \gamma) \pm \sqrt{(\gamma - \alpha)^2 - 4(\beta\delta - \alpha\gamma)}}{2} \qquad (A1)$$

with

$$\alpha = \frac{k_L a + h_L s}{L}$$

$$\beta = \frac{k_L a}{mL}$$

$$\gamma = \frac{k_L a/m + h_G s}{G}$$

$$\delta = \frac{k_L a}{G}$$

Thus

$$\alpha - \gamma = \frac{(k_L a + h_L s)}{L} - \frac{(k_L a/m + h_G s)}{G} = \frac{(Gk_L a - Lk_L a/m) + (Gh_L - Lh_G)s}{GL}$$

$$\alpha - \gamma = \frac{d + cs}{GL} \qquad (A2)$$

where

$$d = (G - L/m)k_L a$$

$$c = (Gh_L - Lh_G)$$

and

$$(\alpha-\gamma)^2 = \frac{c^2s^2+2dcs+d^2}{(GL)^2} = (\gamma-\alpha)^2 \qquad (A3)$$

Now

$$4(\beta\gamma-\alpha\gamma) = \frac{4(k_La)^2/m}{GL} - \frac{4(k_La)^2/m+4(k_Lah_G+k_Lah_L)s+4h_Lh_Gs^2}{GL}$$

$$= -\frac{bs+as^2}{(GL)^2} \qquad (A4)$$

where

$$b = 4GL(h_G+h_L/m)k_La$$

$$a = 4GLh_Lh_G$$

Substitution of A_2, A_3, and A_4 into A_1 gives

$$p_{1,2} = \frac{(d+cs) \pm \sqrt{(c^2+a)s^2+(b+2dc)s+d^2}}{2GL}$$

Substitution of $s=i\omega$, where $i=\sqrt{-1}$, gives

$$p_{1,2} = \frac{(d+c\,\omega i) \pm \sqrt{d^2-(c^2+a)\,\omega^2+(b+2dc)\,\omega i}}{2GL} \qquad (A5)$$

The numerator of the above expression is, in general, a complex number. Let this complex number be $w_{1,2}$, where $w_{1,2}=u_{1,2}+v_{1,2}i$. With this notation the general solution for $\bar{y}$ becomes

$$\bar{y} = C_1\, e^{\frac{w_1}{2GL}z} + C_2\, e^{\frac{w_2}{2GL}z} \qquad (A6)$$

By applying the boundary condition that $\bar{y}=0$ at $z=\infty$ and noting that $\exp(\frac{zv_{1,2}}{2GL}i)$ is bounded for all z it can be be concluded that the constant C_1 or C_2 must be zero if u_1 or u_2 respectively is positive. To determine which is the non-zero constant one proceeds as follows:

Let the complex number represented by the terms under the radical be given by $n+mi$. The radical then becomes,

$$\sqrt{n+mi} = \sqrt{r}\ (\cos\frac{\theta}{2} + i\sin\frac{\theta}{2}) \qquad (A7)$$

where

$$r = \sqrt{n^2+m^2}$$

$$\theta = \tan^{-1}\frac{m}{n}$$

or

$$\sqrt{n+mi} = (r\cos^2\frac{\theta}{2})^{\frac{1}{2}} + i(r\sin^2\frac{\theta}{2})^{\frac{1}{2}}$$

But,

$$\cos^2\frac{\theta}{2} = \frac{\cos\theta+1}{2}, \quad \sin^2\frac{\theta}{2} = \frac{1-\cos\theta}{2}, \text{ and } \cos\theta = \frac{n}{r}$$

Therefore, the radical becomes:

$$\sqrt{n+mi} = (\frac{n+r}{2})^{\frac{1}{2}} + i(\frac{r-n}{2})^{\frac{1}{2}} \qquad (A8)$$

where, from Equations A5 and A7,

$$n = d^2-(c^2+a)\omega^2$$

and

$$r=\sqrt{\left[d^2-(c^2+a)\,\omega^2\right]^2+\left[(b+2dc)\omega\right]^2}$$

The conditions will now be determined under which the real part of the radical term in A5, $(\frac{r+n}{2})^{\frac{1}{2}}$, is larger than the real part of the first term of A5, d. The question is, thus:

$$\text{Is } (\tfrac{r+n}{2})^{\frac{1}{2}} > d?$$

Since

$$r+n = d^2-(c^2+a)\,\omega^2+\sqrt{\left[d^2-(c^2+a)\,\omega^2\right]^2+\left[(b+2dc)\omega\right]^2}$$

then $r+n>2d^2$ if $-(c^2+a)\,\omega^2+\sqrt{\left[d^2-(c^2+a)\omega^2\right]^2+\left[(b+2dc)\omega\right]^2}>d^2$.

If $r+n>2d^2$, then $(\frac{r+n}{2})^{\frac{1}{2}}>d$.

Thus the condition for the required inequality, $(\frac{r+n}{2})^{\frac{1}{2}}>d$, is

$$-(c^2+a)\,\omega^2+\sqrt{\left[d^2-(c^2+a)\,\omega^2\right]^2+\left[(b+2dc)\omega\right]^2}>d^2$$

or

$$\sqrt{\left[d^2-(c^2+a)\,\omega^2\right]^2+\left[(b+2dc)\omega\right]^2}>d^2+(c^2+a)\,\omega^2$$

and

$$\left[d^2-(c^2+a)\,\omega^2\right]^2+\left[(b+2dc)\omega\right]^2>\left[d^2+(c^2+a)\,\omega^2\right]^2 \qquad \text{(A9)}$$

A sufficient, although not necessary, condition for the above step is that

$$\sqrt{\left[d^2-(c^2+a)\,\omega^2\right]^2+\left[(b+2dc)\omega\right]^2}>0,$$

which is obviously the case, and that $d^2+(c^2+a)\,\omega^2>0$. The

latter condition is satisfied when $(c^2+a) > 0$, since $d^2 > 0$ and $\omega > 0$. That $(c^2+a) > 0$ is clear from Equations A2 and A4 where

$$c^2+a = (Gh_L-Lh_G)^2+4GLh_Lh_G = (Gh_L+Lh_G)^2$$

and

$$(Gh_L+Lh_G)^2 > 0$$

Inequality A9 may be expanded and reduced to give

$$b^2+4bcd-4d^2a > 0 \qquad \text{(A10)}$$

By the notation of Equations A2 and A4

$$b^2 = 16\ GL(k_La)^2(h_G+\frac{h_L}{m})^2\ GL$$

$$4bcd = 16\ GL(k_La)^2(h_G+\frac{h_L}{m})(G-\frac{L}{m})(Gh_L-Lh_G)$$

$$4d^2a = 16\ GL(k_La)^2(G-\frac{L}{m})^2\ h_Lh_G$$

Thus, A10 becomes

$$(h_G+\frac{h_L}{m})^2GL+(h_G+\frac{h_L}{m})(G-\frac{L}{m})(Gh_L-Lh_G)-(G-\frac{L}{m})^2h_Lh_G > 0$$

Upon expansion and reduction this becomes

$$\frac{G^2h_L^2}{m} + 2\frac{LGh_Lh_G}{m} + \frac{L^2h_G^2}{m} > 0$$

or

$$(Gh_L + Lh_G)^2 > 0$$

Since the above inequality is true for all operating conditions and is independent of the frequency, ω, the inequality $(\frac{n+r}{2})^{\frac{1}{2}} > d$ has no restriction. Therefore, since $u_{1,2}=d\pm(\frac{n+r}{2})^{\frac{1}{2}}$, u_1 is positive and thus $C_1=0$. With this, Equation A6 becomes

$$\bar{y} = C_2 \exp(\frac{w_2 z}{2GL})$$

By the boundary condition that $\bar{y}=\bar{y}_o$ at $z=0$, $c_2=\bar{y}_o$ and the above becomes:

$$\bar{y} = \bar{y}_o \exp(\frac{w_2 z}{2GL}) \qquad \text{(A11)}$$

With $\frac{w_2}{2GL}=p_2$, combination of Equations A1 and A11 yields the final general solution:

$$\bar{y} = \bar{y}_o \exp\left\{z\left[\frac{(\alpha-\gamma)-\sqrt{(\gamma-\alpha)^2-4(\beta\delta-\alpha\gamma)}}{2}\right]\right\} \qquad \text{(A12)}$$

APPENDIX B

DETERMINATION OF THE AMPLITUDE RATIO AND PHASE ANGLE FROM THE THEORETICAL TRANSFER FUNCTIONS

I. SLUG FLOW MODEL

It has been shown in Appendix A that the general solution for the transformed gas phase composition $\bar{y}$ is given by,

$$\bar{y} = \bar{y}_o \exp\left\{z\left[\frac{(\alpha-\gamma) - \sqrt{(\gamma-\alpha)^2 - 4(\beta\delta-\alpha\gamma)}}{2}\right]\right\}$$

Thus, the transfer function for the gas absorption bed, defined as $\frac{\bar{y}_Z}{\bar{y}_o}$, becomes:

$$\frac{\bar{y}_Z}{\bar{y}_o} = \exp\left\{Z\left[\frac{(\alpha-\gamma) - \sqrt{(\gamma-\alpha)^2 - 4(\beta\delta-\alpha\gamma)}}{2}\right]\right\} \quad (B1)$$

By substitution of Equations A2 through A4 and $s=i\omega$ of Appendix A, the above assumes the form of A5, or,

$$\left[\frac{\bar{y}_Z}{\bar{y}_o}\right]_{i\omega} = \exp\left\{\frac{Z}{2GL}\left[(d+c\omega i) - \sqrt{d^2-(c^2+a)\omega^2+(b+2dc)\omega i}\right]\right\} \quad (B2)$$

Let the complex number represented by the terms of the bracket be given by $w=u+iv$. The transfer function then becomes:

$$\left[\frac{\bar{y}_Z}{\bar{y}_o}\right]_{i\omega} = \exp\left\{\frac{Z}{2GL}(u+iv)\right\} \qquad (B3)$$

As has been stated in Chapter II, the modulus of the complex number resulting from the substitution of $i\omega$ for the Laplace transform parameter in the transfer function is the ratio of the amplitude of the outgoing sine wave to the amplitude of the incoming sine wave (amplitude ratio) while the argument of the complex number represents the phase shift between the two waves. Thus, if one writes the resulting complex number in polar form the transfer function becomes:

$$\left[\frac{\bar{y}_Z}{\bar{y}_o}\right]_{i\omega} = r' e^{\theta' i} \qquad (B4)$$

where

r' is the amplitude ratio (modulus)

θ' is the phase shift (argument)

Expressing B3 in this form yields

$$\left[\frac{\bar{y}_Z}{\bar{y}_o}\right]_{i\omega} = e^{\frac{Z}{2GL}u} \; e^{\frac{Zv}{2GL}i}$$

Thus, it can be immediately seen by analogy with B4 that the amplitude ratio is $\exp(\frac{Zu}{2GL})$ and the phase shift is

$\frac{Zv}{2GL}$ where u and v are the real components of the as yet undetermined complex number of the bracketed term of Equation B2.

To determine u and v , one proceeds as follows:

From Equation A8 of Appendix A, the radical term of B2 becomes:

$$\sqrt{d^2-(c^2+a)\omega^2 + (b+2dc)\omega i} = (\frac{r+n}{2})^{\frac{1}{2}} + (\frac{r-n}{2})^{\frac{1}{2}} i \quad (B5)$$

where

$$n = d^2 - (c^2+a)\omega^2$$

$$r = \sqrt{\left[d^2 - (c^2+a)\omega^2\right]^2 + \left[(b+2dc)\omega\right]^2}$$

By Equations A2 and A4 of Appendix A

$$d^2 = (G-\frac{L}{m})^2 (k_L a)^2$$

$(c^2+a) = (Gh_L-Lh_G)^2 + 4GLh_Lh_G$, which upon reduction becomes:

$$(c^2+a) = (Gh_L+Lh_G)^2$$

and

$$b+2dc = 4GL(h_G+\frac{h_L}{m})k_L a + 2k_L a(G-\frac{L}{m})(Gh_L-Lh_G)$$

Upon expansion and reduction this becomes:

$$b+2dc = 2k_L a(G+\frac{L}{m})(Gh_L+Lh_G)$$

Therefore,

$$n = (G-\frac{L}{m})^2(k_La)^2 - (Gh_L+Lh_G)^2\omega^2$$

and (B6)

$$r = \sqrt{\left[(G-\frac{L}{m})^2(k_La)^2-(Gh_L+Lh_G)^2\omega^2\right]^2 + \left[2k_La(G+\frac{L}{m})(Gh_L+Lh_G)\omega\right]^2}$$

With

$$d = (G-\frac{L}{m})k_La \qquad \text{and} \qquad c = (Gh_L-Lh_G)$$

the complex number, w, representing the terms in the brackets of Equation B2 can be evaluated by direct combination of real and imaginary parts of the first term with those of the radical term as given by Equation B5. Thus,

$$u = d - (\frac{r+n}{2})^{\frac{1}{2}} = (G-\frac{L}{m})k_La - (\frac{r+n}{2})^{\frac{1}{2}}$$

and (B7)

$$v = c\omega - (\frac{r-n}{2})^{\frac{1}{2}} = (Gh_L-Lh_G)\omega - (\frac{r-n}{2})^{\frac{1}{2}}$$

With these results the amplitude ratio, $\frac{A(Z)}{A(0)}$, and the phase shift, ϕ, can be calculated since

$$\frac{A(Z)}{A(0)} = \exp(\frac{Zu}{2GL}) \qquad \text{and} \qquad \phi = \frac{Zv}{2GL}$$

Thus

$$\frac{A(Z)}{A(0)} = \exp\left\{\frac{Z}{2GL}\left[(G-\frac{L}{m})k_La - (\frac{r+n}{2})^{\frac{1}{2}}\right]\right\}$$

and (B8)

$$\phi = \frac{Z}{2GL}\left[(Gh_L-Lh_G)\omega - (\frac{r-n}{2})^{\frac{1}{2}}\right]$$

where n and r, expressed in terms of the column operating conditions, are given by Equation B6.

II. MIXING CELL MODEL

The first step in establishing the complex number resulting from substitution of $s=i\omega$ in Equation 66 will be the determination of the complex numbers $D_{1,2}$ (Equations 67). By Equations 50, T_L and T_G become:

$$T_L = \tau_L \omega i + \frac{Hk_L a}{L} + 1$$

and

$$T_G = \tau_G \omega i + \frac{Hk_L a}{Gm} + 1$$

Thus,

$$T_L T_G = \left(\frac{Hk_L a}{L}+1\right)\left(\frac{Hk_L a}{Gm}+1\right) - \tau_L \tau_G \omega^2 + \omega\left[\tau_G\left(\frac{Hk_L a}{L}+1\right) + \tau_L\left(\frac{Hk_L a}{Gm}+1\right)\right] i$$

or

$$T_L T_G = u + vi \tag{B9}$$

where

$$u = \left(\frac{Hk_L a}{L}+1\right)\left(\frac{Hk_L a}{Gm}+1\right) - \tau_L \tau_G \omega^2$$

and (B10)

$$v = \omega\left[\tau_G\left(\frac{Hk_L a}{L}+1\right) + \tau_L\left(\frac{Hk_L a}{Gm}+1\right)\right]$$

Now, by Equations 51

$$T_L T_G - fg + 1 = (u - fg + 1) + vi$$

or

$$T_L T_G - fg + 1 = k + vi \tag{B11}$$

where

$$k = u - fg + 1 = \left(\frac{Hk_L a}{L} + 1\right)\left(\frac{Hk_L a}{Gm} + 1\right) - \tau_L \tau_G \omega^2 - \frac{(Hk_L a)^2}{LGm} + 1 \tag{B12}$$

With this nomenclature (which is unique to this section),

$$(T_L T_G - fg + 1)^2 = (k^2 - v^2) + 2kvi$$

and

$$(T_L T_G - fg + 1)^2 - 4T_L T_G = (k^2 - v^2 - 4u) + 2v(k-2)i$$

or

$$(T_L T_G - fg + 1)^2 - 4T_L T_G = n + mi \tag{B13}$$

where

$$n = k^2 - v^2 - 4u$$

$$m = 2v(k-2)$$

From Equation A8 of Appendix A, the square root of a complex number, $n+mi$, is given by:

$$\sqrt{n+mi} = \left(\frac{n+r}{2}\right)^{\frac{1}{2}} + i\left(\frac{r-n}{2}\right)^{\frac{1}{2}}$$

where

$$r = \sqrt{n^2+m^2}$$

Thus,

$$\sqrt{(T_L T_G - fg + 1)^2 - 4T_L T_G} = \left(\frac{r+n}{2}\right)^{\frac{1}{2}} + \left(\frac{r-n}{2}\right)^{\frac{1}{2}} i \qquad \text{(B14)}$$

where

$$\begin{aligned} r &= \sqrt{\left[k^2 - v^2 - 4u\right]^2 + \left[2v(k-2)\right]^2} \\ n &= k^2 - v^2 - 4u \end{aligned} \qquad \text{(B15)}$$

With Equations B14 and B11, the complex numbers represented by D_1 and D_2 (Equation 67), can be obtained. This is

$$\begin{aligned} D_{1,2} &= \frac{(T_G T_L - fg + 1) \pm \sqrt{(T_G T_L - fg + 1)^2 - 4T_G T_L}}{2} \\ &= \left[\frac{k \pm \left(\frac{r+n}{2}\right)^{\frac{1}{2}}}{2}\right] + \left[\frac{v \pm \left(\frac{r-n}{2}\right)^{\frac{1}{2}}}{2}\right] i \end{aligned} \qquad \text{(B16)}$$

Thus, with $D_{1,2}$ expressed in the polar form,

$$D_{1,2} = r_D \, e^{\theta_D i} \qquad \text{(B17)}$$

where

$$\begin{aligned} r_D &= \sqrt{\frac{\left[k \pm \left(\frac{r+n}{2}\right)^{\frac{1}{2}}\right]^2 + \left[v \pm \left(\frac{r-n}{2}\right)^{\frac{1}{2}}\right]^2}{4}} \\ \theta_D &= \tan^{-1}\left[\frac{v \pm \left(\frac{r-n}{2}\right)^{\frac{1}{2}}}{k \pm \left(\frac{r+n}{2}\right)^{\frac{1}{2}}}\right] \end{aligned} \qquad \text{(B18)}$$

(Plus sign for D_2; negative sign for D_1)

In general, therefore,

$$D_{1,2}^{\,n} = r_D^{\,n}\, e^{n\theta_D i} = r_D^{\,n} \cos n\theta_D + i r_D^{\,n} \sin n\theta_D \qquad \text{(B19)}$$

From Equation B9, it is clear that

$$T_L T_G - fg \cong T_L T_G \quad \text{if} \quad u \gg fg$$

or, from Equation B10 and Equation 51 if

$$\frac{Hk_L a}{L} + \frac{Hk_L a}{Gm} + 1 - \tau_L \tau_G \omega^2 \gg 0$$

For the ranges of operation conditions used in this work the above inequality holds and, therefore, the denominator of Equation 66 can be written as:

$$T_L T_G (D_2^{\,N} - D_1^{\,N} - D_2^{\,N-1} + D_1^{\,N-1}) \cong (T_L T_G - fg)(D_2^{\,N} - D_1^{\,N}) - T_L T_G (D_2^{\,N-1} - D_1^{\,N-1}) \qquad \text{(B20)}$$

Equation B19 is used to reduce the second term of the above expression.

$$D_2^{\,N} - D_1^{\,N} - D_2^{\,N-1} + D_1^{\,N-1} = \left[r_{D_2}^{\,N} \cos N\theta_{D_2} - r_{D_1}^{\,N} \cos N\theta_{D_1} - r_{D_2}^{\,N-1} \cos(N-1)\theta_{D_2} - r_{D_1}^{\,N-1} \cos(N-1)\theta_{D_1} \right] + \left[r_{D_2}^{\,N} \sin N\theta_{D_2} - r_{D_1}^{\,N} \sin N\theta_{D_1} - r_{D_2}^{\,N-1} \sin(N-1)\theta_{D_2} - r_{D_1}^{\,N-1} \sin(N-1)\theta_{D_1} \right] i$$

Let the above complex number be expressed in the polar form as

$$D_2^N - D_1^N - D_2^{N-1} + D_1^{N-1} = r_N e^{\theta_N i} \tag{B21}$$

where

$$r_N = \left[\left(r_{D_2}^N \cos N\theta_{D_2} - r_{D_1}^N \cos N\theta_{D_1} - r_{D_2}^{N-1} \cos (N-1)\theta_{D_2} - r_{D_1}^{N-1} \cos (N-1)\theta_{D_1} \right)^2 + \left(r_{D_2}^N \sin N\theta_{D_2} - r_{D_1}^N \sin N\theta_{D_1} - r_{D_2}^{N-1} \sin (N-1)\theta_{D_2} - r_{D_1}^{N-1} \sin (N-1)\theta_{D_1} \right)^2 \right]^{\frac{1}{2}}$$

(B22)

$$\theta_N = \tan^{-1} \left[\frac{r_{D_2}^N \sin N\theta_{D_2} - r_{D_1}^N \sin N\theta_{D_1} - r_{D_2}^{N-1} \sin (N-1)\theta_{D_2} - r_{D_1}^{N-1} \sin (N-1)\theta_{D_1}}{r_{D_2}^N \cos N\theta_{D_2} - r_{D_1}^N \cos N\theta_{D_1} - r_{D_2}^{N-1} \cos (N-1)\theta_{D_2} - r_{D_1}^{N-1} \cos (N-1)\theta_{D_1}} \right]$$

where, in general, r_D and θ_D are given by Equations B18.

By Equation B9

$$T_L T_G = u + vi$$

Writing this in polar form gives

$$T_L T_G = r_{LG} e^{\theta_{LG} i} \tag{B23}$$

where

$$r_{LG} = \sqrt{u^2 + v^2}$$
$$\theta_{LG} = \tan^{-1} \frac{v}{u} \tag{B24}$$

where u and v are given by Equations B10.

The numerator of Equation 66 will now be expressed in polar form. First consider the term T_L^N. Since

$$T_L = \left(\frac{Hk_L a}{L}+1\right) + \tau_L \omega i$$

$$T_L = r_L e^{\theta_L i} \quad \text{and} \quad T_L^N = r_L^N e^{N\theta_L i} \tag{B25}$$

where

$$r_L = \sqrt{\left(\frac{Hk_L a}{L}+1\right)^2 + \tau_L^2 \omega^2}$$

$$\theta_L = \tan^{-1} \frac{\tau_L \omega}{\frac{Hk_L a}{L}+1} \tag{B26}$$

The term $\sqrt{(T_L T_G - fg + 1)^2 - 4T_G T_L}$ can be expressed in polar form as

$$\sqrt{(T_L T_G - fg + 1)^2 - 4T_G T_L} = r_T e^{\theta_T i} \tag{B27}$$

where, by Equations B14 and B15

$$r_T = \left[(k^2 - v^2 - 4u)^2 + (2v(k-2))^2\right]^{\frac{1}{4}} = r^{\frac{1}{2}}$$

$$\theta_T = \frac{\tan^{-1}\left[\frac{2v(k-2)}{k^2 - v^2 - 4u}\right]}{2} \tag{B28}$$

Finally, substitution of Equations B20, B21, B23, B25, and B27 into Equation 66 yields the system transfer function in polar form:

$$\left[\frac{\bar{y}_n}{\bar{y}_o}\right]_{i\omega} = \frac{(r_L^N\, e^{N\theta_L i})(r_T\, e^{\theta_T i})}{(r_{LG}\, e^{\theta_{LG} i})(r_N\, e^{\theta_N i})}$$

or

$$\left[\frac{\bar{y}_n}{\bar{y}_o}\right]_{i\omega} = \frac{r_L^N\, r_T}{r_{LG}\, r_N}\, e^{(N\theta_L+\theta_T-\theta_{LG}-\theta_N)i} \qquad \text{(B29)}$$

Thus, since the modulus of $\left[\frac{\bar{y}_n}{\bar{y}_o}\right]_{i\omega}$ is the amplitude ratio while the argument is the phase shift, Equation B29 yields:

$$\frac{A(Z)}{A(0)} = \frac{r_L^N\, r_T}{r_{LG}\, r_N} \qquad \text{(B30)}$$

and

$$\phi = N\theta_L + \theta_T - \theta_{LG} - \theta_N \qquad \text{(B31)}$$

where

r_L and θ_L are given by Equations B26

r_T and θ_T are given by Equations B28

r_{LG} and θ_{LG} are given by Equations B24

r_N and θ_N are given by Equations B22

The value of the height of packing equivalent to a mixing cell, H, used throughout this analysis is given by

$$H = \frac{Z}{N} \qquad \text{(B32)}$$

Thus, both the amplitude ratio and phase shift are functions of the parameter N.

III. AXIAL DIFFUSION MODEL

Equation 90 of Chapter II becomes, upon substitution of $s=i\omega$

$$\left[\frac{y_Z}{y_o}\right]_{i\omega} = \exp\left\{\left[1 - \sqrt{1+\frac{4h_G^2 E_G \omega i}{G^2}}\right]\frac{GZ}{2h_G E_G}\right\} \qquad (B33)$$

The radical of the above expression can be expanded by noting that,

$$\sqrt{1+x} = 1 + \frac{x}{2} - \frac{x^2}{8} + \frac{x^3}{16} - \frac{5x^4}{128} + \text{-----} \quad \text{for} \quad x^2 \leq 1$$

Thus,

$$\sqrt{1 + \frac{4E_G \omega i}{U^2}} = 1 + \frac{2\omega E i}{U^2} + \frac{2\omega^2 E^2}{U^4} - \frac{4\omega^3 E^3 i}{U^6} - \frac{10\omega^4 E^4}{U^8} + \text{----} \qquad (B34)$$

where

$U = \frac{G}{h_G}$ = intersticial velocity, ft/hr

for $\frac{16\omega^2 E^2}{U^4} \leq 1$, which is certainly the case.

From Equation B34,

$$\left[1 - \sqrt{1+\frac{4E_G \omega i}{U^2}}\right]\frac{UZ}{2E_G} = -\frac{Z\omega i}{U} - \frac{Z\omega^2 E_G}{U^3} + \frac{2Z\omega^3 E_G^2 i}{U^5} + \frac{5Z\omega^4 E_G^3}{U^7} - \text{---}$$

When real and imaginary terms are collected the above becomes:

$$\left[1 - \sqrt{1+\frac{4E_G\omega i}{U^2}}\right]\frac{UZ}{2E_G} = \left(\frac{Z\omega^2E_G}{U^3} + \frac{5Z\omega^4E_G^3}{U^7} + \cdots\right) + \left(\frac{Z\omega}{U} + \frac{2Z\omega^3E_G^2}{U^5} - \cdots\right) i$$

or

$$\left[1 - \sqrt{1+\frac{4E_G\omega i}{U^2}}\right]\frac{UZ}{2E_G} = -\frac{Z\omega^2E_G}{U^3}\left(1+\frac{5\omega^2E_G^2}{U^4} + \cdots\right) - \frac{Z\omega}{U}\left(1-\frac{2\omega^2E_G^2}{U^4} + \cdots\right) i \qquad \text{(B36)}$$

If the second and higher-order terms of Equation B36 are small compared to one, or if

$$\frac{5\omega^2E_G^2}{U^4} \ll 1 \qquad \text{(B37)}$$

where

$$U = \frac{G}{h_G}$$

then B36 becomes:

$$\left[1 - \sqrt{1+\frac{4E_G\omega i}{U^2}}\right]\frac{UZ}{2E_G} \cong -\frac{Z\omega^2E_G}{U^3} - \frac{Z\omega}{U} i$$

With this, Equation B33 becomes

$$\left[\frac{y_Z}{y_o}\right]_{i\omega} = \left[\exp\left(-\frac{Z\omega^2 E_G}{U^3}\right)\right] e^{-\frac{Z\omega i}{U}} \qquad (B38)$$

Thus, under the above approximation, the amplitude ratio and phase shift, by direct analogy with B4, become

$$\frac{A(Z)}{A(0)} \cong \exp\left(-\frac{Z\omega^2 E_G}{U^3}\right) = \exp\left(-\frac{ZE_G h_G{}^3 \omega^2}{G^3}\right) \qquad (B39)$$

and

$$\phi \cong -\frac{Z\omega}{U} = -\frac{Zh_G\omega}{G} \qquad (B40)$$

where

$$U = \frac{G}{h_G} \qquad (B41)$$

and condition B37 holds.

APPENDIX C

CONCENTRATION SINUSOID GENERATOR

I. HISTORICAL BACKGROUND

A primary requirement of any frequency response experiment is the generation of a sinusoidal variation of some input variable such as temperature, voltage, pressure, composition, etc. Numerous devices have been constructed to supply such sine-waves for pneumatic, mechanical, and electrical input signals (107). Composition sinusoids, though, have received less attention and the problems involved have not yet been satisfactorily resolved (33, 40). In any type of frequency response experiment, deviation from a pure sinusoidal input requires analysis of the experimental results by the more difficult methods of harmonic analysis (40). Thus there was a strong incentive to design a superior concentration sinusoid generator for this work.

Ideally, a true sinusoidal flow rate can be obtained through a linear valve whose stem is displaced in a sinusoidal manner. A number of difficulties arose in attempting to accomplish this in practice. The first of these difficulties was to obtain a truly linear valve. A number of valves were tested in the experimental setup shown in Figure C-1. The procedure was to maintain the pressure upstream of the valve

constant (usually at 2 psig) with the pressure regulator while the valve position was varied from closed to full open. The relative valve stem position was measured to the nearest 0.0001 cm by a cathetometer. The test valve flow rate was measured at each setting by one of two Tri-Flat rotameters. Nitrogen was used as the gas for these tests.

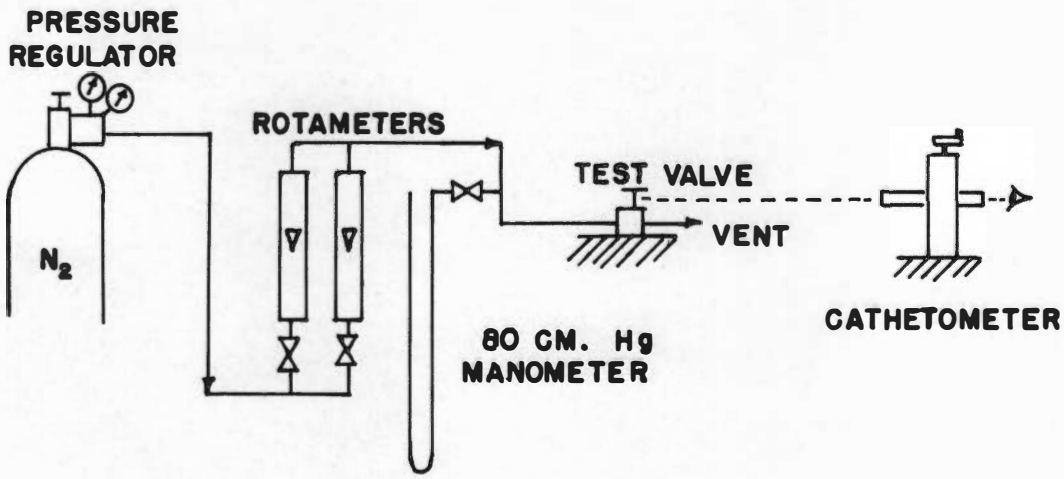


Figure C-1. Valve Linearity Test Setup

The results of tests on the available valves indicated that none were linear, i.e., the volume flows were not directly proportional to the valve stem position. A survey of the major control valve manufacturers also showed that no control valve of suitable size and linearity was available commercially. For these reasons it was decided to design and

build a special linear valve suitable for the proposed sine-wave generator of this work.

II. LINEAR VALVE DEVELOPMENT

The control valve sizing nomographs of Berg et al. (10) were used to determine the relationship between valve flow rate and valve flow area, for a pressure drop of 2 psi to atmospheric pressure. For carbon dioxide at these conditions this relationship was found to be:

$$(\text{Flow area - sq. in.}) = (1.8 \times 10^{-4})(\text{Flow rate - CFH})$$

for a flow rate range of 10 to 520 CFH. The direct proportionality of this relation suggested a design in which the flow area would vary directly with valve stem position. A valve was designed to provide a rectangular flow area for any valve stem position. By making the length of the flow area rectangle vary directly with the valve stem position, the total flow area, and hence the volume flow rate, became directly proportional to the valve stem position. The valve was designed and constructed of stainless steel. The flow area could be varied from zero to approximately 0.015 sq in. The construction details are shown in Figure C-2.

A sinusoidal valve stem motion was obtained by driving the stem with a scotch yoke powered by a variable-speed DC motor. The DC motor was connected to the scotch yoke through

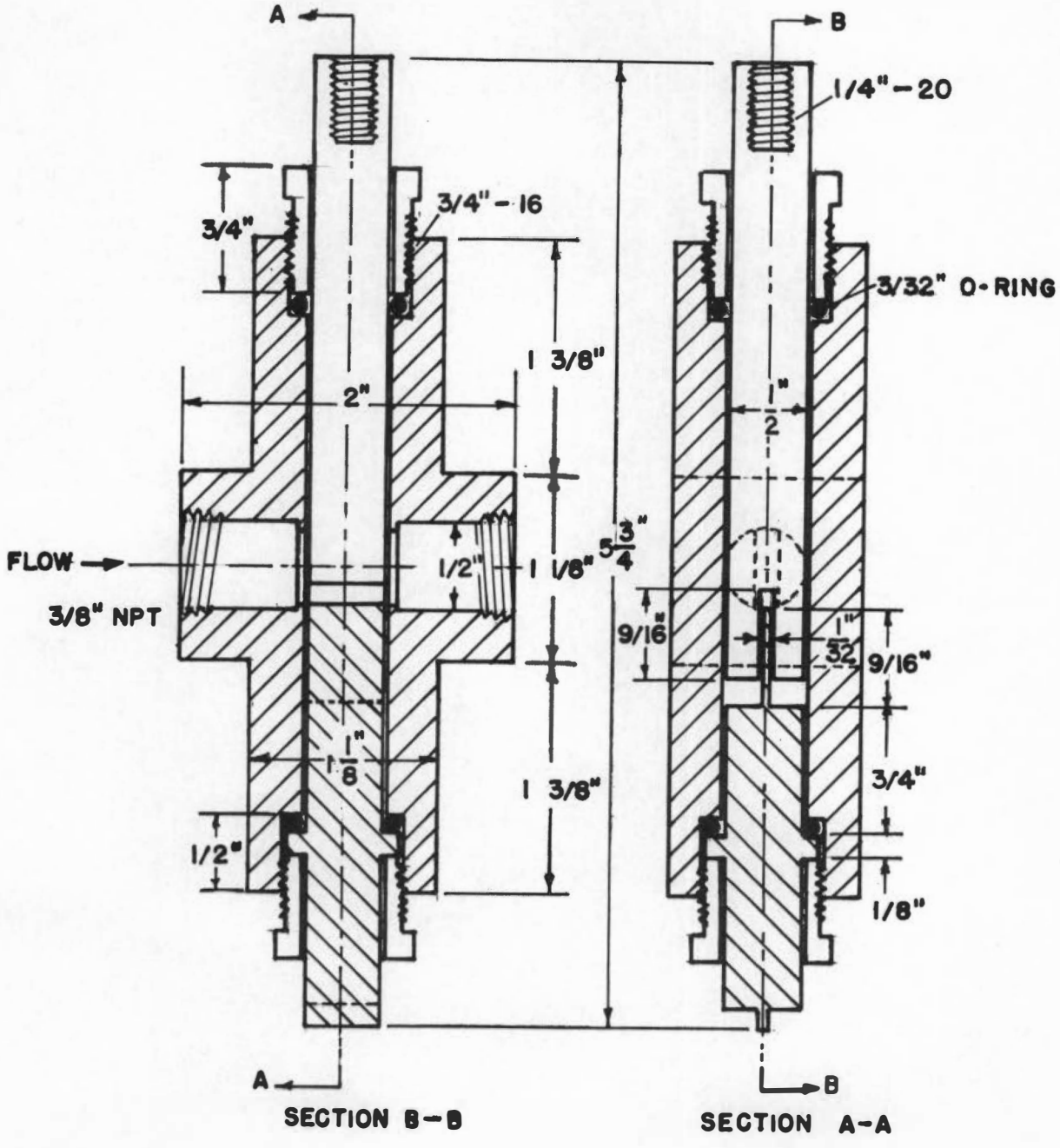


Figure C-2. Linear valve.

a 25:1 reduction worm gear and a set of spur gears which could be arranged in 1:1, 5:1, and 1:5 ratios. By combined adjustment of the spur gear ratio and the DC motor control the valve frequency could be continuously adjusted from 0.1 to 15 cycles per minute. The scotch yoke was designed to provide amplitude variation to 1/2-inch and a mean valve position from full open to full closed. Figure 5 shows the arrangement of the DC motor, gear train, scotch yoke, and linear valve.

The desired concentration sinusoid was formed by mixing the sinusoidal flow of carbon dioxide from the linear valve with a constant-flow air stream. The resulting stream had a sinusoidally varying carbon dioxide concentration; and, if the amplitude of the wave was small, the mixture flow rate was approximately constant.

Another practical difficulty in obtaining an ideal sinusoidal flow through the linear valve was anticipated in attempting to maintain the valve upstream pressure constant. It was clear that, at higher flow rates, even a good pressure regulator could not hold this pressure completely constant. It was proposed, therefore, to place a large gas reservoir between the valve and the pressure regulator to act as a surge stabilizer or pressure capacitance element.

III. THEORETICAL FREQUENCY RESPONSE ANALYSIS

In an effort to size the stabilizer tank and check the steady state behavior of the system the following analysis of the dynamics of the valve, tank, and pressure regulator was carried out:

The linearity of the designed valve was measured with nitrogen and, as shown in Figure C-3, proved satisfactory. The flow rate of the valve with carbon dioxide flowing was assumed to be inversely proportional to the square root of the gas density. With this connection the linear valve volume flow rate at some constant upstream pressure, P, can be given by

$$Q_p = M(P)X \qquad \text{(C-1)}$$

where

M is the linear valve position characteristic--a function of the upstream pressure, P

X is the valve position, inches

It is also reasonable to assume that, at some fixed valve position, X, the valve volume flow is

$$Q_X = K(X)\sqrt{P-P_o} \qquad \text{(C-2)}$$

where

K is the valve pressure characteristic--a function of the valve position

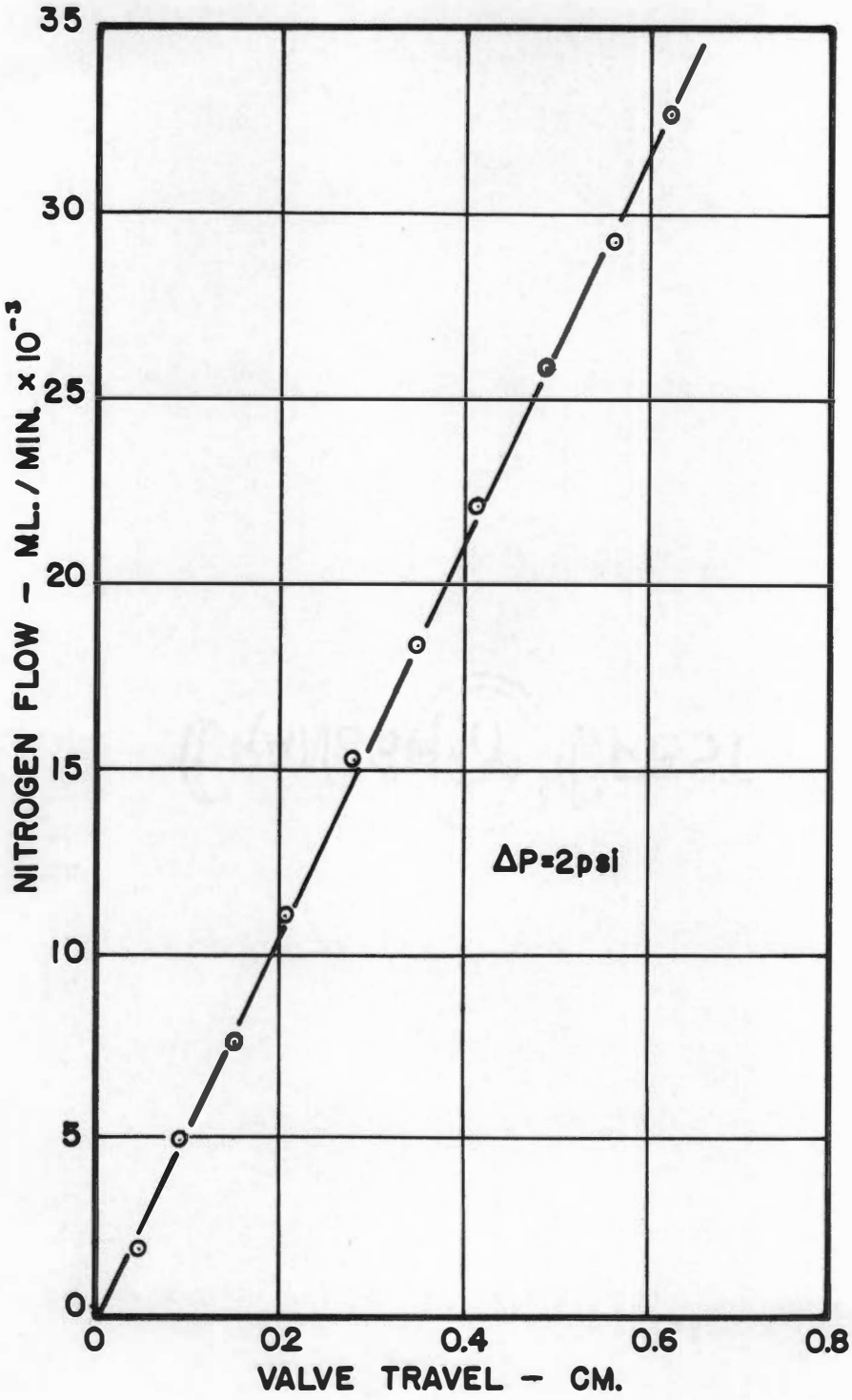


Figure C-3. Linear valve position characteristic.

P is upstream pressure, psia

P_o is constant downstream pressure, psia

Thus, since

$$\frac{\partial^2 Q}{\partial P\, \partial X} = \frac{\partial^2 Q}{\partial X\, \partial P}$$

then

$$\frac{\partial M}{\partial P} = \frac{(P-P_o)^{\frac{1}{2}}}{2} \quad \frac{\partial K}{\partial X} \qquad \text{(C-3)}$$

but

$$K = \frac{Q}{\sqrt{P-P_o}} = \frac{MX}{\sqrt{P-P_o}}$$

Substitution of the above expression in C-3 yields

$$\frac{dM}{M} = \frac{dP}{2(P-P_o)}$$

which, upon integration, results in the general equation,

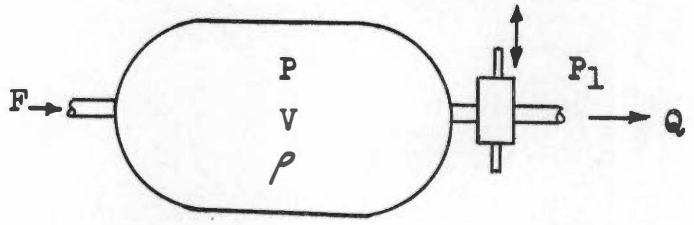
$$Q = B\ X\ \sqrt{P-P_o} \qquad \text{(C-4)}$$

where

B = constant given by $\dfrac{M(P_1)}{\sqrt{P_1-P_o}}$

The valve, whose flow is described by Equation C-4, is connected to the stabilizer tank as illustrated below. The volume of the tank is V in^3 while the pressure and density

of the gas in the tank are P psia and ρ lb/in^3, respec-



tively. The flow into the tank is F lb/min.

A mass balance about the tank gives

$$\frac{V d\rho}{dt} = F - Q\rho$$

which, upon substitution of Equation C-4 and $\rho = \frac{PW}{R_g T}$, assuming the temperature is constant, becomes

$$\frac{VW}{R_g T} \frac{dP}{dt} = F - \frac{BW}{R_g T} XP \sqrt{P-P_o} \qquad (C-5)$$

If the valve stem is now driven sinusoidally its position can be given by

$$X = X_m + A \sin \omega t \qquad (C-6)$$

Substitution of C-6 into C-5 and rearrangement results in the following:

$$\frac{dP}{dt} + C (X_m + A \sin \omega t) P \sqrt{P-P_o} = D \qquad (C-7)$$

where

$$C = \frac{B}{V} = \frac{M(P_1)}{V\sqrt{P_1 - P_o}}$$

and

$$D = \frac{F\,R_g\,T}{VW}$$

The above first order, non-linear differential equation with variable coefficients can be solved by several methods. When several values of the parameters F and ω are to be investigated, analog computer solution becomes, by far, the most convenient. Two cases will be studied: the case in which the inlet mass flow, F, is constant and the case in which the inlet mass flow is that delivered by a conventional gas pressure regulator from a constant upstream pressure.

Case I, F = constant

The following are the operating conditions for this case:

V = 2100 cu in.

P_o = 15 psia

P_1 = 17 psia

T = 68°F = 528°R

$M(P_1)$ = 6470 cu in. CO_2 per in./min

A = 0.1 inches

F = 0.08 lb/min (Flow for X_M=0.19 in.
P_1=17 psia
P_o=15 psia)

R_g= 18,550 lb-in./lb mole-^oR

W = 44 lb/lb mole

X_m= 0.19 in.

Thus

$$C = \frac{M(P_1)}{V\sqrt{P_1-P_o}} = \frac{6470}{2100\sqrt{17-15}} = 2.18$$

and

$$D = \frac{FR_gT}{VW} = \frac{(0.08)(18,550)(528)}{(2100)(44)} = 8.48$$

With these values Equation C-7 becomes:

$$\frac{dP}{dt} = 8.48 - 2.18(0.19 + 0.1 \sin \omega t)P\sqrt{P-15} \quad (C-8)$$

This equation is time-scaled by substituting $t=\frac{\tau}{15}$ (one minute real time equal 15 seconds machine time). Thus Equation C-8 becomes

$$\frac{dP}{d\tau} = 0.565 - \frac{(27.60 + 14.52 \sin \frac{\omega}{15}\tau)}{[100]} \frac{[P]}{[100]} \left[10\sqrt{P-15}\right] \quad (C-9)$$

where

ω = radians/min

Since the second term on the right side of C-5 (thus, also C-9), represents the mass flow from the valve, then

$$\text{valve mass flow (time)} = \frac{BWX}{R_g T} P\sqrt{P-P_o}$$

$$= \frac{VW}{R_g T} C\,(X_m + A \sin \omega t) P \sqrt{P-P_o}$$

where

$$\frac{VW}{R_g T} = \frac{(2100)(44)}{(18,550)(528)} = 0.00944$$

Therefore, by C-9,

$$\text{valve mass flow} = 0.1415 \left\{ \frac{(27.60+14.52 \sin \frac{\omega}{15}\tau)}{[100]} \frac{[P]}{[100]} \left[10\sqrt{P-15}\right] \right\} \quad \text{(C-10)}$$

The analog computer diagram for solution of Equations C-9 and C-10 is shown in Figure C-4. The results of this computation were expressed by plotting the stabilizer tank pressure, P, and the valve mass flow rate versus real time. Figure C-6, page 195, shows such a plot for a valve frequency of 1/2 cycle per minute ($\omega = 3.14$ radians/min). From these graphs it can be seen that, after the initial transient period, the stabilizer tank pressure, P, oscillated approximately 2 psia, and, thus, the valve mass flow rate was not sinusoidal in time. This effect was more prominent at low valve frequencies. In an effort to smooth the stabilizer tank pressure fluctuations and obtain a more sinusoidal output flow, a standard pressure regulator was added to the

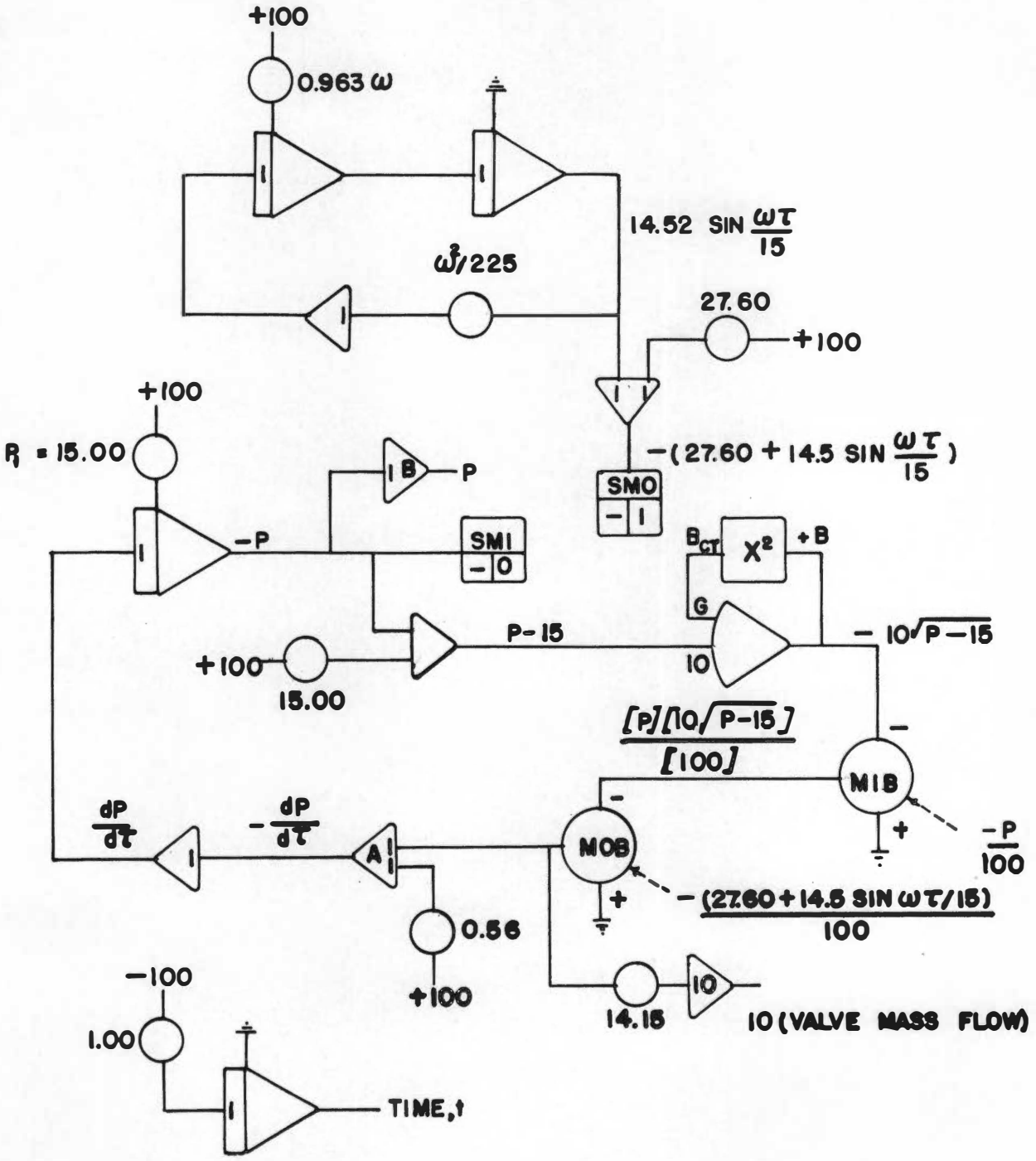


Figure C-4. Analog computer solution of sinusoid generator behavior.

system upstream of the stabilizer tank. The effect of this pressure regulator is described below.

Case II. F = Pressure Regulator Supply

The gas flow delivered by a pressure regulator is inversely proportional to the regulator downstream pressure. The operating characteristics of the proposed gas regulator were determined experimentally by the equipment shown in Figure C-1 and with a downstream static setting of 5 psig. The results can be approximately expressed as,

$$\text{regulator flow } \left(\frac{\text{cu in.}}{\text{min}}\right) = 2.96\text{x}10^{4} - 1542P$$

where

P = stabilizer tank pressure, psi

Since

$$F = (\text{regulator flow})\ \rho_T$$

and, assuming ideal gas conditions,

$$\rho_T = \frac{PW}{R_g T} = \frac{P(44)}{(18{,}550)(528)} = 4.49\text{x}10^{-6}P \text{ lb/cu in.}$$

Therefore,

$$F = P\left[0.1329 - 0.00693P\right] \text{ lb/min}$$

or

$$F = 0.1329\ P - 0.693\left[\frac{P^2}{100}\right] \qquad \text{(C-11)}$$

In this case, D becomes, by Equation C-7,

$$D = \frac{R_g T}{VW} \left(0.1329\ P - 0.693 \left[\frac{P^2}{100}\right]\right)$$

where

$$\frac{R_g T}{VW} = 106$$

and the constant term on the right side of Equation C-9 is replaced by the term, $\frac{R_g TF}{15VW}$, where

$$\frac{R_g TF}{15VW} = 7.07 \left(0.1329\ P - 0.693 \left[\frac{P^2}{100}\right]\right) \qquad (C\text{-}12)$$

The effect of the pressure regulator is incorporated in the analog solution of Figure C-4 by addition of the components shown in Figure C-5 at the amplifiers marked A and B. The results of the analog computer solution of the sinusoid generator system with the pressure regulator supplying the stabilization tank is shown in Figure C-6, page 195. The improvement over the unregulated system is obvious in that the stabilization tank pressure oscillations are reduced by a factor of two, resulting in a considerable improvement in the valve output flow wave. The flow rate closely approximated the desired sinusoid; therefore, the system which was built for the experimental sinusoid generator consisted of a 2100 cu in. stabilization tank supplied by the pressure

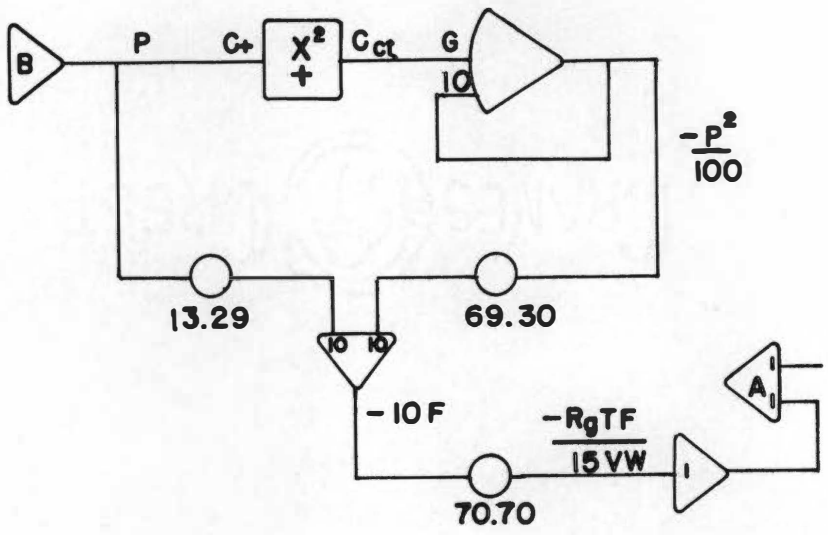


Figure C-5. Analog Simulation of Pressure Regulator Supply

regulator tested for this analysis.

IV. DISCUSSION

The performance of the sinusoid generator under actual operating conditions was very satisfactory. The system was capable of satisfactory sinusoidal flows from 0.1 lb/min, and greater, down to 0.01 lb/min. All adjustments and gear changes proved to be rapid and were easily accomplished. The quality of the concentration sinusoid, as discussed in Chapter V, was good; and the stabilizer tank pressure oscillations were within 1/2 psig of those predicted by the analog solutions when the system was operating at similar conditions.

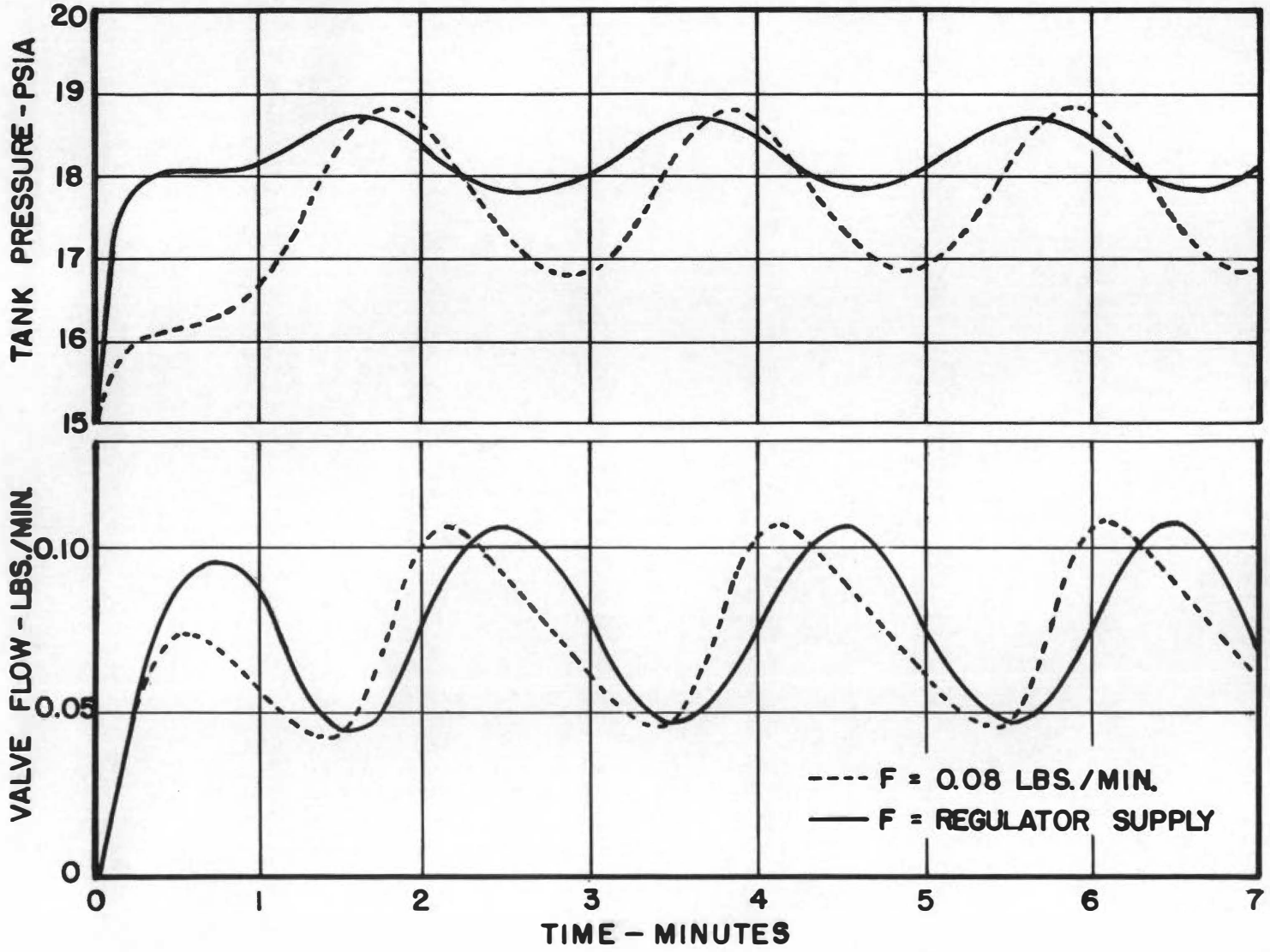


Figure C-6. Sinusoid generator dynamic response.

APPENDIX D

THERMAL CONDUCTIVITY CELL DEVELOPMENT

I. HISTORICAL BACKGROUND

The analysis of gases by thermal conductivity measurement is one of the oldest and most reliable methods used in the chemical process industry. The development and application of a practical apparatus took place simultaneously in Great Britain, Germany, and the United States around the turn of the century. A text of 357 pages by Daynes (31) presents the early development and basic theory up to 1930 and remains the classic reference in the field. Weaver (119) presents a review and discussion of the work between 1930 and 1945. In more recent times thermal conductivity analysis has received much attention as a detection method used in gas chromatography columns (38, 60).

The principle employed by this method is quite simple. When a wire or other resistive element is enclosed in a "cell" and heated by an electric current its temperature will rise until the loss in heat from the wire exactly balances the input of electrical energy to it. Since the heat transfer rate from the wire is some function of the thermal conductivity of the surrounding gas the final steady-state wire temperature is a measure of the gas thermal conductivity.

Thus, since the thermal conductivity of a binary gas mixture is directly related to the composition of the mixture (65), the wire temperature reflects the gas composition. If the hot wire or sensing element is made of a material that has a high temperature coefficient of resistance, the temperature of the wire can be determined from its resistance at steady-state conditions. The usual method to supply current to the wire and to measure its resistance simultaneously is to place the wire in one branch of a Wheatstone bridge.

The advantages of thermal conductivity analysis are simplicity of construction and reliability of operation. The disadvantages of the method are the difficulty of measuring other than binary mixtures and the inherently slow speed of response. Since most commercial cells have time constants* of 30 to 60 seconds (105, 24), they have not been used in unsteady-state experiments. The problem of complex mixture analysis is not so restrictive and its solution is described in detail later in this appendix.

The characteristic slow response speeds of commercial thermal conductivity cells are explained by the physical design of the cell and the nature of the sensing element. In most commercial instruments the gas to be analyzed is transferred to the sensing element by diffusion, natural convection,

---

*Time necessary for cell signal to reach 63 per cent of its final value.

or some combination of these two mechanisms. In addition, the sensing element is, in many cases, a long, relatively massive platinum or tungsten wire (21). Thus, the slow response speed or long time constant results from the time delay in delivering the concentration change to the sensing element and thermal lag of the element itself. The logical manner, therefore, to decrease the time constant of a thermal-conductivity cell is to eliminate, as far as possible, both these types of lags. Preliminary design calculations indicated that time constants of one second or less were possible if the transportation delay could be made negligible.

To reduce the transportation lag a "direct flow" cell was proposed. In this arrangement the sensing element is placed directly in the flowing sample stream (94). In addition, a high linear sampling velocity was proposed to further reduce any transportation lag. Unfortunately, both these approaches would produce, according to past theory and experience, nonlinear response and flow sensitivity (36, 55).

Although a number of elegant theoretical developments have shown that pure conduction heat transfer is necessary for a linear response (bridge signal directly proportional to thermal conductivity change) (31, 15, 118), this author would argue that, even in "diffusion" cells where linear responses are commonly observed, the primary heat transfer mechanism is, in reality, natural convection. For this rea-

son this consideration was not influential in the final cell design.

The problem of flow sensitivity, i.e., the variation of bridge signal due to gross or random turbulent flow fluctuations, was considered more serious. To avoid this situation, it was proposed to create a fully developed laminar flow through the cell to minimize turbulence and to control the average flow rate carefully to eliminate gross flow variations.

The logical way to reduce the thermal lag of the sensing element is to reduce the total heat capacity of the element and/or to increase the heat transfer rate from it. The gas film heat transfer coefficients would increase from those of natural convection to those of forced convection by repositioning the sensing element directly in the sample flow stream. The total heat capacity of the element could be reduced by using an element of the smallest possible mass. This reasoning led to the selection of thermistors for the sensing elements of the proposed thermal conductivity cells.

A thermistor is a termperature sensitive, semi-conductor with the unique property of having a negative coefficient of resistivity (9). Figure D-1 shows a typical resistance-temperature characteristic for a thermistor and indicates, by comparison with a platinum wire, its great superiority in sensitivity. Thermistors are manufactured in a variety of

shapes, sizes, and resistive values (110). Beads as small as

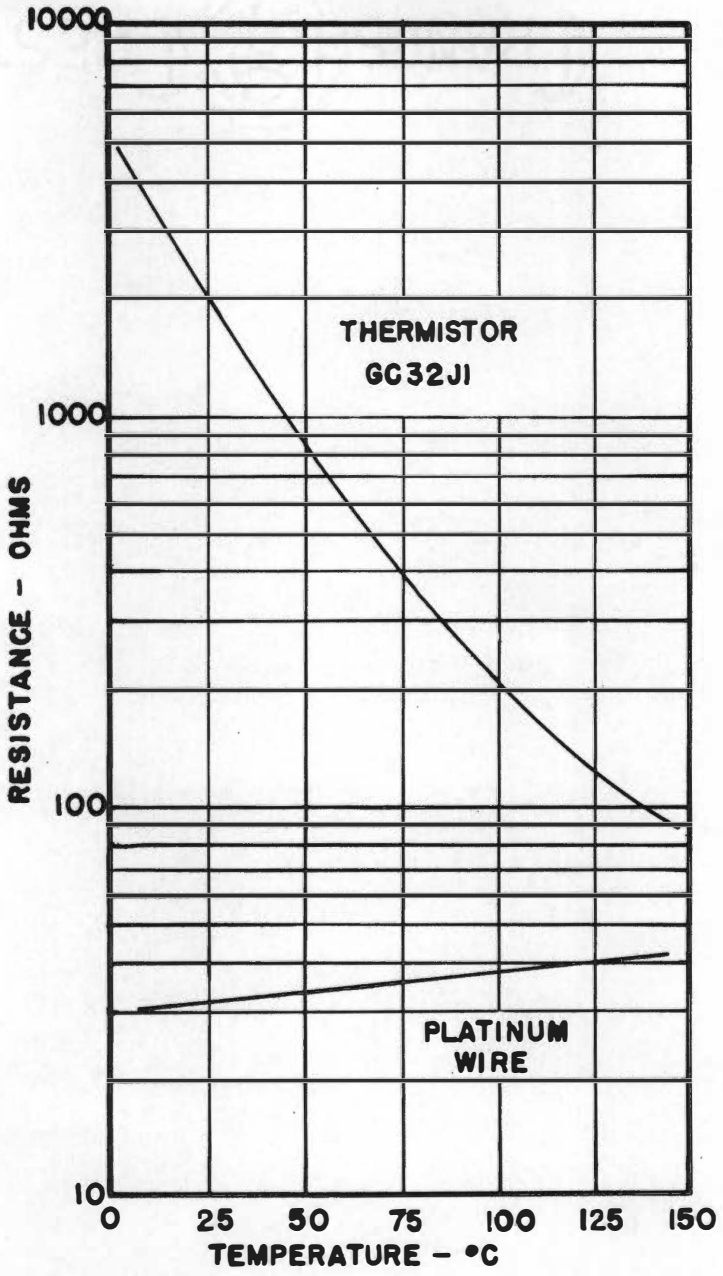


Figure D-1. Thermistor Resistance Temperature Characteristic

0.01 in. in diameter are available and it was this type of thermistor which seemed appropriate for a high speed thermal

conductivity cell application. It is a manufacturer's practice to characterize thermistors by a thermal "time constant" which has significance only in determining the relative heat capacities of the several different thermistors. Thus, this specification was used to determine the thermistors of lowest total heat capacity (those with the lowest "time constant").

The use of thermistors as sensing elements was not a new idea and several cells have been designed to take advantage of their high sensitivity (30, 35, 111). The work of Walker and Westenberg (118) deserves particular attention as an example of a well designed cell, while Cowan and Sterling's (27) study on thermistor selection and operation was of extreme value.

The physical design of thermal conductivity cells has received a great variety of treatments (36, 55, 30, 111, 54, 112) with each individual cell designed to the particular needs of the application at hand. The construction details of the cell used in this work is shown in Figure D-2. The design considerations applied to this cell are discussed below.

II. THERMAL CONDUCTIVITY CELL DESIGN

Although several methods have been devised to apply thermal conductivity analysis to other than binary mixtures (71, 83), the gas system used in this work (air-CO_2-water

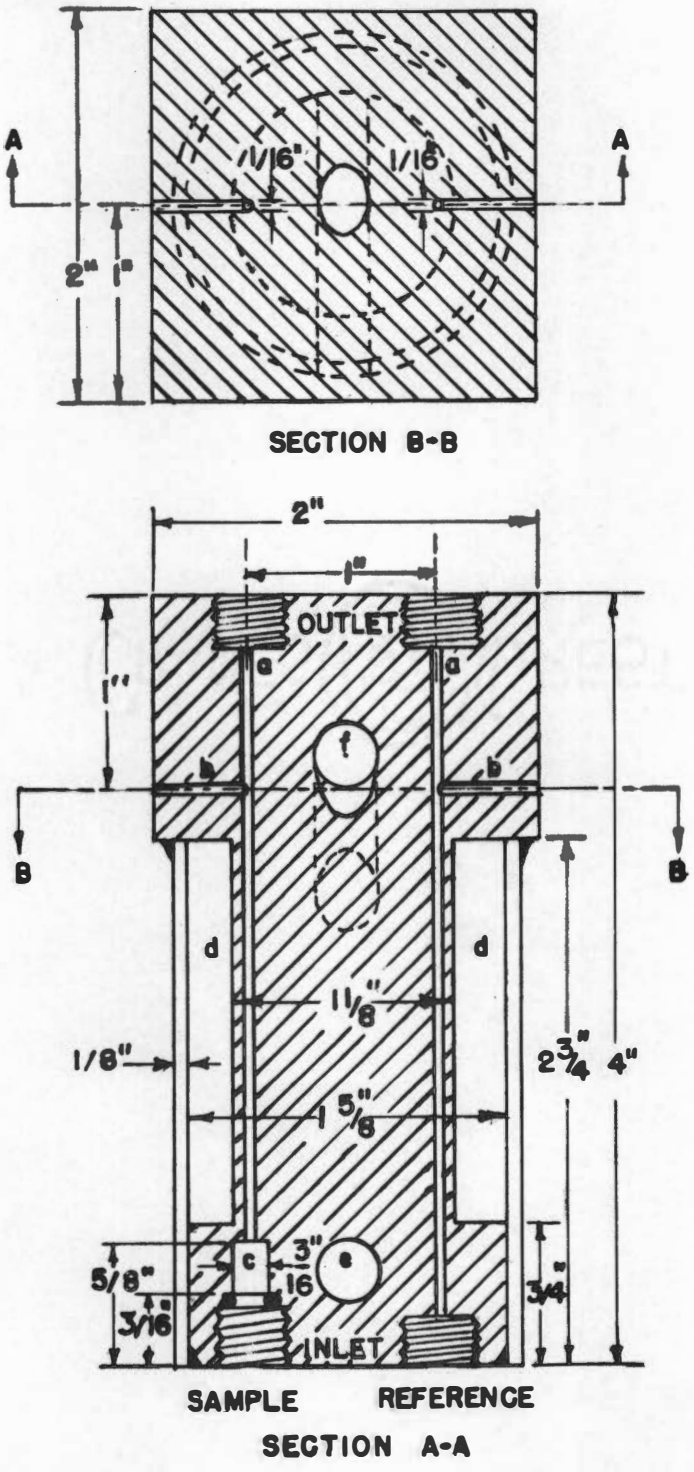


Figure D-2. Thermal conductivity cell.

vapor) allowed the simpler arrangement of the reference gas method to be used. In this method an additional sensing element is placed in a reference gas containing all the constituents of the sample gas except the component of interest. This reference sensing element is then placed in the arm of the Wheatstone bridge opposite the sample sensing element with the result that the bridge signal reflects only changes in concentration of the sample gas component of interest. Thus Figure D-2 shows two gas passages, a; one for continuous sample withdrawal and one for continuous reference gas flow. The gas passages were made intentionally small so as to insure viscous flow (small Reynolds numbers) with large gas sampling velocities. The thermistor access holes, b, were placed approximately fifty passage diameters from the gas passage entrance to eliminate entrance flow effects and to provide sufficient length for the gas to come to the cell temperature. These access holes were also 1/16-inch in diameter.

The thermistor bead was mounted in a two-hole, 0.056-inch OD by 1-inch long ceramic tube as shown in Figure D-3. The 3/8-inch long, 0.001-inch diameter, Pt-Ir thermistor leads were soft soldered to 0.010-inch diameter Pt wire threaded through the ceramic tube. The platinum wire was sealed to the ceramic tube with low melting vacuum wax. In turn the ceramic tube was sealed to the cell body at the

entrance of the access hole with the same material. This mounting arrangement allowed the thermistor to be conveniently located at any position in the sample stream and to

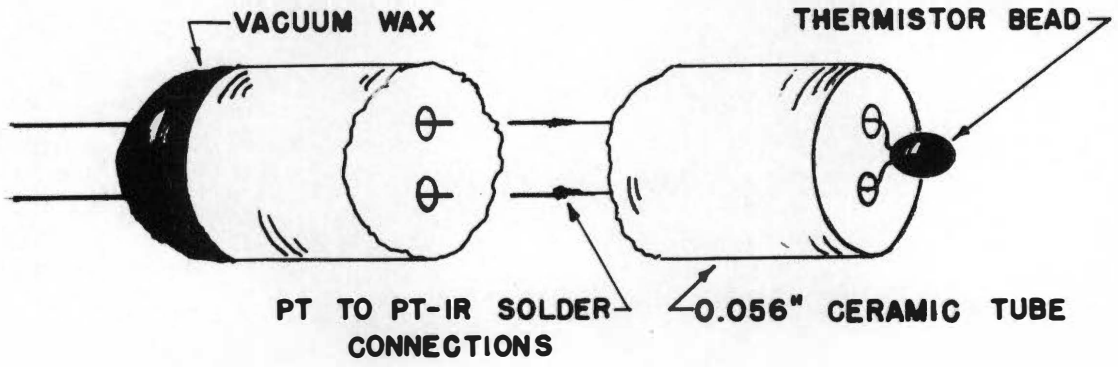


Figure D-3. Thermistor Mounting Arrangement

be withdrawn entirely from the stream if necessary.

The stainless steel cell body was drilled and tapped for 1/8-inch N.P.T.x1/4-inch stainless steel flare fittings at all inlets and outlets except at the sample gas inlet. At this position (c), the entrance hole was recessed approximately 1/2-inch to permit the cell to be placed on the 3/16-inch OD sampling tube. An "O-ring" was used to seal the sampling tube to the cell body and a specially designed fitting held the cell in place.

Although a few thermal conductivity cells have been operated without external temperature control (91, 111) most sensitive applications require careful cell temperature

regulation (55, 27, 118, 70, 48). The temperature of the cell designed for this work was controlled by continuously circulating a constant temperature oil through the cell body. The oil entered the cell point e of Figure D-2, flowed upward past the gas passages in the chamber d and left the cell through the port at point f.

III. WHEATSTONE BRIDGE THEORY AND DEVELOPMENT

The number and variety of cell designs used in thermal conductivity analysis is surpassed only by the number and variety of Wheatstone bridge designs which have been applied to the method (36, 55, 111, 71, 5, 79). Of the numerous statements and generalizations which have been made on the subject of bridge design, the developments of Cowan and Sterling (27) seem the most complete. A modification of these authors' developments is given below to serve as the theoretical justification for the bridge design used in this work.

Consider the Wheatstone bridge shown in Figure D-4 where R_s and R_r are the sample and reference gas thermistor resistances, respectively, R_1 and R_2 are the bridge fixed resistors, I_t is the total bridge current, and ϵ is the unbalanced bridge voltage as measured by an absolute potentiometric detector.

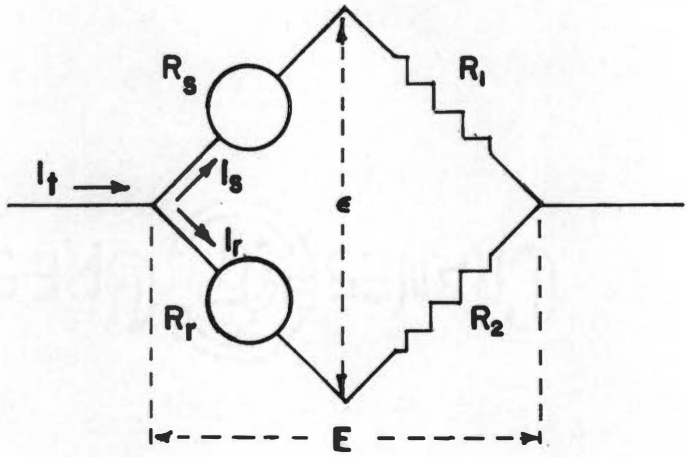


Figure D-4. Wheatstone Bridge

Thus

$$\epsilon = I_s R_s - I_r R_r \tag{D1}$$

also

$$I_s (R_s+R_1) = I_r (R_r+R_2) \tag{D2}$$

Elimination of I_s from Equations D1 and D2 and rearrangement gives

$$\epsilon = \frac{I_r \left[R_s(R_r+R_2) - R_r (R_s+R_1)\right]}{R_s + R_1} \tag{D3}$$

But

$$I_t = I_s + I_r \tag{D4}$$

Elimination of I_s from Equations D2 and D4 and rearrange-

ment yields

$$I_r = \frac{I_t(R_s+R_1)}{R_r + R_s + R_1 + R_2}$$

Substitution of this equation into Equation D3 gives

$$\epsilon = \frac{I_t(R_sR_2-R_rR_1)}{R_r+R_s+R_1+R_2} \tag{D5}$$

For a constant voltage source

$$E = R_e\, I_t \tag{D6}$$

where

$$R_e = \frac{(R_s+R_1)(R_r+R_2)}{R_1+R_2+R_r+R_s}$$

Elimination of I_t from Equations D5 and D6 with rearrangement yields

$$\epsilon = \frac{E(R_sR_2-R_rR_1)}{(R_s+R_1)(R_r+R_2)} \tag{D7}$$

If the special conditions that $R_1=R_2=R$ and $R_s=R_r+\delta R_r$ are imposed on Equation D7 it becomes,

$$\epsilon = \frac{ER\cdot\delta R_r}{(R_r+\delta R_r+R)(R_r+R)}$$

and upon rearrangement

$$\epsilon = \frac{E}{R_r+R}\left[\frac{R_r+\delta R_r}{1+\delta R_r/(R_r+R)} - R_r\right] \tag{D8}$$

Since $\frac{1}{1+a} = 1 - a + a^2 - a^3 + \text{----}$ for $|a| < 1$,

$$\frac{1}{1+\delta R_r/(R_r+R)} = 1 - \frac{\delta R_r}{R_r+R} - \left[\frac{\delta R_r}{R_r+R}\right]^2 - \text{----} \qquad \text{(D9)}$$

Substitution of Equation D9 into D8 with subsequent rearrangement and neglect of δR_r^2 and higher order terms gives,

$$\epsilon \cong \frac{E\,\delta R_r}{R_r+R}\left[1 - \frac{R_r}{R_r+R} - \frac{\delta R_r}{R_r+R}\left(1 - \frac{R_r}{R_r+R}\right)\right] \qquad \text{(D10)}$$

Now let the bridge fixed resistance R be expressed in terms of the thermistor resistance R_r as

$$R = a\,R_r$$

Substitution of this relation into Equation D10 gives

$$\epsilon \cong \frac{E}{1+a}\left(\frac{\delta R_r}{R_r}\right)\left[1 - \frac{1}{1+a} - \frac{1}{1+a}\left(\frac{\delta R_r}{R_r}\right)\left(1 - \frac{1}{1+a}\right)\right]$$

or

$$\epsilon \cong \frac{a\,E}{(1+a)^2}\left(\frac{\delta R_r}{R_r}\right)\left[1 - \frac{\delta R_r}{R_r(1+a)}\right] \qquad \text{(D11)}$$

The second term in the brackets of the above equation causes the unbalanced bridge voltage ϵ to be nonlinear in δR_r. Define the "relative nonlinearity" as the ratio of this nonlinear component at any value of a to its value when a=1 or $R_r=R=R_1=R_2$. Thus,

$$\text{"relative nonlinearity"} = \frac{2}{1+a} \qquad \text{(D12)}$$

If R_r and/or a are large, then

$$\frac{\delta R_r}{R_r(1+a)} \ll 1$$

and Equation D11 becomes

$$\epsilon \cong \frac{aE}{(1+a)^2} \left(\frac{\delta R_r}{R_r}\right) \qquad \text{(D13)}$$

Now define the "relative bridge signal" as the ratio of the unbalanced bridge signal, ϵ, for any a to the unbalanced bridge signal for $a=1$. Thus, by Equation D13 with constant current conditions ($\frac{\delta R_r}{R_r}$ = constant),

$$\text{"relative bridge signal"} = \frac{4a\ E}{(1+a)^2 E'} \qquad \text{(D14)}$$

where

E = bridge voltage at I_t and a

E' = bridge voltage at I_t and $a=1$

Under the conditions that $R_1=R_2=aR_r=aR_s$, Equation D6 becomes

$$E = R_e\ I_t \qquad \text{(D15)}$$

where

$$R_e = \frac{(1+a)R_r}{2}$$

From these equations the "relative bridge voltage" becomes,

$$\text{"relative bridge voltage"} \equiv \frac{E}{E_T} = \frac{1+a}{2} \qquad \text{(D16)}$$

Substitution of Equation D16 into Equation D14 gives

$$\text{"relative bridge signal"} = \frac{2a}{1+a} \qquad \text{(D17)}$$

Thus, as can be seen from Equation D17, the relative bridge signal increases toward a limit of 2 as the ratio of the matched fixed resistance to the matched thermistor resistance, a, increases. Also, by Equation D12, the relative nonlinearity decreases in the process. These favorable effects result at the cost of increased bridge voltage as can be seen from Equation D16. Table II shows the quantitative effects of increasing $a=R/R_r$ on relative bridge signal, the relative nonlinearity, and on the relative bridge voltage.

The calculations shown in Table II suggested that a practical compromise between increased sensitivity (relative bridge signal) and increased power supply requirements (relative bridge voltage) occurred at a value of $a=R/R_r$ somewhere between 5 and 10. This meant that the matched thermistor resistances $R_s=R_r$ should be as small as possible so that the total bridge voltage, E, could be maintained at a

reasonable value (Equation D15) for some fixed thermal condition (bridge current).

The thermistor found to possess the desirable properties of low resistance, low "thermal time constant," and a

TABLE II

MATCHED BRIDGE RELATIVE CHARACTERISTICS

a (R/R_r)	Relative Bridge Signal $(2a/1+a)$	Relative Nonlinearity $(2/1+a)$	Relative Bridge Voltage $(1+a/2)$
1	1.00	1.00	1.0
2	1.33	0.67	1.5
3	1.50	0.50	2.0
5	1.66	0.33	3.0
7	1.75	0.25	4.0
9	1.80	0.20	5.0
19	1.90	0.10	10.0
49	1.96	0.04	25.0

lead arrangement which would allow mounting as in Figure D-3 was Fenwal Electronics' Thermistor GC32J1. This thermistor was available also as a factory matched pair (G170). The designation "matched pair" means that the two thermistors concerned have, within some specified limits, the same resistance-temperature characteristic (see Figure D-1). The necessity for matching is demonstrated by Equation D11 which shows that the unbalanced bridge signal, ϵ, is a direct function of the difference in sample and reference resistance, δR_r. Thus, if the cell temperature and/or bridge current

should fluctuate it would cause, in a bridge of unmatched thermistors, a variation of δR_r. This would result, in turn, in an unstable "null point" or "base line" (27, 118).

From the resistance-temperature and voltage-current characteristics of Thermistor GC32J1 it was estimated that the operating resistance of the thermistor would be approximately 200 ohms. With a value of $a=7.5$ the matched fixed resistance, R_r, therefore, should be approximately 1500 ohms. These values of the bridge element resistances resulted in, by Equation D15, an equivalent bridge resistance, R_e, of 850 ohms and required, with an approximate total bridge current I_t of 10 ma, a bridge voltage of 8.5 volts. The additional resistance added to the bridge circuit for current control and measurement required a power supply of at least 15 volts and effectively eliminated the use of storage batteries for this application. Instead and electronic, variable voltage, regulated DC power supply was obtained for the Wheatstone bridge.

The final bridge design used to detect the thermal conductivity cell signals is shown in Figure 7. A detailed explanation of the function of the individual components and of the operation of the bridge is given in Chapters III and IV. As stated in these chapters, the Sanborn Low-Level Preamplifier with its associated recorder acted as a potentiometric detector since it had imput impedance of 5300 ohms.

A parallel feed arrangement was used to avoid thermal runaway which is possible with a series thermistor bridge (i.e., detector and power supply of Figure 7 interchanged). In addition, the changes in bridge current are much smaller for the parallel arrangement than for the series bridge so that the regulation is better when electronic power supplies are used (27).

IV. CELL TESTS AND CALIBRATIONS

Gas analysis by thermal conductivity is not accomplished by absolute determination of the gas mixture thermal conductivity but, instead, by measurement of a relative cell and bridge signal and by comparison of this signal with a previously determined empirical calibration (21, 119). Thus the accuracy of the analysis is limited by the accuracy of the calibration.

In principle, calibration of a cell is a deceptively simple process involving only the measurement of the cell signal for several gas mixtures of known composition. The difficulty arises with the formation of gas mixtures of accurately known compositions. This exacting task can be divided into two general approaches: batch mixing and continuous mixing. Numerous techniques have been devised for both approaches (31, 119). The flow sensitivity tests of this investigation required that the continuous mixing method

be used.

Descriptions of equipment capable of continuous generation of gas mixtures with accurately known compositions have been published in the recent literature (95, 114, 118). These devices served as an aid in the design of the standard gas mixer used for calibration of the thermal conductivity cell.

Figure D-5 is a schematic diagram of the calibration gas mixer. This mixer utilized the two stage dilution method to obtain gas mixtures of low concentration. The building compressed air supply was used as the air source for the mixer. It supplied air at 30 psig to a Climax type 245 filter regulator followed by a Matheson, low pressure "pancake" regulator. This series regulator arrangement was found necessary to eliminate the effects of periodical pressure cycling of the building air supply. The low pressure regulator supplied air to the mixer at approximately 2-1/2 psig. The air volume flow rate, F_{PA}, to the primary dilution point was measured with one of the specially designed capillary flowmeters (CFM #2) which have been described in Chapters III and IV.

The carbon dioxide used in these tests was "bone dry" grade taken from a cylinder through a Matheson, "two-stage" pressure regulator and a Matheson, low pressure "pancake" regulator. The CO_2 flow rate to the primary dilution point,

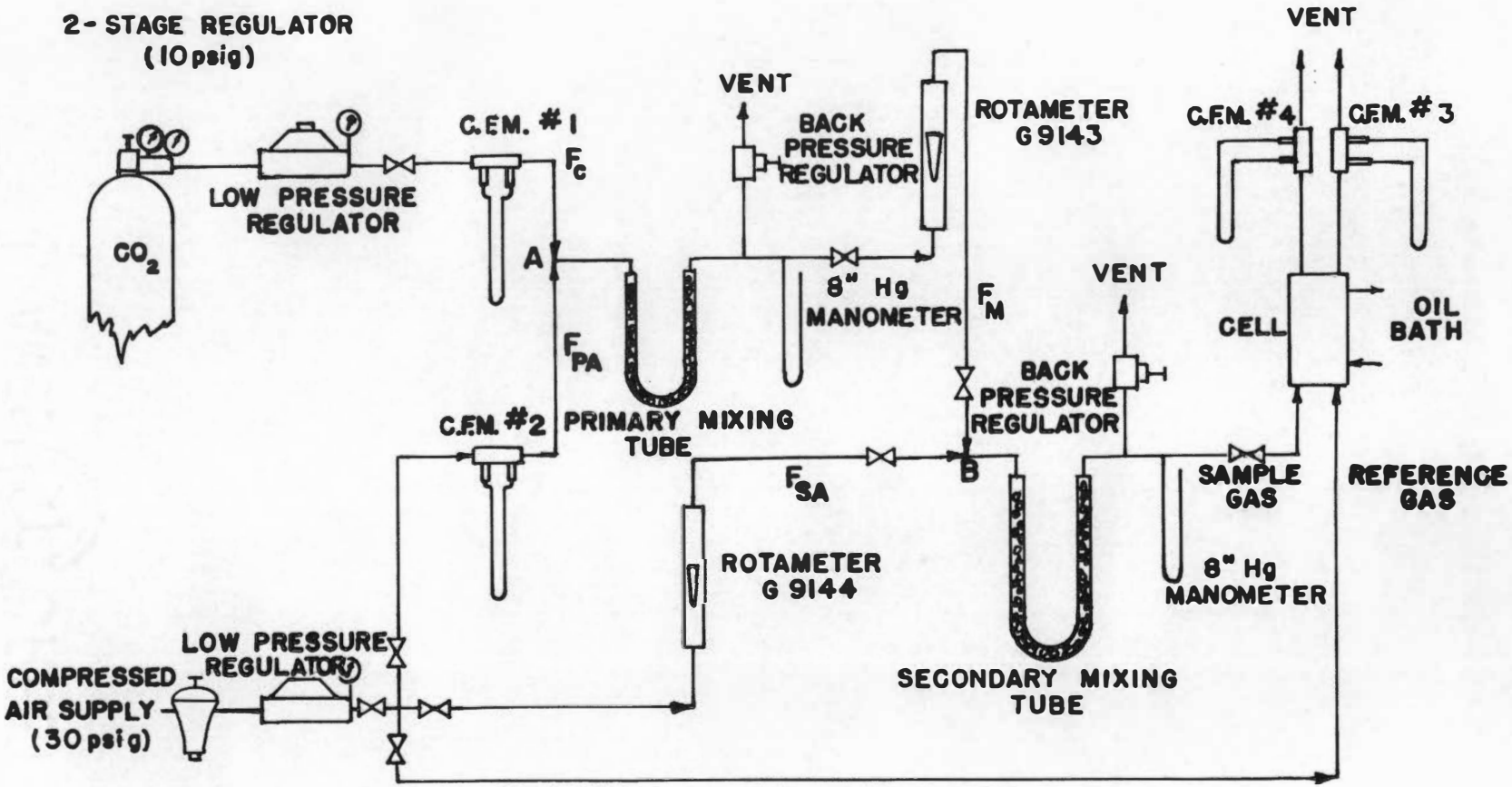


Figure D-5. Schematic diagram of calibration gas mixer.

F_C, also was measured with a capillary flowmeter (CFM #1). These capillary flowmeters were calibrated by the method described in Chapter IV the results of which are given in Figure E-5 of Appendix E.

The primary air flow and the CO_2 flow met at point A, and were well mixed in the primary mixing tube--a 2-foot long 1/2-inch tygon tube filled with 5 mm glass beads. The pressure of this mixing section was maintained at approximately 5 inches of mercury by a standard Taylor instrument-air regulator which was modified to act as a back-pressure regulator.

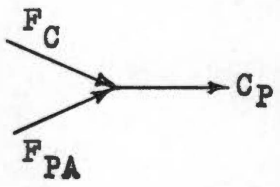
A portion, F_M, of the primary gas mixture was bled from this section, measured with a Tri-flat Predictability rotameter (G9143--stainless float), and introduced to the secondary dilution section at point B. The secondary air flow, F_{SA}, entered the system at the air manifold, was measured with a Tri-flat Predictability rotameter (G9144--sapphire float), and mixed with the primary dilution mixture, F_M, in the secondary mixing tube. These rotameters also were calibrated with the soap-film flowmeter described in Chapter IV. Figures E-6 and E-7, Appendix E, give the calibration curves for these meters.

The pressure in the secondary dilution section was held at about 4 inches of mercury with another Taylor instrument-air regulator modified for use as a back-pressure

regulator.

A portion of the secondary gas mixture was then bled from the system through the thermal conductivity cell for calibration purposes. The cell reference gas was taken directly from the inlet air manifold. The sample gas and reference gas flow rates were measured with capillary flowmeters #4 and #3, respectively, the calibration curves for which are shown in Figure E-4 of Appendix E.

The concentration of the final gas mixture, C_S, flowing to the thermal conductivity cell was calculated from the following simple relationships. The primary dilution section can be illustrated by



where

F_C = CO_2 volume flow rate, ml/min

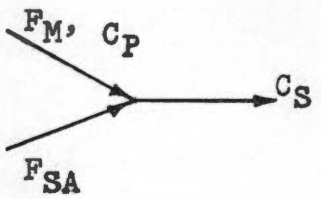
F_{PA} = primary air volume flow rate, ml/min

C_P = concentration of primary gas mixture, vol. %

If the mixing is assumed isothermal and the gases are ideal, then define

$$d_P \equiv \text{"primary dilution factor"} = \frac{F_C}{F_{PA}+F_C} = C_P \qquad (D18)$$

The mixing in the secondary dilution section occurs as



Thus

$$C_S = \frac{F_M C_P}{F_{SA} + F_M} = \frac{F_M F_C}{(F_{SA} + F_M)(F_{PA} + F_C)}$$

When the "secondary dilution factor," d_S, is defined as

$$d_S \equiv \frac{F_M}{F_{SA} + F_M} \tag{D19}$$

then

$$C_S = d_P \cdot d_S \tag{D20}$$

Thus, the concentration of the gas mixture leaving the secondary dilution section was simply the product of the primary and secondary dilution factors which are defined by Equations D18 and D19, respectively. The dilution factors which could be obtained from the mixer flowmeter ranges were such that a variation in concentration of 0.04 per cent to 100 per cent CO_2 could be obtained. The maximum relative error in concentration for this calibration gas mixer was estimated to be 9 per cent.

With the completion of the calibration gas mixer and

the thermal conductivity cells and bridge, a series of tests was conducted on the equipment to determine, among other things, flow, current, pressure, and temperature sensitivity. Figure D-6 shows a photograph of the calibration gas mixer and other equipment used in these tests and calibrations. The operation of the preamplifier and recording oscillograph and a description of the techniques for bridge current determination have been described in detail in Chapter IV.

Cowan and Stirling (27) have shown that maximum bridge sensitivity is obtained when the temperature difference between the operating thermistor and the cell body is in the neighborhood of 50°C. From estimated values of thermistor current and the resistance-temperature characteristic for the thermistor used here (Figure D-1), it was estimated that this condition would exist when the cell body was at 35°C (95°F). For this reason all tests and calibrations, except where noted, were carried out at this cell temperature.

At the start of the thermal conductivity tests a determination of the thermistor mismatch at operating conditions was made. This was accomplished by first adjusting the current balancing potentiometer (see Figure 7) for equal bridge arm currents ($I_s = I_r$) by the method described in Chapter IV. Under these conditions

$$I_s = I_r = I_t/2$$

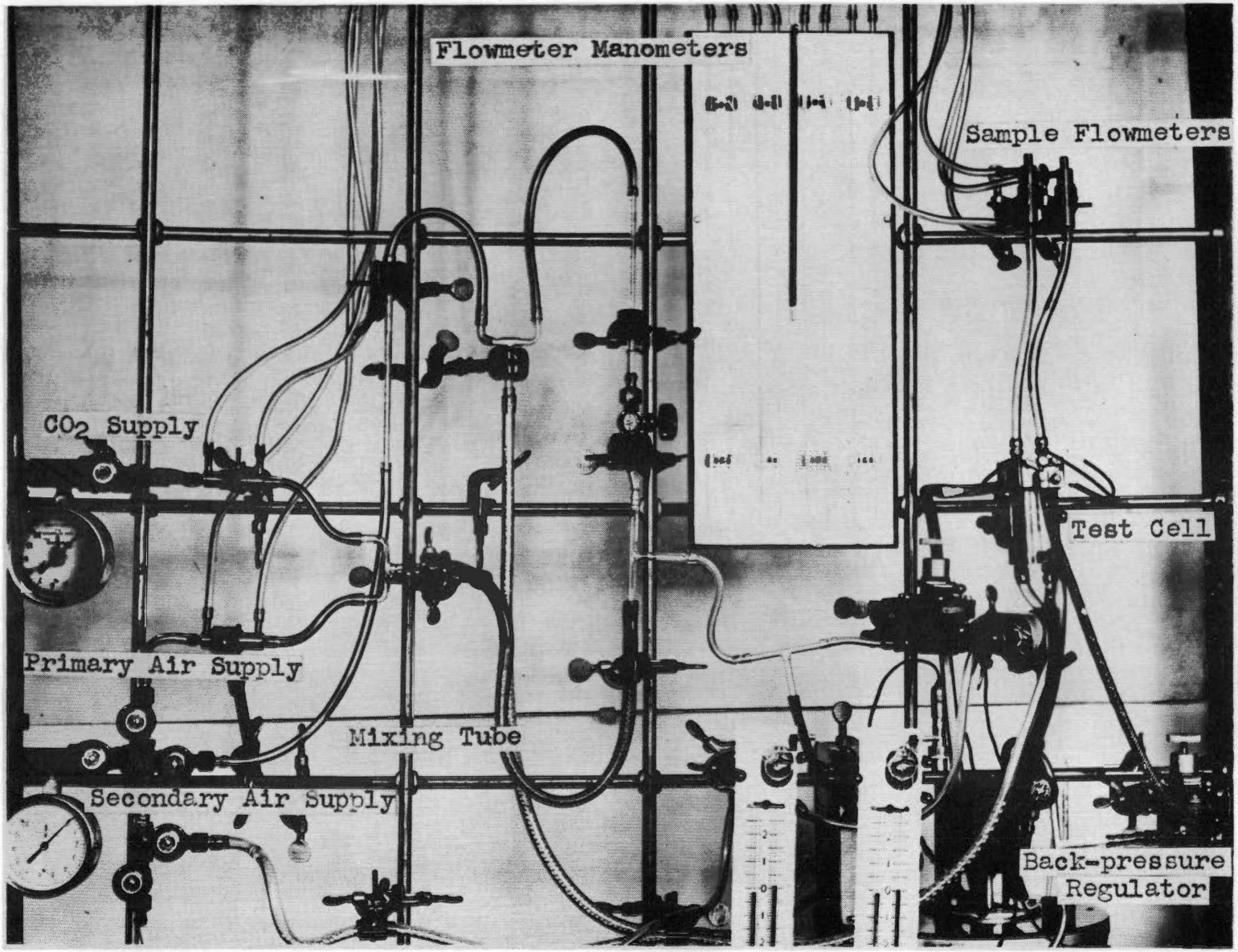


Figure D-6. Thermal conductivity cell test and calibration equipment.

and by Equation D1

$$R_s - R_r = 2\epsilon / I_t$$

the bridge signal, ϵ, was obtained with the bridge balancing potentiometer full counterclockwise. From measurement of the total bridge current and the unbalanced bridge signal at these conditions the thermistor mismatch was found to be

$$R_r - R_s = \pm 21.6 \Omega$$

This was, unfortunately, a rather large difference although it almost met the manufacturer's specifications ($\pm$10%). The effects of this mismatch will be discussed presently.

Previously reported studies of thermal conductivity cells utilizing thermistors (27, 118) have shown that the cells exhibit a maximum in sensitivity (unbalanced bridge signal) with increasing thermistor current. Therefore, a series of tests was made on the cells and bridge designed for this work in an effort to determine the bridge current which would result in maximum sensitivity.

The procedure for these tests was as follows:

The current balance potentiometer was set for equal bridge arm currents and the power supply voltage was set arbitrarily at 30.0 volts. The flowmeters of the calibration gas mixer were set so as to generate a gas of 10 per cent CO_2 concentration. With this gas mixture and a reference gas

flowing through the cell, the unbalanced bridge signal was determined for several different values of the bridge current. The results of these tests are shown in Figure D-7.

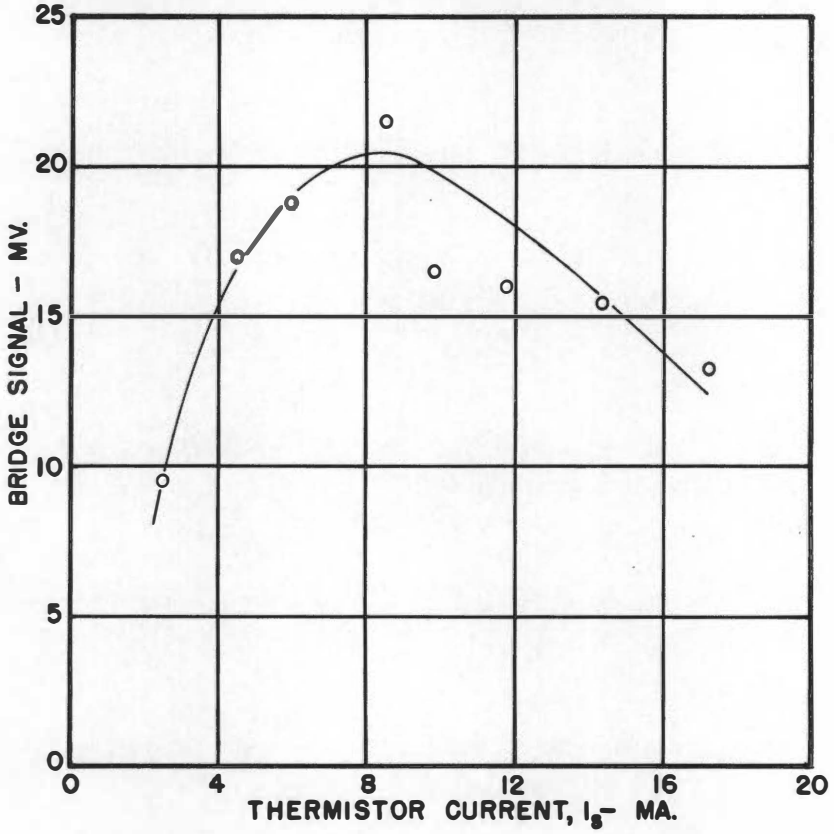


Figure D-7. Bridge Signal vs. Thermistor Current

The scatter of these data resulted from two effects. Since the thermistors were not matched perfectly, changes in the bridge current resulted in null point shifts which required the unbalanced bridge signal due only to CO_2 to be calculated from the difference in bridge signal with 10-per cent CO_2 in the sample stream and with 0-per cent in the sample stream at the same flow rate. Thus, the required

changes of the mixer flows introduced uncertainty about the constancy of the CO_2 concentration. In addition, some difficulty was experienced in keeping the sample flow rate through the cell constant and the cells appeared to be sensitive to sampling flow changes.

Nevertheless, the data do show a broad maximum and were considered sufficiently accurate to justify the selection of an optimum thermistor current of 8 ma. This thermistor current was used for subsequent tests, calibrations, and operation of the cells.

To investigate more thoroughly the effects of sampling flow rates a series of tests was made at various cell flow conditions. These tests consisted of first measuring the unbalanced bridge signal for the sample flow, F_t, of 100-per cent air, equal to the reference flow, F_r, at various cell flow rates. The test was then repeated with the sample flow, F_s, having a concentration of 10-per cent CO_2. The results of these tests are shown in Figure D-8 in which the unbalanced bridge signal is plotted against the flow rate $F_r=F_s$. This technique was used to obviate the continual re-establishment of a constant 10-per cent CO_2 mixture.

In an effort to obtain a maximum speed of response the thermistors were initially mounted at approximately the center line of the cell gas passages with the result, as seen from Figure D-8, that the bridge null point was seriously

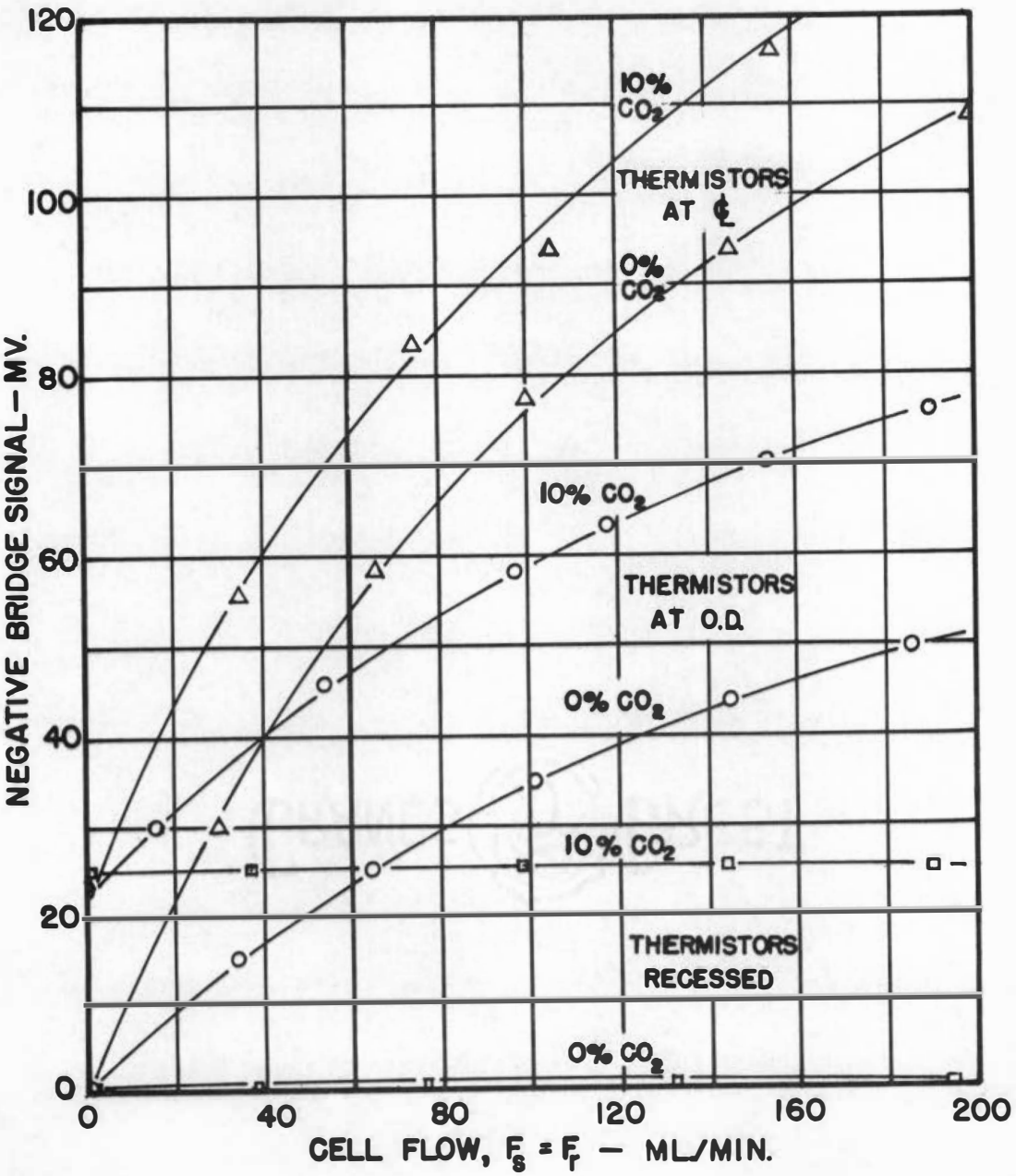


Figure D-8. Bridge signal vs. cell flow rate.

affected by flow rate variation. In the final analysis this flow sensitivity resulted from the thermistor mismatch. Changes in flow rate caused corresponding changes in heat transfer coefficient and thus in thermistor temperature. This, because of the mismatched thermistor temperature coefficients of resistance, resulted in altered bridge signals. In addition to the gross changes in bridge signal a serious fluctuating flow effect was noted with the thermistor at the center line position. These random disturbances were significant at the 1/2-mv/cm sensitivity level.

The thermistors were also tested for flow sensitivity when placed at the outer edge of the cell gas passages and at a position approximately 1/32 inch removed from the flow stream. The results of these tests are also plotted in Figure D-8. As can be seen the flow sensitivity was significantly reduced and effectively eliminated with the thermistors in these two respective positions. Not only was the gross bridge signal made insensitive to cell flow rate but also the signal due to CO_2 content (the difference between the F_s=air and F_s=air+CO_2 curves at any position) became essentially independent of sampling rates--a very desirable condition. In addition, the rapid turbulent variations were eliminated. From these data it was decided to use the cells with the thermistors in the withdrawn position, at the cost of some reduction in speed of response.

In passing it should be mentioned that the smallest of leaks at the vacuum wax seal between the thermistor ceramic tube and the cell body caused extreme flow sensitivity with thermistors in the withdrawn position and that great care had to be taken to assure an absolutely tight system.

As has been discussed, any variation of operating conditions which can alter the thermal condition of the thermistor will result, in a bridge using mismatched thermistors, in undesirable changes in the absolute unbalanced bridge signal. Thus, since mismatched thermistors were used in the cells, a check of the cell body temperature regulation and the stability of the bridge current was in order.

With the cell operated at constant sampling flow rates the bridge signal was found to cycle about ± 0.3 mv with the same frequency as the off-on control of the constant temperature bath. Under zero flow conditions the cycling was only about ± 0.1 mv. From cell temperature drift data this latter condition was estimated to be equivalent to a cell body temperature variation of $\pm 0.16^{\circ}F$.

Bridge current stability was tested by turning off the constant temperature bath and allowing the cell to come to thermal equilibrium with room conditions which were presumed constant. Then, at zero cell flows, the current measuring resistor, R_M, was monitored for 30 minutes. A total current variation of approximately ± 0.015 ma was noted. Thus

the thermistor current regulation was 8.0±0075 ma. Assuming that the thermistor mismatch was 20 ohms (R_r-R_s=20 ohms), the variation of bridge signal due to current instability was calculated to be ±0.15 mv.

Although the degree of temperature and current stability found in the above tests would not have been satisfactory for a sensitive absolute analysis (27, 118), they were believed suitable for the concentration ranges to be used in this investigation.

The previously mentioned thermal drift test was made to determine how much the bridge signal would change with gross variations of cell body temperature. With equal gas flow in the cell (F_r=F_s=60 ml/min of 100% air), the bridge was balanced when at thermal equilibrium with ambient conditions (88°F). The thermostatting bath was then turned on and adjusted to 96°F. After the cell reached this temperature the bridge signal was recorded. This procedure was repeated at 104°F. The results of these tests are shown in Figure 9. Also shown are the bridge signals due to a 10.5-per cent CO_2 gas mixture at each temperature. The magnitude of these signals was the result of CO_2 only--the null point effects having been removed. These curves clearly demonstrate the necessity for good cell temperature regulation.

Although the kinetic theory of gases predicts that the thermal conductivity of a gas should be independent of

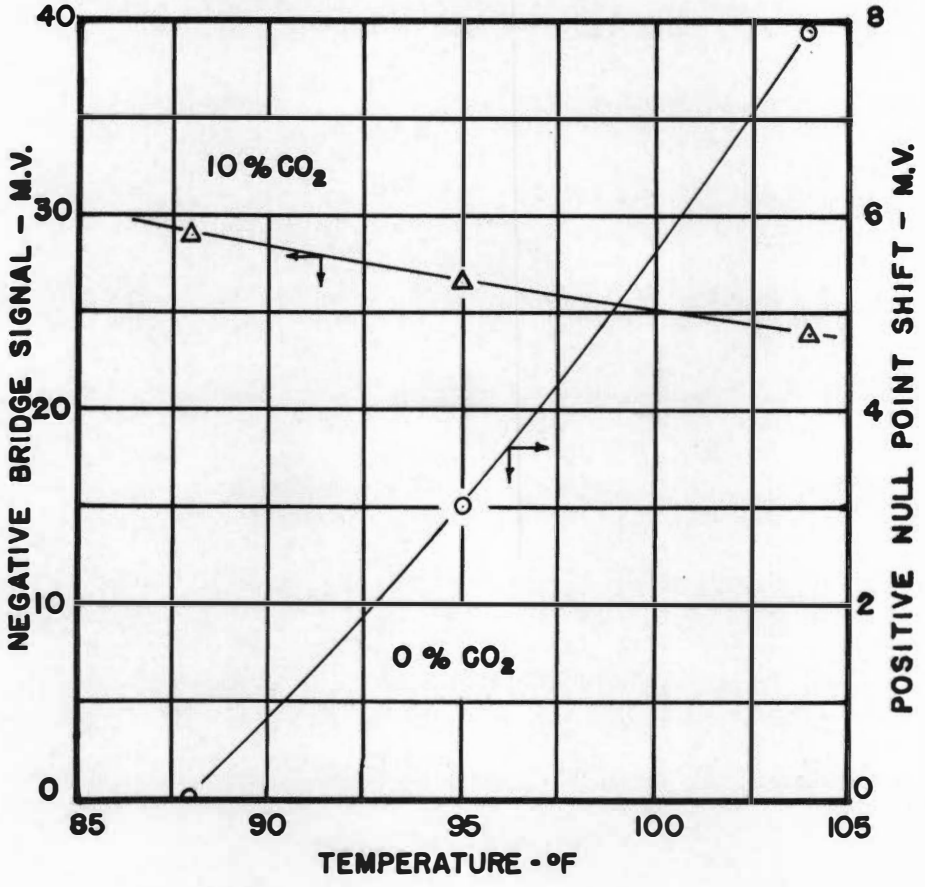


Figure D-9. Null Point and Sensitivity Temperature Effects

pressure, a verification of this hypothesis, with the thermal conductivity cells used in this investigation, seemed in order. Thus the bridge was balanced with $F_s=F_r=60$ ml/min of 100-per cent air and a constant cell temperature of 35°C

(95°F). A change in the sample gas concentration to 10.5-per cent CO_2 resulted in a negative bridge signal of 27.6 mv. The sample and reference gas was then cut off and the cell pressure increased to 3.1 inches of mercury (1.5 psi) above atmospheric pressure. Under these conditions the bridge signal decreased slightly to 27.1 mv. This slight change was believed due to the change in the flow condition (see Figure D-8) since the 27.1 mv signal remained constant when the cell pressure was returned to atmospheric conditions. A repeat of this test gave similar results, thus indicating that small changes in pressure would not alter the cell sensitivity. Similar results have been observed by Walker and Westenberg (118).

The gas stream which would leave the top of the packing under absorption operating conditions would contain water vapor in addition to air and carbon dioxide. Thus, if this gas were passed through a thermal conductivity cell using atmospheric air as its reference gas (presumably at a considerably lower absolute humidity), the resulting bridge signal would reflect not only the CO_2 concentration but also the difference in absolute humidity between the sample and reference gas. A series of tests was carried out, therefore, to determine the quantitative effects of the column gas humidity and to assess means to overcome them.

The building air supply humidity was first determined

from wet and dry bulb temperature readings. Data taken over several days and at different times during the day indicated that the humidity of the compressed air supply varied from 0.0085 to 0.009 lb water/lb dry air, but that it occasionally (in the early morning) would drop as low as 0.005 lb water/lb dry air. In contrast, the humidity of atmospheric air, as measured with a sling hygrometer, varied between the values of 0.011 and 0.016 lb water/lb dry air.

In order to determine the quantitative effects of water vapor in the column outlet gas, a series of tests was carried out with the sample gas stream taken from the operating column and the reference gas stream taken from the compressed air supply. The column gas sample was withdrawn by a vacuum pump acting downstream of a flow control valve and the thermal conductivity cell, respectively. The procedure was to balance the bridge for $F_s=F_r=160$ ml/min 100-per cent compressor air when, as in all these tests, $I_s=I_r=8$ ma and $T_{cell}=35^{\circ}C$. The column humid air (column conditions: $T_{water}=75^{\circ}F$, $T_{air}=89^{\circ}F$, $G=400$ lb/hr-ft^2, $L=5000$ lb/hr-ft^2) was then introduced to the cell as the sample stream with $F_s=160$ ml/min and the resulting bridge signal recorded. The results of several such tests made at different times of different days showed a consistent positive bridge signal of 8.0 ± 0.25 mv. Thus it appeared that the moisture content of the column exit gas could result in a serious error in the

determination of the gas CO_2 concentration if the calibration data were based on dry or near-dry gas mixtures.

Two possible methods were available to avoid this problem. The first, which involved making calibration curves for gas mixtures at the column exit gas moisture content, was thought to offer too many experimental uncertainties. The alternate procedure, and the one used in this work, was to provide a reference gas with the same absolute humidity as the column exit gas. By this method the humidity effects for the sample and reference gas would be the same and the resulting bridge signal would reflect only the CO_2 concentration.

Two methods to obtain a humidified gas stream were investigated. The first involved the continuous bubbling of an air stream through a gas washing bottle filled with water. Because of the batch nature of this technique the air stream humidity from the bottle and the temperature of the water in it experienced a transient condition which lasted for a period of hours. A range of humidities from 0.016 to 0.030 lb water/lb dry air were experienced in this transient period and, although the stream was able to suppress the column gas moisture effects when it was intorudced to the cell as the reference gas, the method was abandoned.

In its place a small continuous countercurrent air-water contactor was built from a 1-inch ID, 20-inch long glass tube packed with 3/16-inch ceramic rings. Tests indicated

that this device would produce a gas stream of constant moisture content. However, when this stream was put through the thermal conductivity cell as the reference gas, with the sample gas taken from the column operating at the previously mentioned conditions, the bridge could not be completely balanced (bridge signal=+3.2 mv), thus indicating that the reference gas had not been sufficiently humidified. This effect, probably due to insufficient contact in the humidifier, was overcome by electrically heating the humidifier inlet water stream. Thus, the outlet humidity from the contactor could be adjusted by varying the voltage across the electric heater.

This arrangement, though somewhat sluggish, was found satisfactory and it was included in the experimental equipment. Figure 9 and Chapter III give the details of how the humidifier was used in the sample flow system.

As has been previously mentioned, it is extremely important to use rapid measuring techniques in any type of process dynamic experiment (42, 46, 2). This, it should be recalled, was the primary reason for the development of a special thermal conductivity cell for this study. Thus, in an effort to obtain some quantitative measure of the cell's speed of response and, thereby, a verification of the design philosophy, the thermal conductivity cells were given a series of transient response tests. These tests were con-

ducted by introducing a step change in CO_2 concentration to the cell and by measuring the resulting speed of response. The most satisfactory arrangement found to make these transient tests is shown in Figure D-10. A three-way solenoid valve was mounted in the sample flow line between the gas

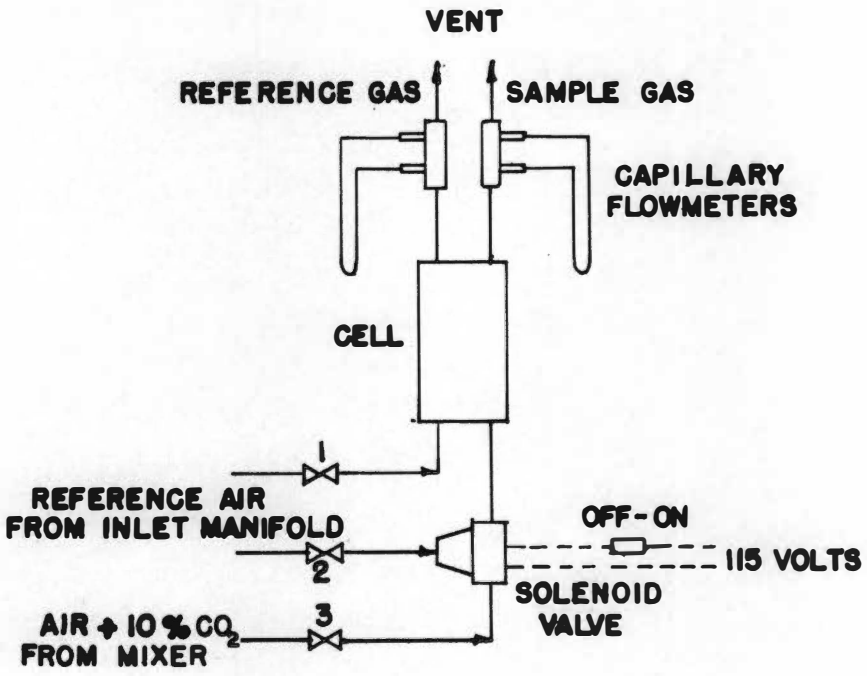


Figure D-10. Transient Test Equipment Modifications

mixer and the thermal conductivity cell. With the valve energized a 10-per cent CO_2 mixture passed through the valve, cell, and flowmeter. In this position valve 3 was adjusted to produce a sample flow rate of 60 ml/min. The solenoid was then turned off, thereby opening flow passage C-A and allowing a reference gas of zero-per cent CO_2 concentration to

flow through the cell and flowmeter. Valve 2 adjusted this flow rate to 60 ml/min. The standard reference gas flow rate was also set to 60 ml/min with valve 1.

Under these conditions the step change in carbon dioxide concentration (from 0% to 10%) was introduced to the cell by energizing the solenoid valve. With the oscillograph chart speed set at 4 mm/sec the solenoid was switched on and the transient recorded. The results of three such transient tests gave an average time constant (time for the recorded concentration trace to reach 63 per cent of its final steady-state value) of 1.8±.1 seconds. This response can be attributed wholly to the cell as the rise time for the preamplifier, drive amplifier, and recorder combined was reported to be only 0.03 seconds.

Although this response speed was somewhat slower than the original optimistic estimate, it was still three to four times faster than the very best commercial equipment.

The tests which have been described in the previous pages were not carried out, in all cases, for both thermal conductivity cells. Both cells were tested, though, for flow sensitivity and speed of response and, as would be expected, showed identical characteristics.

Calibration data were obtained for each thermal conductivity cell used in this work. As has been previously discussed, these data were obtained by measuring the

unbalanced bridge signal with sample gas mixtures of various CO_2 concentrations. The gas mixtures were generated with equipment shown in Figures D-5 and D-6.

Two sets of calibration data were obtained for each cell. The first data were taken for a carbon dioxide concentration range of 0 to 50 per cent by volume to determine the general behavior of the cells. The results showed that both cells were linear over this concentration range, i.e., the unbalanced bridge signal was directly proportional to gas concentration. The sensitivities of the cells were about the same (the outlet cell was slightly higher) with an approximate value of 2.5 mv/mole per cent CO_2. These qualitative and quantitative observations were in excellent agreement with Walker and Westenberg's (118) data obtained from a thermistor thermal conductivity cell and N_2-CO_2 gas mixtures.

A second and more precise set of calibration data were taken over the CO_2 concentration range of 0 to 20 per cent by volume as this was the range in which the column would be operated. The results of these tests are plotted in Figure D-11, which shows the initial calibration curves for both the inlet and outlet thermal conductivity cells. As can be seen, the curves are unquestionably linear and, again, quite similar. The inlet cell sensitivity (slope of the curve) was 2.55 mv per mole per cent carbon dioxide while the outlet cell sensitivity was somewhat greater (2.66 mv per mole

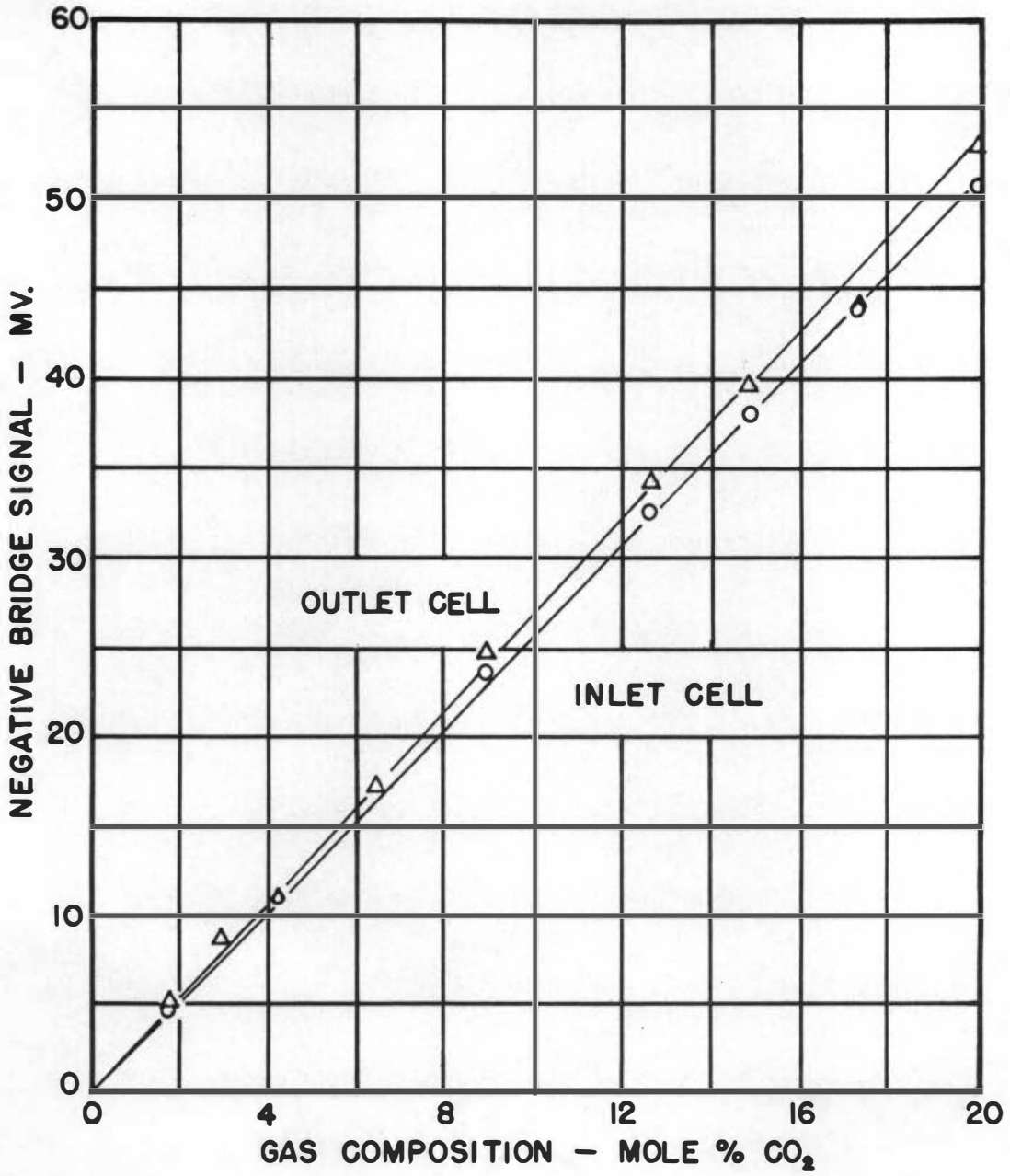


Figure D-11. Thermal conductivity cell calibration data.

per cent).

V. DISCUSSION

In concluding this discussion of the development, testing, and calibration of the thermal conductivity cells designed for this study, several general observations can be made.

Actual experimental operation of the sinusoid generator and inlet thermal conductivity cell showed that speed of response of the instrument was more than adequate as evidenced by the lack of attenuation of the recorded inlet sinusoid at the highest experimental frequencies. Nevertheless, it is believed possible to obtain even better response characteristics by returning the thermistors to their original flow, mid-stream position. This would require excellent cell flow control which, from sampling system operation experience, appears possible.

A considerable amount of difficulty was encountered with failure of the extremely fine (0.001-inch) thermistor leads. These failures were attributed to poor solder joints, rough handling, chemical attack, or a combination of these (30). It is suggested that alternate mounting methods and heavier electrical leads be considered in future work.

The excellent sensitivity of these cells (changes as small as 0.1 per cent are easily detected) suggests their

application to absolute concentration analysis such as that required by steady state absorption studies. An absolute requirement, though, for this type of application is the use of a set of thermistors which are precisely matched within 1 per cent throughout their entire resistance range (27). This, combined with superior cell temperature and bridge current regulation, would assure the necessary null point stability. In addition to these cell and bridge improvements, absolute concentration determination would require a considerably improved method of water vapor compensation.

APPENDIX E

CALIBRATION DATA

Calibration data are presented in this appendix in the form of graphs. The curves associated with equipment of a particular system are grouped together in the following order:

Column Air System

- E-1 orifice meter calibration
- E-2 rotameter calibration

Column Water System

- E-3 rotameter calibration

Thermal Conductivity Cell Sampling Flowmeter

- E-4 capillary flowmeter calibrations

Standard Gas Mixer

- E-5 capillary flowmeter calibrations
- E-6 rotameter G9143 calibration
- E-7 rotameter G9144 calibration

Thermal Conductivity Cells

- E-8 inlet and outlet cell calibrations

Sinusoid Generator

- E-9 DC motor speed control calibration

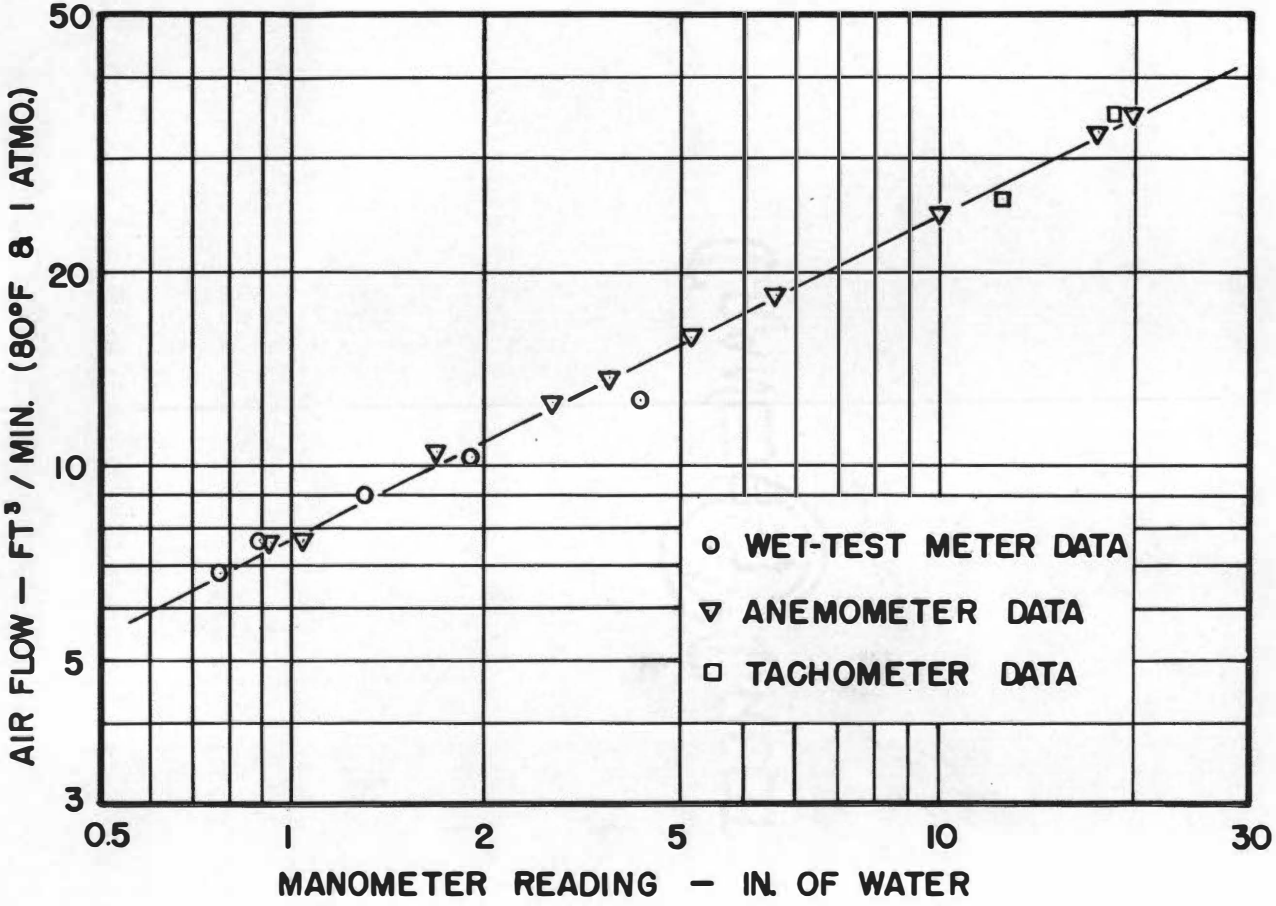


Figure E-1. Air orifice meter calibration data.

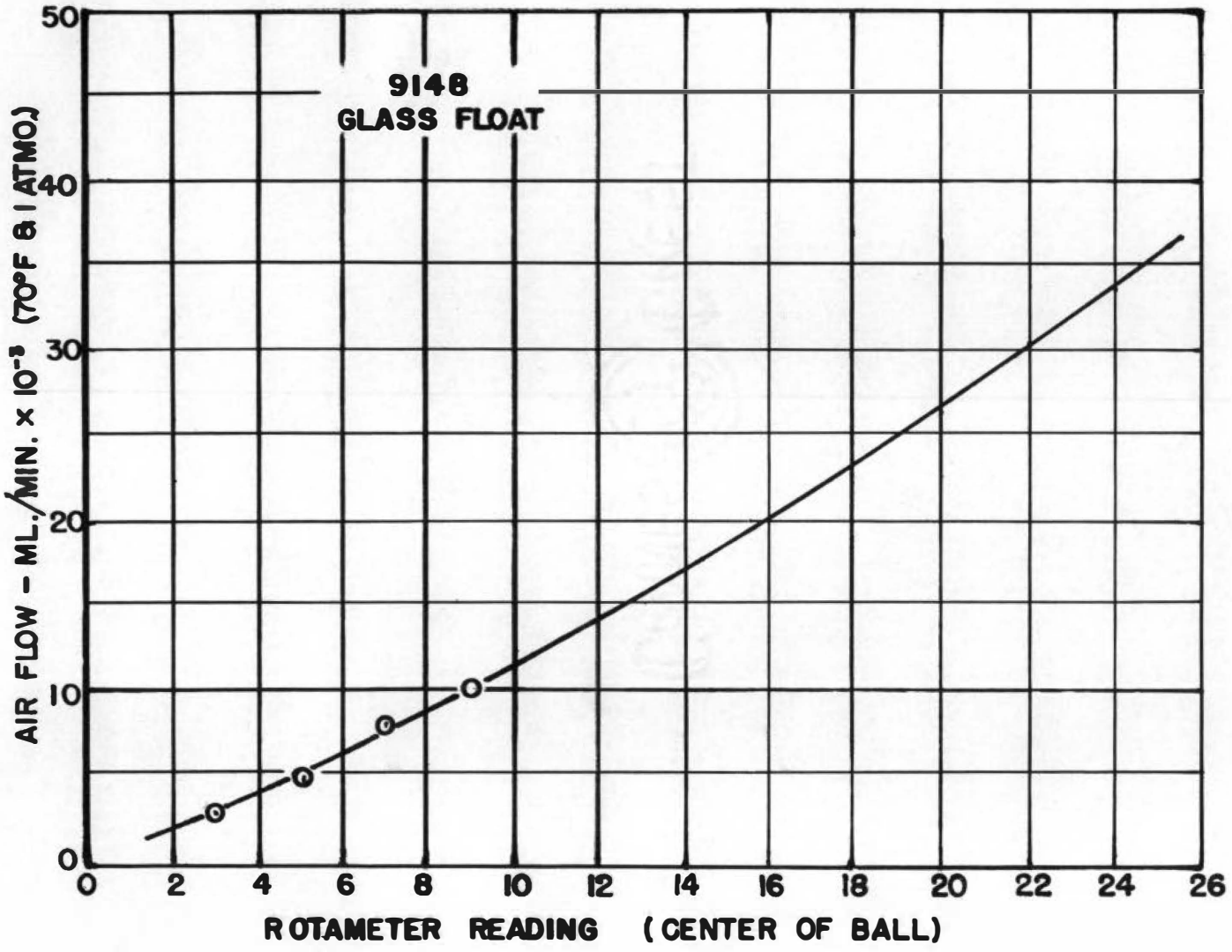


Figure E-2. Air rotameter calibration data.

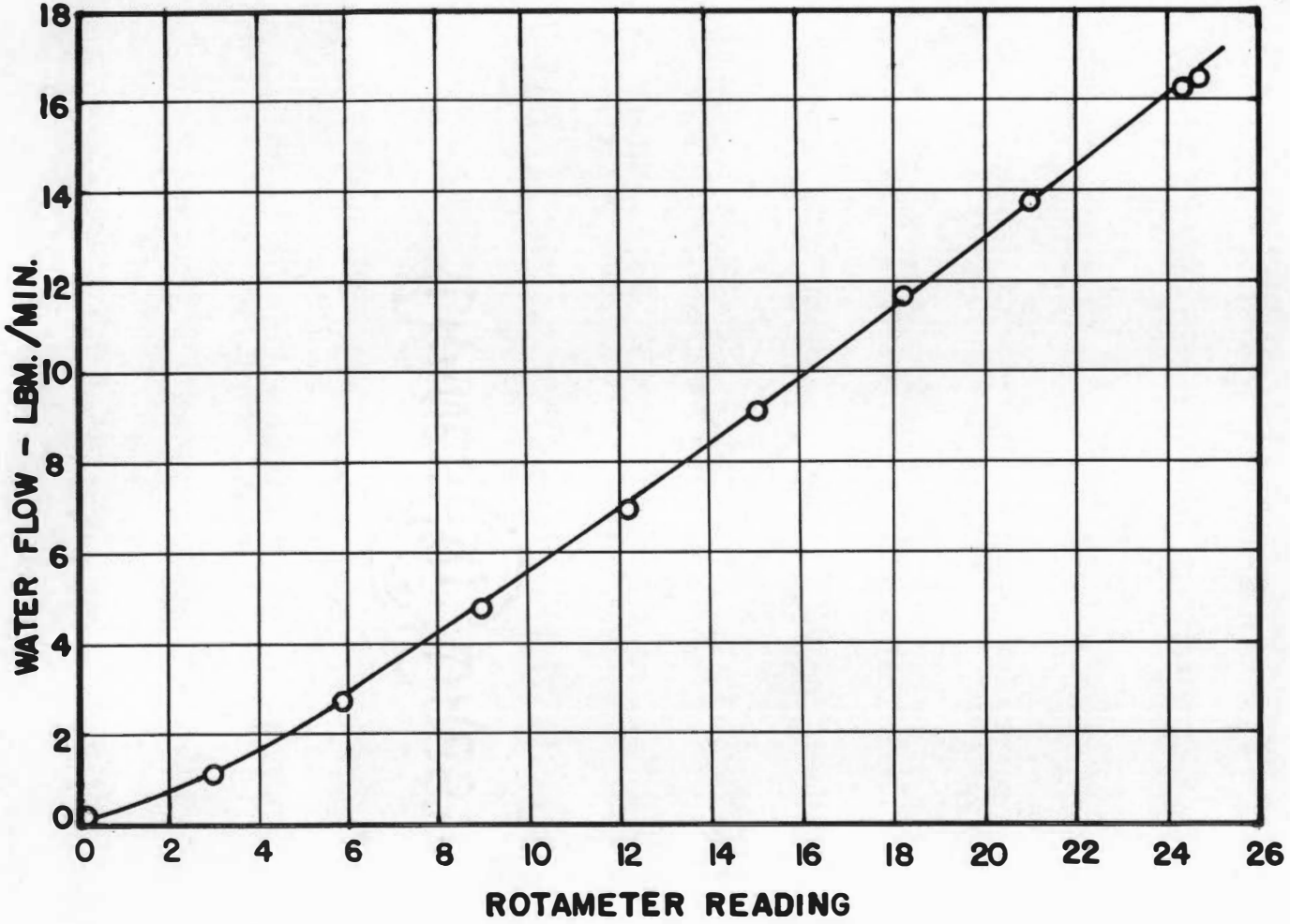


Figure E-3. Water rotameter calibration data.

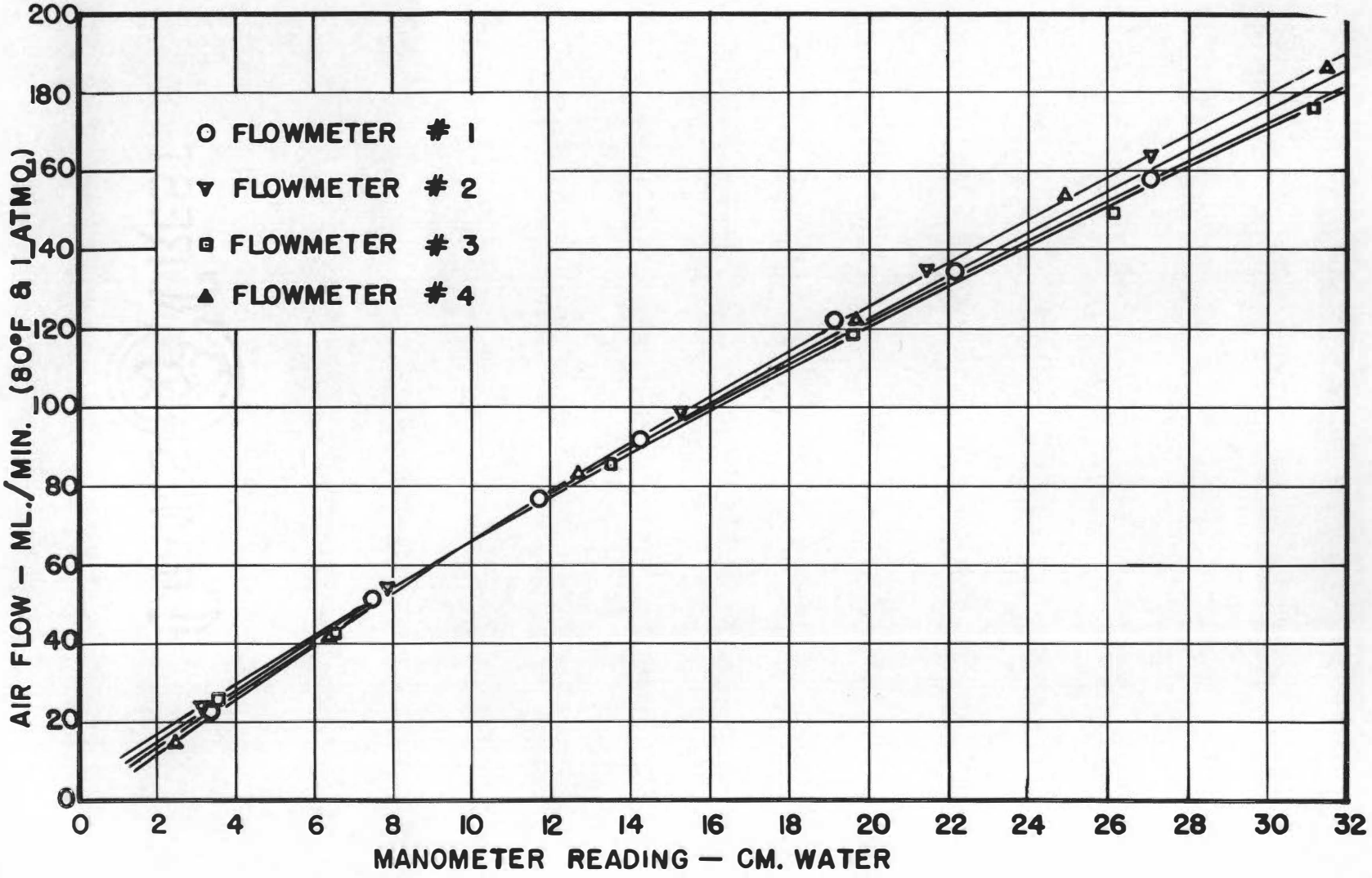


Figure E-4. Capillary flowmeter calibration data for air.

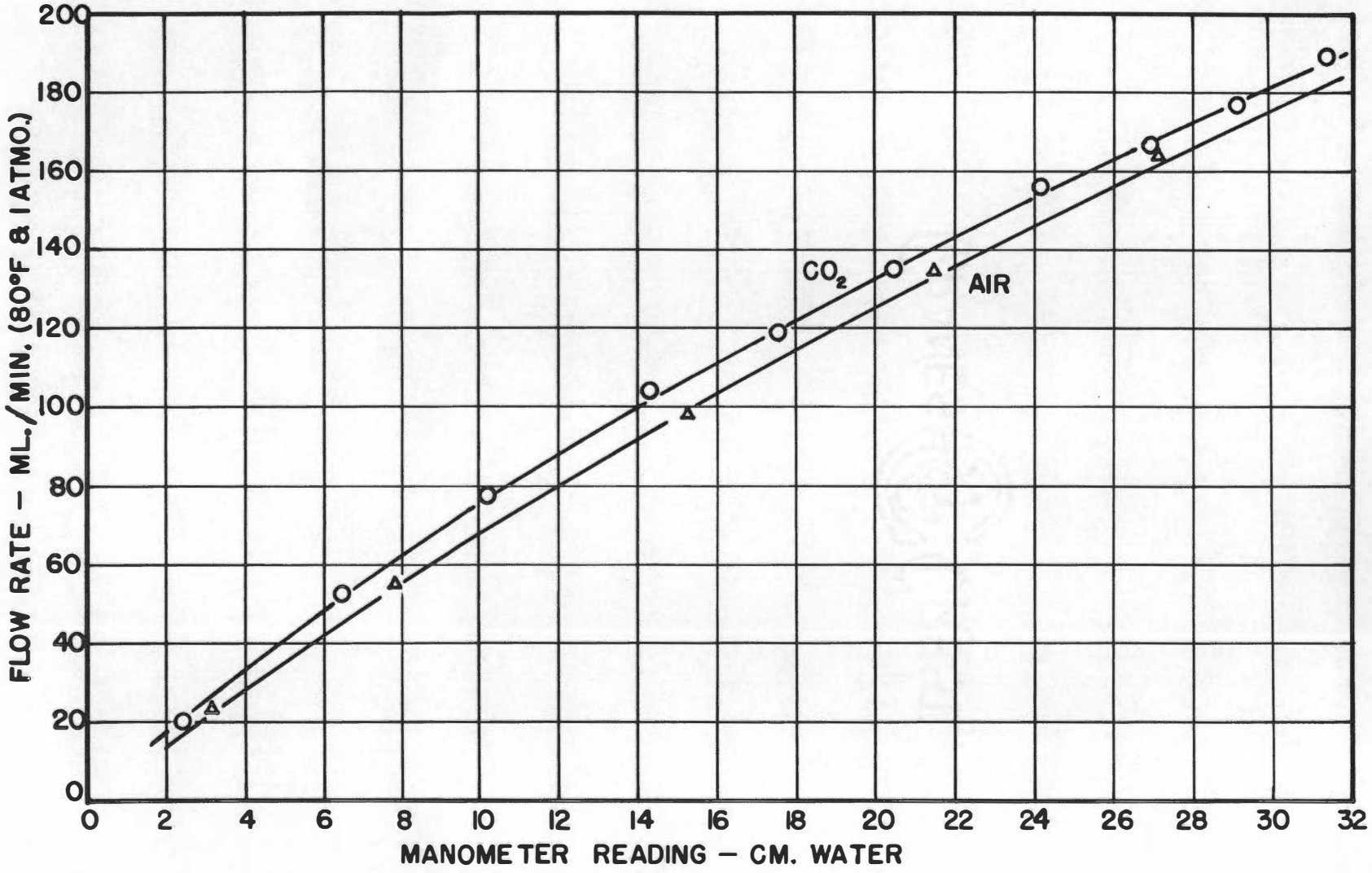


Figure E-5. Mixer capillary flowmeter calibration data for carbon dioxide and air.

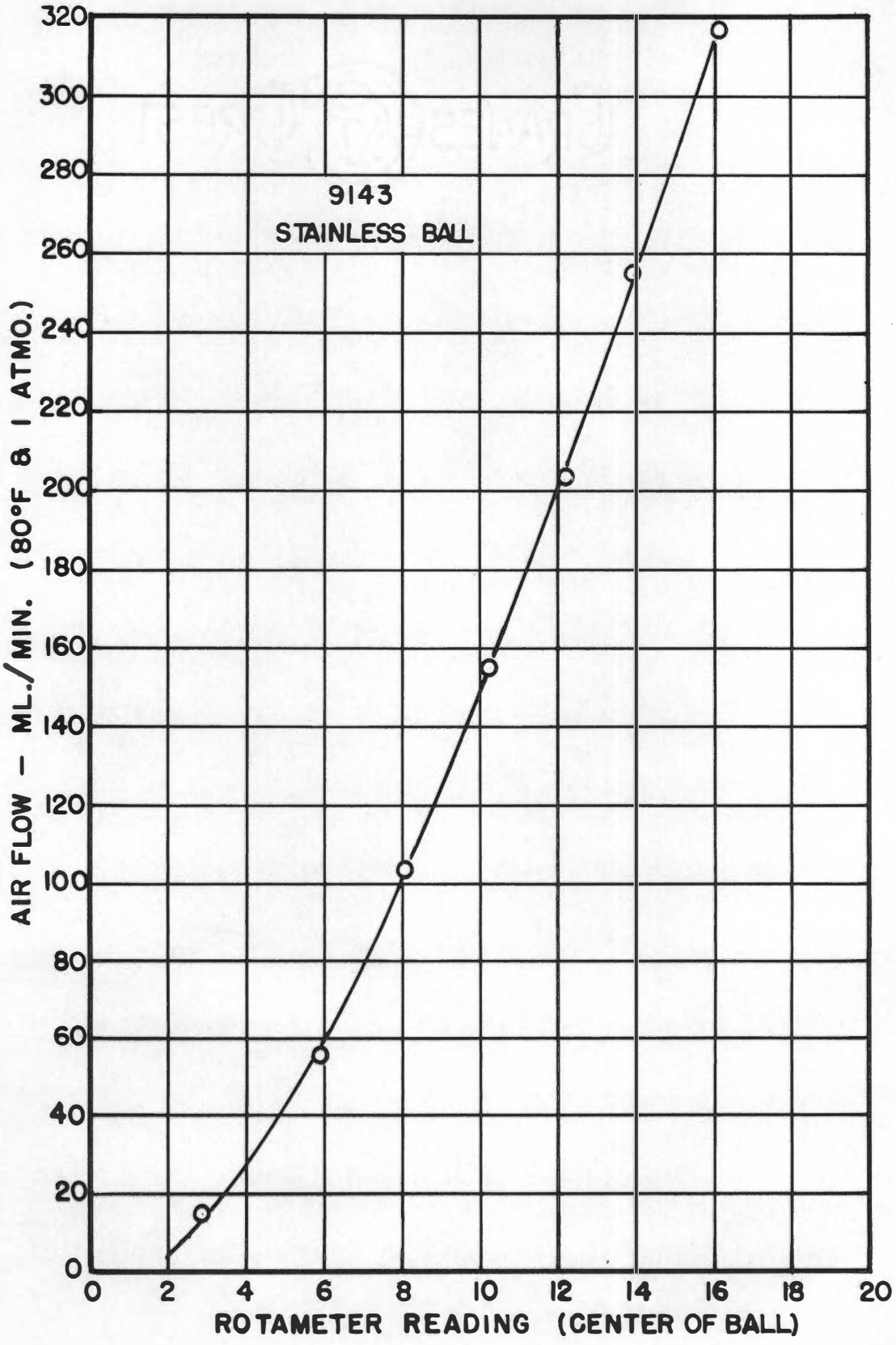


Figure E-6. Mixer rotameter calibration data, G-9143.

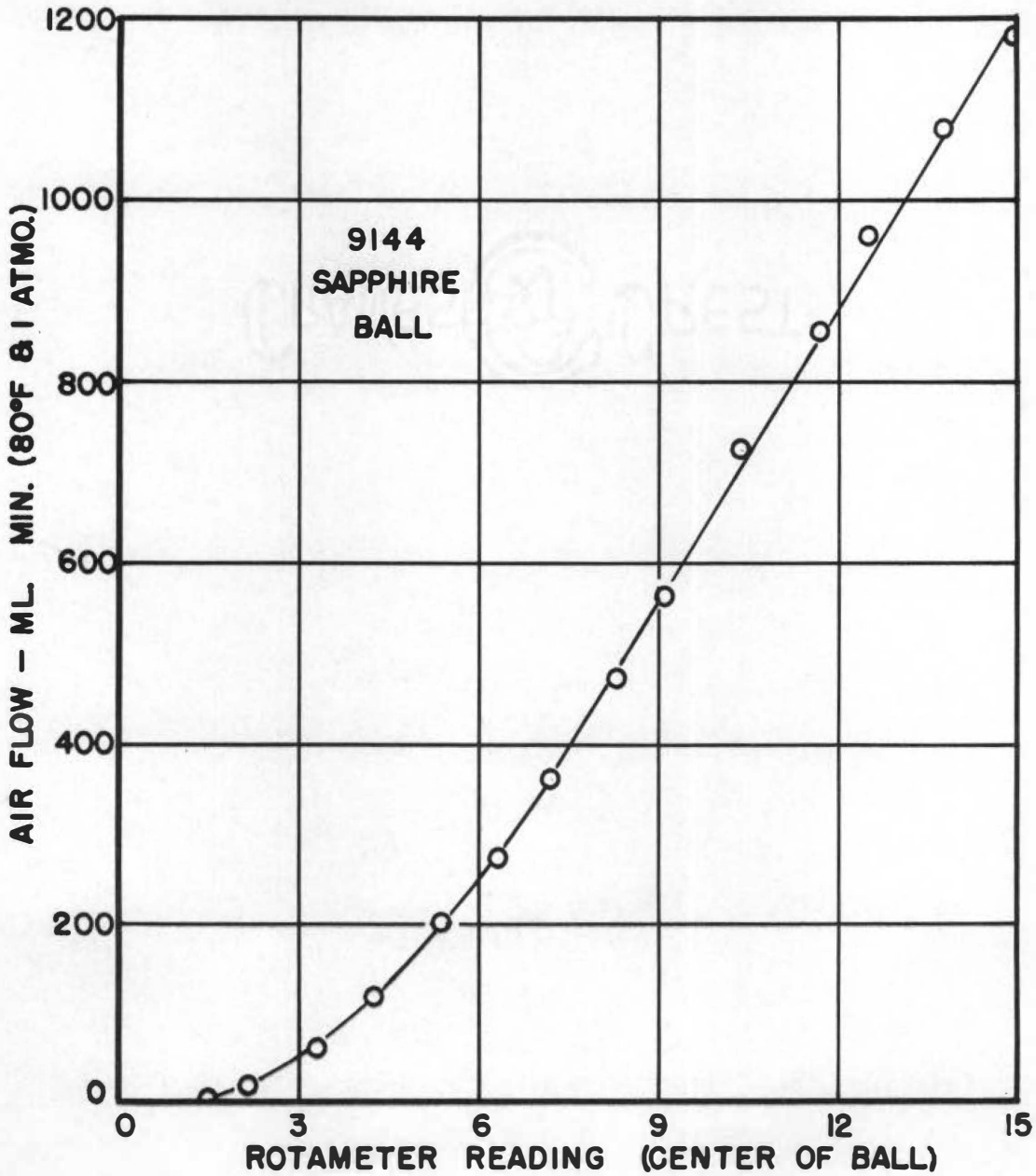


Figure E-7. Mixer rotameter calibration data, G-9144.

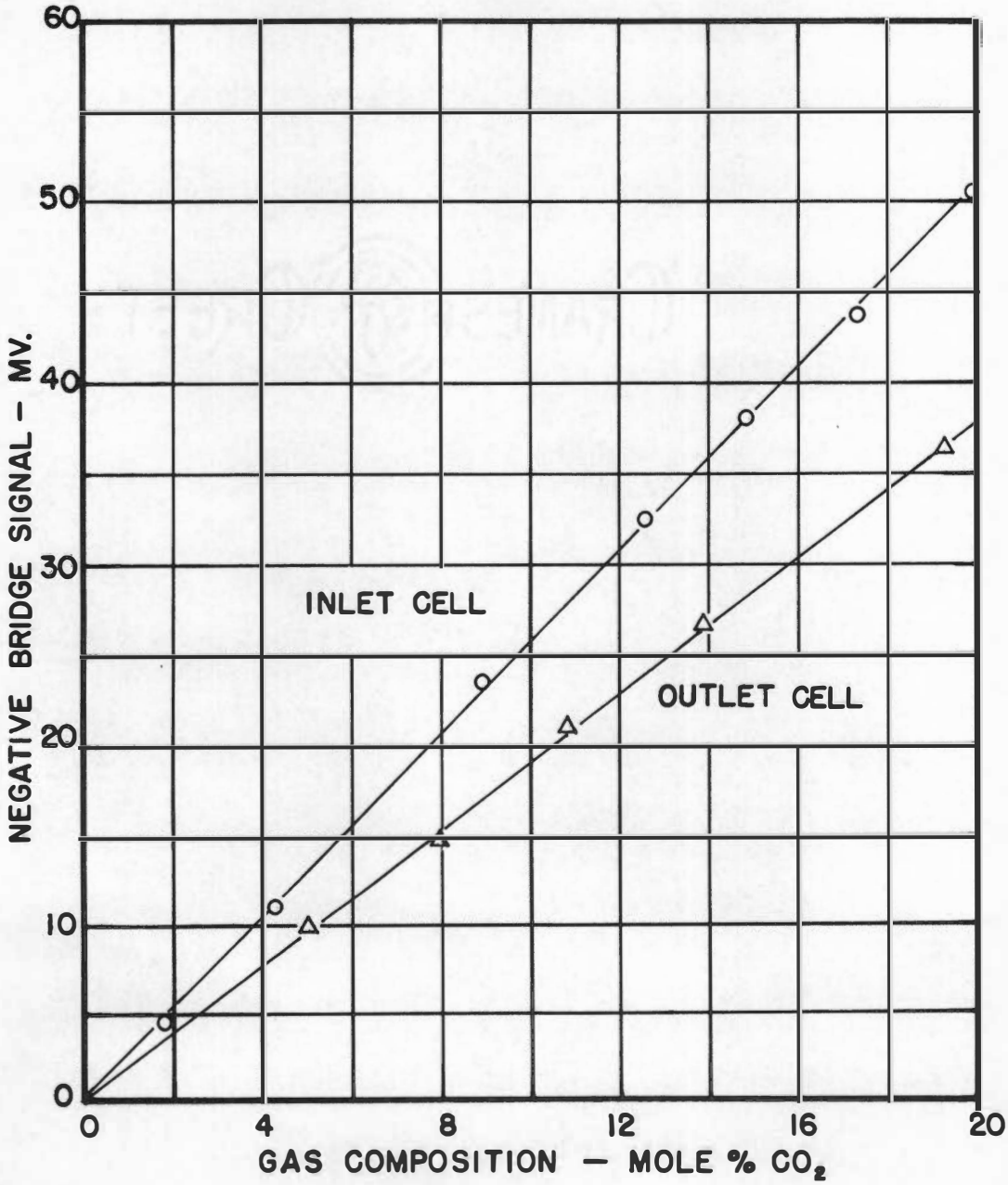


Figure E-8. Inlet and outlet thermal conductivity cell calibration data.

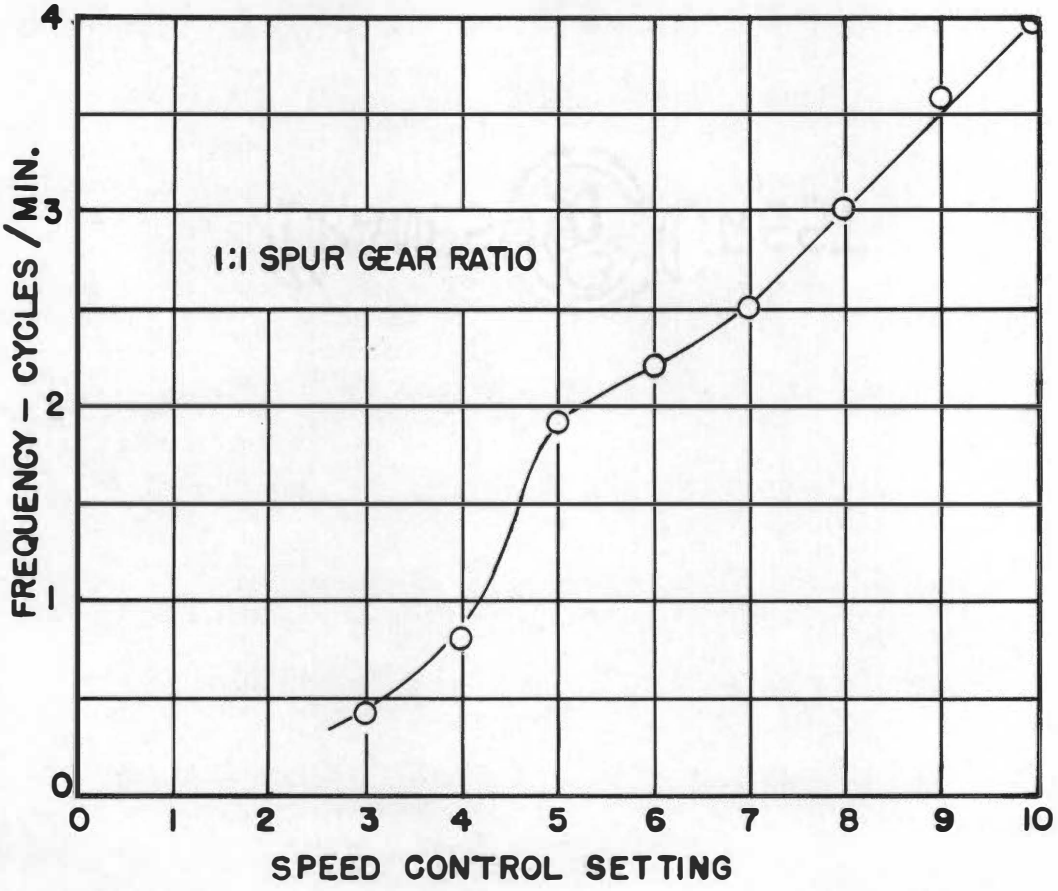


Figure E-9. Sinusoid generator frequency calibration data.

APPENDIX F

EXPERIMENTAL FREQUENCY RESPONSE DATA

The following tables give the amplitude and phase measurements taken from the concentration sinusoid traces. The thermal conductivity cell and column operating conditions are also included for each run. The runs are numbered in the order that they were made--the run number indicating the last digit of the data sheet page number starting with page 24451. The Original Record of Research and the concentration traces are on file with the Department of Chemical Engineering, University of Tennessee. For convenience, the tables are arranged in order of increasing nominal gas phase flow rate, G, as in Table I of Chapter V. The significance of the terms is explained in Appendix G.

TABLE III

EXPERIMENTAL DATA - RUN 1

G = 1 lb mole/hr-ft^2 (nominal) L = 0 lb mole/hr-ft^2

Period		Frequency		Inlet Amplitude		Outlet Amplitude		Amplitude Ratio	R_P*	Phase Shift
min-sec	min	rad/min	cpm	mv	mole %	mv	mole %			degrees
2-25	2.417	2.60	.414	25.5	10.0	14.8	7.80	.78	.378	136
1-13.3	1.222	5.14	.818	25.0	9.8	10.7	5.63	.574	.704	258
0-52.6	0.876	7.17	1.142	25.0	9.8	8.0	4.21	.430	1.0	360
0-32.4	0.540	11.62	1.85	25.0	9.8	4.1	2.16	.220	1.44	518
0-19.7	0.328	19.15	3.05	24.0	9.41	1.25	0.654	.695	2.2	780
0-15.0	0.250	25.1	4.0	23.0	9.02	0.5	0.263	.0292	2.8	1010

*R_P = phase ratio (ratio of outlet wave displacement to period)

Atmospheric Conditions
- Temperature - 82°F
- Pressure - 74.05 cm Hg

Cell Conditions (both cells)
- Total Bridge Current - 16.0 ma
- Cell Temperature - 35°C
- Sample Flow Manometers - 9 cm H_2O

Column Conditions
- Inlet Air Flow - 21.5 (rotameter reading)
- Inlet Gas Temperature - 82°F
- Column Pressure Drop - 0 in. H_2O
- Inlet Water Flow - 0 (rotameter reading)
- Inlet Water Temperature -
- Inlet Gas Mean Concentration - 9.1 mole % CO_2

TABLE IV

EXPERIMENTAL DATA - RUN 3

G = 1 lb mole/hr-ft^2 (nominal) L = 55 lb moles/hr-ft^2

Period		Frequency		Inlet Amplitude		Outlet Amplitude		Amplitude Ratio	R_P*	Phase Shift
min-sec	min	rad/min	cpm	mv	mole %	mv	mole %			deg
0-15.0	0.25	25.1	4.0	22.8	8.94	.39	.205	.023	8.50/3.00	1020
0-19.6	0.367	19.2	3.06	23.8	9.33	.915	.481	.0516	2.80/1.34	754
0-34.5	0.576	11.1	1.77	24.5	9.61	3.15	1.66	.173	2.10/1.47	515
0-54.0	0.90	6.99	1.11	25.0	9.81	6.9	3.63	.370	1.0	360
1-15.8	1.163	5.40	.860	25.0	9.81	9.8	5.16	.526	1.0/1.5	240
2-19.8	2.330	2.69	.429	25.5	10.0	14.9	7.84	.784	1.09/2.73	143
3-30.2	3.504	1.79	.285	25.5	10.0	16.5	8.68	.868	1.10/4.19	95
4-56.0	4.934	1.28	.203	25.5	10.0	17.3	9.11	.911	1.2/5.88	72

*R_P = phase ratio (ratio of outlet wave displacement to period)

Atmospheric Conditions
- Temperature - 81°F
- Pressure - 73.96 cm Hg

Cell Conditions (both cells)
- Total Bridge Current - 16.0 ma
- Cell Temperature - 35°C
- Sample Flow Manometer - 9 cm H_2O

Column Conditions
- Inlet Air Flow - 21.5 (rotameter reading)
- Inlet Gas Temperature - 80°F
- Column Pressure Drop - 0 in. H_2O
- Inlet Water Flow - 6.8 (rotameter reading)
- Inlet Water Temperature - 74°F
- Inlet Gas Mean Concentration - 10.0 mole % CO_2

TABLE V

EXPERIMENTAL DATA - RUN 2

G = 1 lb mole/hr-ft^2 (nominal) L = 222 lb moles/hr-ft^2

Period		Frequency		Inlet Amplitude		Outlet Amplitude		Amplitude Ratio	R_P*	Phase Shift
min-sec	min	rad/min	cpm	mv	mole %	mv	mole %			deg
4-41.0	4.684	1.335	.214	24.5	9.61	16.2	8.53	.889	1.2/5.5	78.5
3-46.0	3.767	1.665	.265	24.5	9.61	15.6	8.21	.854	1.11/4.50	89
2-24.3	2.405	2.61	.416	25.2	9.88	13.35	7.02	.711	1.18/2.80	152
1-14.0	1.233	5.09	.811	25.2	9.88	8.55	4.50	.456	1.00/1.47	245
0-51.8	.863	7.35	1.17	25.2	9.88	5.40	2.84	.288	1.0	360
0-32.8	.547	11.50	1.83	24.8	9.73	2.50	1.315	.135	1.28/1.30	493
0-20.2	.337	18.65	2.97	23.8	9.33	.75	.395	.0424	1.60/0.80	720
0-15.0	.25	25.1	4.0	22.8	8.94	.345	.184	.0205	4.77/1.48	1100

*R_P = phase ratio (ratio of outlet wave displacement to period)

Atmospheric Conditions

Temperature - 79°F
Pressure - 74.0 cm Hg

Cell Conditions (both cells)

Total Bridge Current - 16.0 ma
Cell Temperature - 35°C
Sample Flow Manometer - 9 cm of H_2O

Column Conditions

Inlet Air Flow - 21.5 (rotameter reading)
Inlet Gas Temperature - 73°F - 76°F - 78°F
Column Pressure Drop - 0 in.H_2O
Inlet Water Flow - 20.3 (rotameter reading)
Inlet Water Temperature - 74°F
Inlet Gas Mean Concentration - 9.5% CO_2 ± 5% CO_2

TABLE VI

EXPERIMENTAL DATA - RUN 10

G = 1 lb mole/hr-ft^2 (nominal) L = 222 lb moles/hr-ft^2

Period		Frequency		Inlet Amplitude		Outlet Amplitude		Amplitude Ratio	R_P*	Phase Shift
min-sec	min	rad/min	cpm	mv	mole %	mv	mole %			deg
4-54.2	4.903	1.28	.204	24.8	9.72	17.0	8.95	.921	1.11/5.74	72
3-25.8	3.414	1.85	.294	25.3	9.92	16.0	8.42	.849	1.12/4.03	100
2-19.7	2.328	2.70	.430	25.0	9.81	13.7	7.21	.735	1.07/2.70	143
1-13.8	1.230	5.10	.813	25.0	9.81	8.6	4.53	.462	1.00/1.47	245
0-50	.833	7.54	1.20	25.0	9.81	5.6	2.95	.301	1.90/1.98	345
0-31.6	.526	11.92	1.90	24.4	9.57	2.4	1.262	.132	1.77/1.24	517
0-27.5	.375	16.8	2.67	23.9	9.37	1.0	.562	.0562	3.83/2.20	626
0-19.4	.323	19.4	3.10	23.2	9.10	.58	.305	.0335	3.82/1.87	736
0-15.0	.25	25.1	4.0	23.0	9.02	.35	.184	.0204	3.70/1.45	919

*R_P = phase ratio (ratio of outlet wave displacement to period)

Atmospheric Conditions
Temperature - 76°F
Pressure - 74.36 cm Hg

Cell Conditions (both cells)
Total Bridge Current - 16 ma
Cell Temperature - 35°C
Sample Flow Manometer - 9 cm H_2O

Column Conditions
Inlet Air Flow - 21.5 (rotameter reading)
Inlet Gas Temperature - 72°F
Column Pressure Drop - 0 in. H_2O
Inlet Water Flow - 20.3 (rotameter reading)
Inlet Water Temperature - 71°F
Inlet Gas Mean Concentration - 14.9 mole % CO_2

TABLE VII

EXPERIMENTAL DATA - RUN 11

G = 1 lb mole/hr-ft^2 (nominal) L = 0 lb mole/hr-ft^2

Period		Frequency		Inlet Amplitude		Outlet Amplitude		Amplitude Ratio	R_p*	Phase Shift
min-sec	min	rad/min	cpm	mv	mole %	mv	mole %			deg
4-45.5	4.743	1.33	.211	24.7	9.69	17.0	8.95	.925	0.62/5.57	40
3-23.6	3.393	1.85	.295	25.0	9.80	16.1	8.43	.865	0.56/3.98	51
2-21.0	2.350	2.67	.425	25.0	9.80	15.0	7.90	.805	0.53/2.75	69
1-11.6	1.193	5.25	.836	25.0	9.80	12.0	6.31	.644	0.42/1.42	107
0-50.7	.845	7.43	1.18	25.0	9.80	10.0	5.26	.536	0.78/2.00	142
0-30.8	.513	10.2	1.95	24.7	9.69	5.6	2.95	.304	0.70/1.23	205
0-23.1	.385	16.3	2.60	24.2	9.50	3.4	1.79	.188	1.40/2.20	229
0-19.3	.321	19.6	3.11	23.8	9.33	1.9	1.00	.107	1.33/1.85	259
0-14.8	.247	25.4	4.05	23.1	9.06	1.0	.526	.0581	1.10/1.45	274

*R_p = phase ratio (ratio of outlet wave displacement to period)

Atmospheric Conditions
- Temperature - 79°F
- Pressure - 74.20 cm Hg

Cell Conditions (both cells)
- Total Bridge Current - 16 ma
- Cell Temperature - 35°C
- Sample Flow Manometer - 9 cm H_2O

Column Conditions
- Inlet Air Flow - 21.5 (rotameter reading)
- Inlet Gas Temperature - 75°F
- Column Pressure Drop - 0 in. H_2O
- Inlet Water Flow - 0
- Inlet Water Temperature - --
- Inlet Gas Mean Concentration - 14.5 mole % CO_2

TABLE VIII

EXPERIMENTAL DATA - RUN 4

G = 10 lb moles/hr-ft^2 (nominal) L = 0 lb mole/hr-ft^2

Period		Frequency		Inlet Amplitude		Outlet Amplitude		Amplitude Ratio	R_P*	Phase Shift
min-sec	min	rad/min	cpm	mv	mole %	mv	mole %			deg
4-55.7	4.93	1.27	.202	13.5	5.30	9.7	5.10	.962	0.20/5.87	12.2
3-35.0	3.583	1.75	.279	13.5	5.30	9.7	5.10	.962	0.20/4.20	17.1
2-14.0	2.234	2.82	.448	15.2	5.96	10.9	5.74	.964	0.27/2.67	29.6
1-9.3	1.07	5.87	.935	17.0	6.67	12.5	6.57	.984	0.20/1.32	54.6
0-50.3	.838	7.48	1.19	18.0	7.06	13.0	6.87	.968	0.16/0.98	58.9
0-31.4	.523	12.0	1.91	19.0	7.45	13.5	7.10	.953	0.17/0.63	97.2
0-19.0	.317	19.8	3.15	20.0	7.85	12.6	6.63	.845	0.90/1.84	176
0-15.0	.25	25.1	4.0	20.0	7.85	11.4	6.00	.764	0.83/1.42	210
0-10.2	.17	37.0	5.88	20.0	7.84	8.9	4.69	.598	0.79/0.99	287
0-6.0	.10	62.8	10.0	19.0	7.45	5.2	2.74	.368	0.78/0.57	493
0-5.0	.0834	75.4	12.0	18.5	7.26	3.85	2.03	.280	1.51/0.95	572
0-4.1	.0684	90.8	14.6	17.3	6.74	2.15	1.13	.168	2.0	720

*R_P = phase ratio (ratio of outlet wave displacement to period)

Atmospheric Conditions

Temperature - 82°F
Pressure - 74.37 cm Hg

Cell Conditions (both cells)

Total Bridge Current - 16.0 ma
Cell Temperature - 35°C
Sample Flow Manometer - 9 cm H_2O

Column Conditions

Inlet Air Flow - 1.3 in. H_2O (manometer)
Inlet Gas Temperature - 83°F
Column Pressure Drop - 0.3 in. H_2O
Inlet Water Flow - 0 (rotameter reading)
Inlet Water Temperature - --
Inlet Gas Mean Concentration - 13.7 mole % CO_2

TABLE IX

EXPERIMENTAL DATA - RUN 9

G = 10 lb moles/hr-ft^2 (nominal) L = 55 lb moles/hr-ft^2

Period		Frequency		Inlet Amplitude		Outlet Amplitude		Amplitude Ratio	R_p*	Phase Shift
min-sec	min	rad/min	cpm	mv	mole %	mv	mole %			deg
0-3.8	.0633	99.3	15.8	17.3	6.79	1.7	.895	.132	1.40/0.71	710
0-5.0	.0833	75.3	12.0	18.8	7.38	3.3	1.74	.234	1.39/0.93	539
0-6.0	.10	62.8	10.0	19.1	7.49	4.6	2.42	.323	1.47/1.11	477
0-8.0	.133	47.2	7.5	19.2	7.53	7.1	3.74	.497	1.50/1.57	344
0-13.7	.229	27.5	4.39	20.2	7.92	10.8	5.69	.718	0.77/1.13	245
0-15.0	.25	25.1	4.0	20.0	7.85	11.3	5.95	.758	0.78/1.47	191
0-19.4	.323	19.4	3.10	20.0	7.85	10.6	6.64	.845	0.78/1.94	145
0-23.2	.387	16.2	2.58	19.8	7.76	13.0	6.85	.882	0.83/2.26	132
0-37.8	.630	10.0	1.58	18.0	7.45	13.2	6.95	.931	0.86/3.20	97
0-54.5	.909	6.92	1.1	17.8	6.98	12.4	6.54	.935	0.34/2.14	57

*R_p = phase ratio (ratio of outlet wave displacement to period)

Atmospheric Conditions

Temperature - 81°F
Pressure - 74.20 cm Hg

Cell Conditions (both cells)

Total Bridge Current - 16 ma
Cell Temperature - 35°C
Sample Flow Manometer - 9 cm H_2O

Column Conditions

Inlet Air Flow - 1.0 in. H_2O (manometer)
Inlet Gas Temperature - 82°F
Column Pressure Drop - 0.4 in. H_2O
Inlet Water Flow - 6.8 (rotameter reading)
Inlet Water Temperature - 72°F
Inlet Gas Mean Concentration - 13.7 mole % CO_2

TABLE X

EXPERIMENTAL DATA - RUN 8

G = 10 lb moles/hr-ft^2 (nominal) L - 222 lb moles/hr-ft^2

Period		Frequency		Inlet Amplitude		Amplitude		Amplitude Ratio	R_p*	Phase Shift
min-sec	min	rad/min	cpm	mv	mole %	mv	mole %			deg
0-54.3	.905	6.94	1.10	16.6	6.5	12.0	6.32	.973	0.37/2.18	64.5
0-33.2	.553	11.34	1.81	18.5	7.25	12.7	6.69	.923	0.34/1.31	93.5
0-24.0	.40	15.8	2.5	19.1	7.49	12.0	6.31	.843	0.36/0.91	142
0-19.2	.32	19.7	3.13	20.0	7.84	11.5	6.05	.772	0.82/1.90	156
0-15.0	.25	25.1	4.0	20.0	7.84	10.7	5.63	.720	0.80/1.46	197
0-13.8	.23	27.4	4.35	20.2	7.92	10.1	5.31	.670	0.79/1.33	214
0-8.0	.133	47.2	7.5	20.0	7.84	6.8	3.58	.456	0.75/0.77	350
0-5.6	.0933	67.3	10.7	19.0	7.45	4.3	2.26	.304	1.42/1.10	465
0-4.8	.080	78.5	12.5	18.1	7.10	2.95	1.55	.218	1.45/0.96	545
0-3.8	.0633	99.3	15.8	17.5	6.86	1.60	0.847	.123	1.37/0.71	695

*R_p = phase ratio (ratio of outlet wave displacement to period)

Atmospheric Conditions
Temperature - 81°F
Pressure - 74.20 cm Hg

Cell Conditions (both cells)
Total Bridge Current - 16 ma
Cell Temperature - 35°C
Sample Flow Manometers - 9 cm H_2O

Column Conditions
Inlet Air Flow - 1.2 in. H_2O (manometer)
Inlet Gas Temperature - 82°F
Column Pressure Drop - 0.7 in. H_2O
Inlet Water Flow - 20.3 (rotameter reading)
Inlet Water Temperature - 72°F
Inlet Gas Mean Concentration - 14.1 mole % CO_2

TABLE XI

EXPERIMENTAL DATA - RUN 12

G = 10 lb moles/hr-ft^2 (nominal) L = 0 lb mole/hr-ft^2

Period		Frequency		Inlet Amplitude		Outlet Amplitude		Amplitude Ratio	R_p*	Phase Shift
min-sec	min	rad/min	cpm	mv	mole %	mv	mole %			deg
0-50.2	.837	7.50	1.193	21.8	8.55	15.4	8.11	.95	0.40/4.98	29
0-31.1	.518	12.13	1.93	23.3	9.10	15.5	8.16	.897	0.39/3.04	46
0-22.1	.369	17.0	2.71	24.0	9.41	15.2	8.00	.830	0.42/2.20	69
0-18.4	.307	20.5	3.26	24.5	9.61	14.8	7.79	.811	0.45/1.80	90
0-14.6	.243	25.9	4.12	24.5	9.61	13.7	7.21	.750	0.41/1.42	104
0-12.5	.208	30.2	4.81	24.5	9.61	12.5	6.58	.685	0.39/1.22	115
0-7.6	.1267	49.6	7.90	24.0	9.41	9.0	4.74	.504	0.38/0.75	182
0-6.0	.100	62.8	10.0	23.5	9.22	6.8	3.58	.388	0.69/1.10	226
0-5.0	.0834	75.3	12.0	22.8	8.94	6.30	3.32	.370	0.64/0.94	245
0-3.8	.0634	99.0	15.8	21.5	8.43	4.30	2.26	.268	1.22/1.42	309

*R_p = phase ratio (ratio of outlet wave displacement to period)

Atmospheric Conditions
Temperature - 80°F
Pressure - 73.91 cm Hg

Cell Conditions (both cells)
Total Bridge Current - 16 ma
Cell Temperature - 35°C
Sample Flow Manometers - 9 cm H_2O

Column Conditions
Inlet Air Flow - 1.3 in. H_2O (manometer)
Inlet Gas Temperature - 76°F
Column Pressure Drop - 0.1 in. H_2O
Inlet Water Flow - 0
Inlet Water Temperature - --
Inlet Gas Mean Concentration - 12.5 mole % CO_2

TABLE XII

EXPERIMENTAL DATA - RUN 5

G = 20 lb moles/hr-ft^2 (nominal) L = 0 lb mole/hr-ft^2

Period		Frequency		Inlet Amplitude		Outlet Amplitude		Amplitude	R_p*	Phase
		rad			mole		mole			Shift
min-sec	min	min	cpm	mv	%	mv	%	Ratio		deg
0-3.8	.0633	99.4	15.8	7.25	2.84	2.92	1.54	.5412	0.76/0.70	391
0-5.0	.0834	75.3	12.0	7.95	3.12	3.78	1.99	.638	0.75/0.13	290
0-6.0	.100	62.8	10.0	8.05	3.16	4.45	2.34	.709	0.77/1.13	245
0-8.0	.133	47.3	7.52	8.50	3.34	5.23	2.76	.826	0.40/0.78	184
0-15.0	.25	25.1	4.0	8.50	3.34	6.10	3.21	.961	0.47/1.45	109
0-19.7	.578	19.2	3.05	8.55	3.35	6.25	3.29	.982	0.47/1.92	88
0-31.0	.516	12.2	1.94	8.35	3.25	6.2	3.21	1.0	0.19/1.21	56.5
0-59.1	.902	6.95	1.11	7.5	2.94	5.6	2.84	1.0	0.17/2.10	29

*R_p = phase ratio (ratio of outlet wave displacement to period)

Atmospheric Conditions
Temperature - 82°F
Pressure - 74.28 cm Hg

Cell Conditions (both cells)
Total Bridge Current - 16.0 ma
Cell Temperature - 35°C
Sample Flow Manometers - 9 cm H_2O

Column Conditions
Inlet Air Flow - 7.5 in. H_2O (manometer)
Inlet Gas Temperature - 88°F
Column Pressure Drop - 1.55 in. H_2O
Inlet Water Flow - 0
Inlet Water Temperature - --
Inlet Gas Mean Concentration - 5.61 mole % CO_2

TABLE XIII

EXPERIMENTAL DATA - RUN 7

G = 20 lb moles/hr-ft^2 (nominal) L = 55 lb moles/hr-ft^2

Period		Frequency		Inlet Amplitude		Outlet Amplitude		Amplitude Ratio	Rp*	Phase Shift
min-sec	min	rad/min	cpm	mv	mole %	mv	mole %			deg
0-3.8	.0634	97.5	15.8	7.90	3.10	2.90	1.53	.493	0.77/0.75	370
0-5.0	.0834	75.3	12.0	8.50	3.33	3.90	2.05	.616	0.75/1.00	270
0-6.6	.110	57.1	9.1	8.50	3.33	4.40	2.32	.696	0.79/1.20	237
0-8.7	.145	43.3	6.9	8.90	3.49	5.10	2.68	.768	0.41/0.82	180
0-15.8	.263	23.9	3.8	8.70	3.42	5.80	3.05	.892	0.42/1.51	100
0-20.2	.337	18.6	2.97	8.60	3.37	6.00	3.16	.937	0.18/0.73	89
0-23.5	.392	16.0	2.55	8.60	3.37	6.10	3.21	.952	0.42/2.30	66
0-33.2	.554	11.4	1.80	8.15	3.20	5.80	3.05	.953	0.45/3.23	50
1-14.6	1.143	5.5	.875	7.00	2.74	5.20	2.74	1.0	0.23/2.88	28

*R_p = phase ratio (ratio of outlet displacement to period)

Atmospheric Conditions
Temperature - 84°F
Pressure - 74.28 cm Hg

Cell Conditions (both cells)
Total Bridge Current - 16.0 ma
Cell Temperature - 35°C
Sample Flow Manometer - 9 cm H_2O

Column Conditions
Inlet Air Flow - 6.9 in. H_2O (manometer)
Inlet Gas Temperature - 88°F
Column Pressure Drop - 2.6 in. H_2O
Inlet Water Flow - 6.8 (rotameter reading)
Inlet Water Temperature - 74°F
Inlet Gas Mean Concentration - 7.52 mole % CO_2

TABLE XIV

EXPERIMENTAL DATA - RUN 6

G = 20 lb moles/hr-ft^2 (nominal) L = 222 lb moles/hr-ft^2

Period		Frequency		Inlet Amplitude		Outlet Amplitude		Amplitude Ratio	R_P*	Phase Shift
min-sec	min	rad/min	cpm	mv	mole %	mv	mole %			deg
0-56.0	.933	6.73	1.07	7.40	2.90	5.5	2.90	1.00	0.22/2.20	36
0-32.5	.542	11.6	1.85	8.55	3.35	5.94	3.13	.935	0.16/1.21	48
0-23.8	.397	15.6	2.52	8.90	3.49	6.00	3.16	.905	0.17/0.82	75
0-19.6	.327	19.2	3.06	9.00	3.53	6.00	3.16	.895	0.19/0.75	91
0-15.0	.25	25.1	4.0	9.05	3.55	5.95	3.13	.882	0.44/1.45	109
0-8.6	.1434	43.8	6.98	8.90	3.49	4.90	2.58	.739	0.42/0.82	184
0-6.2	.1034	60.8	9.68	8.90	3.49	4.15	2.185	.626	0.42/0.60	252
0-4.8	.080	78.5	12.5	8.75	3.43	3.55	1.87	.542	0.75/1.60	270
0-4.0	.0667	94.1	15.0	8.50	3.33	2.80	1.475	.443	00.77/0.76	365

*R_P = phase ratio (ratio of outlet wave displacement to period)

Atmospheric Conditions

Temperature - 84°F
Pressure - 74.28 cm Hg

Cell Conditions (both cells)

Total Bridge Current - 16.0 ma
Cell Temperature - 35°C
Sample Flow Manometers - 9 cm H_2O

Column Conditions

Inlet Air Flow - 7.7 in. H_2O (manometer)
Inlet Gas Temperature - 88°F
Column Pressure Drop - 4.6 in. H_2O
Inlet Water Flow - 20.3 (rotameter reading)
Inlet Water Temperature- 73°F
Inlet Gas Mean Concentration - 6.74 mole % CO_2

TABLE XV

EXPERIMENTAL DATA - RUN 13

G = 20 lb moles/hr-ft^2 (nominal) L = 0 lb mole/hr-ft^2

Period		Frequency		Inlet Amplitude		Outlet Amplitude		Amplitude Ratio	R_p*	Phase Shift
min-sec	min	rad/min	cpm	mv	mole %	mv	mole %			deg
0-3.8	.0634	99.0	15.8	8.8	3.45	3.85	2.02	.587	0.73/1.41	188
0-5.0	.0834	75.3	12.0	9.5	3.72	4.7	2.48	.665	0.80/1.87	154
0-6.0	.10	62.8	10.0	9.8	3.84	5.2	2.74	.714	0.82/2.19	135
0-8.1	.135	46.5	7.41	10.0	3.92	6.0	3.16	.805	1.00/3.17	113
0-13.2	.220	28.5	4.55	10.4	4.08	6.8	3.58	.877	0.52/3.61	72
0-15.0	.250	25.1	4.0	10.3	4.04	7.0	3.68	.911	0.43/1.88	54
0-18.6	.310	20.2	3.27	10.3	4.04	7.25	3.82	.944	0.49/3.68	48
0-22.6	.377	16.6	2.65	10.1	3.96	7.1	3.74	.949	0.25/2.17	41.5
0-31.4	.524	12.0	1.91	9.9	3.88	7.1	3.74	.964	0.27/4.05	19.5
0-52.4	.874	7.18	1.14	9.5	3.72	6.8	3.58	.962	0.10/2.08	17.3

*R_p = phase ratio (ratio of outlet wave displacement to period)

Atmospheric Conditions

Temperature - 80°F
Pressure - 73.91 cm Hg

Cell Conditions (both cells)

Total Bridge Current - 16 ma
Cell Temperature - 35°C
Sample Flow Manometers - 9 cm Hg

Column Conditions

Inlet Air Flow - 7.4 in. H_2O (manometer)
Inlet Gas Temperature - 77°F
Column Pressure Drop - 0.4 in. H_2O
Inlet Water Flow - 0
Inlet Water Temperature - --
Inlet Gas Mean Concentration - 4.65 mole % CO_2

APPENDIX G

AMPLITUDE RATIO AND PHASE SHIFT SAMPLE CALCULATIONS

This appendix presents a sample of the analytical methods used to calculate the amplitude ratios and phase shifts resulting from the experimental and theoretical portions of this study. The calculation procedures for the experimental and theoretical responses will be presented separately but at the common nominal operating conditions of $G=1$ lb mole/hr-ft^2, $L=222$ lb mole/hr-ft^2, and $\omega=1.0$ cycles per minute.

I. EXPERIMENTAL RESPONSES

The experimental amplitude ratios and phase shifts were determined from the oscillograph concentration traces such as the samples shown in Figure 12.

As discussed in Chapter IV, the exact sinusoid frequency for any nominal frequency control setting was determined from the period between flashes of the remote marker light. Thus, for a nominal frequency of one cycle per minute at the above column operating conditions (Table V, Appendix F), the measured period was 51.8 seconds or 0.863 minutes and the true sinusoid frequency was 1.17 cycles per minute.

The amplitude of the concentration waves at this

frequency was carefully measured with dividers and the bridge signal amplitude was calculated from these divider measurements and the existing preamplifier sensitivity (chart calibration). As can be seen from Table V of Appendix F, the bridge signal amplitudes measured by this method for the frequency 1.17 cpm were 25.2 mv and 5.40 mv for the inlet and outlet thermal conductivity cells, respectively. Since, as discussed in Appendix D, the thermal conductivity cell response was linear throughout the concentration range used in this experiment, a constant cell sensitivity factor could be used to convert the bridge signal amplitude to concentration amplitude. These cell sensitivity factors were calculated from the slopes of the cell calibrations curves (Figure E-8) and were found to be 2.55 mv/per cent CO_2 and 1.90 mv/per cent CO_2 for the inlet and outlet cells, respectively. Thus, by dividing the bridge signal amplitudes by their respective cell sensitivity factors, the following concentration amplitudes were determined:

inlet gas concentration amplitude = 9.88% CO_2
outlet gas concentration amplitude = 2.84% CO_2

Since the amplitude ratio was defined as the ratio of the outlet wave amplitude to the inlet wave amplitude, this became:

$$\frac{A(Z)}{A(0)} = \frac{2.84}{9.88} = 0.288$$

The phase shifts between the inlet and outlet waves were calculated from a term called the "phase ratio." The "phase ratio" was simply the ratio of the displacement of the outlet wave with respect to the inlet wave, measured in some arbitrary units, to the wave period measured in the same units. The wave period was determined, for each frequency, from the remote marker indications on the chart paper by measuring the distance between marks with a divider. The outlet wave displacement was the distance from the marker indication on the outlet trace to a position on the outlet wave which corresponded to the position on the inlet wave at which the frequency indicator made its mark. This method of determining phase shifts was used because it was rapid and accurate. The phase shift in degrees was calculated from the phase ratio by multiplying by 360 or an integral multiple of 360.

Thus, at a frequency of 1.17 cpm and the previously mentioned column conditions, the phase ratio was fortuitously 1.0 This meant that the phase shift was 0, 360, or 720, etc., degrees. The choice of these multiples was made from the phase shift calculated for the waves at the next smallest measured frequency. Table V shows that this was 245 degrees. Thus the phase shift at 1.17 cpm was 360 degrees.

II. THEORETICAL RESPONSES

The theoretical amplitude ratios and phase shifts were

calculated, for the various models, by the equations of Chapter II and Appendix B.

To make a theoretical response calculation at some fixed column flow conditions it was necessary to know certain system physico-chemical parameters. These were: 1) packing liquid phase holdups, 2) mass transfer coefficients, and 3) equilibrium data. The values for these parameters used in the theoretical response calculations were obtained from the very best available information in the literature. A presentation of these data and a brief discussion of their source follows.

The packing porosity or void volume tests, described in Chapter IV, gave the volume of water necessary to fill the packed section of the column. The porosity was calculated as the ratio of this volume (presumably the void volume) to the empty column volume. The value so obtained was $\epsilon = 0.604$.

The liquid phase holdup, h_L, was obtained from the data of Shulman, et al. (104). His data were interpolated to determine the relationship between the holdup on 5/8-inch Raschig rings and the liquid phase flow rate, L, at gas flows less than loading conditions. Figure G-1 gives the results of this interpolation. The gas phase holdups were calculated from the packing section porosity, ϵ, and the liquid phase holdup by the simple expression:

$$h_G = \epsilon - h_L \qquad \text{(G-1)}$$

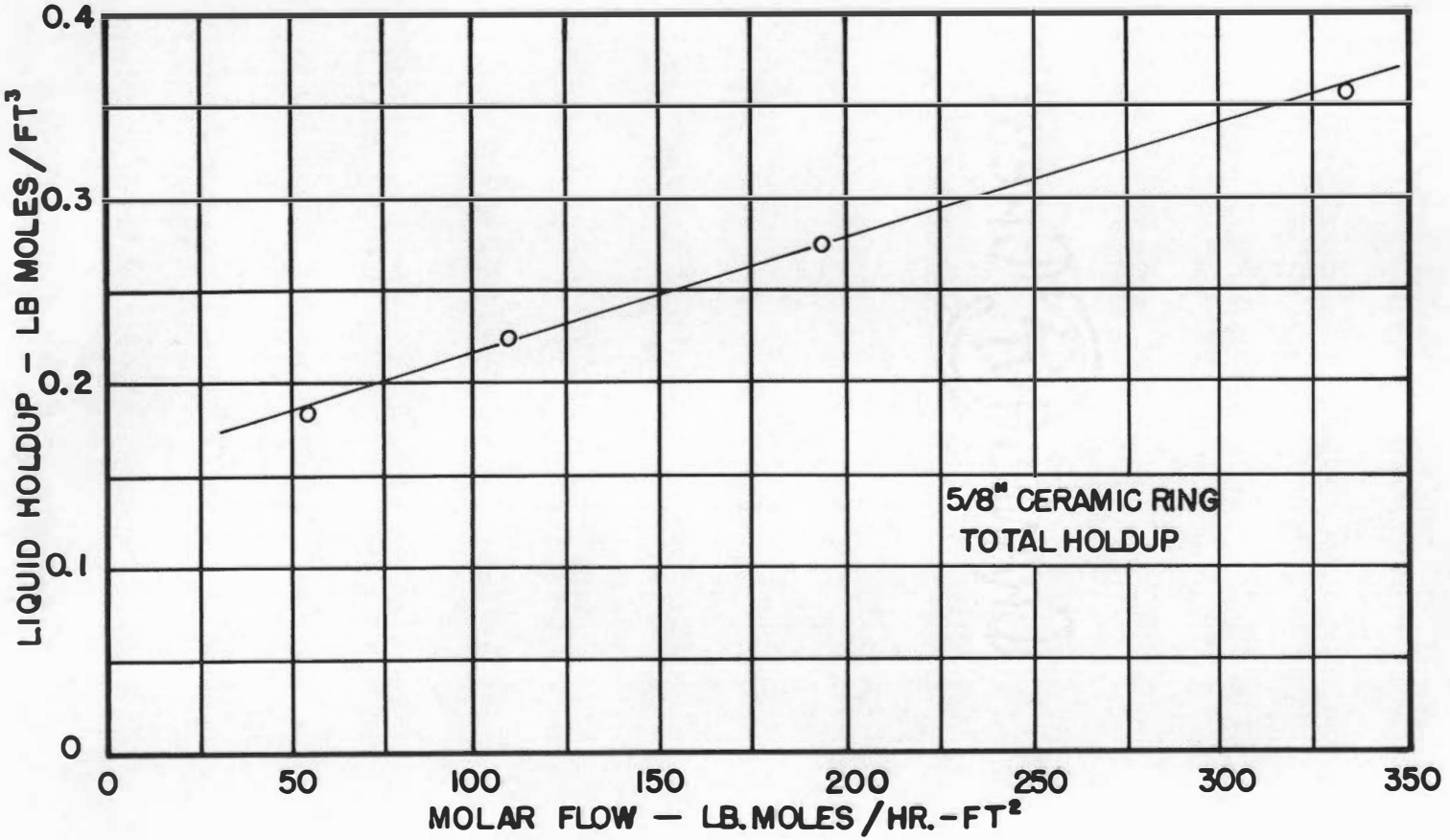


Figure G-1. Packing liquid phase holdup.

Since, as demonstrated by Shulman, et al. (104), and others, the liquid phase holdup is independent of the gas phase flow rate up to the loading point, the holdup values used in the theoretical response calculations were assumed independent of gas phase flow rate. This, of course, was the case since the column was operated below loading condition for all runs except Run 6 (L=222 lb mole/hr-ft^2, G=17.5 lb mole/hr-ft^2) for which loading conditions were only slightly exceeded. Figure G-2 shows the limiting conditions for loading and flooding of the 5/8-inch ceramic Raschig rings used in the absorption column. The data for this figure were calculated from the generalized correlations given by Treybal (113).

A large number of experimental studies have been carried out to determine mass transfer coefficients for the air-carbon dioxide-water system; and, as with most mass transfer data, the results show little consistency (101, 26). Sherwood and Holloway (99, 100) made by far the most careful and comprehensive study of the system and of liquid film coefficients in general, and their data have become the standard of comparison for subsequent research. Shulman and De Gouff (103) and Deed et al. (32) have verified Sherwood and Holloway's results for the air-carbon dioxide-water system and Raschig ring packings. Since the Sherwood and Holloway data appeared to be the most reliable and the most widely accepted mass transfer information on liquid film coefficients for

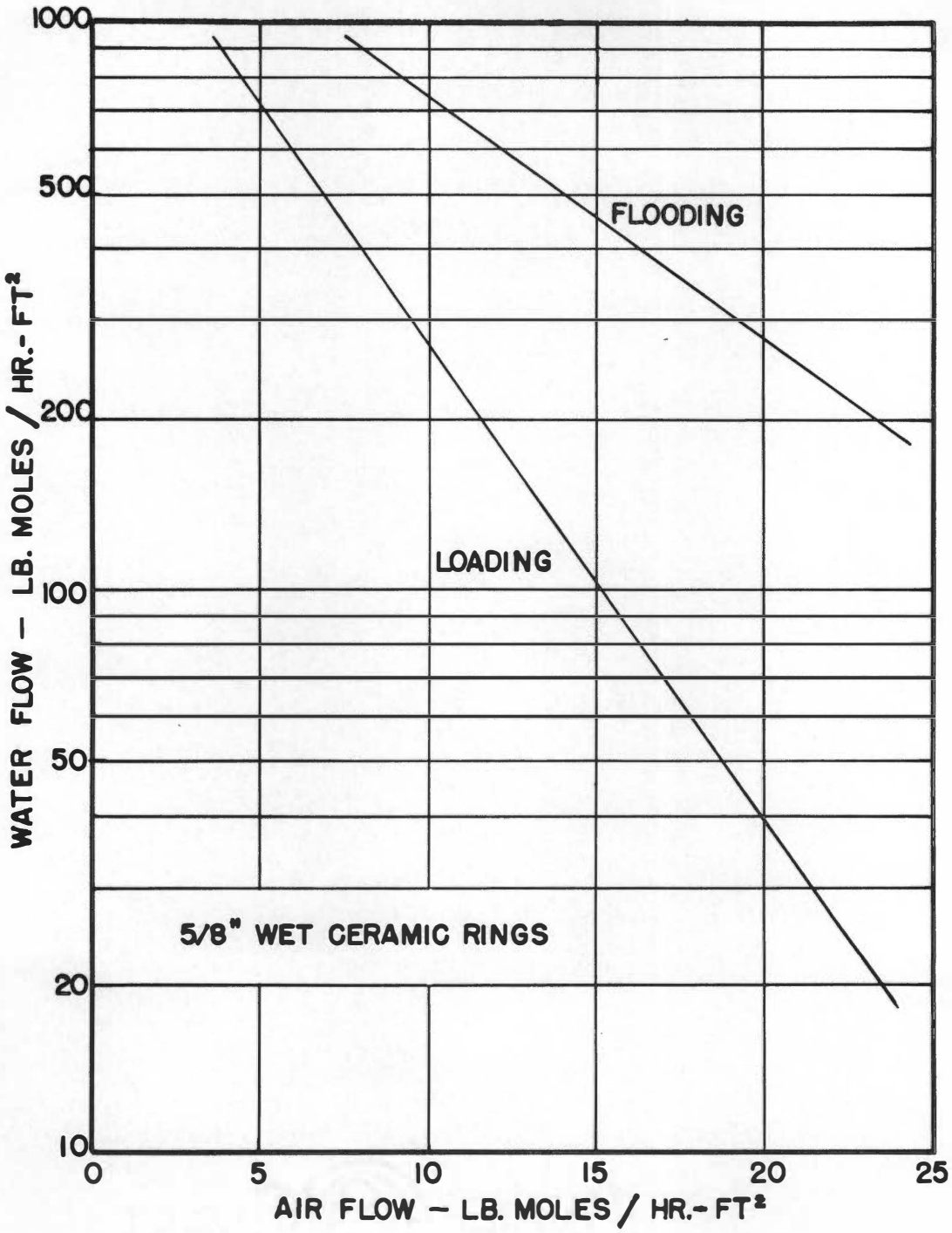


Figure G-2. Loading and flooding limiting conditions.

Raschig rings, they were used to determine the values of k_La needed for the calculation of the theoretical amplitude ratios and phase shifts. Figure G-3 shows a plot of desorption coefficients, k_La, versus the liquid phase flow, L, for 1/2-inch rings. The data for 1/2-inch rings were used since Sherwood and Holloway did not test 5/8-inch rings, and since only small differences existed between the k_La values for 1/2-inch and 1-inch rings, particularly at higher liquid flows. Desorption mass transfer coefficients have been shown by Sherwood and Holloway (100) to be equal to absorption coefficients and, as in the case of liquid holdup, these liquid film coefficients were found to be independent of gas phase flow rates up to the loading point. Thus the data of Figure G-3 were used for all the gas phase flow rates considered in this work.

The equilibrium data for the air-carbon dioxide-water system obey Henry's Law; i.e., the ratio of the gas phase composition to the liquid phase composition is constant at fixed temperatures. But, while the relationship $y=mx^*$ (Equation 4) is linear over a range of compositions, the slope, m, of this equilibrium expression is temperature dependent. Figure G-4 gives the value of m as a function of system temperature (80, 72). In this work, the system temperature was assumed to be that of the liquid phase.

The values of liquid phase holdup, mass transfer

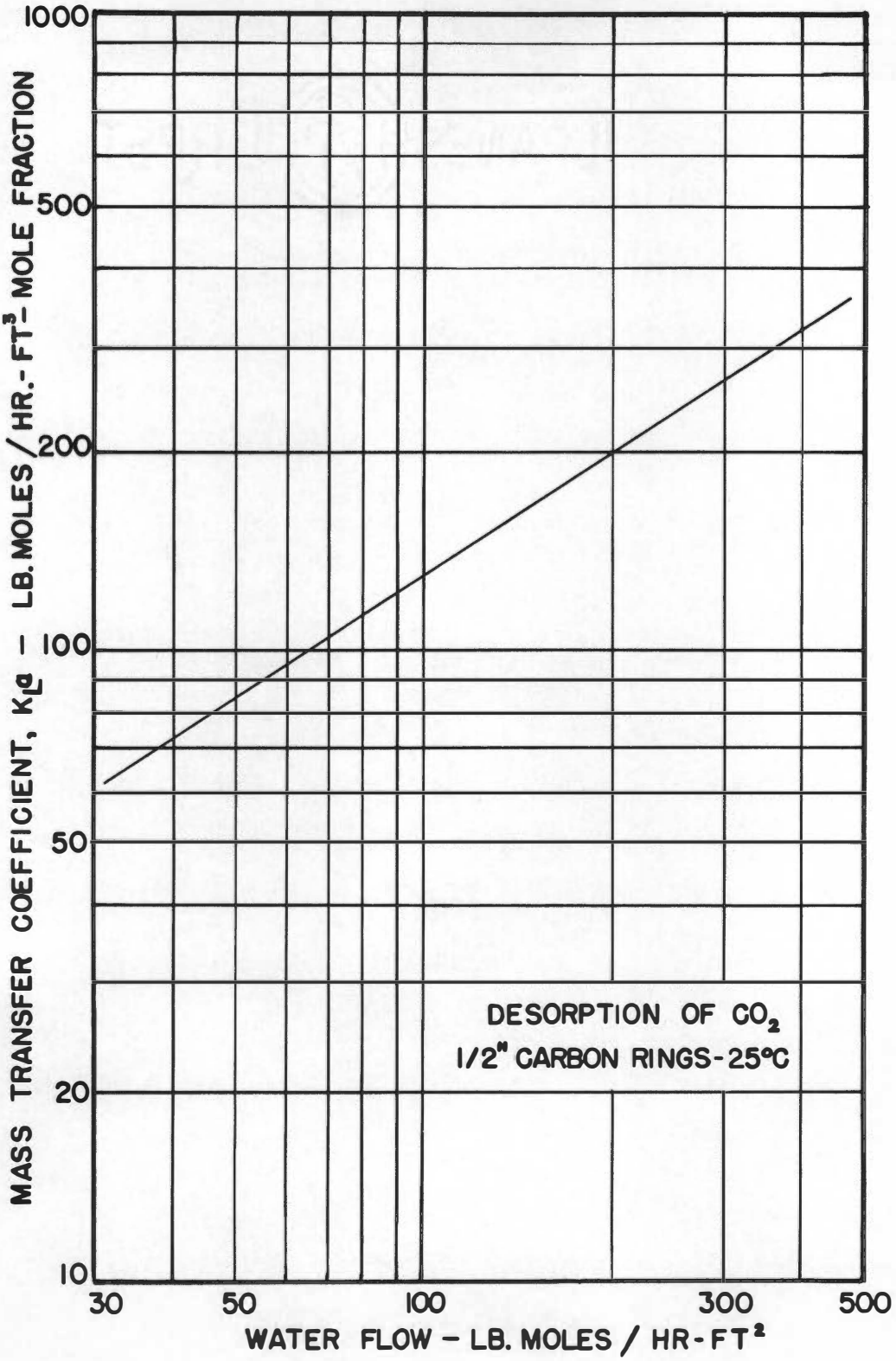


Figure G-3. Liquid film mass transfer coefficients.

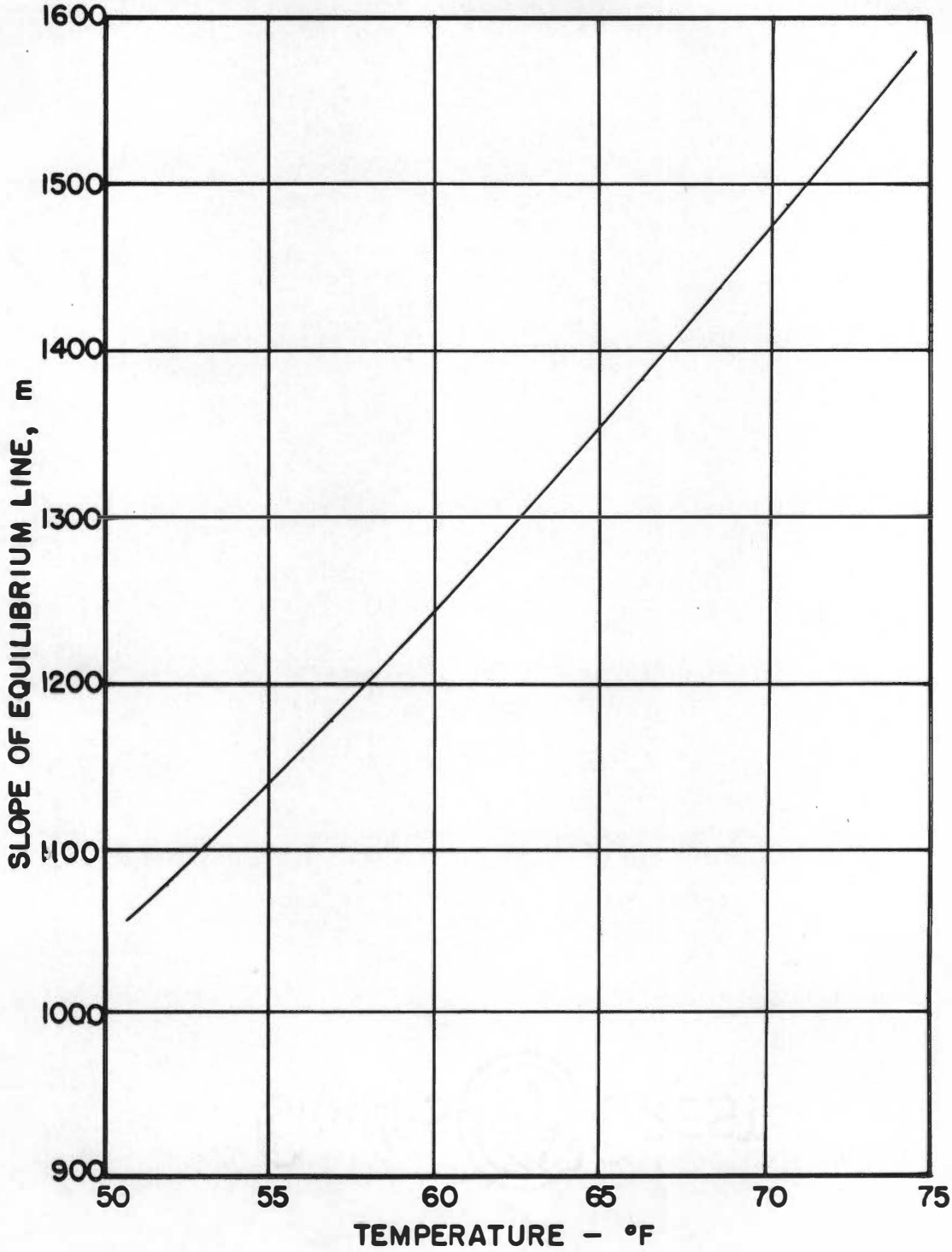


Figure G-4. Equilibrium data temperature dependence.

coefficients, etc., discussed above were used to calculate the theoretical frequency responses of the flow models presented in Chapter II. Sample calculations for these models are given below. Each calculation was made at the actual column operating conditions which the theoretical model was attempting to describe. These conditions are given in Table I.

III. SLUG FLOW MODEL

Two Phase Countercurrent with Absorption

Table I gives the column operating conditions as:

$G = 0.874$ lb mole/hr-ft^2

$L = 222$ lb mole/hr-ft^2

column temperature = 74°F

packing height = 5.12 ft

Figure G-1 gives

$$h_L = 0.291 \frac{\text{lb moles water}}{\text{ft}^3} = 0.084 \frac{\text{ft}^3 \text{ water}}{\text{ft}^3}$$

Thus the gas phase holdup by Equation G1 becomes

$$h_G = 0.604 - .084 = 0.52 \text{ ft}^3 \text{ gas/ft}^3$$

or, assuming 394 ft^3/lb mole gas

$$h_G = 0.00132 \text{ lb mole/ft}^3$$

From Figure G-3,

$$k_L a = 222 \text{ lb mole/hr-ft}^3$$

and Figure G-4 gives

$$m = 1565$$

Consider the frequency

$$= 1.5 \text{ cycle/min} = 568 \text{ radians/hr}$$

With the above conditions the values of n and r, as given by Equation B6, become

$$n = (0.874-\frac{222}{1565})^2(222)^2 - (0.874x0.291 + 222x0.00132)^2(568)^2$$
$$= -6.90x10^4$$

and

$$r = \sqrt{\left[-6.90x10^4\right]^2 + \left[2x222(0.874+\frac{222}{1565})(0.874x0.291+222x0.00132)\right]^2}$$
$$= 15.57x10^4$$

Thus, the amplitude ratio and phase shift can now be calculated from Equations B8 of Appendix B. These are,

$$\frac{A(Z)}{A(0)} = \exp\left\{\frac{5.12}{2x0.874x222}\left[(0.874-\frac{222}{1565})222 - (\frac{15.57x10^4-6.90x10^4}{2})\right]\right\}$$
$$= .548$$

and

$$\phi = \frac{5.12}{2x0.874x222}\left[(0.874x0.291+222x0.00132)(568)-\left(\frac{15.57x10^4+6.90x10^4}{2}\right)^{\frac{1}{2}}\right]$$

$$= -4.73 \text{ radians}$$

or

$$\phi = -271 \text{ degrees}$$

The limit of the amplitude ratio as the sinusoid frequency approaches infinity is given by Equation 32. Thus,

$$\lim_{\omega\to\infty} \frac{A(Z)}{A(0)} = e^{-\frac{(5.12)(222)}{(0.874)(1565)}}$$

$$= 0.435$$

The inflection frequency given by Equation 34 becomes,

$$\omega_i = \frac{222(0.874-\frac{222}{1565})}{(0.874x0.291+222x0.00132)} = 297 \text{ radians/hr}$$

$$= 0.788 \text{ cycles/min}$$

and the amplitude ratio and phase shift at this frequency are given by Equations 35 and 36, respectively. These are,

$$\left[\frac{A(Z)}{A(0)}\right]_i = \exp\left\{\frac{5.12x222}{2x0.874x222}\left[(0.874-\frac{222}{1565})-(0.874^2-\frac{222^2}{1565^2})^{\frac{1}{2}}\right]\right\}$$

$$= 0.681$$

and

$$\phi_i = \frac{5.12 \times 222}{2 \times 0.874 \times 222}\left[\frac{(0.874 \times 0.291 - 222 \times 0.00132)}{(0.874 \times 0.291 + 222 \times 0.00132)}\left(0.874 - \frac{222}{1565}\right) - \left(0.874^2 - \frac{222^2}{1565^2}\right)^{\frac{1}{2}}\right]$$

or

$$\phi_i = -2.68 \text{ radians} = -154 \text{ degrees}$$

Single Phase Flow without Absorption

As is pointed out in Chapter II the amplitude ratio for this model is identically unity for all frequency, ω. The phase shift, however, is given by Equation 42. In this case, where there is no liquid flow, the gas phase holdup is given directly by the porosity. Thus,

$$h_G = 0.604 \text{ ft}^3/\text{ft}^3$$

or

$$h_G = \frac{0.604}{394} = 0.00153 \text{ lb mole/ft}^3$$

and

$$\phi = -\frac{0.00153 \times 5.12}{0.874} \times 568 = -5.09 \text{ radians}$$

or

$$\phi = -292 \text{ degrees}$$

IV. MIXING CELL MODEL

Two Phase Countercurrent Flow with Absorption

The procedure for the calculation of the theoretical amplitude ratio and phase shift for this model is given in Appendix B. The use of a desk calculator is necessary for this calculation because five or more significant figures are required for an accurate solution.

In this case a sinusoid frequency of $\omega = 1.0$ cpm=377 radians per hour will be used. Consider the case where the column is to be represented by forty mixing cells, i.e., N=40. By Equations 44 and 47 and the values of the operating conditions used in the calculation of the slug flow model τ_L and τ_G become:

$$\tau_G = \frac{h_G Z}{GN} = \frac{0.00132 \times 5.12}{0.874 \times 40} = 1.9340 \times 10^{-4} \text{ hr}$$

$$\tau_L = \frac{h_L Z}{LN} = \frac{0.291 \times 5.12}{222 \times 40} = 1.6771 \times 10^{-4} \text{ hr}$$

Also,

$$H = \frac{Z}{N} = \frac{5.12}{40} = 0.12800 \text{ ft}$$

Thus by Equations B10,

$$u = \left(\frac{0.128 \times 222}{222} + 1\right)\left(\frac{0.128 \times 222}{0.874 \times 1565} + 1\right) - (1.934 \times 10^{-4})(1.6771 \times 10^{-4})(377)^2$$

$$= 1.1467$$

and

$$v = 377\left[1.934\times10^{-4}\left(\frac{0.128\times222}{222}+1\right)+1.6771\times10^{-4}\left(\frac{0.128\times222}{0.874\times1565}+1\right)\right]$$
$$= 0.14672$$

Also, from Equations B12 and 51

$$k = u - \frac{(Hk_La)^2}{LGm} + 1 = 1.1467 - \frac{(0.128\times222)^2}{222\times0.874\times1565} + 1$$
$$= 2.1441$$

With these values of u, v, and k, Equations B15 can be used to obtain values of r and n. Thus,

$$r = \sqrt{\left[(2.1441)^2-(0.14672)^2-4(1.1467)\right]^2-\left[2\times0.14672(2.1441-2)\right]^2}$$
$$= 0.043739$$

and

$$n = (2.1441)^2-(0.14672)^2-4(1.1467)$$
$$= -0.11101$$

By Equations B18

$$r_{D_1} = \sqrt{\frac{\left[2.1441-\left(\frac{0.043739+0.11101}{2}\right)^{\frac{1}{3}}\right]^2+\left[0.14762-\left(\frac{0.043739-0.11101}{2}\right)^{\frac{1}{3}}\right]^2}{4}}$$
$$= (1.0201)^{\frac{1}{3}}$$

and

$$\theta_{D_1} = \tan^{-1}\left[\frac{0.14672 - \left(\frac{0.43739-0.11101}{2}\right)^{\frac{1}{2}}}{2.144 - \left(\frac{0.43739+0.11101}{2}\right)^{\frac{1}{2}}}\right]$$

$$= -0.633 \text{ degree}$$

Similarly, from these equations,

$$r_{D_2} = (1.3157)^{\frac{1}{2}}$$

and

$$\theta_{D_2} = 7.834 \text{ degrees}$$

With these values of r_{D_1}, r_{D_2}, θ_{D_1}, and θ_{D_2} the terms of Equations B22 can be evaluated. Thus,

$$r_{D_1}{}^{N} = (1.0201)^{20} = 1.4860$$

$$r_{D_1}{}^{N-1} = (1.0201)^{19.5} = 1.4715$$

$$r_{D_2}{}^{N} = (1.3157)^{20} = 241.0$$

$$r_{D_2}{}^{N-1} = (1.3157)^{19.5} = 211.0$$

and

$$\sin N\theta_{D_1} = \sin (40)(-0.633) = -0.4276$$

$$\cos N\theta_{D_1} = \cos (40)(-0.633) = 0.9040$$

$$\sin(N-1)\theta_{D_1} = \sin (39)(-0.633) = -0.4176$$

$$\cos(N-1)\theta_{D_1} = \cos (39)(-0.633) = 0.9086$$

$$\sin \quad N\theta_{D_2} = \sin\,(40)(7.834) = -0.7310$$
$$\cos \quad N\theta_{D_2} = \cos\,(40)(7.834) = 0.6821$$

$$\sin\,(N-1)\,\theta_{D_2} = \sin\,(39)(7.834) = -0.8139$$
$$\cos\,(N-1)\,\theta_{D_2} = \cos\,(39)(7.834) = 0.5810$$

Substitution of these values into Equations B22 yields

$$r_N = 42.118$$
$$\theta_N = 353.9 \text{ degrees}$$

The values of r_{LG} and θ_{LG} are determined from Equations B24. Therefore,

$$r_{LG} = (u^2 + v^2)^{\frac{1}{2}} = (1.1467^2 + 0.1467^2)^{\frac{1}{2}}$$
$$= 1.1560$$

and

$$\theta_{LG} = \tan^{-1} \frac{0.1467}{1.1467}$$
$$= 7.11 \text{ degrees}$$

Equations B26 yield r_L and θ_L:

$$r_L = \sqrt{\left(\frac{0.128 \times 222}{222} + 1\right)^2 + (1.6771 \times 10^{-4} \times 377)^2}$$
$$= (1.27638)^{\frac{1}{2}}$$

and

$$\theta_L = \tan^{-1}\left[\frac{1.6771\times10^{-4}\times377}{\frac{0.128\times222}{222}+1}\right]$$

$$= 3.20 \text{ degrees}$$

Also, the values of r_T and θ_T are determined from Equations B28, where

$$r_T = r^{\frac{1}{3}} = (0.043739)^{\frac{1}{3}}$$

$$= 0.2090$$

and

$$\theta_T = \frac{\tan^{-1}\left[\frac{2\times0.14672(2.1441-2)}{(2.1441)^2-(0.14672)^2-4(1.1467)}\right]}{2}$$

$$= 52.0 \text{ degrees}$$

Finally, the amplitude ratio can be calculated from Equation B30. Thus

$$\frac{A(Z)}{A(0)} = \frac{r_L^{\,N}\, r_T}{r_{LG}\, r_N} = \frac{(1.27638)^{20}(0.2090)}{(1.1560)(42.118)}$$

$$= 0.565$$

The phase shift is found from Equation B31:

$$\phi = N\,\theta_L + \theta_T - \theta_{LG} - \theta_N$$

$$= 40\times3.20 + 52.0 - 7.11 - 353.9$$

$$= -181 \text{ degrees}$$

Single Phase Flow without Absorption

In this simple case the amplitude ratio and phase shifts can be determined directly from Equations 75 and 76, respectively. Here, as in the slug flow model,

$$h_L = 0.00153 \text{ lb mole/ft}^3$$

Then

$$\frac{A(Z)}{A(0)} = \left[\left(\frac{0.128 \times 0.00153 \times 377}{0.874}\right)^2 + 1\right]^{-\frac{40}{2}}$$

$$= 0.871$$

and

$$\phi = -40 \tan^{-1} \left(\frac{0.128 \times 0.00153 \times 377}{0.874}\right)$$

$$= -190 \text{ degrees}$$

V. AXIAL DIFFUSION MODEL

Two Phase Countercurrent Flow with Absorption

As discussed in Chapter II, an analytical determination of the theoretical amplitude ratio and phase shift cannot be obtained for this case.

Single Phase Flow without Absorption

The reduction and simplification of Equation 90 given in Appendix B required that

$$\frac{5 \omega^2 E_G^2}{U^4} \ll 1$$

where

$$U = \frac{G}{h_G}$$

and, again,

$$h_G = 0.00153 \text{ lb mole/ft}^3$$

At the conditions of these sample calculations, the interstitial velocity, U, becomes

$$U = \frac{0.874}{0.00153} = 572 \text{ ft/hr}$$

If the axial eddy diffusivity, E_G, is assumed to be approximately 15 ft^2/hr (Peclet number $\cong$ 2.0) then

$$\frac{5\ \omega^2\ E_G{}^2}{U^4} = \frac{5x377^2x15^2}{572^4} = 1.5x10^{-3}$$

and the above inequality is satisfied. Thus the amplitude ratio and phase shift for this case are given by Equations B39 and B40, respectively, or

$$\frac{A(Z)}{A(0)} = \exp\left(-\frac{512x377^2x15}{572^3}\right)$$

$$= 0.950$$

and

$$\phi = \frac{5.12x377}{572} = 3.38 \text{ radians}$$

$$= -193 \text{ degrees}$$

APPENDIX H

NOTATION

Symbol	Meaning
A	amplitude of harmonic oscillation
$A_{1,2}$	roots of a characteristic equation
a	$4\ GL\ h_L\ h_G$ or mass transfer area, ft^2/ft^3 packing
B	constant
b	$4\ GL\ k_L a(h_G + h_L/m)$
$C_{1,2}$	constants
c	$(G\ h_L - L\ h_G)$; or concentration, volume %
D	constant; or diameter, ft
$D_{1,2}$	$\frac{(T_G T_L - fg + 1) \pm \sqrt{(T_G T_L - fg + 1)^2 - 4 T_G T_L}}{2}$ (positive sign D_2)
d	$(G - \frac{L}{m})\ k_L a$; or dilution factor
E	bridge voltage, volts; or axial eddy diffusivity, $\frac{ft^2}{hr}$
F	mass flow rate, lbm/min; or volume flow rate, ml/min
f	$\frac{H k_L a}{Lm}$
G	molar mass velocity of gas phase, lb moles/hr-ft^2
g	$\frac{H k_L a}{G}$
H	$\frac{Z}{N}$ packing height equivalent to a mixing cell, ft
h	total holdup, lb moles/ft^3
I	current, amperes
i	imaginary unit, $\sqrt{-1}$

Symbol	Meaning
K	linear valve pressure characteristic, $\frac{ft^3}{min-\sqrt{psi}}$
$K_{1,2}$	roots of a characteristic equation
k_L	mass transfer coefficient, lb moles/hr-ft^2 transfer area
L	molar mass velocity of liquid phase, lb moles/hr-ft^2
M	linear valve position characteristic, ft^3/min-in
m	slope of equilibrium line
N	mass transfer rate, lb moles/hr-ft^2 transfer area; or number of mixing cells
P	pressure, lbf/in^2 absolute
Peclet number	$= \frac{D_p U}{E_G}$
$P_{1,2}$	roots of a characteristic equation
Q	volume flow rate, ft^3/min
R	resistance, ohms
Reynolds number	$= \frac{D_p U \epsilon}{V}$
R_g	gas constant = 18,550 lbf-in/lb mole-$^\circ$R
R_p	phase ratio, outlet wave displacement to wave period
r, r'	moduli of complex numbers
S	transformed dependent variable (signal)
s	Laplace transform parameter
T	absolute temperature, $^\circ$R
T_G	$\tau_G s + \frac{H k_L a}{Gm} + 1$
T_L	$\tau_L s + \frac{H k_L a}{L} + 1$
t	time dimension, hr

Symbol	Meaning
U	interstitial velocity, hr
u,v,n,m	= components of imaginary numbers
V	volume, $in.^3$
W	molecular weight, lbm/lb mole
X	linear valve position, inches
x	mole fraction solute in liquid phase
y	mole fraction solute in gas phase
$\left\lvert \frac{\bar{y}_Z}{\bar{y}_o} \right\rvert$	attenuation or amplitude ratio
z	length dimension, ft

Greek Letters

α	$\frac{k_L a + h_L s}{L}$
β	$\frac{k_L a}{mL}$
γ	$\frac{k_L a/m + h_G s}{G}$
δ	$\frac{k_L a}{G}$
ϵ	porosity, ft^3/ft^3; or unbalanced bridge signal, volts
$\mathcal{P}$	$\frac{G}{k_L a} + \frac{L E_G}{k_L a E_L}$

Meaning

η $\quad \left(\frac{1}{m} - \frac{LG}{E_L\ k_L a} - \frac{E_G}{E_L}\right) + \left(\frac{h_G}{k_L a} - \frac{h_L\ E_G}{k_L a\ E_L}\right) s$

θ , θ' arguments of complex numbers

κ $\quad \frac{-E_G}{k_L a}$

λ $\quad \left(\frac{G}{E_L} - \frac{L}{E_L m}\right) + \left(\frac{h_L G}{k_L a\ E_L} - \frac{h_G L}{k_L a\ E_L}\right) s$

μ $\quad \left(\frac{k_L a + h_L s}{E_L}\right)\left(\frac{k_L a/m + h_G s}{k_L a}\right) - \frac{k_L a}{E_L m}$

ν kinematic viscosity, ft^2/hr

τ_G $\quad \frac{H\ h_G}{G}$

τ_L $\quad \frac{H\ h_L}{L}$

ϕ phase shift, degrees or radians

ω circular frequency, radians/hr

Subscripts

A air

C carbon dioxide

c cell

G gas phase

i inflection point or inlet

L liquid phase

M measuring or mixture

m	mean value
o	outlet
P	pressure P fixed or primary
p	packing
r	reference gas thermistor
S	secondary
s	system or sample gas thermistor
T	tank
t	total
X	position X, fixed

VITA

Robert I. Gray was born in White Plains, New York, in 1930. His primary and secondary schooling took place in the public schools of Hastings on Hudson, New York, from which he received a diploma in 1948. He entered Syracuse University in September, 1948, and received a Bachelor of Chemical Engineering degree from that institution in 1952. He completed work for a Master of Chemical Engineering degree at Syracuse University in 1953. From September, 1953, to December, 1957, he was employed by Pratt and Whitney Aircraft at East Hartford, Connecticut and Oak Ridge, Tennessee. He entered the Graduate School of The University of Tennessee in the fall of 1954 and is now employed as an instructor at this university. He resides with his wife, Elise, and son, Dean, at 1625 Laurel Avenue, Knoxville, Tennessee.